Nuffield Department of Orthopaedics, Rheumatology and Musculoskeletal Sciences
University of Oxford

Mapping the pro-inflammatory epitope of tenascin-C

Lorena Zuliani Alvarez
St Cross College
DPhil in Musculoskeletal Sciences

Trinity Term 2016

Lorena Zuliani Alvarez

St. Cross College, DPhil in Musculoskeletal Sciences

Trinity Term 2016

Mapping the pro-inflammatory epitope of tenascin-C

Abstract

Endogenous molecules, including extracellular matrix (ECM) proteins, have been shown to induce inflammation via toll-like receptor (TLR) activation in order to drive an immune response to tissue damage. Tenascin-C, an ECM glycoprotein transiently induced in injury and persistently expressed during chronic inflammatory diseases, stimulates cytokine synthesis via activation of TLR4 by its C-terminus fibrinogen-like globe (FBG-C) domain. However, the specific epitope of FBG-C that activates TLR4 is not known. Unlike tenascin-C, other tenascin family members (tenascin-R, -W and -X) are constitutively expressed in healthy adult tissues but also contain a highly homologous FBG domain. I have used comparative analysis of the tenascin family FBG domains to elucidate the molecular mechanism by which FBG-C activates TLR4. The ability of each tenascin FBG domain to activate NF-κB in ThP1 cells and cytokine synthesis in primary human macrophages was assessed. Direct binding to TLR4 was evaluated *in vitro* using a solid phase binding assay. Peptide mapping and site-directed mutagenesis were used to elucidate specific residues within the FBG domain involved in TLR4 binding and activation. Molecular modelling and docking simulations were performed to analyse the structural basis of the FBG-TLR4 interaction. I've shown for the first time that, in addition to tenascin-C, other tenascin family members (-R and -W) can induce a TLR4 mediated inflammatory response, whereas tenascin-X cannot. The active FBG domains bound directly to TLR4, in the absence of any co-receptor, with low nM affinity. The pro-inflammatory epitope of the FBG domain of tenascins lies in loop 5 in the P-subdomain, where positively charged amino acids are necessary for the activation of TLR4, whilst two other regions in loops 7 and 10 assist in mediating high affinity binding to this receptor. Introducing these sites into FBG-X enabled this domain to bind to TLR4 and to induce an inflammatory response. Together these data revealed how endogenous molecules can induce an immune response and may help in the design of specific inhibitors of TLR stimuli that contain FBG domains.

Table of Contents

List of figures

List of tables

Acknowledgements

"It is not the critic who counts; not the man who points out how the strong man stumbles, or where the doer of deeds could have done them better. The credit belongs to the man who is actually in the arena, whose face is marred by dust and sweat and blood; who strives valiantly; who errs, who comes short again and again, because there is no effort without error and shortcoming; but who does actually strive to do the deeds; who knows great enthusiasms, the great devotions; who spends himself in a worthy cause; who at the best knows in the end the triumph of high achievement, and who at the worst, if he fails, at least fails while daring greatly, so that his place shall never be with those cold and timid souls who neither know victory nor defeat." Theodore Roosevelt

These lines are dedicated to the people that I have been fortunate to be surrounded by during my DPhil; people who "dare greatly" everyday, which have been giving me support and encouragement to develop this project.

First, I would like to thank my supervisor Kim, for trusting me from day one and for the unconditional help and support she has always given me. Thank you for being my mentor, for motivating me every day and teaching me, with patience and enthusiasm, to be a better scientist.

I also want to especially thank my second supervisor Anna, who has been working with me side by side during all my DPhil. She has been an example of perseverance and dedication, and I would like to thank her for giving me her support, continuous advice and friendship, which I will always treasure.

Thanks to the great laboratory group with which I had to share every day: Wing, Anja, Sean, Susan… thank you for helping me, not only with the experiments, but for all our discussion about science and life. Thank you for your friendship and for all the great moments inside and outside the lab.

Thanks to the matrix biology group, especially Rob, Linda and Noriko, for helping me with the cloning and protein purification protocols. Thanks to the rest of the group for all the helpful feedback during our lab meetings, as well as the good times that we spent together outside the institute. Thanks also to Brian for his assistance with the protein modelling and docking.

I will end acknowledging my family, as without them I would not be here today. Thanks mum for being the first person who took me to a lab and made me fell in love with science. Thanks dad for always believing in me and for your guidance whenever I needed it. Thanks to my brother Adrian for being my inspiration and teaching me that research is about curiosity and being open to learn something new each day. Finally, I want to thank my partner, Manuel. Thank you for making our home a place of peace and joy that I can always return to. Thank you for hearing my presentations a 100 times not fully understanding all of them, and for showing me that passion and motivation is what move us forward to achieve what we dream of.
To all the people who have been in the arena with me and contributed along the way in this project, Many Thanks!

Abbreviations

Ab: antibody

AIM2: absent in melanoma 2

ALR: AIM2-like receptor

β-ME: β-mercaptoethanol

Bmp-2: bone morphogenetic protein 2

BSA: bovine serum albumin

CALEB: chicken acidic leucine-rich EGF-like domain containing brain protein

CD: circular dichroism

CLR: C-type lectin receptor

CNS: central nervous system

DAMP: damage-associated molecular pattern

DC-SING: dendritic cell-specific ICAM3-grabbing non integrin

dsRNA: double-stranded RNA

EDA: extra domain A

EDS: Ehlers-Danlos syndrome

EGF: epidermal growth factor

EGF-L: epidermal growth factor-like repeats

ELISA: enzyme-linked immunosorbent assay

ETM: epithelial-to-mesenchymal

FACS: fluorescence-activated cell sorting

FBG: fibrinogen-like globe

FIBCD-1: fibrinogen C domain-containing protein-1

FNIII: fibronectin type III-like repeats

FReD: fibrinogen related domain

FReP: fibrinogen related proteins

FRET: Förster resonance energy transfer

GLAST: glutamate aspartate transporter

GMQE: global quality estimation score

GPI: glycosylphosphatidylinositol

HMGB1: high mobility group box 1

HNK-1: human natural killer-1

HSP: heat shock protein

HUVEC: human umbilical vein endothelial cells

ICM: internal coordinate mechanics

IFI16: gamma-interferon-inducible protein

IL: interleukin

IFN: interferon

IRAK: IL-1R-associated kinase

IRF: interferon-regulatory factor

kDa: kilo dalton

LBP: LPS-binding protein

LDL: low density lipoprotein

LGP2: laboratory of genetics and physiology 2

LPS: lipopolysacharide

LRR: leucine rich repeat

LRRCT: LRR modules C-terminus

LRRNT: LRR modules N-terminus

LTA: lipoteichoic acid

Mab: monoclonal antibody

Mal: MyD88-adaptor like

MAPK: mitogen-activated protein kinases

M-CSF: macrophage colony-stimulating factor

MD-2: myeloid differentiation factor 2

MMP: matrix metalloproteinase

MSC: mesenchymal stem cell

MTT: tetrazolium salt

MyD88: myeloid differentiation factor 88

NF-κB: nuclear factor-κB

NLR: NOD-like receptor

NLRP3: NLR family pyrin domain containing 3

NMR: nuclear magnetic resonance spectroscopy

NOD1: nucleotide-binding oligomerization domain-containing protein 1

OA: osteoarthritis

OD: optical density

PAb: polyclonal antibody

PAMP: pathogen-associated molecular pattern

PBST: phosphate buffered saline, 0.05% tween

PCR: polymerase chain reaction

PDB: protein data bank

PMB: polymyxin B

PRR: pattern recognition receptor

RA: rheumatoid arthritis

RIG-I: retinoic acid-inducible gene-I

RLR: RIG-I-like receptor

RPTP- ζ /β: receptor protein-tyrosine phosphatase- ζ /β

SD: standard deviation

SDS-PAGE: sodium dodecyl sulphate polyacrylamide gel

SEAP: soluble embryonic alkaline phosphatase

SEM: standard error of the mean

SLC: small latent complex of TGF-β

SLE: systemic lupus erythematosus

SPR: surface plasmon resonance

ssRNA: single-stranded RNA

STING: stimulator of interferon genes

TGF-β: transforming growth factor β

TIR: toll/IL1R homology

TLR: toll-like receptor

TNF: tumour necrosis factor

TRAF-6: TNF receptor-associated factor 6

TRAM: TRIF-related adaptor molecule

TRIF: TIR domain containing adapter inducing interferon-β

Chapter 1 – Introduction

Chapter 1. Introduction

1.1. The immune response: stranger vs danger

An immune response is activated by both exogenous infectious agents as well as sterile tissue damage. The stranger model suggested by Charles Janeway in 1989 [1] proposed that upon infection the immune system recognises "infectious non-self" or molecules from pathogens that are not part of the host, and which activate the innate immune response. These pathogen-associated molecular patterns (PAMPs) are diverse microbial structures that are unique to microorganisms and necessary for their survival, but which also alert the host to pathogen invasion [2]. PAMPs activate the inflammatory machinery which recruits immune cells to the site of infection, destroys pathogens and infected cells and modulates the adaptive immune response [3].

However, this model did not explain how the immune system becomes activated in the absence of infectious stimuli such in the case of sterile injury, cell necrosis, tumours, transplants or autoimmune diseases [4]. In 1994, Polly Matzinger [5] described the danger theory, which proposed that the immune system not only recognises pathogenic stimuli but that it can also be activated by endogenous danger signals. Damage-associated molecular patterns (DAMPs) are molecules generated upon tissue trauma caused by mechanical forces or chemical insults, among other factors [6]. They are not normally active in healthy tissue but they are released or induced upon tissue damage. DAMPs can be located intracellularly and released under conditions of cellular stress or injury. DAMPs can also be found outside the cell, for example one extracellular source of DAMPs are matrix fragments, which are generated as a result of proteolysis by enzymes released from dying cells or by proteases that participate in tissue remodelling and repair. In addition, another source of DAMPs are extracellular

matrix (ECM) proteins that are induced upon tissue injury [7]. Inflammation triggered by endogenous danger signals is a vital physiological cellular response, but it can become a problem when it is excessive or persistent, leading to chronic inflammation that causes further cellular and tissue damage.

In the last two decades, numerous studies have presented strong evidence that supports both models, and shown how both PAMPs and DAMPs are recognized by overlapping subsets of cellular pattern recognition receptors (PRRs).

1.2. Pattern recognition receptors (PRRs)

PRRs are expressed by cells of the innate immune system, including macrophages, monocytes and dendritic cells, but have also been shown to be expressed by a wide variety of other cell types including endothelial cells, epithelial cells and fibroblasts [8]. After the recognition of PAMPs or DAMPs, PRRs induce the activation of signalling pathways that result in the release of pro-inflammatory cytokines, type I interferons, chemokines and antimicrobial proteins. In addition, PRRs can induce other cell processes such as phagocytosis, cell death and autophagy, and together this initial response limits the spread of pathogens or damage, and triggers the activation of the adaptive immune system [3, 9].

There are five classes of PRRs: NOD-like receptors (NLRs), C-type lectin receptors (CLRs), Toll-like receptors (TLRs), RIG-I-like receptors (RLRs) and AIM2-like receptors (ALRs). TLRs and CLRs are located in the cell membrane or in the endosome and NLRs, RLRs and ALRs are present in the cytoplasm. In this way, PRRs can sense both intracellular and extracellular pathogens or DAMPs and activate the

innate immune response. Table 1-1 summarises key examples of each of these PRR families and highlights their role in detecting different inflammatory stimuli.

Table 1-1. Examples and functions of the five different classes of mammaliam PRRs.

PRR	Examples	Functions
CLRs	DEC-205, dectin 1, dectin 2, dendritic cell-specific ICAM3-grabbing non integrin (DC-SIGN)	Recognise carbohydrate epitopes from bacteria and viruses including mannose, fucose and glucan structures [10, 11].
	Macrophage-inducible C-type lectin (Mincle), DC NK lectin group receptor-1 (DNGR-1)	Recognise DAMPs associated with necrotic cell death including spliceosome-associated protein 130 and exposed actin filaments [12-14]
NLRs	Nucleotide-binding oligomerization domain-containing protein 1 (NOD1)	Recognises peptidoglycan motifs from the bacterial membrane of gram-positive and negative bacteria [15-18]
	NLR family pyrin domain containing (NLRP) 3, NLRP7, NLRP1, NLR family CARD domain containing (NLRC) 4	Recognise diverse bacterial components including flagellin, lipopeptides and toxins and are involved in the activation of the inflammasome [19]
	NLRP3	Recognises bacterial RNA, virulence factors and DAMPS such as hyaluronan and uric acid crystals [20-23]
TLRs	TLR1, TLR2, TLR4, TLR5, TLR6	Recognise pathogenic molecules including lipopeptides, flagellin and lipopolysaccharides. Recognise proteins, proteoglycans and fatty acids [24]
	TLR3, TLR7, TLR8, TLR9	Recognise pathogenic and self-nucleic acids [24]
RLRs	Retinoic acid-inducible gene-I (RIG-I) and melanoma differentiation-associated gene 5 (MDA5)	Recognise short and long double stranded (ds) RNA from viruses [25, 26]
	Laboratory of genetics and physiology 2 (LGP2)	Negative regulator of antiviral response and RIG-I activation [27]
ALRs	Absent in melanoma 2 (AIM2) gamma-interferon-inducible protein (IFI16)	Recognise double stranded DNA from bacteria and viruses [28]

CLRs are calcium-dependent carbohydrate-binding lectins, which can recognise different sugar epitopes derived from bacteria and viruses. Detection of these

carbohydrate-derived structures by CLRs results in pathogens being internalised, degraded and presented as antigens [11]. CLRs contain at least one carbohydrate recognition domain, which has conserved residues that determine the carbohydrate specificity of the CLR [29]. NLRs can recognise a diverse range of pathogenic molecules such as peptidoglycan, flagellin, viral RNA and fungal hyphae [30]. They contain a central nucleotide-binding and oligomerization domain (NACHT) and C-terminal leucine rich repeats (LRRs) domain involved in ligand binding. At the N-terminus NLRs contain a caspase recruitment domain (CARD), a baculoviral inhibitory repeat (BIR)-like domain, an acidic transactivation domain or a pyrin domain [31]. The pyrin domain is involved in the assembly of the inflammasome, a multiprotein complex that activates procaspase-1 and participates in the maturation of IL-1 cytokine family [19]. RLRs can recognise short and long double stranded (ds) RNA from viruses and are essential for interferon (IFN) antiviral responses in different types of cells such as fibroblasts, dendritic cells and epithelial cells [32]. RLRs comprise two caspase recruitment domains (CARDs) at the N-terminus, a central box helicase/ATPase domain and a regulatory domain at the C-terminal region [33]. Finally, ALRs are cytosolic DNA sensors. They comprise a HIN200 domain that can bind to pathogenic double stranded DNA and a pyrin domain that confers the ability to associate with other pyrin-containing proteins that leads to assembly of the inflammasome [28]. A new DNA sensor has been discovered recently named cGAS, which in the presence of DNA is able to generate cyclic di-GMP/AMP that binds to stimulator of interferon genes (STING) inducing an antiviral response [34]. A few of these PRRs have also been shown to sense DAMPs. For example, CLRs can detect DAMPs released by necrotic cells such as spliceosome-associated protein 130 and exposed actin filaments [13], while NLRs can recognise hyaluronan and uric acid crystals [30].

1.3. Toll-like receptors

One of the best characterized groups of PRRs is the toll-like receptor family. The protein Toll was initially found in *D. melanogaster* and associated with dorsoventral polarity in the developing embryo [35, 36]. The human homologue called hToll was then discovered [37] and found to be involved in pro-inflammatory signalling in mammals. This receptor was later renamed TLR4 when other family members were also characterised [38]. Eleven TLRs have been described to date in humans but only ten are expressed. TLRs have a variety of ligands including exogenous and endogenous danger signals. TLR 1, 2, 4, 5, 6 and 10 are located in the cell membrane and recognise pathogenic molecules including lipopolysaccharide, lipopetides, peptidoglycans, zymosan and flagellin, as well as endogenous molecules such as hyaluronan fragments, S100 proteins, uric acid, HMGB1, heat shock proteins and fatty acids. TLR 3, 7, 8, 9 are located intracellularly in the endosomal compartment and recognise pathogenic and self nucleic acids (Table 1-2). TLRs are expressed by immune cells including macrophages, dendritic cells and mast cells, but they are also found in the epithelial lining of organs providing the first line of defense against pathogens and lesion. TLRs can be also expressed by fibroblasts, keratinocytes and endothelial cells. TLRs play an essential role in triggering the innate immune response against pathogenic infection and tissue damage. TLR activation also promotes the release of antimicrobial peptides [39], reactive oxygen species [40] and induces cell phagocytosis [41] to enhance microbial killing. Knock out mice have been generated for all TLRs, and have shown that they play an important role against infection *in vivo*. For example, deletion of TLR4, TLR1/TLR2 or TLR2/TLR6 resulted in reduced cytokine synthesis and impaired immune response against pathogenic stimuli such as lipopolysaccharide (LPS) and lipoproteins respectively [42-44]. Additionally, TLRs contribute to tissue homeostasis

being involved in regeneration and tissue repair, providing anti-apoptotic signals and regulating cell proliferation [45-47].

Table 1-2. Human TLRs with their exogenous and endogenous activators. HSP: heat shock protein. HMGB1: high mobility group box 1. LPS: lipopolysacharide. LDL: low density lipoprotein. GPI: glycosylphosphatidylinositol. EDA: extra domain A. FBG: fibrinogen-like globe. *Adapted from* [48], [49] and [50].

Receptor	PAMPs	DAMPs
TLR1	Triacyl lipopeptides	β-defensin-3
TLR2	Virus envelop protein, GPI-linked proteins, lipoproteins, lipoteichoic acid, peptidoglycans, zymosan	HSP, HMGB1, β-defensin-3, eosinophil-derived neurotoxin, antiphospholipid antibodies, serum amyloid A, biglycan, versican, hyaluronic acid fragments, fibronectin EDA domain, oxidised LDL, uric acid
TLR3	Pathogenic dsRNA	Self-mRNA
TLR4	LPS, mannan, glycoinositolphospholipids	HMGB1, fibronectin EDA domain, fibrinogen, tenascin-C FBG domain, surfactant protein A, D, β-defensin-2, HSP, S100 proteins, neutrophil elastase, antiphospholipid antibodies, lactoferrin, serum amyloid A, oxidised LDL, saturated fatty acids, biglycan, uric acid, hyaluronic acid fragments, fetuin A
TLR5	Flagellin	
TLR6	Diacyl lipopeptides, lipoteichoic acid, zymosan	Versican
TLR7	Pathogenic single-stranded RNA	Self-single-stranded RNA, antiphospholipid antibodies
TLR8	Pathogenic single-stranded RNA	Self-single-stranded RNA, antiphospholipid antibodies
TLR9	CpG containing DNA	HMGB1, osteopontin, IgG-chromatin complexes, mitochondrial DNA
TLR10	Unknown	Unknown

However, increased TLR expression and/or persistent activation has been linked to autoimmune diseases, cancer and other pathologies [3, 51] (Table 1-3).

Table 1-3. Examples of TLRs driven pathologies and ligands involved in the activation of TLRs in disease. RA: rheumatoid arthritis, OA: osteoarthritis, SLE: systemic lupus erythematosus.

TLR	Disease	TLR	Disease
TLR2	Irritable bowel syndrome [52]	**TLR7**	RA [60, 61]
	RA [53]		SLE [62]
	OA [54]		Multiple myelomas [57]
	Atherosclerosis [55]		Pancreatic cancer [63]
	Diabetic nephropathy [56]		
	Multiple myelomas [57]		
	Colorectal cancer [58]		
	Type-2 diabetes [59]		
TLR3	RA [64, 65]	**TLR8**	RA [69]
	Type-2 diabetes [66]		SLE [62]
	Allergic contact dermatitis [67]		Pancreatic cancer [63]
	Nasopharyngeal carcinoma [68]		
TLR4	Sepsis [70]	**TLR9**	SLE [82]
	RA [71]		Chronic obstructive pulmonary disease [83]
	OA [54]		Colorectal cancer [84]
	Non-alcoholic steatohepatitis [72]		Prostate cancer [85, 86]
	Alcoholic liver disease [73]		
	Atherosclerosis [74, 75]		
	Type-2 diabetes [59]		
	Allergy [76, 77]		
	Ischemia/reperfusion injury [78]		
	Multiple myelomas [57]		
	Colorectal cancer [79, 80]		
	Prostate cancer [81]		

PAMPs have been associated with the development of infectious diseases, but other chronic inflammatory diseases have no pathogen related aetiology. In this context, DAMPS are thought to play a role. Several TLR endogenous ligands have been associated with chronic conditions. Endogenous ligands of TLR4 and TLR2 including HMGB1 [87, 88], tenascin-C [89] and hyaluronan fragments [87, 90, 91] can sustain inflammation in autoimmune diseases such as rheumatoid arthritis (RA). In addition, RNA released from necrotic cells can activate TLR3 in synovial fibroblast and also contributes to inflammation in RA [92]. Self RNA and DNA have been associated with the development of systemic lupus erythematosus (SLE) via the activation of endosomal TLR7-9 [93]. Biglycan can exacerbate chronic inflammation in ischemia/reperfusion injury by triggering TLR-2 and TLR-4-signalling [94], while fibronectin extra domain A (EDA) [95, 96] and saturated fatty acids [97] promote atherosclerosis via activation of TLR4-mediated inflammatory response. Together these data show that TLRs are key players contributing to the inflammatory response in diverse pathologies. Moreover, the induction or release of endogenous ligands as a result of tissue damage triggers TLR signalling and perpetuates inflammation in these conditions.

1.3.1. Overall structure and mode of activation of toll-like receptors

The TLR family members have a conserved structure, which is composed of an N-terminal ectodomain formed by 20-25 leucine rich repeats (LRRs), a transmembrane domain and a cytoplasmic Toll/IL1R homology (TIR) domain (Figure 1-1). TLR7, 8 and 9 are the largest members of the family containing 25 LRRs. Each LRR module is 20–30 amino acids long and contains one LxxLxLxxN sequence motif. The central LxL part of the module creates a β sheet that forms a concave surface. The leucines in this

region pointing towards the interior of the protein generate a hydrophobic core. The other 9 residues in this sequence are exposed to solvent, making them available to mediate interactions with ligands. The structure of the TLR proteins resembles a horseshoe in which the central β strands are stacked together making up the entire concave surface of the horseshoe. Different amino acids outside the conserved LxxLxLxxN motif of each LRR module generate the convex part of the structure, which is composed of a mixture of α-helices and random loops. The LRR modules have cysteine-rich structures at the N-terminus and C-terminus named LRRNT and LRRCT [98, 99] (Figure 1-1). The extracellular domain of the TLRs is connected via a transmembrane helix to the intracellular TIR domain, which comprises a central β sheet surrounded by α helices [100-102].

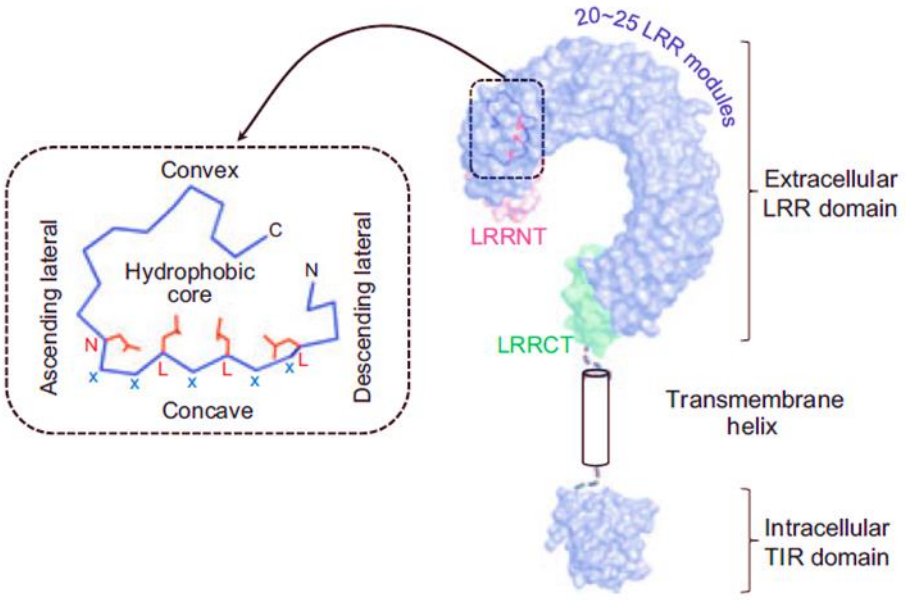

Figure 1-1. Structure of toll-like receptors. Overall structure of a TLR monomer showing the extracellular and intracellular domains. Amplification of one leucine-rich repeats (LRR) module where the side chains of the conserved leucines and asparagine are shown. The LRR N-terminal (LRRNT) and LRR C-terminal (LRRCT) modules are coloured pink and green, respectively. Adapted from [103].

TLRs recognise a variety of different ligands including lipopolysaccharides, lipopeptides, nucleic acids, peptidoglycans, proteins and fatty acids. The crystal structures of cell surface TLRs (Figure 1-2) and endosomal TLRs (Figure 1-3) have been published in complex with pathogenic ligands and the crystal structure of TLR4 will be discussed in detail later in the introduction. These studies have highlighted both differences and similarities in the mode of ligand recognition by the TLRs.

TLR1, TLR2, TLR6 and TLR4 showed a similar sub-domain organization which is not present in the other members of the family. The extracellular domain of TLR1, TLR2, TLR6 and TLR4 are divided into three regions: N-terminal, central and C-terminal sub-domains. The N-terminal sub-domain comprises the typical 24 residues LRR modules, which include conserved asparagines that form a continuous hydrogen-bonding ladder and the phenylalanines which form a hydrophobic spine. The asparagine and phenylalanine ladders are not present in the central sub-domain, and both the central and C-terminal region contain LRR modules of variable length ranging from 20-30 amino acids [104-106]. This domain organization is not present in other members of the TLR family. TLR7, 8 and 9 also exhibit a common structural feature not found in other TLRs; they contain a ~40 amino acids insertion between LRR14- LRR15. This region was named Z-loop and comprises an α helix and random loops that are exposed in the concave surface of these TLRs. Biochemical and structural studies have shown that proteolytic processing of the Z-loop is essential for TLR9 dimerization and DNA sensing [107, 108].

Crystal structures revealed that all TLRs exist in complex with their ligands as dimers, creating an “M” shape structure. However, some TLRs form homodimers, whilst others form heterodimers. TLR2 forms heterodimers with TLR1 or TLR6 to recognise triacyl or diacyl-lipopeptides respectively, while the other members of the

family form homodimers. Using Förster resonance energy transfer (FRET) to measure the distance among two molecules, it was found that TLR2 was associated with TLR1 and TLR6 before cell stimulation, existing as pre-formed dimer, but the number of heterodimers increased after cell stimulation [109]. This technique was also used to demonstrate that TLR9 is also found as an homodimer prior to cell stimulation, and conformational changes after ligand binding bring the C-terminal regions closer together to induce receptor activation [110]. This has also been demonstrated by the crystal structure of TLR8 and its synthetic agonistic ligand resiquimod (R848). Gel filtration showed that un-ligated TLR8 is found as a dimer in solution, and the crystal structure revealed that the distance between the C-terminal regions of ligand-free TLR8 homodimer is 53Å. When R848 binds to TLR8, it brings the C-terminus of the two receptors into close proximity shortening this distance to 30 Å [111]. However, in solution, purified TLR1, TLR2, TLR6 and TLR3 have been found mainly as a monomer, and when the agonistic ligand is added, it enhances dimer formation [104, 105, 112]. In summary, strong evidence suggest that endosomal TLRs exist as pre-formed dimers (with the exception of TLR3) and ligand binding induces conformational changes that activate the receptor. In contrast, cell membrane TLRs exists mainly as monomers, but ligand recognition leads to dimerization and stabilisation of the dimeric complex.

Ligand recognition doesn't induce major structural changes in the TLR overall horseshoe-like structure, and only minor adaptations of flexible loops or amino acid side chains are observed. TLR4 is the only family member that has been crystallised with a co-receptor, myeloid differentiation factor 2 (MD-2), which is essential for binding to its ligand LPS. The TLR4-MD-2 heterodimer can bind two molecules of LPS, and ligand binding with 2:2 stoichiometry has also been observed for TLR5,

TLR8 and TLR9 homodimers. In contrast, TLR1-TLR2, TLR2-TLR6 and TLR3 dimers interact only with one ligand molecule per dimer. As well as differences in ligand-receptor binding ratios, the location of the ligand binding sites and the types of residues and bonds formed also differs between TLRs. TLR1-TLR2 and TLR2-TLR6 recognised triacyl or diacyl-lipopeptides mainly via hydrophobic interactions, involving the central LRRs (LRR9 to LRR12) of TLR2 [104] [105]. TLR3 has two RNA binding sites, one at the N-terminus and other at the C-terminus, where ligand binding is driven by hydrogen bonding and electrostatic interactions [113]. TLR5 complex with flagellin is dominated by hydrophilic interactions, where this pathogenic molecule binds to a large area from the N-terminal region all the way up to the LRR9 module of TLR5 [114]. TLR8 synthetic agonist R848 binds to a hydrophobic pocket at LRR11 in TLR8 [111] and the same binding site has been reported for the degradation product of single-stranded RNA uridine [115]. CpG DNA binds via hydrophobic and hydrophilic interactions to the N-terminal region of the first TLR9 and to loop regions in the C-terminal part of the second TLR9 [108].

In all TLRs, the interaction of the ligand with two TLR monomers simultaneously induces the convergence of the C-terminus of the ectodomains to a distance of 20-40 Å. These data has supported the hypothesis that the dimerization of the TLRs induces the juxtaposition of the intracellular domains of the receptors, leading to their oligomerization and recruitment of adapter molecules for the initiation of signalling cascades [104, 105, 113, 114, 116]. In summary, the ectodomains of TLR are formed by LRRs and can recognise a variety of ligands of diverse structure. TLRs form dimers when they are in complex with their ligands, and dimerization of the receptor induces the activation of downstream signalling pathways.

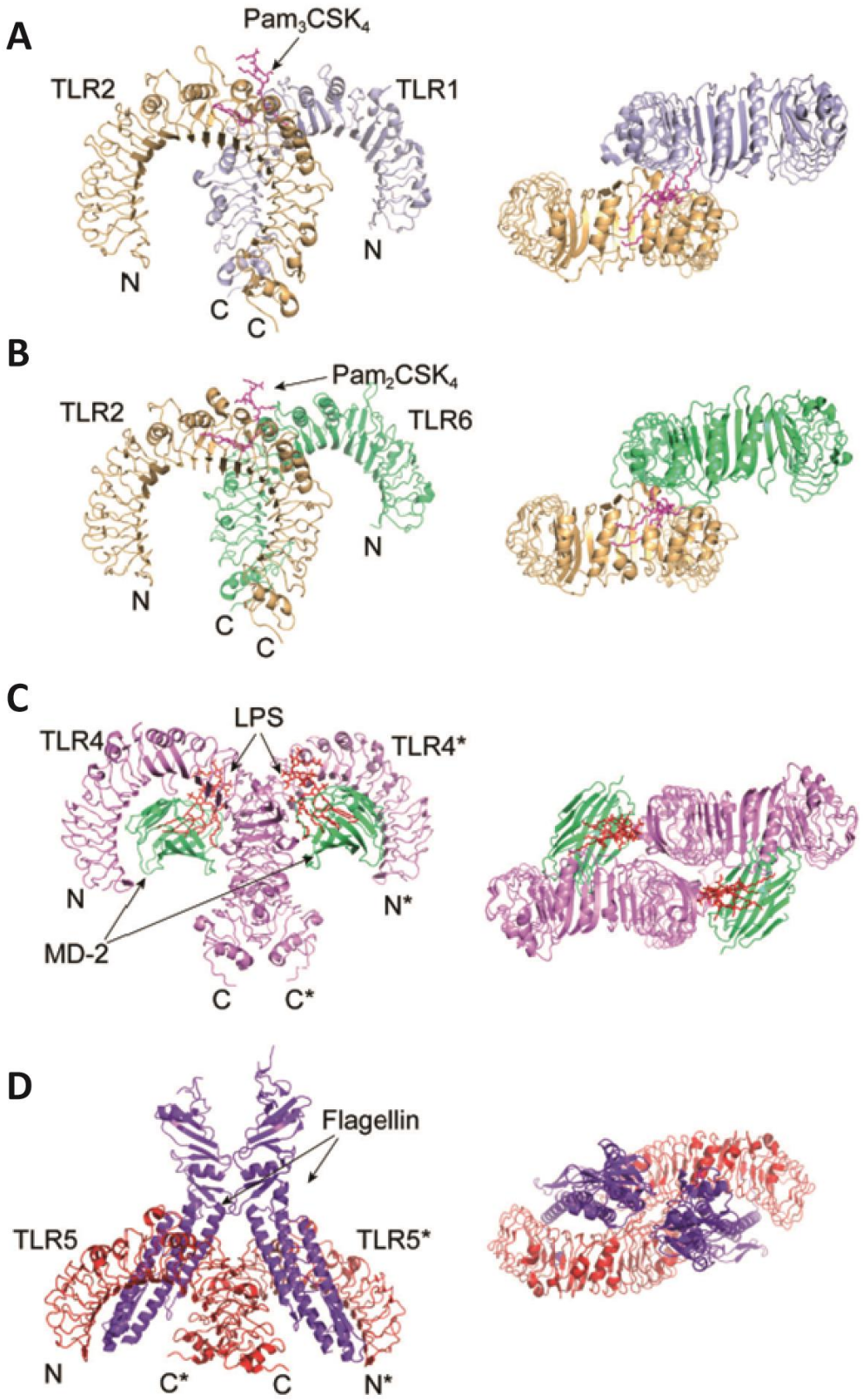

Figure 1-2. Crystal structure of cell surface TLRs. A. 3D structure of TLR1/TLR2 in complex with Pam_3CSK_4. **B.** 3D structure of TLR2/TLR6 in complex with Pam_2CSK_4. **C.** Crystal structure of TLR4 in complex with MD-2 and LPS **D.** 3D structure of TLR5 homodimer in complex with flagellin. C and N denote the C-terminal and N-terminal region. * indicates the second TLR of the dimer. Adapted from [99].

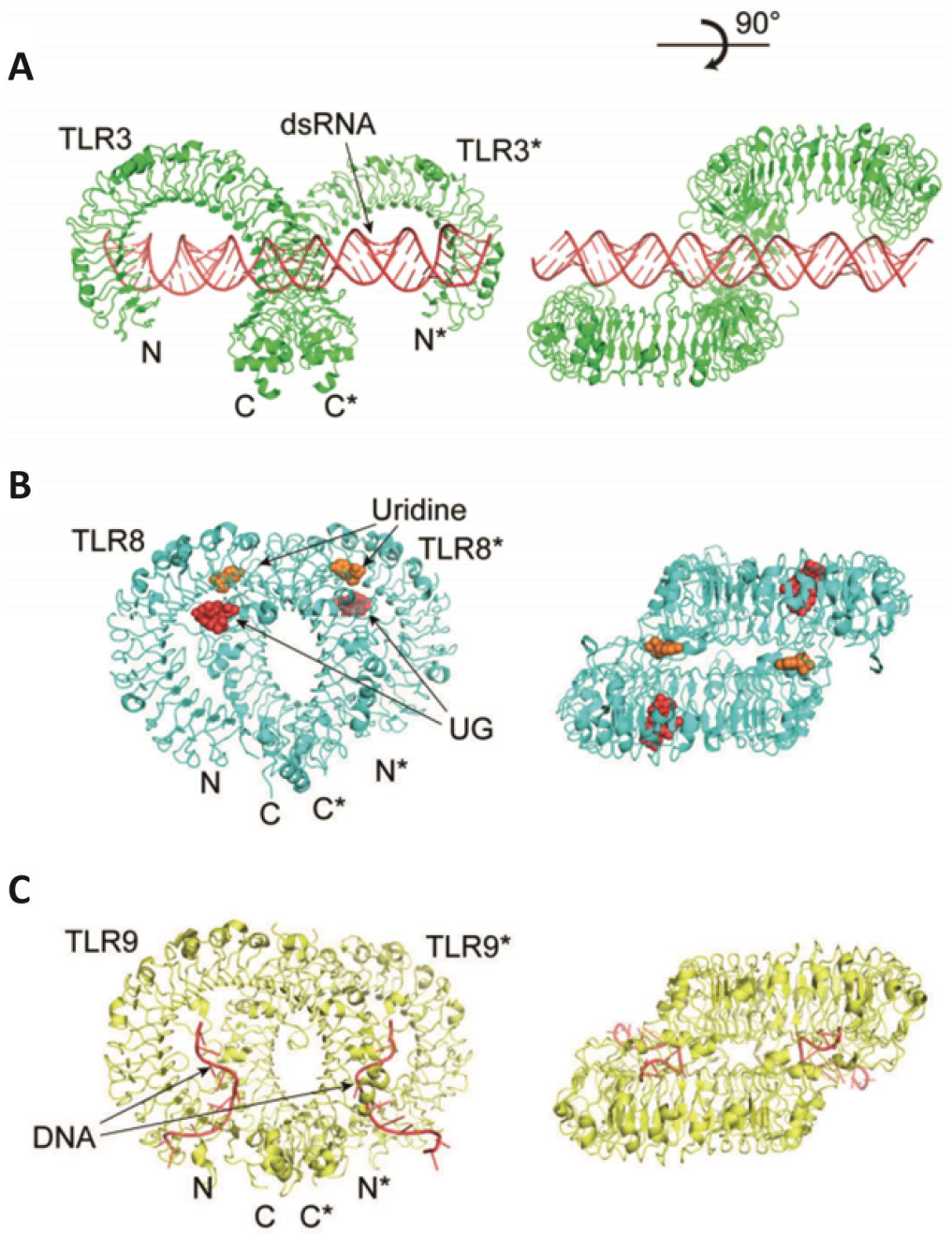

Figure 1-3. Crystal structure of endosomal TLRs. A. 3D structure of TLR3 in complex with double stranded RNA (dsRNA). **B.** 3D structure of TLR8 in complex with uridine or RNA degradation product UG. **C.** 3D structure of TLR9 in complex with DNA. C and N denote the C-terminal and N-terminal region. * indicates the second TLR of the homodimer. Adapted from [99].

1.4. TLR4

TLR4 was the first pattern recognition receptor to be discovered [38]. Lipopolysaccharide (LPS), a component of the outer membrane of Gram-negative bacteria, was the first described activator of TLR4 and has been extensively studied [42, 117]. LPS is a glycolipid composed of a hydrophobic lipid A region followed by a core oligosaccharide and a variable O-antigen (Figure 1-4 A). The lipid A has two glucosamine sugars, where phosphate groups are attached giving the molecule a negative charge. Large variability has been observed in this region, four to seven lipid chains can be connected to the glucosamine sugars in lipid A, and the phosphate groups can be deleted or modified [118]. Lipid A has been identified as the region responsible of the pro-inflammatory activity of LPS [119, 120]. The carbohydrate chain of LPS is divided into two areas: the inner and the outer core. The inner core has conserved oligosaccharide chains containing multiple copies of the sugars 3-deoxy-D-manno-oct-2-ulosonic acid (Kdo) and L-glycero-D-mannoheptose (Hep). The outer core region contains the O-specific chain which is formed by multiple copies of galactoses, galactosamines, and other sugars. This structure is different among bacterial species and can change depending on culture conditions *in vitro* [120].

TLR4 requires carriers and co-receptors to recognise LPS (Figure 1-4 B). LPS is first sensed and recruited by the LPS-binding protein (LBP) in the bloodstream, and *in vivo* studies have shown that this protein is essential for a rapid induction of inflammation after injection of LPS or Gram-negative bacteria to mice [121]. LBP forms a complex with LPS and transfer monomeric units of LPS to CD14, a co-receptor of TLR4 expressed in immune cells [122]. CD14 belongs to the LRR family and is able to bind LPS at picomolar concentration. CD14 interacts with LPS via a hydrophobic

pocket located between the LRRNT and first LRR module of the protein [123]. CD14 then presents and transfers monomer units of LPS to MD-2 [124], which can exist in a soluble form or in a preformed complex with TLR4. MD-2 is part of the superfamily of lipid binding proteins, and is essential for the binding of LPS to TLR4 [125]. The TLR4-MD-2 complex has been shown to bind with higher affinity (3 nM) to LPS than soluble MD-2 (65 nM) [126]. LPS recognition by TLR4-MD-2 assembly leads to TLR4 dimerization and activation of the receptor [127]. Different studies have shown that LPS is essential for TLR4 dimerization in solution, by analysing heterodimer formation using gel filtration and native PAGE gels, and these finding were corroborated by the crystallography data [106, 116, 128].

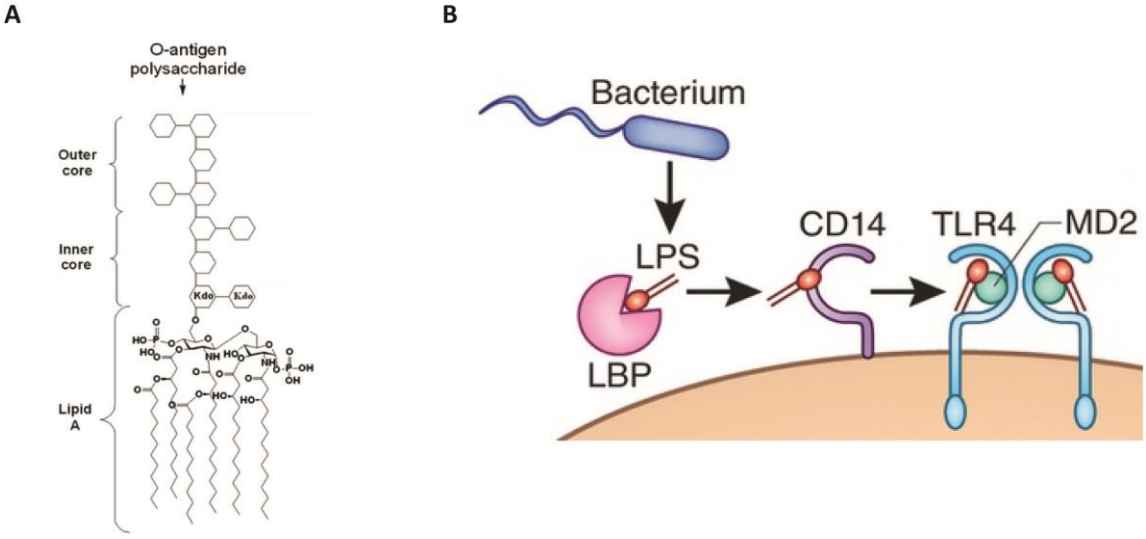

Figure 1-4. Structure of LPS and detection by TLR4. A. Chemical structure of LPS showing three modules: lipid A, a core oligosaccharide and a highly variable O-antigen. The core is covalently linked to lipid A and can be further divided into inner and outer core. Sugar 3-deoxy-D-manno-oct-2 ulosonic acid (Kdo) is linked to lipid A. Adapted from [129]. **B.** Schematic representation of LPS recognition. Soluble LPS-binding protein (LBP) extracts and disaggregates LPS from the outer membrane of bacteria that have infected the host. The cell-surface receptor CD14 then transfers LPS to a heterodimeric complex of MD-2 bound to TLR4, which triggers an intracellular response. Adapted from [130].

1.4.1. Crystal structure of TLR4 and PAMPs

The crystal structure of TLR4 in complex with MD-2 and LPS was published by Park *et al.* in 2009 [116]. MD-2 is an 18 kDa glycoprotein formed by two anti-parallel β sheets, which create a hydrophobic pocket that can accommodate lipid ligand such as LPS. MD-2 has two interaction interfaces with TLR4, a primary and a dimerization interface (Figure 1-5 B). The primary interface consists of ionic and hydrogen bonds, where an edge of MD-2 binds to the concave surface close to the N-terminus of the first TLR4 (TLR4-1). This interaction doesn't require LPS binding, and allows the formation of a stable heterodimer composed of one molecule of TLR4 and MD-2. The binding of LPS to MD-2 facilitates the dimerization of the TLRs ectodomains. The dimerization interface occurs between the opposite region of MD-2 and the convex surface of the second TLR4 (TLR4-2), at the C-terminal region between the LRR modules 15-17 (Figure 1-5 A). In this region, hydrophobic interactions occur between TLR4-2, MD-2 and one lipid chain of LPS. In addition, hydrophilic interactions between TLR4-2 and MD-2 support this hydrophobic core. The two phosphate groups of LPS contribute to the stability of the dimerization interface interacting with a positive cluster of amino acids in TLR4-1 (R263, K341, K362), TLR4-2 (K388) and MD-2 (K58, K122). Protein-protein interactions, mainly via polar residues, among the two TLR4 molecules are also observed in this interface. The dimerization of the receptor brings into close proximity the C-terminal region of the ectodomains, which is predicted to initiate the signalling cascade.

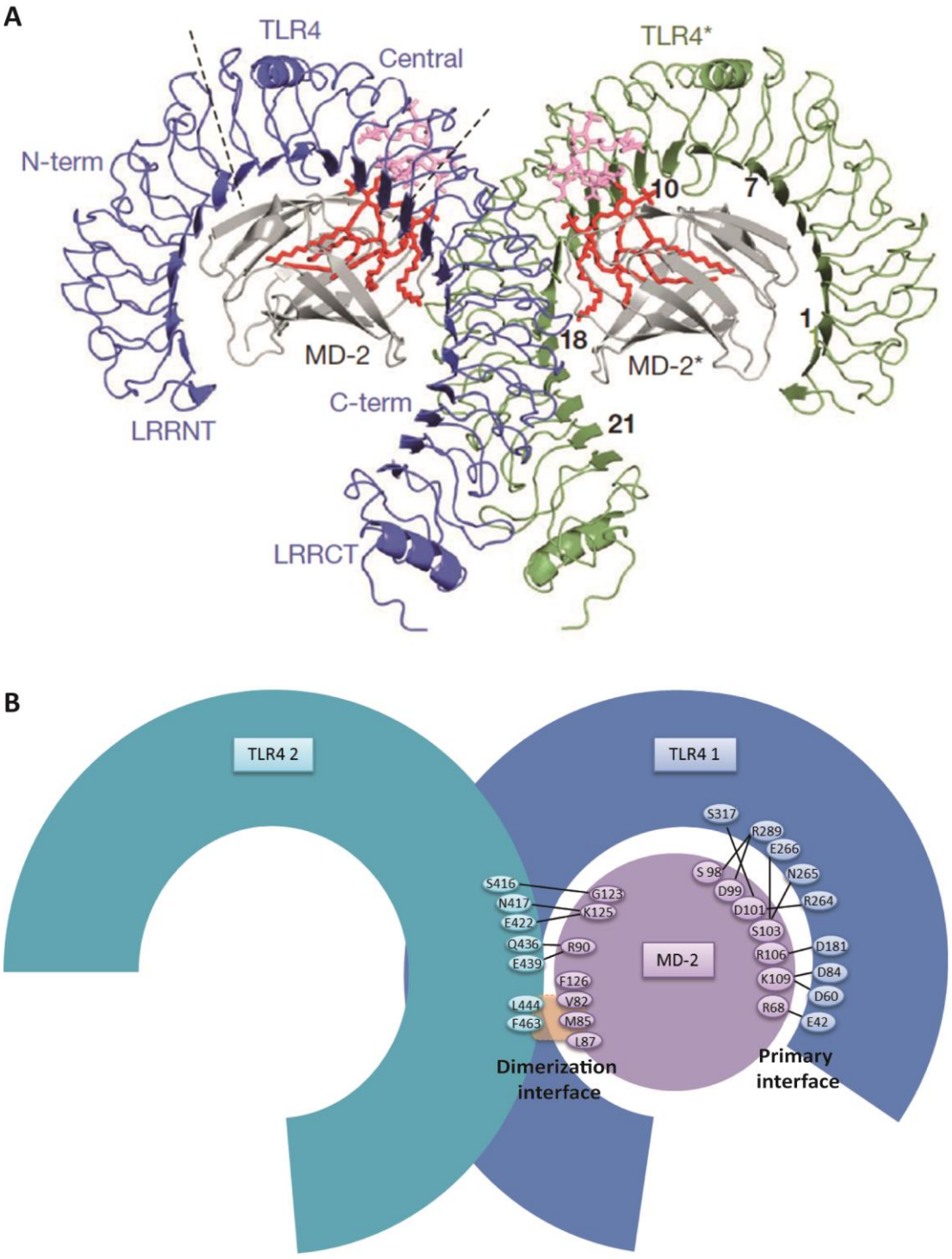

Figure 1-5. Crystal structure of TLR4-MD-2 heterodimer in complex with LPS. A. 3D structure of TLR4-MD-2-LPS complex. The lipid A component of LPS is coloured in red, and the inner core carbohydrates of LPS are coloured in pink. The module numbers of the LRRs in TLR4 are written in black. TLR4 is divided into N-, central and C-terminal domains. The LRRNT and LRRCT modules cover the amino and carboxy termini of the LRR modules. * denotes the second TLR4 or MD2. Adapted from [116]. **B.** Schematic representation of TLR4 in complex with MD-2 showing key amino acids involved in the interaction of these proteins.

The numbers of lipid chains of LPS has an impact on TLR4 activation. The crystal structure of hexa-acyl immunogenic LPS with TLR4-MD-2 showed that 5 acyl chains are accommodated in the hydrophobic pocket of MD-2, creating a conformational change in this protein and the position of the hydrophobic amino acid F126. This amino acid locates in the core of the dimerization interface, and together with surrounding hydrophobic residues of MD-2, interacts with the free exposed acyl chain of LPS and TLR4-2 [116]. Mutations in F126 inhibit the ability of LPS to induce TLR4 dimerization [131, 132]. Less than six lipid chains have an effect on TLR4 activation and dimerization as observed in the crystal structures of the TLR4 antagonist eritoran with TLR4-MD2 and lipid IVa with MD-2 [106, 133]. Eritoran and lipid IVa have only 4 acyl-chains, which are buried inside of the hydrophobic pocket of MD-2. This structure lacks the exposure of a free lipid chain that is part of the dimerization interface. In addition, the phosphate groups are positioned downwards compared to hexa-acyl LPS and cannot interact with the positively charged residues in TLR4 stabilizing the dimerization of the receptor [78]. The phosphate groups of LPS are also essential for its immunogenic activity and deletions of these groups result in a reduction of the endotoxin activity by ~100 fold [134, 135].

Two single-nucleotide polymorphisms of human TLR4, D299G and T399I have been associated with LPS hyporesponsiveness [136]. The structure of polymorphic TLR4 with MD-2 and LPS has been determined by Ohto *et al.* [128]. They found that the SNPs were localized far from the binding site of MD-2 and LPS to the receptor, and the overall structure of polymorphic TLR4-MD-2-LPS complex was very similar to the wildtype determined structure. Differences were observed in loop structures in the region around D299G (LRR10-13) compared to wildtype TLR4. In contrast, T399I SNP site was almost structurally identical in polymorphic and wildtype TLR4. These

few differences in the SNPs regions didn't affect TLR4 dimerization as shown by native PAGE analysis. For that reason, the authors suggested that these TLR4 SNPs could be affecting other functional processes such as binding affinity, protein folding efficiency and stability, and cell surface expression. Other studies have found that D299G and T399I SNPs reduced cell surface accumulation of functional TLR4 in HEK293 cells [137], while D299G mutation decreased expression of TLR4 in human airway epithelial cells [136]. In addition, D299G SNP has been shown to modify TLR4 signalling by interfering with the recruitment of adaptor molecules to the intracellular domain [138].

Publication of TLR crystal structures has shed light on the molecular mechanisms by which PRRs sense inflammatory stimuli. These studies have also contributed to the development of inhibitors to limit excessive inflammation driven by these receptors in different diseases. Detailed information of TLR antagonists under development and their stage in clinical trials are reviewed in [139-141], but perhaps the best example of where detailed knowledge of the mode of action of a TLR has accelerated drug design is TLR4. The TLR4 antagonist eritoran has been used for the treatment of patients with severe sepsis [142]. The crystal structure of eritoran in complex with TLR4 and MD-2 has highlighted the difference in receptor activation by this molecule compared to LPS. Eritoran is a synthetic form of lipid A, which is composed by only 4 acyl-chains and cannot induce TLR4 dimerization. The crystal structure shows that eritoran binds to only one TLR4-MD-2 heterodimer, as it lacks the exposure of a free lipid chain and the phosphate groups essentials for binding to the second TLR4 and induce receptor dimerization [106]. Another examples is the TLR4 antibody (NI0101) developed by NovImmune, which has recently completed phase I in clinical trials and will be used for the treatment of chronic inflammatory conditions including RA [141]

[http://www.novimmune.com/pipeline/ni-0101.html]. Mutagenesis and structural analysis revealed that this antibody binds to a cluster of positively charged amino acids close to the dimerization interface of TLR4 preventing dimer formation and receptor activation [143]. In this way, a better understanding of TLR activation has had real impact on drug design for a number of inflammatory diseases. The structure of TLR4 has been published in complex with pathogenic stimuli. However, no crystal structure has been published of TLR4 with other activators (DAMPs and allergens), and this information could be useful for the development of new TLRs inhibitors that could reduce endogenous activation of TLR4 in chronic inflammatory diseases.

1.4.2. Mode of activation of TLR4 by metals and allergens

In recent years, TLR4 has emerged as a receptor involved in allergen recognition. TLR4 is involved in the development of allergies to metals such as Ni^{2+}, which can directly bind and activate this receptor inducing an immune response. Mutagenesis studies revealed that Ni^{2+} induces TLR4 dimerization and activation by binding to histidines (H431, H456 and H458) located in the dimerization interface and cross-linking the two TLR4 ectodomains (Figure 1-6 A). Ni^{2+} can activate human TLR4 but not mouse TLR4, as these histidines residues are only found in the human protein [77]. Similar results were found with the metal Co^{2+}, which can also induce TLR4 dimerization and activation [144]. Interestingly, both Ni^{2+} and Co^{2+} require MD-2 to induce an inflammatory response via TLR4; however, they can induce receptor homodimerization in the absence of MD-2 *in vitro*. The authors suggested that MD-2 might be involved in further shaping the metal-TLR4 receptor complex to induce effective signalling, but additional structural studies are necessary to answer this question [144].

The house dust mite allergen Der p 2 is a protein structurally similar to MD-2 comprising a β sheet sandwich with a hydrophobic core, which can bind to lipid ligands [145] (Figure 1-6 B). Trompette *et al.* [146] proposed that Der p 2 can recognise LPS and mimic MD-2 function, activating TLR4 and inducing an allergic response to low levels of endotoxin. The study showed that endotoxin contaminated Der p 2 preparations can activate HEK cells expressing TLR4 only, but also could augment cytokine production in cells expressing TLR4 and MD-2. In addition, Der p 2 was able to induce experimental allergic asthma in a TLR4-dependent manner. This results were confirmed by another study from Hammad *et al.*, where house dust mite allergen activated lung cells via TLR4, leading to the development of asthma and activation of mucosal dendritic cells [147]. Co-immunoprecipitation experiments have shown that Der p 2 can be pulled down in complex with TLR4. In addition, mutations in Y91 in Der p 2, an amino acid conserved in MD-2, halts the ability of Der p 2 to induce cytokine synthesis via this receptor [146].

Another allergen that signals through TLR4 is the cat allergen Fel d 1. Structurally, this protein is composed mainly of α helices and doesn't resemble MD-2, but it can also bind to lipid ligands [148]. Unlike Der p 2, this protein doesn't interact directly with TLR4 or MD-2, but it can enhance the signalling downstream of the receptor when it is bound to LPS [149]. Similar results were found with another animal allergen from dog, the protein Can f 6, suggesting that a lipid transfer mechanism might be involved in the induction of airway hypersensitivity reactions to these allergens [149]. Further structural studies will elucidate the mechanism of activation of TLR4 by these allergens, which is still poorly understood.

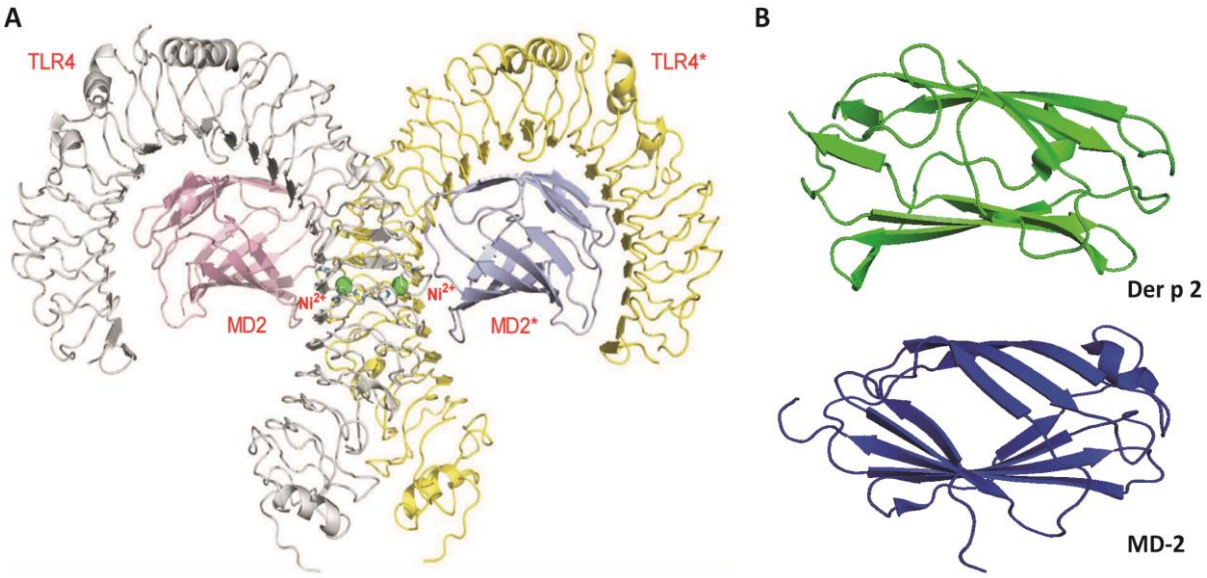

Figure 1-6. Allergens that activate TLR4. A. Model of Ni^{2+} in complex with TLR4 showing the position of the bound Ni^{2+}. Adapted from [77]. **B.** Crystal structure of Der p 2 and MD-2. Taken from protein data bank (PDB), accession numbers: Der p 2: 1KTJ and MD-2: 2E56.

Table 1-4 summarises the modes of TLR4 activation that have been described for bacteria, metal ions and other allergens. Pathogen recognition by TLR4 requires the co-receptor MD-2. Metal ions and the allergen Der p 2 can bind to TLR4 in the absence of MD-2 *in vitro*. However, they still can activate TLR4-MD-2 heterodimer and induce an inflammatory response.

Table 1-4. TLR4 mode of activation by pathogenic stimuli, allergens and metals.

Ligand	Type	Mode of activation of TLR4
LPS	Component of the bacterial outer membrane	Requires MD-2 to induce TLR4 dimerization
Nickel	Metal	Binds to histidines in the dimerization interface and induces activation of the receptor
Der p 2	House dust mite allergen	Lipid binding protein that mimics MD-2. *In vitro* can bind to TLR4 only but can also activate TLR4-MD-2 complex
Fel d 1 **Can f 6**	Animal allergens	Lipid binding proteins composed of α helices, which could transfer lipid ligands to TLR4-MD2 complex

1.4.3. Mode of activation of TLR4 by DAMPs

Different endogenous stimuli can also activate TLR4 such as fibronectin EDA domain, fibrinogen, S100 proteins, oxidised LDL and uric acid, among others. Direct interaction between DAMPs and TLR4 have been reported in biochemical studies including HMGB1 [150], surfactant protein D [151], biglycan [94] and decorin [152]. No crystal structures have been published of DAMPs in complex with TLR4, but studies have suggested a different mode of TLR4 activation by DAMPs compared to PAMPs or allergens. Endogenous stimuli require different co-receptors compared to pathological stimuli like LPS. Some DAMPs do require MD-2 and CD-14 to activate TLR4 including heat-shock protein 60 and 70 [153, 154], biglycan [155], S100 proteins [156, 157] and oxidised LDL [158]. However, other DAMPs require only CD14 to activate the receptor such as lactoferrin [159] and surfactant protein A, D [151, 160]; or only MD-2, such as fibronectin extra domain A [161]. Other DAMPs such as tenascin-C don't require CD14 or MD-2 to activate TLR4 [89]. Another group of DAMPs

require a different subset of co-receptors. Hyaluronan requires CD44 to form a complex with TLR4 [162] and biglycan can activate NLPR3 inflammasome in mouse macrophages via TLR2/4 and $P2X_4$/$P2X_7$ receptors [155].

Little is known about how DAMPs activate TLRs and to date HMGB1 is the best characterised endogenous TLR4 ligand. HMGB1 requires MD-2 to bind to TLR4 and site-directed mutagenesis revealed that cysteine 106 in HMGB1 is essential for binding to the TLR4-MD-2 complex [150]. In addition, the peptide tetramer FSSE comprising the residues 105-108 in HMGB1 can block the interaction of HMGB1 and MD-2. This peptide is predicted to accommodate inside the hydrophobic pocket of MD-2; however, it doesn't affect the binding capability of LPS to MD-2, suggesting a different mode of binding of HMGB1 to this region [150, 163]. The immune activity of HMGB1 also depends on the redox state of three cysteine residues at positions 23, 45 and 106. HMGB1 can interact with TLR4-MD-2 and induce cytokine production when having a disulphide bond at positions 23 and 45 and a free thiol at position 106 [164, 165]. The carbohydrate domain of surfactant protein D can also bind directly to TLR4. Mutations in this domain which reduce the ability of surfactant protein D to bind to phosphatidylinositol or LPS, did not affect the interaction to TLR4, suggesting a different mechanism of binding to this receptor compared to other ligands [151].

Mutations in TLR4 also have a different effect on PAMPs and DAMPs. The common polymorphism mutations D299G and T399I reduce the ability of TLR4 to respond to LPS, but increase the activation of TLR4 signalling by fibrinogen [166]. These data suggest a diverse mechanism of interaction between fibrinogen and TLR4 compared to LPS, which results in a different response and activation of the signalling pathways downstream of the receptor. The large variety of TLR4 endogenous ligands

and their structural diversity highlight the complexity of DAMPs-TLR4 interactions and the different requirements for receptor activation. Further studies are necessary to understand the molecular mechanism of TLR4 activation by endogenous stimuli.

1.4.4. Signalling pathways activated downstream of TLR4: differences in PAMPS and DAMPS

After ligand recognition, TLRs activate signalling pathways that induce inflammatory mediators such as cytokines, chemokines and tissue-degrading enzymes. The formation of TLR4 ectodomain complex leads to the dimerization of the TIR domain. TLR4 is the only TLR member able to activate both the myeloid differentiation factor 88 (MyD88) dependent pathway and the TIR domain containing adapter inducing interferon-β (TRIF) pathway. The MyD88 dependent pathway is activated at the plasma membrane and involves the recruitment of adaptor molecules including MyD88-adaptor like (Mal), the IL-1R-associated kinase (IRAK) 4 and 1, and TNF receptor-associated factor 6 (TRAF-6). This complex called "the Myddosome" [167] leads to the phosphorylation of signalling kinases and activation of transcription factors such as nuclear factor-κB (NF-κB) and activator protein 1 (AP1) to induce the synthesis of pro-inflammatory cytokines [168]. TLR4 activation of the TRIF pathway occurs later when the receptor is endocytosed and trafficked to the endosome, where the TIR domain of TLR4 forms a complex with other adaptor molecules such as TRIF and TRIF-related adaptor molecule (TRAM) [169]. The activation of this pathway results in the phosphorylation of interferon-regulatory factor (IRF) 3 and the production of interferons [170], in addition to the late-phase activation of NF-κB and mitogen-activated protein kinases (MAPK) [171, 172].

Pathogenic stimuli such as LPS activate both the MyD88 dependent pathway and the TRIF pathway. Endogenous TLR4 stimuli can signal through the MyD88 pathway including tenascin-C [89], biglycan [155] and heat shock protein (HSP) 60 [173] or induce the activation of MyD88 and TRIF pathways such as HMGB1 [174]. Formation of different receptor complexes of DAMPs and PAMPs with TLR4 suggests that each stimulus triggers a signature response that is translated to diverse cellular responses. Indeed, the cytokine profiles induced by LPS differ from the ones induced by DAMPs. For example, LPS induces TNF, IL-6 and IL-8 in primary human macrophages as well as IL-6 and IL-8 in synovial fibroblasts. However, tenascin-C induces TNF, IL-6, IL-8 in primary human macrophages, but only induces IL-6 in synovial fibroblasts [89]. S100A12 protein induces more strongly IL15RA, IL-7, and IL-18 in monocytes compared to LPS [157]. Hyaluronan induces a different set of genes in MH-S macrophages compared to LPS. Only hyaluronan promotes matrix metalloproteinase (MMP)-3, MMP-13, and suppressor of cytokine signalling 3 (Soc3) synthesis, while LPS induces chemokine receptor 6 and defensin β5 [162]. Similarly, intrathecal injections of the endogenous ligand HSP60 or LPS to the brain of mice generated a different effect after activation of TLR4. HSP60 produced neurodegeneration and demyelination but did not induce an exacerbated inflammatory response as observed with the injection of LPS, which did not cause neuronal injury [173]. The different outcomes from PAMPs and DAMPs suggest a different mode of receptor complex formation and activation of the signalling pathways downstream of TLR4. However, compared to PAMPs, the signalling pathways activated by DAMPs are still poorly understood. Therefore, TLRs inhibitors that have been developed against PAMPs may not prevent DAMPs activation of the receptors and further studies will be needed to establish the differences among endogenous and pathogenic-induced TLR4 signalling.

1.5. Tenascin-C as a DAMP

During tissue injury or infection, a subset of ECM proteins is specifically induced that contribute to tissue repair. One example is the ECM glycoprotein tenascin-C. This protein is highly expressed during embryogenesis in the nervous, skeletal and vascular system and in areas of organ morphogenesis. In adulthood, tenascin-C is down-regulated and expressed only in restricted areas [175]. However, tenascin-C expression is induced as a consequence of tissue damage or infection independently of the location of the insult [176].

1.5.1. Structure and physiological role of tenascin-C

The tenascin-C monomer comprises diverse structural domains. The N-terminal region contains a chaperone-like sequence that forms a coiled coil structure and interchanges disulphide bonds necessary for oligomerisation. Next are the epidermal growth factor (EGF)-like repeats, of which there are 14.5 in human tenascin-C, followed by 17 fibronectin type III-like repeats (FNIII). Finally in the C-terminal region is the fibrinogen-like globe (FBG) [177] (Figure 1-7 A). The FNIII domain contains a region that is alternatively spliced and the molecular weight of tenascin-C may vary from 180 to 330 KDa depending on the number of alternatively spliced domains [178]. The tenascin monomers assemble into a 6-armed hexabrachion structure (Figure 1-7 B) via the N-terminal region to form a large protein of approximately 1.5 million Daltons. The protein also undergoes post-translational modification including N- and O-glycosylation, and most of the glycosylation sites are predicted to be in the FNIII domain [178, 179].

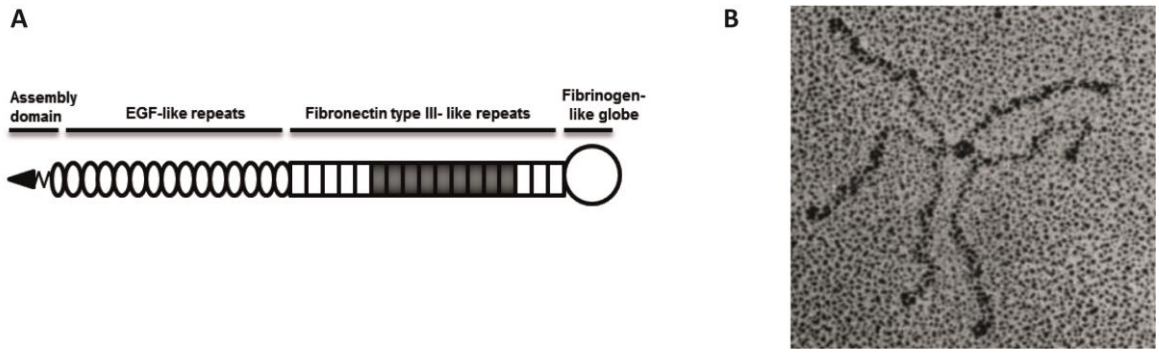

Figure 1-7. Tenascin-C structure. A. Each tenascin monomer comprises an N-terminal assembly domain, epidermal growth factor-like repeats, fibronectin type III-like repeats (constitutively expressed in white boxes and alternatively spliced in grey boxes) and a C-terminal fibrinogen-like globe (FBG). **B.** Electron micrographs from tenascin-C hexabrachion. Taken from [180].

Tenascin-C was first described as an ECM protein with anti-adhesive properties. Initial studies found that cells that were plated on a tenascin-C substratum showed a proliferative phenotype and did not adhere well [181, 182]. When cells were plated on a combination of tenascin-C and fibronectin, tenascin-C inhibited cell adhesion and spreading via blocking the interaction of syndecan-4 and fibronectin, reducing the activities of RhoA and focal adhesion kinase and compromising the formation of focal adhesion complexes [183, 184]. Tenascin-C can also interact with other extracellular matrix proteins, including versican, aggrecan, brevican and neurocan [185]. Lundell *et al.*, showed, using electron micrographs and structural models, that tenascin-C can cross-link aggrecan-hyaluronan complexes playing a role in the structural organisation of extracellular matrix networks [186]. Tenascin-C can also influence cells behaviour via interaction with different receptors modulating cell signalling, migration and proliferation. As a multidomain protein, tenascin-C is able to bind different cell receptors and proteins, which translates into diverse functions some of which are highlighted in Table 1-5.

Table 1-5. Examples of the diverse functions of tenascin-C domains.

Tenascin-C domain	Function
N-terminus assembly domain	Involved in hexamer formation [187]
EGF-like repeats	Interacts with EGF receptor and induces its phosphorylation promoting migration [188, 189]
	Promotes mesenchymal stem cell (MSC) survival by activating EGF receptor [188]
FNIII-like repeats	FNIII 3 interacts with β_1 and β_3 integrins to promote cell adhesion [190-192]
	FNIII A1A2 interacts with fibronectin and inhibits T-cell activation [193]
	FNIII A-D interacts with annexin II to promote loss of focal adhesion, mitogenesis and migration [194]
	FNIII D interacts with contactin and $\alpha_7\beta_1$ integrin to promote neurite outgrowth [195, 196]
	FNIII 1-2, A, B and 6-8 interacts with sodium channel to modulate their localization and activity at nodes of Ranvier [197]
FBG	Interacts with $\alpha_v\beta_3$ to promote cell adhesion [198]
	Interacts with phosphacan/protein-tyrosine phosphatase-ζ/β and modulates neural cells adhesion and neurite outgrowth [199]

In the adult, tenascin-C is expressed in regions of high cell turnover or sites which undergo constant remodelling such as stem cells niche and tendons, but also is upregulated as a result of tissue damage and infection. During physiological tissue repair after injury, tenascin-C expression is transient and down-regulated with the resolution of inflammation and tissue repair [200]. In normal wound healing, tenascin-C is expressed by keratinocytes [201] and fibroblasts during the phases of inflammation, re-epithelisation and granulation tissue formation [202]. Tenascin-C promotes adhesion and migration of keratinocytes [201] and fibroblasts [203] and each domain within this protein can interact with a wide variety of binding partners to mediate diverse effects on

cell behaviour during wound repair. For example, the FBG domain of tenascin-C can modulate endothelial cells adhesiveness and migration enhancing neovascularisation of the wound and endothelial sprouting via binding to $\alpha_v\beta_3$ integrin [198, 204, 205]. The EGF-L repeats of tenascin-C promote mesenchymal stem cell (MSC) survival in wound healing by activating EGF receptor and protecting from Fas ligand (FasL)-induced nuclear DNA damage [206]. Tenascin-C knock-out mice showed only minor defects in wound healing, exhibiting temporarily reduced fibronectin on the granulation tissue [207]. However, impaired tissue repair was observed in these mice after corneal incision injury [208] and articular cartilage damage [209], implying a possible role for tenascin-C in remodelling during repair. Tenascin-C levels return to normal after wound contraction and cannot be detected in scar tissue [210-212], suggesting a restricted and controlled pattern of expression during wound healing.

Different factors have been shown to drive the expression of tenascin-C such as cytokines (TNF, IL-4, IL-1), growth factors (FGF, TFGβ, PDGF), mechanical stress and reactive oxygen species [213]. In addition, tenascin-C expression can be up-regulated during acute infection by the activation of the NF-κB transcription factor downstream of TLRs. LPS, lipoteichoic acid (LTA), PAM3, and flagellin could induce the expression of tenascin-C in human monocyte-derived dendritic cells and protein levels peaked at 24 h [214]. *In vivo* data showed that intraarticular injections of zymosan, a TLR2 ligand, resulted in up-regulation of tenascin-C in the mice joints after 24 h, and the expression of the protein increased overtime up to 4 days after injection [89]. In this study, tenascin-C knock out mice showed faster resolution of inflammation after zymosan injection than wild-type mice, suggesting that tenascin-C could be involved in the maintenance of acute inflammation. Indeed, our group found that tenascin-C was essential for the pro-inflammatory response to LPS *in vivo*, as tenascin-

C null mice presented impaired cytokine production. Tenascin-C modulates the translation of TNF via controlling the expression of the microRNA miR-155, which is a post-transcriptional regulator of TNF production following LPS stimulation [215].

1.5.2. Tenascin-C in chronic inflammation

Tenascin-C expression is tightly regulated during acute infection or injury. However, persistent expression of this protein has been linked to chronic inflammatory conditions. For example, low levels of tenascin-C are found in joints of healthy individuals. In contrast, high levels of tenascin-C have been detected in the synovium, synovial fluid and cartilage of patients with rheumatoid arthritis [216-218]. Up-regulation of tenascin-C has also been associated with fibrotic diseases [219, 220], keloids [221], atherosclerosis [222], asthma [223], multiple sclerosis [224], colitis [225], diabetes [226] and cancer [227]. Serum levels of tenascin-C correlate with disease severity in different inflammatory conditions including inflammatory bowel disease [228], rheumatoid arthritis [229], chronic kidney disease [230], myocardial infarction [231] and pneumonia [232].

Studies using tenascin-C null mice have highlighted the role of tenascin-C in the maintenance of inflammation. In a model of antigen-induced arthritis, our group found that tenascin-C knock out mice are protected from joint destruction, showing less cell infiltration, pannus formation and bone erosion compared to wild type mice [89]. Tenascin-C deficiency also impaired the polarization of Th17 cells and the induction of IL-17 in a mouse model of arthritis, suggesting that this protein has a role driving adaptive immune responses [233, 234]. In a model of OVA-induced allergic asthma, tenascin-C null mice develop less severe bronchial asthma compared to wild type mice,

presenting less numbers of eosinophils and decreased Th2 cell activation and cytokines such as IL-5 and IL-3 in plasma and bronchoalveolar lavage fluids. Furthermore, tenascin-C could increase the secretion if IL-5 and IL-13 by splenic lymphocytes *in vitro*, suggesting that it might be involved in the activation of Th2 cell in this disease [235]. Another example was reported in a mouse model of hepatic ischemia and reperfusion injury, where tenascin-C knock out mice had a reduction in liver damage, lower leukocyte recruitment and decreased expression of cytokines compared to wild-type mice [236]. Tenascin-C null mice showed less amyloid beta (Aβ) plaque formation and reduced neuroinflammation when crossed with the amyloid precursor protein mouse model of Alzheimer, indicating that tenascin-C contributes to the inflammatory pathology of this disease [237].

In the last years different studies have looked at the mechanism involved in tenascin-C induced inflammation. As a multidomain protein, tenascin-C can interact with different cell surface receptors inducing cytokine synthesis and contributing to pro-inflammatory responses. Integrins have been identified as one of these receptors. Tenascin-C promoted the migration of macrophages in a mouse model of cardiac fibrosis and induced the expression of IL-6 by these cells. This was mediated by the engagement of $\alpha_V\beta_3$ integrin in macrophages that resulted in the activation of the NF-κB signalling pathway and the production of pro-inflammatory cytokines [238]. However, the domain mediating these effects is still not known. In addition, the FNIII 3 repeat of tenascin-C can induce cytokine synthesis in murine myeloid cells and human synovial fibroblasts from arthritic joints via activation of α9 integrin [239, 240]. Tenascin-C can also induce inflammation via activation of PRRs. Tenascin-C induces the expression of TNF, IL-6 and IL-8 in primary human macrophages and IL-6 in synovial fibroblasts, as well as TNF, IL-6 and IL-8 in mixed populations of cells from

synovial membranes of individuals with RA [89]. Our group identified the FBG domain as the region of tenascin-C that induces cytokine synthesis in primary human cells, and found that this is mediated *in vitro* and *in vivo* by activation of TLR4 [89]. Tenascin-C activation of TLR4 also induces the expression of IL-6 and IL-8 in human chondrocytes [241] and MMP-9 in mouse isolated neutrophils [236]. Tenascin-C contributes to atherosclerosis in a TLR4-dependent manner by promoting foam cell formation and up-regulating the expression of CD36, which is involved in the uptake of oxLDL [242]. In addition, it can induce constriction of cerebral arteries in rats via activation of TLR4 and downstream signalling pathways [243]. Finally, tenascin-C contributes to the development of autoimmune myocarditis via activation of TLR4 in murine dendritic cells, which leads to Th17 differentiation and enhance the pro-inflammatory response in this model [244]. These data from our group and from other labs indicate that tenascin-C is a pro-inflammatory molecule, acting through TLR4 and being involved in the maintenance of the inflammatory response. However, very little is known about the mechanism of activation of TLR4 by tenascin-C. My thesis seeks to answer this question and one approach I will take relies upon a comparative analysis of tenascin-C with other tenascin family members.

1.6. The tenascin family

The tenascins are a family of four extracellular matrix glycoproteins comprising tenascin-C, -R, -W and -X. Each family member has a distinct pattern of expression and function. However, all the tenascin members have a conserved domain organisation comprising an N-terminal assembly domain, followed by the EGF-like repeats, the FNIII-like repeats, and the C-terminal FBG domain (Figure 1-8) [245]. Tenascin-C was

the first family member to be discovered and is the only tenascin that has been associated with chronic inflammatory conditions and shown to mediate TLR4 activation via its FBG domain. It is not known if the FBG domains of the other tenascin family members are able to activate TLR4 like tenascin-C.

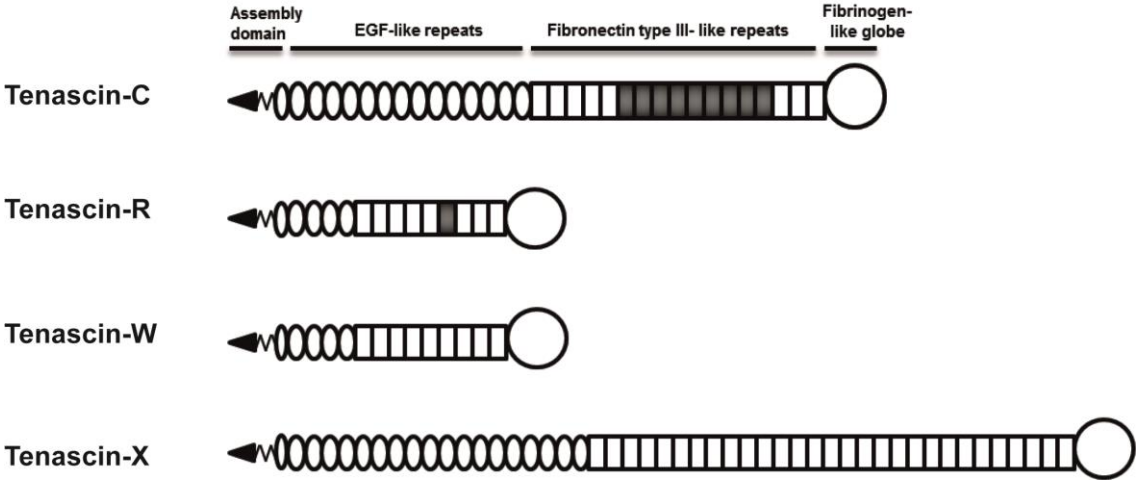

Figure 1-8. Domain organisation of the tenascin family. Each tenascin monomer comprises an N-terminal assembly domain, followed by epidermal growth factor (EGF)-like repeats, fibronectin type III-like repeats (FNIII) (constitutively expressed in white boxes and alternatively spliced in grey boxes) and a C-terminal fibrinogen-like globe (FBG).

1.6.1. Tenascin-R

Tenascin-R was the second family member to be discovered and has a restricted pattern of expression in embryogenesis and adult, being present only in the central nervous system (CNS). During development tenascin-R is found within the pathways of oligodendrocytes precursor migration, during the phases of active myelination and plays a role in the organization of axonal tracts. In adult, tenascin-R is located in the nodes of Ranvier, myelinated axon and the perineuronal nets of interneurons and motorneurons [246-249]. Tenascin-R is expressed as two major isoforms of 160 kDa and 180 kDa generated by alternative splicing of the FNIII-like repeats. The smaller version of the protein dimerises, while the 180 kDa isoform tends to form trimers [250].

Tenascin-R has a role in normal development and contributes to the homeostasis of the central nervous system. Tenascin-R deficiency in mice results in abnormal behaviour such as cognitive deficit, reduced coordination and increased anxiety in open field tests [251, 252]. In humans, homozygous deletion of tenascin-R is associated with global development delay, cognitive deficit and transient hyperkinetic movement disorder [253]. Structural changes in the CNS were observed in tenascin-R knock out mice including abnormal organization of perineuronal nets [254, 255], reduced extracellular space in the brain [256] and abnormal hippocampus [257]. *In vitro* assays using hippocampus slices from tenascin-R null mice showed impaired synaptic plasticity and defects of long-term potentiation that might contribute to the observed cognitive deficits [258]. Moreover, tenascin-R has been proposed as a biomarker for dementia as it is down-regulated in the hippocampus of patients with Alzheimer's disease and could be a direct cause of cognitive impairment in neurodegenerative disorders [259].

In the perineuronal nets, tenascin-R is able to interact with other extracellular matrix proteins cross-linking hyaluronan and chondroitin sulphate proteoglycans such as aggrecan, brevican and lecticans via its EGF and FNII-like repeats [186, 255, 260]. Perineuronal nets are found around inhibitory neurons and regulate interneuronal excitability. In addition, they have been suggested to control the diffusion of cationic ions and synapsis formation being involved in synapsis plasticity [261]. Tenascin-R has been shown to modulate voltage-gated sodium channel potentiation via the interaction of the FNIII 1-2 and 6-8 repeats with the β2 subunit of the ion channel, thus regulating its localization and function in neurons [197, 262]. Tenascin-R also controls glutamate uptake by astrocytes as it up-regulates the expression of the glutamate aspartate transporter (GLAST), which is a major component of astrocytic glutamate transporters

and modulates glutamatergic neurotransmission [263]. In addition, tenascin-R is essential for the transport of the carbohydrate human natural killer-1 (HNK-1), involved in perisomatic inhibition. Deficiency of tenascin-R results in reduced long-term potentiation and increased excitatory transmission, suggesting that tenascin-R, as a carrier of HNK-1, may regulate inhibitory transmission and synaptic plasticity in the hippocampus [258, 264].

The adhesive effects of tenascin-R play a role in the development of the CNS and in synaptic plasticity. Tenascin-R is anti-adhesive for oligodendrocytes precursors expressing disialoganglioside GD3 during development, affecting the phosphorylation of focal adhesion kinases and increasing their migration [265]. Later, tenascin-R becomes an adhesive substratum for oligodendrocyte by interacting with cell membrane sulfatides and promotes their differentiation [266]. Tenascin-R can inhibit neurite outgrowth via the interaction of its EGF-like repeats with the adhesion molecule contactin (F3/F11) [267]. In this manner, tenascin-R acts as a repellent molecule for neurites and promotes axonal defasciculation, creating a barrier for the formation of new neuronal pathways during development and CNS repair [268-270]. Initial studies showed that tenascin-R purified from adult rat brain is an anti-adhesive substratum for microglia cells *in vitro,* and when it is present in brainstem cryosections [271]. However, Liao *et al.* [272] later found that distinct domains of tenascin-R have a diverse effect on microglia adhesion and migration. The EGF-like repeats are anti-adhesive for microglia and this effect is mediated by the activation of the protein kinase A signalling pathway. In contrast, FNIII 6-8 repeats of tenascin-R induce microglia adhesion and migration in a protein kinase C-dependent manner. These data suggest that the different domains of tenascin-R may modulate adhesion and migration of microglia via activation of different receptors on these cells.

In summary, tenascin-R is a member of the tenascin family involved in CNS development and homeostasis. Research focus on understanding the role of the perineuronal nets will reveal new functions of extracellular matrix proteins such as tenascin-R in CNS function.

1.6.2. Tenascin-X

Tenascin-X was the third family member to be discovered. During embryogenesis, tenascin-X is mainly expressed in the epicardium, developing skeletal muscle, connective tissue and tendons [273]. In adults, tenascin-X is constitutively expressed in loose connective tissue, especially in tendons, ligaments and skin, and in some smooth muscle and epimysium [274]. Tenascin-X is the largest member of the tenascin family and has a molecular weight of 450 kDa. Tenascin-X is able to form trimers [275]; however, it is not capable of assembling into a hexamer due to lack of amino-terminal cysteines found in tenascin-C, which allow two trimers to assemble into the hexabrachion structure [276].

Tenascin-X has a structural role in connective tissue integrity. Deficiency of this protein in humans results in Ehlers-Danlos syndrome (EDS), characterized by joint hypermobility, skin hyperextensibility, easy bruising and muscle weakness [277, 278]. This phenotype was confirmed in tenascin-X null mice, which also presented similar features as the human deficiency: hypermobile joints, muscle weakness and decreased number of collagen fibrils in the dermis [279, 280]. Indeed, *in vivo* and *in vitro* studies have involved tenascin-X in the regulation of collagen deposition. Biopsies of dermal tissue from mice or patients lacking tenascin-X have lower amounts of collagen I compared to wild type mice or healthy individuals [279, 281]. *In vitro*, fibroblasts from tenascin-X null mice showed a decreased expression of collagen type I and VI, and

other collagen-fibril associated molecules such as collagen type XII, XIV, lumican and fibromodulin [279, 282]. Tenascin-X participates in the architecture of collagenous networks acting as a bridge between collagen fibrils by directly or indirectly interacting with fibrillar collagens or other matrix component. Tenascin-X can directly bind to collagen type XII N-terminal NC3 domain [283], and the FNIII repeats 10 and 11 of the protein interact with dermatan sulfate chains of decorin contributing to the integrity of the extracellular network [284]. These results correlate with cell-free experiments where recombinant tenascin-X could increase the stiffness of 3D collagen gels, suggesting a role in sustaining molecular interactions between fibrils [285]. In addition, the EGF-like repeats and FBG domain of tenascin-X participate in collagen type I fibrillogenesis, as deletion of these domain resulted in lower rates of collagen fibril formation [286]. The FBG domain and FNIII 29 of tenascin-X can also interact with tropoelastin *in vitro* and the protein has been localised to the elastic fibres *in vivo*, suggesting that it could be involved in skin elastic fibres stability and maturation [287, 288]. However, no major differences have been found in the healing process of EDS patients, although wounded tenascin-X knock out mice exhibit lower wound strength than wild type mice. Unlike tenascin-C, tenascin-X is expressed during the late phases of wound remodelling suggesting a role in matrix assembly and maturation and correlating its expression with tissue homeostasis [289].

Tenascin-X has anti-adhesive properties as the other members of the tenascin family do. When used as a substratum *in vitro*, cells do not attach well and present a rounded morphology. The FBG domain of tenascin-X was shown to mediate the interaction between osteosarcoma (MG63) and bladder carcinoma (ECV304) cells and β1-containing integrin in cell adhesion assays [290]. Mouse fibroblast L cells were also able to attach loosely to tenascin-X substratum, but cells did not spread and showed

lower phosphorylation of the focal adhesion kinase [291]. The mechanism by which tenascin-X modulates cell adhesion is not well understood, however a study demonstrated that phosphorylation of p38 mitogen-activated protein (MAP) kinase induced by tenascin-X might mediate cell detachment [291].

More recently, tenascin-X has been also shown to influence epithelial-to-mesenchymal (ETM) transition converting polarized epithelial cells into motile mesenchymal ones [292]. This process is mediated by the interaction of its FBG domain with the small latent complex of TGF-β (SLC), producing a conformational change that exposes mature TGF-β to activate type I and II TGF-β receptor and induce ETM transition. This mechanism is dependent on the binding of the FBG domain to $\alpha_{11}\beta_1$ integrin in the cell surface [293] and this interaction may play a role in tissue repair.

Together these data indicates that tenascin-X is required for the normal assembly and maintenance of the extracellular matrix of connective tissue, although recent studies have suggested an additional role in ETM transition.

1.6.3. Tenascin-W

Tenascin-W is the most recently discovered family member, first described in zebrafish [294] and then found in mammals [295]. Tenascin-W is expressed in embryogenesis during palate formation, smooth muscle and skeletal development. In adult, its pattern of expression is restricted to bone, kidney, smooth muscle and stem cell niches [295]. The tenascin-W monomer has a molecular weight of 130 kDa and no spliced variants in the FNIII repeats have been reported. Like other tenascin family members, it can oligomerise forming hexamers via the di-sulphide bonds of the N-terminal domain [294, 295].

Tenascin-W knock out mice haven't been reported to date and the protein function is not completely understood. Like the other tenascins, tenascin-W can modulate cell adhesion and spreading when used as a substratum. Mouse embryonic fibroblast, C2C12 precursor osteoblast cells and human umbilical vein endothelial cells (HUVEC) attached loosely to plates coated with tenascin-W. Cells showed a rounded phenotype, failed to spread and did not form focal adhesion complexes [296-298]. This effect might be mediated by the interactions of integrins including $\alpha_8\beta_1$ [295], $\alpha_4\beta_1$ and $\alpha_V\beta_1$ [297] and FNIII repeats of tenascin-W, as culture of osteoblast in plates coated with KGD peptides from this domain induced the same cell phenotype as full-length tenascin-W [299]. A role of tenascin-W in osteogenesis has been proposed, as this protein is induced by the bone morphogenetic protein 2 (Bmp-2) in C2C12 and in mouse embryonic fibroblasts, and is expressed at sites of bone morphogenesis [295, 300, 301]. Tenascin-W can increase bone mineralization *in vitro* and promote osteoblast migration. In addition, frontal bones explants from chicken were thicker after 24 h in culture with recombinant tenascin-W, suggesting that this protein can stimulate bone growth *ex vivo* [299, 302].

Expression of tenascin-W has also been associated with cancer. Tenascin-W is found in solid tumours including melanomas, breast, colon, pancreas, kidney, and lung carcinomas [303]. Tenascin-W has been suggested as potential biomarker for solid tumour, as it is absent in healthy adults but is up-regulated in the serum of patients with breast and colon cancer, where higher levels correlated with unfavourable disease progression [304]. Tenascin-W is expressed in the stroma and around blood vessels of tumours [297, 303]. In contrast with tenascin-C, fibroblasts partially adhere to tenascin-W when used as a substratum, while breast cancer cells did not attached in the presence of this protein. Tenascin-W promotes breast cancer cell migration suggesting that it

might support cancer cell invasion [297]. Indeed, a recent study has shown that tenascin-W contribute to breast cancer cell proliferation in the bone metastatic niche. Growth factors such as TGF-β release by breast cancer cells can induce the expression of tenascin-W in human bone marrow stromal cells. In turn, tenascin-W increased the proliferation and migration of the cancer cells promoting further growth and invasive behaviour [305].

To date tenascin-W has been associated with osteogenesis and cancer. Further research including analysis of the tenascin-W null mice will be needed to determine the functions of this protein as part of the extracellular matrix during development and in adults.

The tenascin family is involved in cell adhesion and signalling in mammals and their members are able to interact with multiple receptors and proteins to exert their functions. A summary of their expression in adult, function and reported role of the FBG domain of these proteins is presented in Table 1-6

Table 1-6. Summary of the expression and functions of tenascin-C, -R, -W and –X.

Family member	Expression in adult	Function	FBG role
Tenascin-C	Absent from most tissues but induced upon tissue injury and infection	Influences cell behaviour, migration and proliferation. Contributes to tissue repair	Modulates cell adhesion and migration via interaction with integrins Induces cytokine synthesis via activation of TLR4
Tenascin-R	Central nervous system	Organization of perineuronal nets. Contributes to the homeostasis of the CNS and synaptic plasticity	Interacts with myelin associated glycoprotein Induces microglia adhesion and migration
Tenascin-W	Bone, kidney, smooth muscle and stem cell niches	Osteogenesis	Unknown
Tenascin-X	Loose connective tissue, smooth muscle and epimysium	Assembly and maintenance of the ECM of connective tissue	Interacts with tropoelastin and β1 integrins Participates in collagen type I fibrillogenesis Involved in ETM transition

1.7. Aims

We and others have shown that tenascin-C is associated with the maintenance of inflammation in autoimmune diseases such as RA, and that it can induce pro-inflammatory cytokine synthesis via activation of TLR4. However, it is unknown how tenascin-C activates or interacts with this receptor. The aim of my project is to identify the key residues within tenascin-C FBG that activate TLR4.

This aim will be achieved by: 1) comparing the immune activity of the FBG domain of tenascin-C (FBG-C) with the FBG domains of the other tenascin family members; 2)

determining the active site of FBG-C by peptide mapping; and 3) creating chimeric FBG proteins by site-directed mutagenesis to asses gain or loss of the ability to activate TLR4.

The activity of the FBG domains, peptides and mutant proteins will be assessed by measuring NF-κB activation in a ThP1 reporter cell line and cytokine synthesis in primary human macrophages. Direct binding to TLR4 will be evaluated *in vitro* using a solid phase binding assay.

Together these results will establish the specific epitopes necessary for the activation of TLR4 and the induction of an inflammatory response by the FBG domain of tenascin-C. This information will contribute to a better understanding of how endogenous molecules activate PRRs. These data might also aid the design of specific inhibitors against the pro-inflammatory epitope of tenascin-C. Inhibitors which target tenascin-C-TLR4 signalling may be useful in reducing persistent inflammation in chronic inflammatory conditions where tenascin is involved in disease pathogenesis.

Chapter 2 – Materials and Methods

Chapter 2. Materials and Methods

2.1. Reagents

All reagents were purchased from Sigma unless stated otherwise below.

Cloning and molecular biology reagents: dNTPs, Phusion HF buffer, Phusion Hot Start II DNA Polymerase, T4 DNA ligase, *Nde1* and *Xho*I restriction enzymes, rapid digestion buffer, pCRBlunt vector, GeneRuler DNA ladder, 6X DNA gel loading dye and GeneJET gel extraction kit were purchased from Thermo Scientific. All the primers and agarose were purchased from Invitrogen. IMAGE consortium cDNA clones of tenascin-R, -W and -X were purchased from Source bioscience.

Protein assays reagents: LB broth was purchased from Invitrogen. Carbenicillin was purchased from Novagen. HCl and pET32b vector was purchased from Merk. Ni^{2+} ProBound resin was purchased from Life technologies. Urea, Coomassie brilliant blue R-250, formic acid, acetic acid and tween were purchased from BDH. 30% acrylamide/ 0.8% bisacrylamide was purchased from Severn Biotech. Imidazole was purchased from MP biomedicals. Silver nitrate was purchased from Fisher chemicals. Phosphate buffered saline 10 X was purchased from VWR. TMB substrate was purchased from KPL. QuikChange II XL Site-Directed Mutagenesis Kit was purchased from Agilent Technologies. MAb hTLR4 (clone HTA125) was purchased from Invivogen. Anti-mouse IgG-HRP was purchased from Biorad. Nunc, Maxisorp 96 well plates was purchased from Thermo Scientific. Tetra-his antibody was purchased from Qiagen. Recombinant human TLR4 and TLR4-MD-2 were purchased from R&D systems. Recombinant TLR4 purity was >95% according to manufacturer and was verified by Dr. Anna Piccinini by SDS-PAGE and silver staining.

Cell culture reagents: RPMI 1640 was purchased from Lonza. FBS and penicillin/streptomycin were purchase from Gibco. LPS from *E. coli*, Serotype EH100 (Ra) (TLRgrade™) was purchased from Enzo, life sciences. Polymyxin B solution was purchased from Fluka. Blasticidin, Normocin™, PAb hTLR4 antibody, IgG isotype control and CLI-095 TLR4 inhibitor (TAK 242) were purchased from Invivogen.

2.2. Buffers and recipes

TAE buffer 50X: 2 M Tris, 1 M acetic acid, 50 mM EDTA pH 8.

TBS buffer: 50 mM Tris pH 8, 150 mM NaCl, 0.02 % Na Azide.

Urea buffer: 8 M urea, 20 mM Tris pH 8.0.

SDS-PAGE loading buffer: 125 mM Tris HCl pH 6.8, 20% glycerol, 4% SDS, 0.2% 2-β-ME, 0.001% bromphenol blue.

TN buffer: 50 mM Tris pH 8, 150 mM NaCl.

Tris-glycine buffer: 0.06 M Tris base, 0.48 M glycine, 1% w/v SDS.

SDS-PAGE 12% gel:

Separating gel 12%: 3 mL of 30% acrylamide/ 0.8% bisacrylamide, 1.87 mL of 4X Tris HCl/ SDS pH 8.8, 2.62 mL of H_2O, 25 µL of 10% ammonium persulfate, 5 µL of TEMED.

Stacking gel 3.9%: 0.32 mL of 30% acrylamide/ 0.8% bisacrylamide, 0.62 mL of 4X Tris HCl/ SDS pH 8.8, 1.52 mL of H_2O, 12.5 µL of 10% ammonium persulfate, 2.5 µL of TEMED.

1.5% Agarose gel: 0.75 g of agarose, 1 mL of TAE buffer 50X, 8 µL ethidium bromide in 49 mL of H_2O.

Coomassie blue solution: 0.1% coomassie blue, 50% methanol, 20% acetic acid in H_2O.

Coomassie destainer: 30% methanol, 1% formic acid in H_2O.

2.3. Cloning tenascin-R, -W, -X FBG domains

The FBG domains of tenascin-R, -W and -X were cloned as described for tenascin-C [89]. The boundaries of the FBG domains of tenascin-R, -W and -X were determined using the domain sequences published in Uniprot for the human tenascin-R, -W and -X sequence (accession numbers in Table 2-1). Primers were designed by adding a His-tag at the N-terminus of the proteins, and a restriction site in the forward primer for *Nde*I and in the reverse primer for *Xho*I (Table 2-2). PCR was performed using 400 nM of each primer, 1 µg DNA template, 200 µM dNTPs, 1X Phusion HF buffer and 0.02 units/µL of Phusion Hot Start II DNA Polymerase in a final volume of 50 µL. The templates used were IMAGE consortium cDNA clones containing full length sequence of tenascin-R (ID: 40114168), tenascin-W (ID: 9020609) and tenascin-X (ID: 5179997). PCR was performed as described in Table 2-3 in Thermocycler PCR machine (Biometra).

Table 2-1. Features of the FBG domains of tenascin family members.

FBG Domain	Accession number	Amino acid position	Molecular Weight (kDa)	Number of amino acids	pI
FBG-C human	P24821	1974-2201	26.1	229	8.78
FBG-R human	Q92752	1128-1359	27.0	232	8.63
FBG-W human	Q9UQP3	1060-1300	27.6	240	9.18
FBG-X human	P22105	4013-4243	26.1	231	5.54

Table 2-2. Forward and reverse primer sequences of tenascin -R, -W and -X FBG. Each sequence has a His-tag (underlined) and a restriction site in the forward primer for *Nde*I (bold) and in the reverse primer for *Xho*I (bold).

Gene	Accession number	Number of base pairs of FBG	Base pairs position	Primer name	Sequence	Size of PCR product
FBG-R	NM_003285.2	696	3937-4632	TNR FBG Forward	GCC **CAT ATG** CAT CAT CAT CAT CAT CAT GGA GGC CGG GTG TTC CCT CAT	735
				TNR FBG Reverse	GCC **CTC GAG** TTA GAA CTG TAA GGA CTG CCG TTT TCT	
FBG-X	NM_019105.6	693	12239-12931	TNX FBG Forward	GCC **CAT ATG** CAT CAT CAT CAT CAT CAT ACCTCTTTCACCACGGGT	732
				TNX FBG Reverse	GCC **CTC GAG** TTA GCC TCC CCC CGC TGG GGA G	
FBG-W	NM_022093.1	723	3291-4013	TNW FBG Forward	GCC **CAT ATG** CAT CAT CAT CAT CAT CAT GTT GGT GCC CGT TTC CCA	762
				TNW FBG Reverse	GCC **CTC GAG** TTA GAA CGT TCG CAG CCT TCC TCT CAG	

Table 2-3. Touch down PCR protocol. PCR protocol used to amplify tenascin-R, -W and -X FBG domain sequence using IMAGE consortium clones as templates.

Step	Temperature	Time	Cycles
Denaturation	94ºC	10 min	1
1	94ºC	1 min	3
	69ºC		
	72ºC		
2	94ºC	1 min	6
	67ºC		
	72ºC		
3	94ºC	1min	20
	65ºC		
	72ºC		
4	94ºC	1min	3
	62ºC		
	72ºC		
5	94ºC	1min	3
	60ºC		
	72ºC		
Elongation	72ºC	10 min	1

5 µL of PCR products were ligated into pCRBlunt vector (1 µL) according to manufacturer's instructions. The clones were sequenced (Eurofins, UK) to ensure no errors had been introduced by PCR. The plasmids with the correct inserts were digested adding 1 µL *Nde1* and *Xho*I to 5 µL DNA, 4 µL rapid digestion buffer and 39 µL H_2O (total volume = 50 µL). The reaction was incubated at 37°C for 1 h. To visualise the DNA, samples were loaded with 6X DNA gel loading dye in 1.5% agarose gels stained with ethidium bromide. Next to the samples, 5 µL DNA ladder (GeneRuler) was loaded to determine the band size. Gel tank (Mupid One gel electrophoresis system) was filled with 1X TAE buffer and the gel was run for 1 h at 100 V. Inserts were extracted from the agarose using GeneJET gel extraction kit according to manufacturer's instructions. Inserts were then ligated into pET32b using *Nde1* and *Xho*I restriction sites, using 1 µL T4 DNA ligase and 2 µL rapid ligation buffer (topped up to 10 µL with H_2O) for 1 h at room temperature.. The inserts were verified by enzyme restriction digestion as explained above. DNA was visualised in 1.5% agarose gels stained with ethidium

bromide. pET32b vector was transformed into *E. coli* BL21 (DE3) cells by heat shock. 100 ng of DNA was added to 45 µL of bacterial cells and incubated on ice for 30 min. Cell were then incubated for 30 s at 42°C and then placed on ice for 2 min. 500 µL of LB media was added to the cells and they were grown for 1 h at 37°C, 220 rpm. Bacterial cells were plated in LB agarose plates + carbenicillin to select transformed colonies. Glycerol stocks were made of the colonies containing the pET32b vector for protein expression.

2.4. Expression of the FBG domains in *E. coli*

2.4.1. Small scale expression

E. coli BL21 (DE3) cells containing pET32b vector including FBG-C, -R, -W or -X, were inoculated in 2 mL of LB media + 1% glucose and 100 µg/mL carbenicillin, and grown overnight at 37 °C, 220 rpm. The next day, the bacterial culture was centrifuged for 10 min, 3000 rpm and resuspended in 1 mL of fresh LB media. This was used to inoculate 20 mL of LB + 100 µg/mL carbenicillin. The culture was incubated at 37 °C, 220 rpm until bacterial growth reached an $O.D._{600}$ between 0.6 and 0.8. 1mM of IPTG was added to induce protein expression for 3 h at 37 °C, 220 rpm. A sample of 100 µL was taken each hour to monitor protein expression.

Bacterial culture was centrifuged for 15 min, 3000 rpm and the pellet was washed with TBS buffer. Bacterial pellet was resuspended in 1 mL of TBS buffer and cells were lysed by sonication using Bioruptor water bath (Diagenode) for 4 cycles (30 sec ON, 30 sec OFF). Bacterial solution was centrifuged at 13000 rpm for 5 min at 4°C. The supernatant was collected and the pellet was resuspended in 1 mL of TBS buffer.

10 µL of each sample + 10 µL of loading buffer were loaded into 12% SDS-PAGE and samples were run for approximately 1 h at 20 mA (for details see section 2.6.1).

2.4.2. Large scale expression

E. coli BL21 (DE3) cells containing pET32b vector including the FBG domain of the tenascin family members, were inoculated in 20 mL of LB media + 1% glucose and 100 µg/mL carbenicillin and grown overnight at 37 °C, 220 rpm. The culture was centrifuged for 10 min, 3000 rpm and resuspended in 10 mL of fresh LB media. This was used to inoculate 1 L of LB + 100 µg/mL carbenicillin. The culture was incubated at 37 °C, 220 rpm until bacterial growth reached an $O.D._{600}$ between 0.6 and 0.8. 1mM of IPTG was added to induce protein expression for 3 h at 37 °C, 220 rpm.

Bacterial culture was centrifuged for 15 min, 3500 rpm and the pellet was washed with TBS buffer. Bacterial pellet was resuspended in 40 mL TBS and lysed with French Press (Thermo Spectronic) at 1500 pound per square inch (PSI) four times. Bacterial solution was centrifuged at 10000 rpm for 15 min at 4°C. The supernatant was discarded and the pellet (inclusion bodies) stored at -20 °C until protein solubilisation.

2.5. Purification of FBG domains using Ni^{2+} chromatography

2.5.1. Protein solubilisation

Inclusion bodies were resuspended in urea buffer + 5 mM β-mercaptoethanol (β-ME). The solution was left overnight on a rotator at 4°C to solubilize the proteins in the inclusion bodies.

2.5.2. Ni^{2+} column chromatography under denaturing conditions

5 mL of Ni^{2+} beads were placed in a Poly-Prep chromatography column (Bio-Rad). Beads were washed with 5 column volumes of ultrapure water and equilibrated with 5 column volumes of urea buffer. 40 mL of solubilised protein pool was loaded into the column and the flow through was collected. The column was washed with 5 column volumes of urea buffer followed by 20 column volumes of 0.1% triton-X114 in urea buffer to remove LPS, and 20 column volumes of urea buffer. Finally, the FBG protein was eluted using 300 mM imidazole in urea buffer. 5 fractions of 5 mL were collected. 10 µL of each sample + 10 µL of loading buffer were loaded into 12% SDS-PAGE gel to visualised protein yields.

2.5.3. Protein refolding

After purification, the protein fractions were pooled together and the concentration measured at $O.D._{280}$ by Nanodrop (Thermo Scientific). The protein solution was diluted until $O.D._{280nm} < 0.2$ in urea buffer + 20 mM cystamine to avoid protein precipitation during dialysis. The diluted protein solution was dialyzed for 4 days:

- Day 1 and 2: dialysed for 24 h against TN buffer + 5 mM β-ME, 1 mM 2-hydroxyethyldisulphide at 4 °C.
- Day 3 and 4: dialysed for 24 h against TN buffer at 4 °C.

After refolding, the protein solution was filtered through 0.45 µm Corning® Vacuum Filter (CN Membrane) to remove any precipitated protein.

2.5.4. Ni^{2+} column chromatography under native conditions

1.5 mL of Ni^{2+} beads (Bio-Rad) were placed in a Poly-Prep chromatography column (Bio-Rad). Beads were washed with 5 column volumes of ultrapure water and equilibrated with 5 column volumes of TN buffer. The refolded protein solution was loaded into the column and the flow through was collected. The column was washed with 5 column volumes of TN buffer followed by 50 column volumes of 0.1% triton-X114 in TN buffer and 30 column volumes of TN buffer. 20 mM imidazole (in TN buffer) was added to remove any unspecific bound protein. Finally, the FBG protein was eluted using 300 mM imidazole in TN buffer. 5 or 6 fractions of 1 mL were collected in total and 10 µL of each sample + 10 µL of loading buffer were loaded into 12% SDS-PAGE gel to visualise protein yields. Fractions were then dialyzed against TN buffer to remove imidazole. The concentration of the protein was measured at $O.D._{280}$ by Nanodrop (Thermo Scientific) and by Bradford assays according to manufacturer's instructions (Bio-rad).

2.6. FBG-C, R, -W, -X protein characterization

2.6.1. Tris-glycine sodium dodecyl sulphate polyacrylamide gel electrophoresis (SDS-PAGE)

Protein samples were prepared using 2X loading buffer and boiled for 5 min before loaded into the gel. Proteins were separated using 12% SDS-PAGE gels. 6 µL of PAGE-ruler plus pre-stained protein ladder were loaded alongside the protein samples to estimate their molecular weight. Gels tank (ATTO) was filled with 1x Tris-glycine buffer and the gel was run for approximately 1 h at 20 mA.

2.6.2. Coomassie staining

Protein gels were stained with Coomassie blue solution for 15 min at RT with shaking. Gels were then rinsed and de-stained with Coomassie destainer until bands were clear above the background.

2.6.3. Silver staining

1 µg of each protein was separated by SDS-PAGE and samples were fixed with 50% methanol, 5% acetic acid solution. Gel was stained with 0.1% silver nitrate solution and bands were developed using 0.04% formalin and 2% sodium carbonate solution. The reaction was stopped using 5% acetic acid.

2.6.4. Western blot

Proteins were separated by SDS-PAGE and were electrotransferred using Trans-Blot® Turbo™ Transfer System to Trans-Blot® Turbo™ Mini Nitrocellulose membranes (BioRad). Membranes were blocked with 5% BSA in phosphate buffered saline, 0.05% tween-20 (PBST) and then incubated with primary antibody in 2% BSA PBST: tetra-his (Qiagen, 1:10000 dilution), anti-human FBG-C (1:500 dilution), anti-human FBG-R (Santa Cruz, 1:3000 dilution) or anti-human FBG-X (Santa Cruz, 1:3000 dilution). Membranes were then incubated with secondary antibody in 2% BSA PBST: anti-mouse IgG-HRP (Biorad, 1:20000 dilution), anti-rabbit IgG-HRP (Dako, 1:3000 dilution), or anti-goat IgG-HRP (Santa Cruz, 1:5000 dilution). Protein bands were visualized using ECL (Amersham).

2.6.5. Circular Dichroism (CD) spectroscopy

200 µL of each sample in TN buffer were analysed using the J-815 Circular Dichroism Spectrometer (Jasco)**.** The CD spectrum was measured in the "far UV" spectral region (190-250 nm) at 20°C or 85°C. Five repeated measured were taken and the average plotted and analysed using Spectra Manager™ II software. CD spectroscopy measures the secondary structure of protein in the "far UV" region. Characteristic spectra from α-helix, β-sheet and random coils are presented in Figure 2-1.

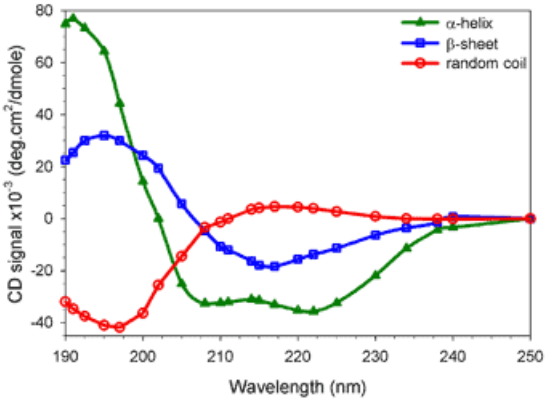

Figure 2-1. CD spectrum of α-helix, β-sheet and random coils. α-helix spectrum has a peak at 208 and 222 nm, β-sheet spectrum peaks at 215 nm and random coils spectrum show a negative peak at 195 nm.

2.6.6. LPS test

The LPS content was measured using the Endpoint Chromogenic LAL Assays (Lonza) according to manufacturer's instructions.

2.7. Mutagenesis

Mutant proteins were made using QuikChange II XL Site-Directed Mutagenesis Kit (Agilent Technologies). Mutant proteins were designed for FBG-C and FBG-X and the amino acids changed are shown in Table 2-4 and Table 2-5.

Table 2-4. Sequence of FBG-C mutant proteins. Wild type amino acids are coloured in blue and mutations are highlighted in red.

FBG-C loop 5 WT	DKFSVGDA**K**T**R**Y**K**L**K**VEGYSGTAGD
FBG-C mutant 1	DKFSVGDA**A**T**A**YKLKVEGYSGTAGD
FBG-C mutant 2	DKFSVGDAKTRY**A**L**A**VEGYSGTAGD
FBG-C mutant 3	DKFSVGDA**A**T**A**Y**A**L**A**VEGYSGTAGD
FBG-C loop10 WT	RPSNFRNLEG**RRKRA**
FBG-C mutant 4	RPSNFRNLEG**GG**
FBG-C mutant 5	DKFSVGDA**A**T**A**Y**A**L**A**VEGYSGTAGD + RPSNFRNLEG**GG**
FBG-C loop 7 WT	KDT**D**SA**I**T**N**CAL
FBG-C mutant 6	KDT**P**SA**L**T**S**CAL
FBG-C mutant 7	DKFSVGDA**A**T**A**Y**A**L**A**VEGYSGTAGD + KDT**P**SA**L**T**S**CAL

Table 2-5. Sequence of FBG-X mutant proteins. Wild type amino acids are coloured in blue and mutations are highlighted in red.

FBG-X loop 5 WT	DSFHV**DS**A**AEY**YRL**H**LEGYHG
FBG-X mutant 1	DSFHVDSA**KAK**YRLHLEGYHG
FBG-X mutant 2	DSFHV**GD**A**KTK**YRL**K**LEGYHG
FBG-X loop 10 WT	RNFRSPAG**GG**
FBG-X mutant 3	DSFHV**GD**A**KTK**YRL**K**LEGYHG + RNFRSPAG**RRKRA**
FBG-X loop 7 WT	DRD**P**NSL**L**I**S**CAVS
FBG-X mutant 4	DSFHV**GD**A**KTK**YRL**K**LEGYHG + RNFRSPAG**RRKRA** + DRD**D**NSL**I**I**N**CAVS

Specific primers were designed for each mutation; in some cases, the mutations were introduced in two steps using 2 sets of primers (Table 2-6). PCR was run according to manufacturer's instructions and adapted to the pET32b vector (Table 2-7). The PCR products were transformed into XL10-Gold ultracompetent cells by heat shock. Plasmids were isolated using QIAprep Spin Miniprep Kit (Qiagen) and were sequenced (Eurofins, UK) to validate the insertion of the mutations. The clones with the correct mutant sequences were transformed into *E. coli* BL21 DE3 cells for protein over-expression and purification as described above (section 2.4 and 2.5). Proteins were also biochemically and biophysically characterised using SDS-PAGE gels, western blots, CD spectroscopy and LPS content was measured as described in section 2.6.6.

Table 2-6. Primer sequences used to insert specific mutations in FBG-C and FBG-X.

Protein		Primer sequence
FBG-C mutant 1	Forward Primer	GTG GGA GAT GCC GCG ACT GCC TAC AAG CTG AAG GTG GAG
	Reverse Primer	CAC CTT CAG CTT GTA GGC AGT CGC GGC ATC TCC CAC GC
FBG-C mutant 2	Forward Primer	GCC AAG ACT CGC TAC GCG CTG GCG GTG GAG GGG TAC
	Reverse Primer	GTA CCC CTC CAC CGC CAG CGC GTA GCG AGT CTT GG
FBG-C mutant 3	Forward Primer	GTG GGA GAT GCC GCG ACT GCC TAC GCG CTG GCG GTG GAG GGG TAC
	Reverse Primer	GTA CCC CTC CAC CGC CAG CGC GTA GGC AGT CGC GGC ATC TCC CAC
FBG-C mutant 4 and 5	Forward Primer	AGC AAC TTC AGA AAT CTT GAA GGC GGG GGC TAA CGG GC
	Reverse Primer	GC CCG TTA GCC CCC GCC TTC AAG ATT TCT GAA GTT GC
FBG-C mutant 6 and 7	Forward Primer	GAC AAG GAC ACA CCT TCA GCC CTC ACC AGC TGT GCT CTG
	Reverse Primer	CAG AGC ACA GCT GGT GAG GGC TGA AGG TGT GTC CTT GTC
FBG-X mutant 1	Forward Primer	CAC GTA GAC TCG GCT AAG GCG AAG TAC CGC CTC CAC TTG
	Reverse Primer	CAA GTG GAG GCG GTA CTT CGC CTT AGC CGA GTC TAC GTG
FBG-X mutant 2	Forward Primer 1	GAC TCC TTC CAC GTA GGC GAT GCT AAG GCG AAG TAC CGC
	Reverse Primer 1	GCG GTA CTT CGC CTT AGC ATC GCC TAC GTG GAA GGA GTC
	Forward Primer 2	GTA GGC GAT GCT AAG ACG AAG TAC CGC CTC AAG TTG GAG GGC
	Reverse Primer 2	GCC CTC CAA CTT GAG GCG GTA CTT CGT CTT AGC ATC GCC TAC
FBG-X mutant 3	Forward Primer 1	TCC CCA GCG GGG AGA CGC AAA CTC GAG CAC CAC CAC
	Reverse Primer 1	GTG GTG GTG CTC GAG TTT GCG TCT CCC CGC TGG GG
	Forward Primer 2	CCA GCG GGG AGA CGC AAA CGC GCG TAG CAC CAC
	Reverse Primer 2	GTG GTG CTA GCG CGC TTT GCG TCT CCC CGC TGG
FBG-X mutant 4	Forward Primer	CGT GAT CGG GAC GAC AAC AGC TTG ATC ATC AAC TGC GCT GTC TCC
	Reverse Primer	GGA GAC AGC GCA GTT GAT GAT CAA GCT GTT GTC GTC CCG ATC ACG

Table 2-7. Mutagenesis PCR steps. PCR protocol for QuikChange II XL Site-Directed Mutagenesis Kit used to amplify FBG-C and FBG-X mutant proteins.

Step	Temperature	Time	Cycles
1	95 °C	1 min	1
2	95 °C	50 s	18
	60 °C	50 s	
	68 °C	6 min	
3	68 °C	7 min	1

2.8. Peptides

Peptides 1-9 were designed to comprise the entire FBG-C sequence with overlapping regions among two contiguous peptides. Additional peptides were made including scrambled versions of P5, P6 and P9, different version of FBG-C loop 5 and mutant versions of FBG-C loop 5. All peptides were synthesised by BioGenes, they had a purity >90% and were provided as a TFA-salt, lyophilised powder. Peptides were reconstituted in sterile PBS, and DMSO was added when required for their solubilisation. The list of all peptides used is presented in Table 2-8.

Table 2-8. Sequences of peptides used in cell and *in vitro* assays.

P1	TIGLLYPFPKDCSQAMLNGDTTSGLYTIYL
P2	YTIYLNGDKAEALEVFCDMTSDGGGWIVFL
P3	WIVFLRRKNGRENFYQNWKAYAAGFGDRRE
P4	GDRREEFWLGLDNLNKITAQGQYELRVD
P5	ELRVDLRDHGETAFAVYDKFSVGDAKTRYK
P6	KTRYKLKVEGYSGTAGDSMAYHNGRSFST
P7	RSFSTFDKDTDSAITNCALSYKGAFWYRN
P8	WYRNCHRVNLMGRYGDNNHSQGVNWFHWKG
P9	FHWKGHEHSIQFAEMKLRPSNFRNLEGRRKRA
P5S	KGVFLTRYVTDARDVHFDKYGASRELEAKD
P6S	YKGTSDHFRVGSNSRYETSMGKGAATLKY
P9S	AFERHMKWKRKLRGAGHREPELHSNSNRIFQF
Loop 5-1	KTRYK
Loop 5-2	GDAKTRYKLKVEG
Loop 5-3	DKFSVGDAKTRYKLKVEGYSG
Loop 5-4	AFAVYDKFSVGDAKTRYKLKVEGYSGTAGD
Loop 5-deletion	GETAFAVYDKFSVGDAVEGYSGTAGDSMAY
Loop 5-mutant 1	AFAVYDKFSVGDA**A**T**A**YKLKVEGYSGTAGD
Loop 5-mutant 2	AFAVYDKFSVGDAKTRY**A**L**A**VEGYSGTAGD
Loop 5-mutant 3	AFAVYDKFSVGDA**A**T**A**Y**A**L**A**VEGYSGTAGD

2.9. FBG proteins and peptides activity

2.9.1. ThP1 NF-κB cells

ThP1-Blue™ NF-κB cells (Invivogen) were cultured in RPMI 1640, 10% FBS, 1% penicillin/streptomycin, 10 µg/ml blasticidin and 100 µg/ml Normocin™. Cells were plated (10^5 cells/mL) in 96 wells plate and stimulated with different doses of LPS, recombinant FBG proteins or peptides. As a control for LPS contamination, the different stimuli were pre-incubated for 30 min with 10 µg/mL polymyxin B or boiled for 15 min prior cell stimulation. After 24 h, supernatant was collected and the presence of SEAP was detected using QUANTI-Blue™ (Invivogen). Absorbance was read at 620 nm on FluoStar Omega plate reader. Tetrazolium salt (MTT) assay was performed to verify cell viability. 10% v/v MTT was added to the cell media and cells were incubated for 2 h at 37ºC. Cells were lysed with 10% SDS, 0.01 M HCl and the formation of purple formazan was measured at 620 nm on FluoStar Omega plate reader.

2.9.2. TLR4 protein activity dependency in ThP1 NF-κB cells

ThP1-Blue™ NF-κB cells were culture as explained above. Cells were incubated with PAb hTLR4 antibody or IgG isotype control (Inivogen) for 1 h at 37ºC, or with 3 µM of TLR4 inhibitor TAK 242 (Invivogen) for 6 h at 37ºC prior to cell stimulation. Cells were stimulated with 1 ng/mL of LPS, 1 µM of FBG proteins or 100 µM of peptides. After 24 h, supernatant was collected and the presence of SEAP was detected using QUANTI-Blue™. Absorbance was read at 620 nm on FluoStar Omega plate reader.

2.9.3. Co-stimulation of ThP1 NF-κB cells with FBG-C and peptides

ThP1-Blue™ NF-κB cells were cultured in RPMI 1640, 10% FBS, 1% penicillin/streptomycin, 10 µg/ml blasticidin and 100 µg/ml Normocin™. Cells were plated (10^5 cells/mL) in 96 wells plate and stimulated with 100 µM of different peptides for 30 min at 37ºC. The cells were then stimulated with FBG-C for 24 h at 37ºC. Supernatant was collected and the presence of SEAP was detected using QUANTI-Blue™. Absorbance was read at 620 nm on FluoStar Omega plate reader.

2.9.4. Primary human macrophages

Human monocytes were isolated from peripheral blood (London Blood Bank) by ficoll gradient and counterflow centrifugation. Cells were plated (1 million cells/mL) in RPMI 1640, 5% (v/v) FBS, 1% penicillin/streptomycin and differentiated into macrophages for 5 days with 100 ng/mL of M-CSF (Peprotech).

Macrophages were plated (10^5 cells/mL) in RPMI 1640, 3% (v/v) FBS and 1% penicillin/streptomycin for 24 h before stimulation with different doses of LPS, recombinant FBG proteins or peptides. As a control for LPS contamination, the different stimuli were pre-incubated for 30 min with 10 µg/mL polymyxin B or boiled for 15 min prior cell stimulation. Macrophages were stimulated for 24 h, the media was collected and cytokines levels detected by ELISA (BD Biosciences) according to the manufacturer's instructions. Absorbance was read at 450 nm on FluoStar Omega plate reader and data analysed using Omega software.

MTT assay was performed to verify cell viability. 10% v/v MTT was added to the cell media and cells were incubated for 2 h at 37ºC. Cells were lysed with 10% SDS,

0.01 M HCl and the formation of purple formazan was measured at 620 nm on FluoStar Omega plate reader.

2.9.5. TLR4 protein activity dependency in primary human macrophages

Primary human macrophages were obtained and cultured as explain above. Cells were incubated with PAb hTLR4 antibody or IgG isotype control for 1 h at 37ºC, or with 3 µM of TLR4 inhibitor TAK 242 for 6 h at 37ºC prior to cell stimulation. Macrophages were stimulated with 1 ng/mL of LPS, 1 µM of FBG proteins or 100 µM of peptides. After 24 h, the media was collected and cytokines levels detected by ELISA according to the manufacturer's instructions. Absorbance was read at 450 nm on FluoStar Omega plate reader and data analysed using Omega software.

2.10. Solid phase binding assay

2.10.1. Equal coating with FBG and TLR proteins

Nunc, Maxisorp 96 well plates were coated with 1 µg/ml solution of recombinant FBG proteins, TLR4 or TLR4-MD-2 in PBS. The plate was incubated with shaking overnight at 4°C. Non-specific binding was blocked with 10% BSA in PBST for 2 h at room temperature with shaking. MAb hTLR4 (Invivogen), FBG-C antibody or tetra-his (Qiagen) was added at a final concentration of 1 µg/ml in 2% BSA/PBST and incubated with shaking for 1 h at room temperature. Secondary antibody anti-mouse IgG-HRP (Biorad) or anti-rabbit IgG-HRP (Dako) (1:1000 dilution) in PBST was added and incubated with shaking for 1 h at room temperature. Colorimetric reaction was started adding TMB substrate and incubating for 5 min in the dark. Colour development was

stopped using 6% sulphuric acid solution and plates were read at 450 nm in FluoStar Omega plate reader.

2.10.2. Solid phase binding assay detecting TLR4

Nunc, Maxisorp 96 well plates were coated with 1 µg/ml solution of recombinant FBG proteins in PBS and incubated with shaking overnight at 4°C. Unspecific binding was blocked with 10% BSA in PBST for 2 h at room temperature with shaking. TLR4 was added at a maximum concentration of 27 µg/ml followed by a series dilution 1:3 in 2% BSA/PBST and incubated with shaking for 2 h at room temperature. MAb hTLR4 (Invivogen) was added at a final concentration of 1 µg/ml in 2% BSA/PBST and incubated with shaking for 2 h at 4°C. Secondary antibody anti-mouse IgG-HRP (Biorad, 1:1000 dilution) in PBST was incubated with shaking for 1 h at room temperature. Colorimetric reaction was started by adding TMB substrate and incubated for 10 min in the dark. Colour development was stopped using 6% sulphuric acid solution and plates were read at 450 nm in FluoStar Omega plate reader.

2.10.3. Blocking TLR4-FBG-C *in vitro* binding with peptides

Nunc, Maxisorp 96 well plates were coated with 1 µg/ml solution of recombinant FBG proteins in PBS and incubated with shaking overnight at 4°C. Unspecific binding was blocked with 10% BSA in PBST for 2 h at room temperature with shaking. TLR4 was pre-incubated with 200 µM of peptides for 1 h at room temperature. This was then added at a maximum concentration of 27 µg/ml followed by a series dilution 1:3 in 2% BSA/PBST and incubated with shaking for 2 h at room temperature. MAb hTLR4 was added at a final concentration of 1 µg/ml in 2% BSA/PBST and incubated with shaking for 2 h at 4°C. Secondary antibody anti mouse IgG-HRP 1:1000 dilution in PBST was incubated with shaking for 1 h at room temperature. Colorimetric reaction was started

by adding TMB substrate and incubated for 10 min in the dark. Colour development was stopped using 6% sulphuric acid solution and plates were read at 450 nm in FluoStar Omega plate reader.

2.11. In-silico analysis of homology and protein modelling.

All protein sequences were obtained from the UniProt Knowledge database and the accession numbers are presented in Table 2-9, with the exception of the FBG domain of *B. floridae* and *C. savignyi*, which predicted sequences were taken from [306]. Pairwise alignments were performed using Clustal Omega 1.2.1. Alignments were coloured using Jalview software. Multiple sequence alignments were performed using Clustal Omega and coloured according to the Clustal colour scheme. SWISSMODEL [307] was used to generate tenascin FBG structural models based on the structure of the C-terminus fibrinogen γ chain (PDB: 1FID) [308]. Protein models were coloured and structurally analysed using Pymol Molecular Graphics System, Version 1.7.4 Schrödinger. Docking of TLR4 and FBG-C was performed in the automated docking software ClusPro [309] and using ICM. ICM protein docking was performed by Brian D. Marsden. Briefly, the model of the FBG-C domain was docked into the TLR4 dimer using the fourier transform protein:protein docking method within ICM using standard parameters and with post-prediction refinement enabled. The structure of TLR4-MD-2-LPS (PDB code 4G8A) [128] was used as a basis for protein:protein docking with the tenascin FBG domain homology model generated within ICM. The MD-2-LPS components of this structure were removed. The glycosylations of the TLR4 molecules were retained but all waters and crystallographic-condition molecules were removed. 5000 models were generated and those with loop 5 and 7 interactions within 3.5Å with TLR4 were retained.

Table 2-9. FBG domains examined by multiple sequence alignment analysis.

FBG Domain	Accession number
FBG-C *S. scrofa*	Q29116
FBG-C *M. musculus*	Q80YX1
FBG-C *R. norvegicus*	B2LYI9
FBG-C *B. taurus*	A0JN60
FBG-C *G. gallus*	P10039
FBG-C *D. rerio*	Q4FAI8
FBG-C *T. rubripes*	Q7SZG1
Angiopoietin 1	Q15389
Angiopoietin 2	O15123
Angiopoietin 4	Q9Y264
Angiopoietin-related protein 1	O95841
Angiopoietin-related protein 2	Q9UKU9
Angiopoietin-related protein 3	Q9Y5C1
Angiopoietin-related protein 4	Q9BY76
Angiopoietin-related protein 5	Q86XS5
Angiopoietin-related protein 6	Q8NI99
Angiopoietin-related protein 7	O43827
Fibrinogen β chain C-terminus	P02675
Fibrinogen ϒ chain C-terminus	P02679
Fibroleukin	Q14314
FIBCD-1	Q8N539
Ficolin-H	075636

Ficolin-L	Q15485
Ficolin-M	O00602
Tenascin-C	P24821
Tenascin-R	Q92752
Tenascin-W	Q9UQP3
Tenascin-X	P22105
FreP *P. parvimensis*	P19477
FreP *B. glabrata*	G3LHF9
FreP *T. tridentatus*	Q9U8W8
FreP *S. domuncula*	Q5W4Y8

2.12. Statistics

The data mean ± standard error of the mean (SEM) or standard deviation (SD), and statistical analysis were calculated using GraphPad Prism 6 software. Multiple group means were analysed by one-way analysis of variance, followed by the Dunnett multiple comparisons test, where appropriate. Two-tailed, un-paired or paired t-test was used for experiments involving only two groups. *P* values less than 0.05 were considered significant.

Chapter 3 – Comparative analysis of the immune function of the tenascin family members

Chapter 3. Comparative analysis of the immune function of the tenascin family members

3.1. Introduction

The aim of my project is to determine the key amino acids within tenascin-C FBG domain (FBG-C) that activate TLR4 to better understand how endogenous molecules trigger the immune system. In addition, this information will be used to design specific inhibitors of tenascin-C-TLR4 signalling that may be useful in treating RA.

To identify specific sequences of FBG-C essential for TLR4 activation, the first approach I will use is to compare the immune activity of the tenascin family members. The tenascin family comprises tenascin-C, -R, -W and -X and they all have an FBG domain at the C-terminus. Pairwise alignment of the sequences of the FBG domain of the tenascin family members revealed that they are highly conserved, exhibiting 50-60% sequence identity (Table 3-1). The ability of the FBG domains of tenascin-R, -W and -X (FBG-R, -W and -X) to induce an inflammatory response hasn't been determined, but tenascin-C is the only member that is induced during tissue damage and infection independently of the injury site. Here, I will assess the activity of the FBG-C, -R, -W and -X by measuring NF-κB activation in ThP1 cells, cytokine synthesis in primary human macrophages and direct binding to TLR4 in a solid phase binding assay. I will then look for common sequences among the proteins that can activate TLR4 and differences among the proteins that lack inflammatory activity. In this manner, I will be able to establish which specific sequences are required for TLR4 activation. Moreover, these data will reveal for the first time if other members of the tenascin family are able to induce an inflammatory response.

Table 3-1. Identity among the FBG domains of human tenascin-C, -R, -W and -X (FBG-C, -R, -W and -X). Pairwise alignment analysis was performed with Clustal Omega software to determine the % of identity among the FBG protein sequences.

	FBG -C	FBG -X	FBG -R
FBG-X	52.89 %	-	-
FBG-R	59.65 %	54.67 %	-
FBG-W	53.02 %	49.56 %	55.74 %

3.2. Cloning of FBG-R, -W and –X

FBG-C was expressed and purified as described previously [89]. The same approach was used to recombinantly synthesise FBG-R, -W and -X. PCR was performed to amplify the sequences of human FBG-R, -W and X and primers were designed to add an His-tag at the N-terminus for purification, and restriction sites (*Nde*I and *Xho*I) for cloning.

The DNA sequence of each FBG domain was first ligated into the pCRblunt vector, cloning validated by restriction enzyme digestion and verification of the correct size of the insert by gel electrophoresis (Figure 3-1). DNA was extracted from the gel and sequenced. The sequences of FBG-R, FBG-W and FBG-X were correct for all the clones validated. FBG-R, -W and -X were then cloned into the pET32b expression vector and the insert was verified by restriction enzyme digestion (Figure 3-2). This vector was transformed into *E. coli* BL21 (DE3) cells for protein over-expression.

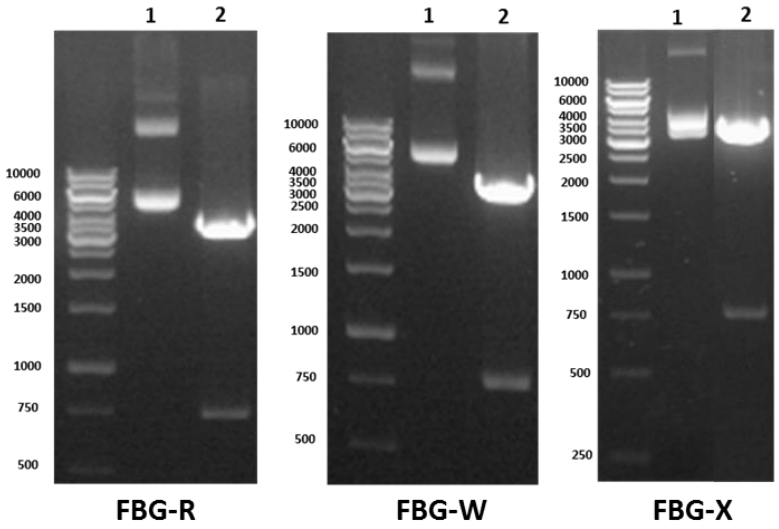

Figure 3-1. Cloning FBG -R, -W and -X into the pCRblunt vector. Each tenascin FBG was cloned initially into pCRblunt vector and the insert was verified by restriction digestion. On each gel, lane 1: Control, undigested vector. Lane 2: Vector digested with *Nde*I and *Xho*I. FBG-R (735 bp), FBG-W (762 bp) and FBG-X (732 bp) were successfully cloned into pCRblunt vector. 1.5% agarose gel stained with ethidium bromide.

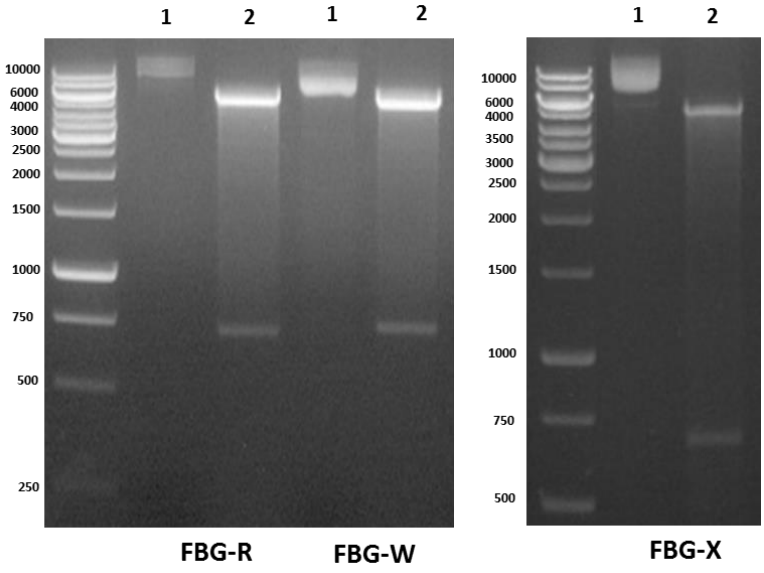

Figure 3-2. Cloning FBG-R, -W and -X into the pET32b vector. Each tenascin FBG was cloned into pET32b vector using *Nde*I and *Xho*I restriction sites and the insert was verified by restriction digestion. On each gel, lane 1: Control, undigested vector. Lane 2: Vector digested with *Nde*I and *Xho*. FBG-R (735 bp), FBG-W (762 bp) and FBG-X (732 bp) were successfully cloned into pET32b vector. 1.5% agarose gel stained with ethidium bromide.

3.3. Expression of FBG-R, -W and -X protein

The expression of FBG-R, -W and -X was assessed first in a small scale (20 mL) culture. Protein expression was induced by adding IPTG and monitored for 3 h. After 3 h, bacteria were lysed and the soluble and insoluble fraction (inclusion bodies) separated by centrifugation. FBG-R, -W and -X were successfully expressed and located in the inclusion bodies fraction (Figure 3-3 A) similarly to FBG-C [89]. Western blotting with an anti-His antibody confirmed that the induced bands at ~27 kDa were the proteins of interest (Figure 3-3 B).

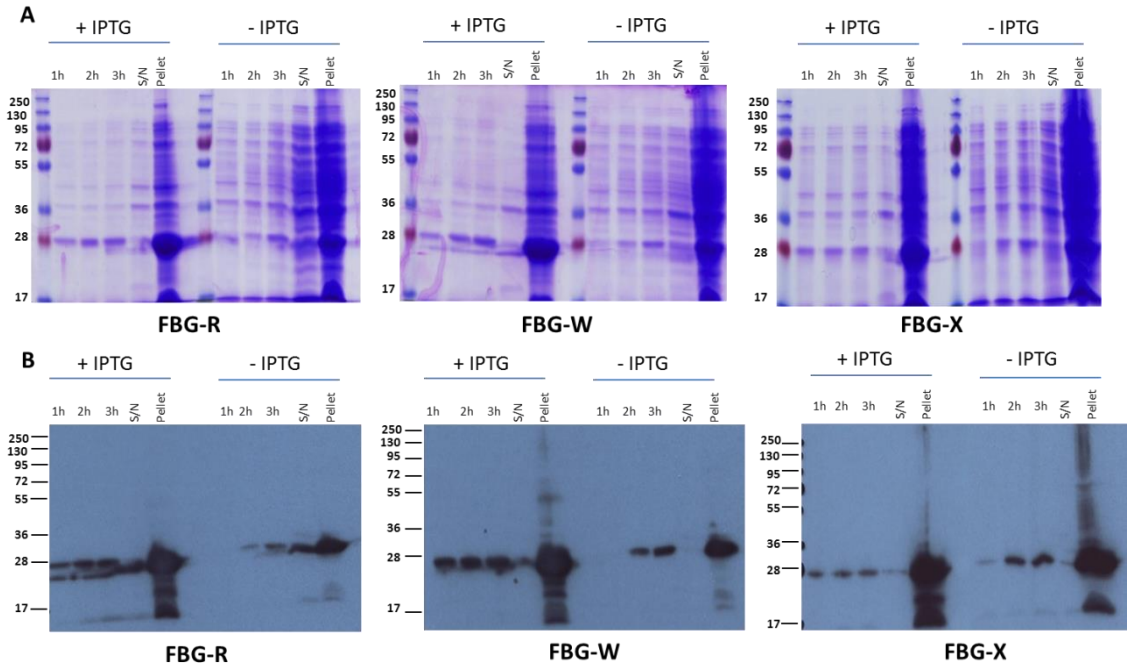

Figure 3-3. Successful small scale expression of FBG -R, -W and -X. *E. coli* BL21 DE3 cells were cultured + or – IPTG for 3 hours. A sample of the bacterial culture was taken every hour to monitor protein expression (1, 2 and 3 hours). Bacterial lysate was centrifuged at 3 h to separate supernatant (S/N) or soluble fraction from the inclusion bodies (pellet). **A.** 12 % SDS gel stained with Coomassie blue. **B.** Anti- His tag Western blot. FBG-R (27.0 kDa), FBG-W (27.6 kDa), FBG-X (26.1 kDa) FBG proteins are located in the inclusion bodies of the bacterial lysate. 10 µL of each sample was loaded on each well.

After verifying protein expression, the bacterial cultures were scaled up to 1 L to produce larger amounts of FBG-R, -W and -X. Large scale protein expression during 3

h was confirmed by SDS-PAGE gel electrophoresis and most of the protein was found in the inclusion bodies. Different levels of expression were observed for each FBG, where the expression of FBG-W was higher than FBG-R and –X (Figure 3-4). The inclusion bodies were solubilised in urea buffer for protein purification.

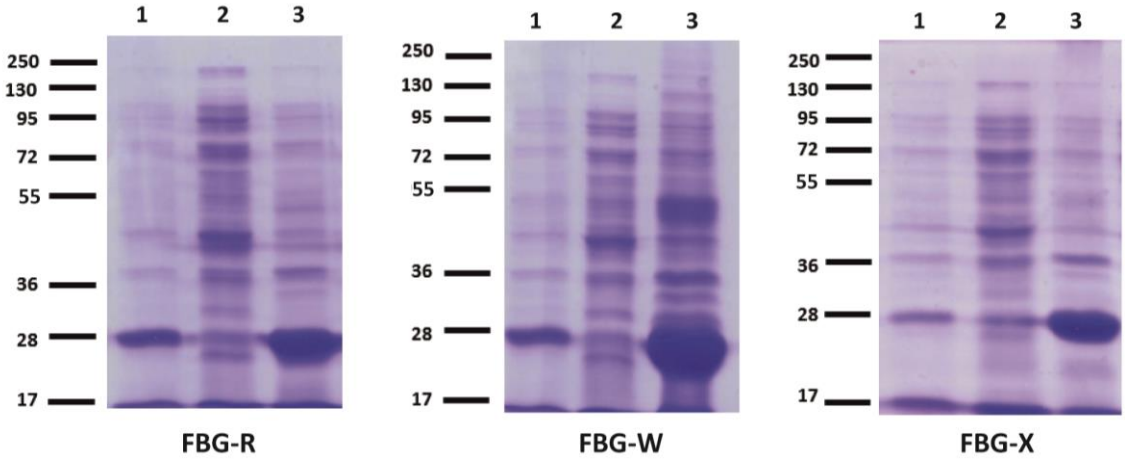

Figure 3-4. Large scale expression of FBG-R, -W and -X. Protein expression was induced during 3 h by adding IPTG to 1 L of bacterial culture. Lane 1: sample of bacterial culture 3 h after protein expression induction with IPTG. Lane 2: Soluble fraction from bacterial lysate. Lane 3: Inclusion bodies from bacterial lysate. FBG-R (27.0 kDa), FBG-W (27.6 kDa), FBG-X (26.1 kDa). FBG proteins are located in the inclusion bodies fraction. 12 % SDS gel stained with Coomassie blue. 10 µL of each sample was loaded on each well.

3.4. Protein purification and characterization

3.4.1. Protein purification

The recombinant FBG proteins contain an N-terminal His-tag sequence that allows purification using Ni^{2+} chromatography. The first step in the purification of the FBG domain of tenascin family members was a Ni^{2+}chromatography under denaturing conditions. This enables protein purification from other contaminant proteins in the inclusion bodies, after which it was refolded for 4 days by dialysis. The protocol was optimised for each protein according to their isoelectric points as this could affect the recovery of the protein after refolding.

Once the protein was refolded, the protein solution was loaded into a second Ni^{2+} column to concentrate and remove LPS contamination. Triton X-114 was added to the 2nd wash to remove LPS. A solution of 0.1% triton X-114 has been proved to be an effective method to remove LPS from protein samples without affecting protein activity [310, 311]. Protein was eluted with imidazole and 5 or 6 fractions of 1 mL each were collected (Figure 3-5).

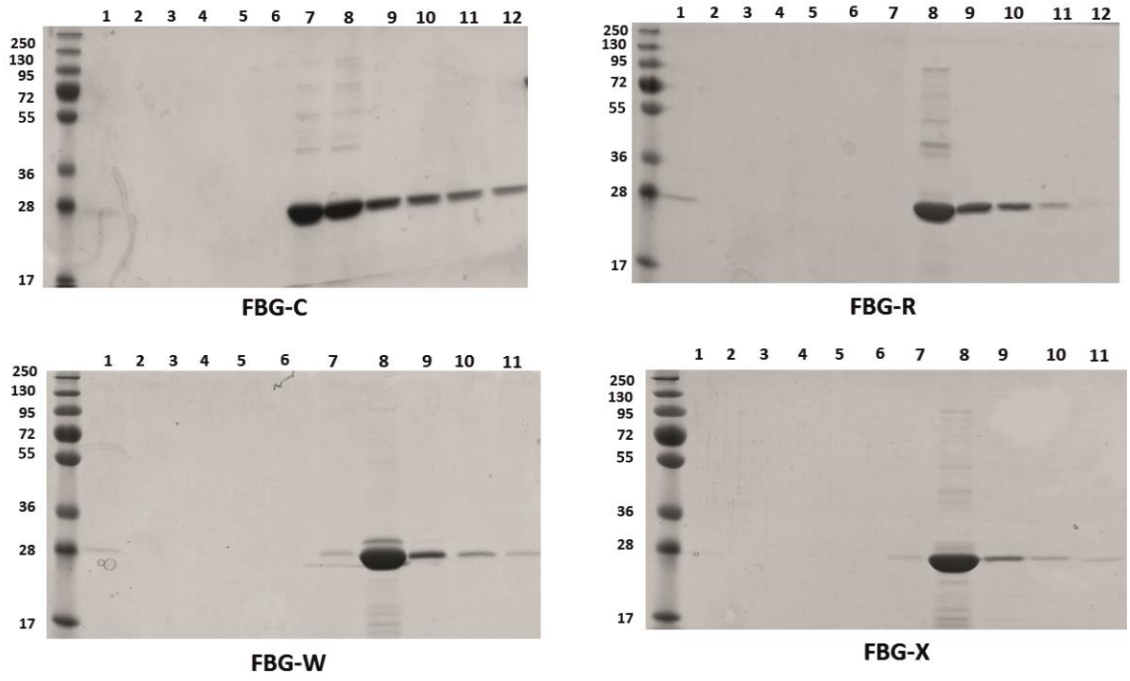

Figure 3-5. FBG-C, -R, -W, -X purification using Ni^{2+} chromatography. On each gel, lane 1: start material, refolded protein solution. Lane 2: Flow through. Lane 3: first wash with TN buffer. Lane 4: Triton X-114 wash. Lane 5: second wash with TN buffer. Lane 6: 20 mM Imidazole wash. Lane 7: 1° FBG fraction. Lane 8: 2° FBG fraction. Lane 9: 3° FBG fraction. Lane 10: 4° FBG fraction. Lane 11: 5° FBG fraction. Lane 12: 6° FBG fraction. 12 % SDS gel stained with Coomassie blue. 10 µL of each sample was loaded on each well.

Western blot using antibodies against the His-tag or specific for the FBG domain of each protein were used to confirm protein identity of each of the fractions after protein purification (Figure 3-6). Antibodies against the FBG domain of tenascin-W are not commercially available, therefore only anti-His tag western blot was performed for this protein. The fractions free from protein contaminants were pooled and dialysed

against TN buffer to remove the imidazole and afterwards, the protein concentration was measured. On average the yields for each protein per 1 L of bacterial culture were: FBG-C: 5.3 mg; FBG-R: 2.31 mg; FBG-W: 2.46 mg; and FBG-X: 1.2 mg.

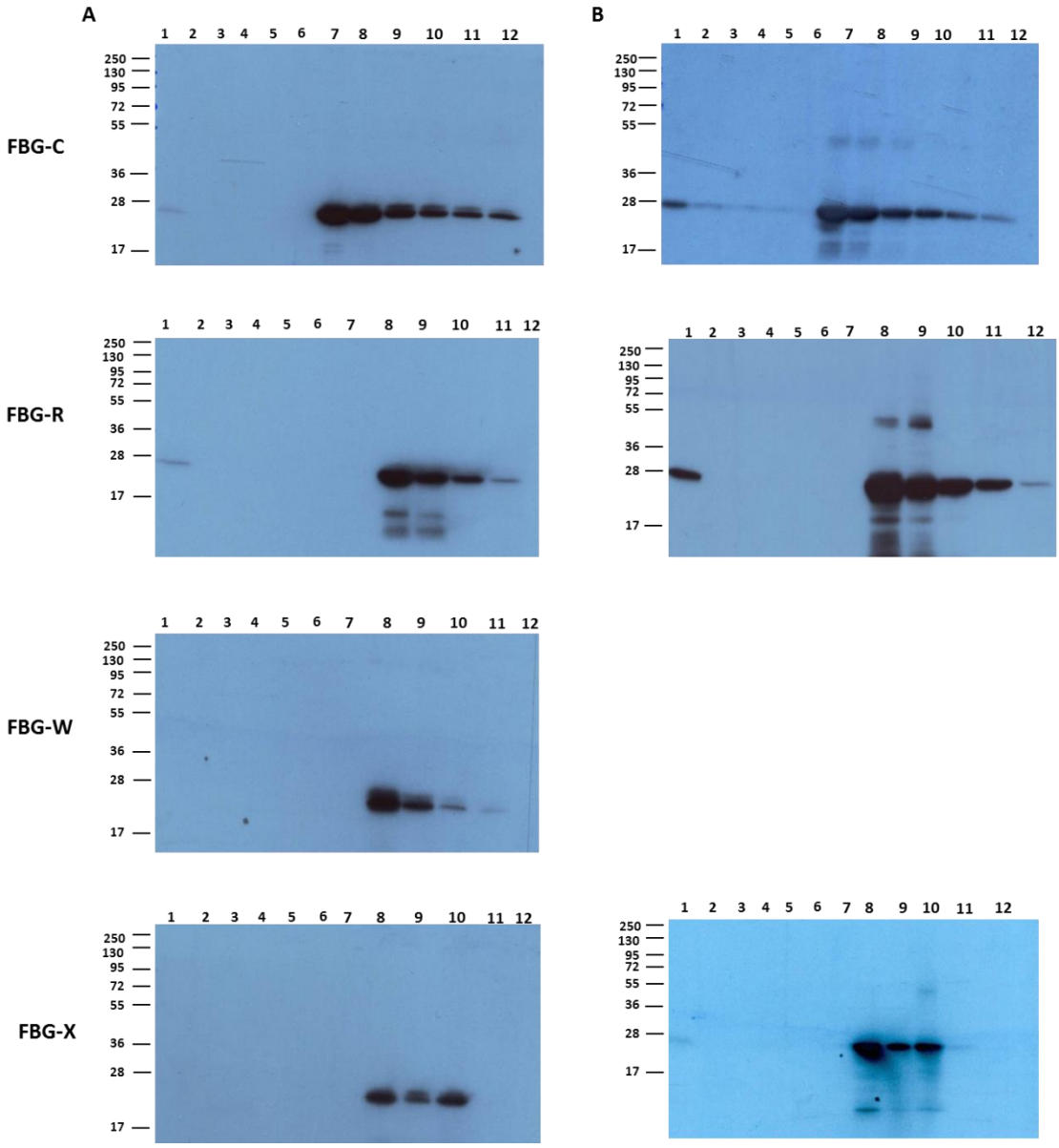

Figure 3-6. Anti-His tag western blot of FBG-C, -R, -W and -X and anti-FBG western blots of FBG-C, -R and -X protein fractions from Ni^{2+} chromatography. Protein identity was confirmed by western blots using antibodies against the His tag (**A**) or the FBG domain (**B**). Lane 1: start material, refolded protein solution. Lane 2: flow through. Lane 3: first wash with TN buffer. Lane 4: Triton X-114 wash. Lane 5: second wash with TN buffer. Lane 6: 20 mM Imidazole wash. Lane 7: 1° FBG fraction. Lane 8: 2° FBG fraction. Lane 9: 3° FBG fraction. Lane 10: 4° FBG fraction. Lane 11: 5° FBG fraction. Lane 12: 6° FBG fraction. 10 µL of each sample was loaded on each well.

3.4.2. Protein characterization

To verify the protein purity after Ni^{2+} chromatography, 1 µg of protein was loaded into a SDS gel. Silver staining showed that all the proteins after purification are pure and do not contain contaminants from other proteins (Figure 3-7 A). An additional band was observed in FBG-W sample, which could correspond to a protein variant formed during the refolding process; or to incomplete protein reduction after treatment with β-ME resulting in two contiguous bands when run in the SDS gel. Anti-His western blot was performed to confirm protein identity on these samples (Figure 3-7 B).

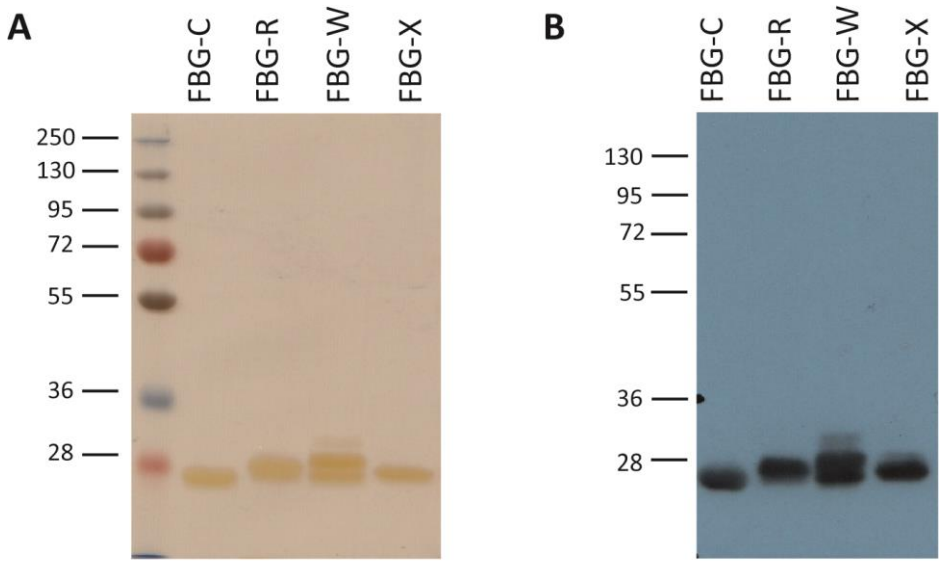

Figure 3-7. SDS PAGE characterization of FBG-C, -R, -W and -X. A. Protein purity was verified by silver staining of 1 µg of FBG-C, -R, -W and -X. **B.** Anti-His tag western blot of 1 µg of FBG-C, -R, -W and -X.

The LPS content of each FBG was measured using the chromogenic LAL assay and all proteins were found to contain less than 10 pg/mL of LPS. To verify protein refolding, circular dichroism (CD) spectroscopy was used. This technique allows assessment of changes in protein secondary structure. Each tenascin FBG domain had a negative peak in their spectra near 220 nm at 20 ºC (Figure 3-8 A), which was lost at 85°C, indicating that these proteins were originally refolded (Figure 3-8 B). Together these data showed that the purification of the FBG domain of the tenascin family members was successful, all the protein samples contain less than 10 pg/mL of LPS and are refolded.

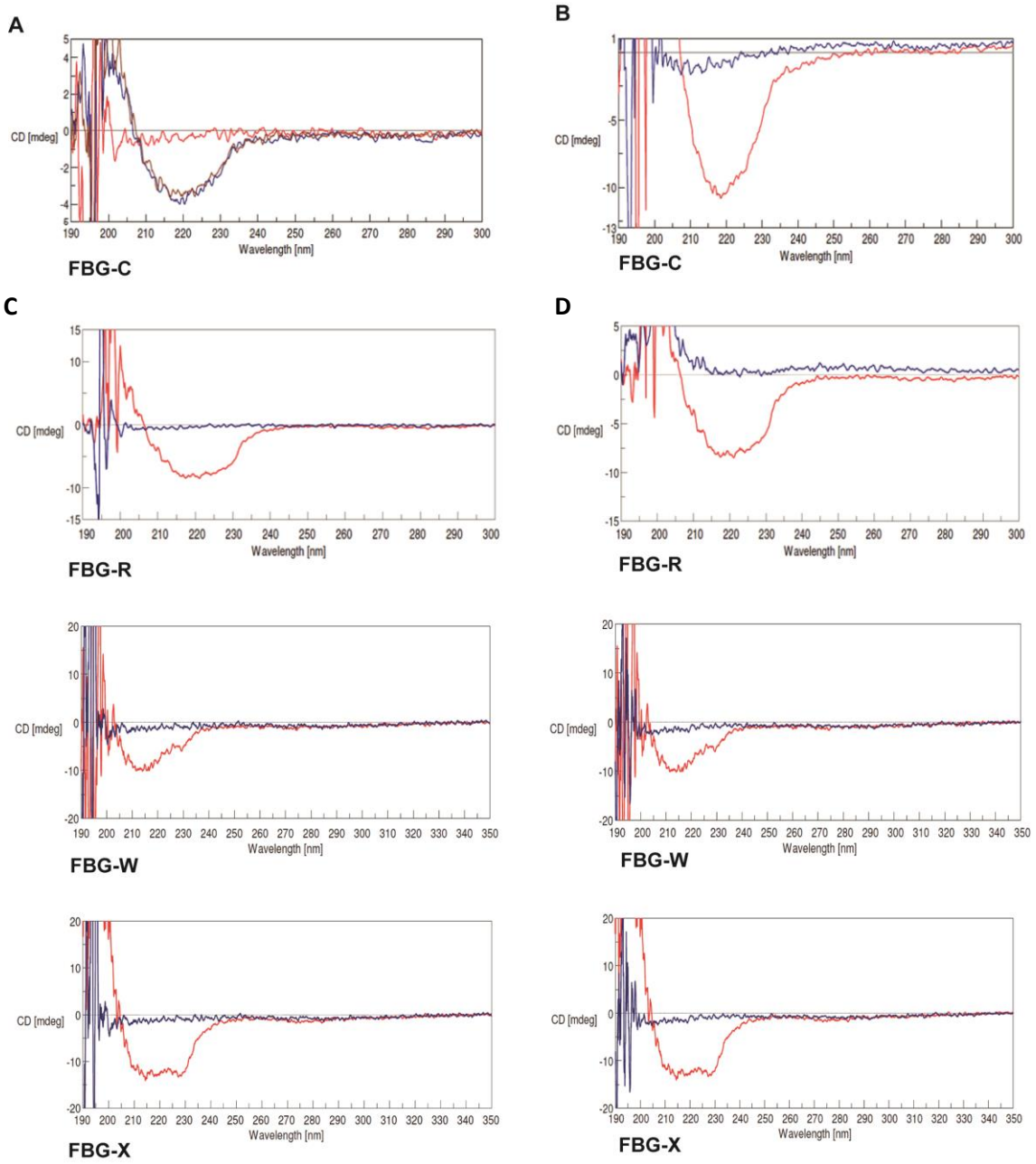

Figure 3-8. Circular dichroism (CD) spectroscopy measurements of FBG-C, -R, -W and -X. 200 µL of each sample in TN buffer were analysed using the J-815 Circular Dichroism Spectrometer. The CD spectra were determined in the "far UV" spectral region (190-250 nm). FBG-C CD spectra **A.** Negative control: TN buffer (red); positive control: reference refolded FBG-C (brown); and FBG-C sample (blue) **B.** CD spectra of FBG-C sample at 20 °C (red) and at 85 °C (blue). FBG -R, -W and -X **C.** CD spectra of negative control: TN buffer (blue); FBG-R, -W and -X sample (red) **D.** CD spectra of FBG-R, -W and -X sample at 20 °C (red) and at 85 °C (blue).

Correct protein refolding was also assessed by gel filtration to verify that the samples obtained were not refolded as protein aggregates. Gel filtration showed a small peak corresponding to the protein dimer and a large peak corresponding to the protein monomer, which is the most abundant form in the refolded material (Figure 3-9 A). These results were corroborated by SDS gel under non-reducing conditions, where it is shown that the protein is refolded mainly as a monomer using these conditions (Figure 3-9 B).

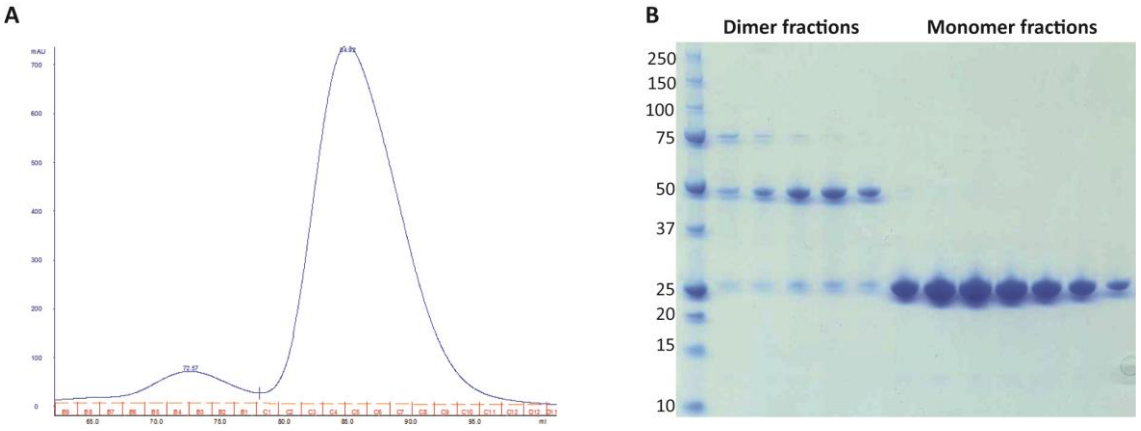

Figure 3-9. Gel filtration chromatography of FBG-C. A. Chromatograph of FBG-C fractions during gel filtration purification using Superdex 75 column (GE healthcare). First peak correspond to fractions containing protein dimer and second peak correspond to fractions containing protein monomer. **B.** SDS-PAGE gel under non-reducing conditions showing fractions from gel filtration column corresponding to the first peak (protein dimer) and second peak (protein monomer). 12 % SDS gel stained with Coomassie blue. 10 µL of each sample was loaded on each well.

3.5. Protein activity in ThP1 NF-κB cells

3.5.1. Optimisation of protein activity assay in ThP1 NF-κB cell line

The ThP1 NF-κB cell is a monocytic cell line, which has an NF-κB reporter gene. Upon activation of TLR4, NF-κB transcription factor is translocated to the nucleus to activate the transcriptional machinery of pro-inflammatory genes. This cell line has a soluble embryonic alkaline phosphatase (SEAP) gene downstream of NF-κB activation which is secreted to the media. The amount of SEAP in the media correlates with the activation of NF-κB and it is measured using QUANTI-Blue™, a colorimetric reagent. The cell line was optimised to be used as a screening protocol to determine FBG protein activity, as it is a quick method to assess activation of NF-κB transcription factor downstream of TLR activation. To determine the optimal dose and time point for assessing NF-κB activation in this cell line, ThP1 NF-κB cells were stimulated with different doses of LPS or FBG-C, and NF-κB activation was measured at different time points. The results showed that 0.5 ng/mL of LPS or 0.5 μM of FBG-C is sufficient to induce similar levels of NF-κB activation, and a robust reading after cell stimulation was obtained at 24 h (Figure 3-10).

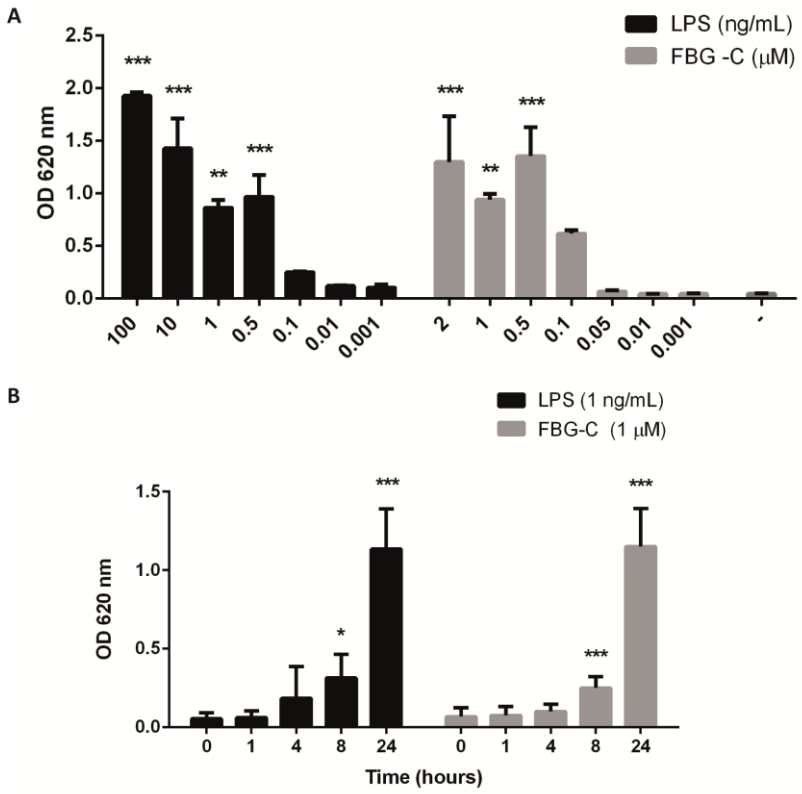

Figure 3-10. Time course and dose response of NF-κB activation in ThP1 NF-κB cells. **A**. Cells were stimulated with different doses of LPS or FBG-C or left unstimulated (-) and after 24 h NF-κB activation was measured using QUANTI-Blue™. **B.** Cells were stimulated with 1 ng/mL of LPS or 1 μM FBG-C and NF-κB activation was measured using QUANTI-Blue™ at different time points. Data shown as mean ± SEM, N=3 independent experiments. One-way ANOVA vs time 0 h or non-stimulated, *p<0.05, **p<0.01, ***p<0.001.

To confirm that the FBG-C activity was not due to LPS contamination, LPS and FBG-C were pre-incubated with polymyxin B for 30 min, or boiled for 15 min prior to cell stimulation. Polymyxin B binds to lipid A chain of LPS and inhibits pathogenic activation of TLR4, however it doesn't affect the FBG-C activity. Boiling the samples doesn't affect LPS activity but denatures the protein, inhibiting FBG-C activity (Figure 3-11).

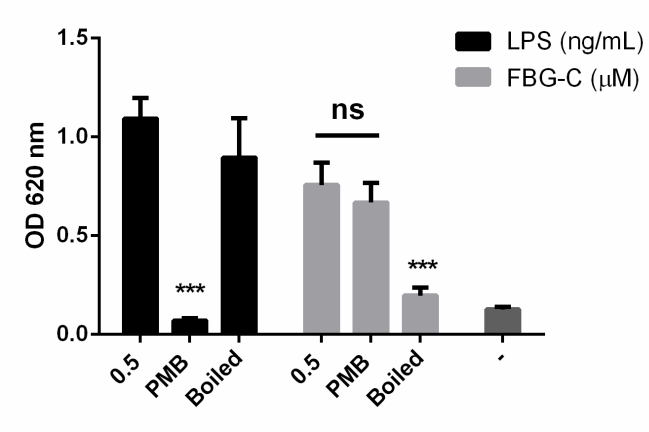

Figure 3-11, Effect of polymyxin B (PMB) and boiling on LPS and FBG-C activity in ThP1 NF-κB cells. Cells were left unstimulated (-) or stimulated with LPS or FBG-C pre-incubated with PMB for 30 min or boiled for 15 min. NF-κB activation was measured using QUANTI-Blue™. Data shown as mean ± SEM, N=4 independent experiments. Paired t-test vs non-treated, ***p<0.001.

Further characterisation of this cell line revealed that the levels of SEAP in the media and NF-κB activation diminished after several passages (Figure 3-12 A). In addition, ThP1 NF-κB cells expressed very low levels of pro-inflammatory cytokines (IL-6, IL-8 and TNF), even when NF-κB transcription factor was activated (Figure 3-12 B).

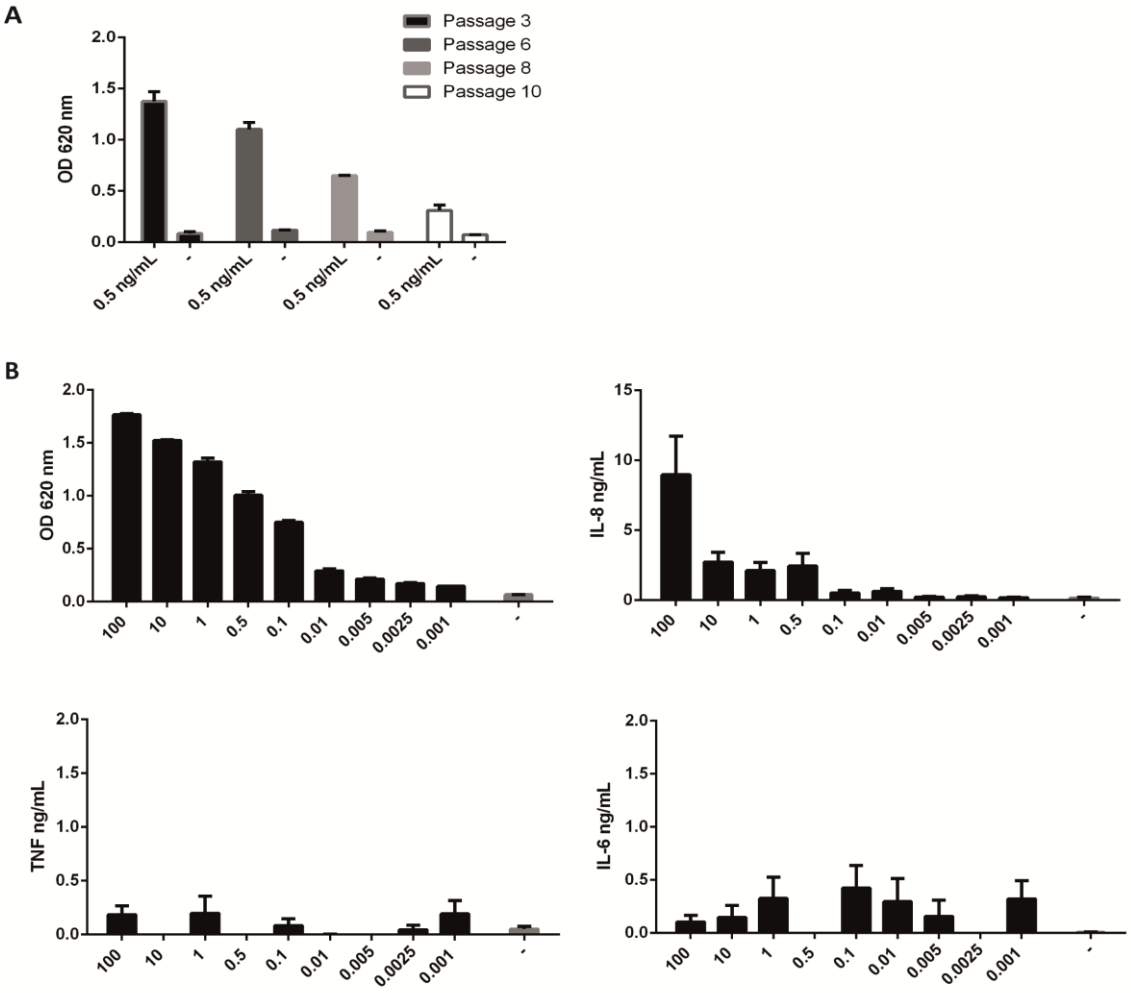

Figure 3-12. Characterization of ThP1 NF-κB cells. A. Cells from different passages were stimulated with 0.5 ng/mL of LPS or left unstimulated (-) and NF-κB activation was measured after 24 h using QUANTI-Blue™. Data shown as mean ± SEM, N=3. **B**. Cells were stimulated with different doses of LPS or left unstimulated (-) and NF-κB activation was measured after 24 h using QUANTI-Blue™; or cytokine synthesis was measured by ELISA. Data shown as mean ± SD, N=2 independent experiments.

Together these data demonstrated that the ThP1 NF-κB cell line is a quick screening method to measure FBG protein activity via activation of the NF-κB transcription, but it is not suitable to measure cytokine synthesis by FBG-C.

3.5.2. Activity of the FBG domain of tenascin family members in ThP1 NF-κB cells

The activity of the recombinant proteins FBG-R, -W and -X was measured in the ThP1 NF-κB cells. FBG-R and -W can induce the activation of NF-κB in a dose dependent manner similarly to FBG-C, but very little activation was observed for FBG-X. In addition, MTT assay was performed to check cell viability in the presence of the recombinant proteins. No effect was observed in cell viability after stimulation with the FBG domain of the tenascin family members compared to non-stimulated cells (Figure 3-13).

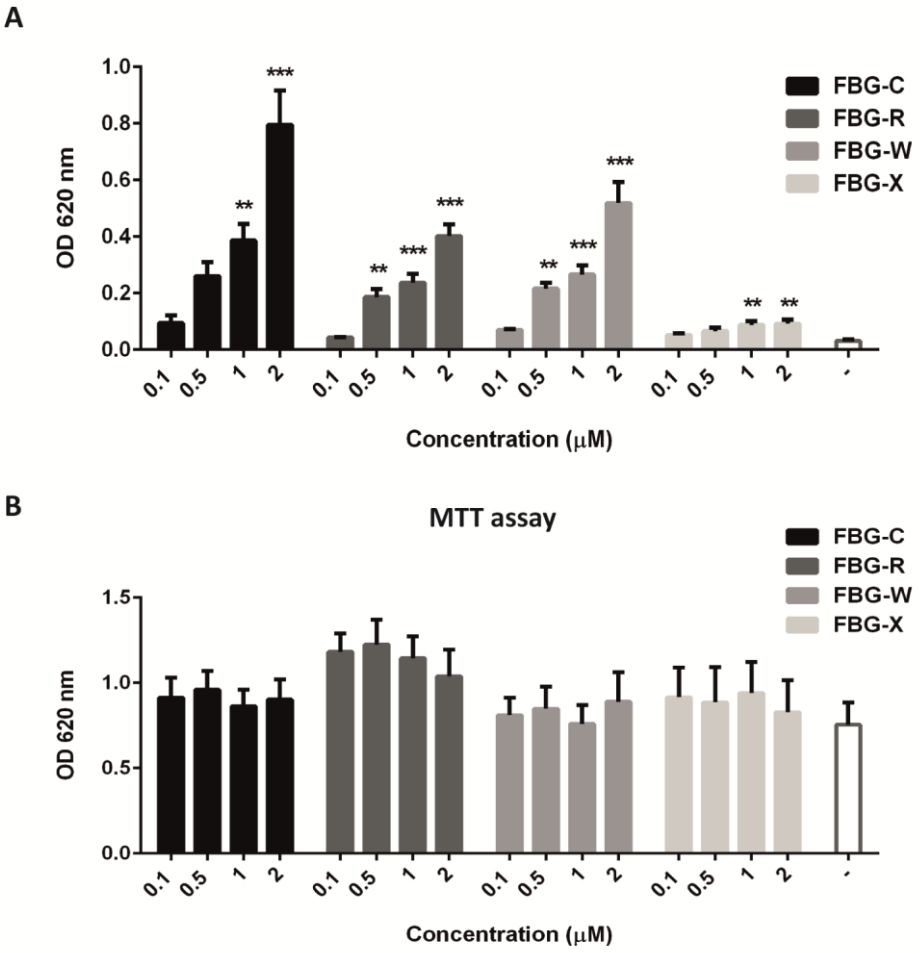

Figure 3-13. FBG-C, -R, -W and -X activation of NF-κB in ThP1 NF-kB cells. **A**. ThP1 NF-κB cells were left unstimulated (-) or stimulated with different doses of FBG-C, -R, -W and -X for 24 h and NF-κB activation was measured using QUANTI-Blue™. **B.** MTT assay of ThP1 NF-κB cells stimulated with different doses of FBG-C, -R, -W and -X or left unstimulated (-) for 24 h. Data shown as mean ± SEM, N=3 independent experiments. One-way ANOVA vs non-stimulated, *p<0.05, **p<0.01, ***p<0.001.

FBG-C, -R, -W and -X were treated with polymyxin B or boiled to verify that protein activity was not due to LPS contamination. The activity of FBG-C, -R and -W was not inhibited by the treatment with polymyxin B; however it was lost by boiling due to protein denaturation. FBG-X activity was affected by polymyxin B treatment indicating that the low activity of FBG-X could be due to low levels of LPS contamination (Figure 3-14).

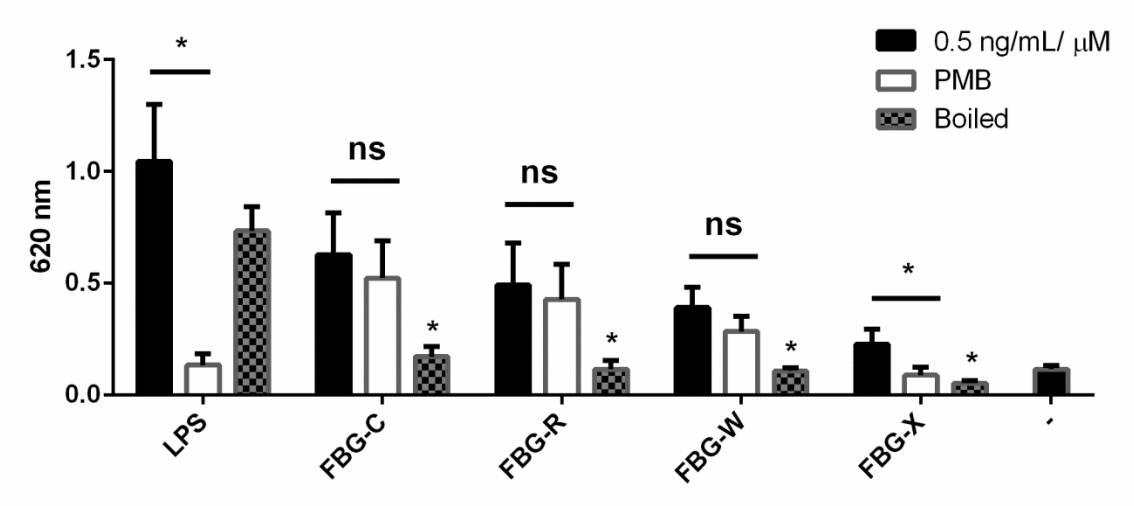

Figure 3-14. FBG-C, -R and -W activity in ThP1 NF-κB cells is not due to LPS contamination. ThP1 NF-κB cells were left unstimulated (-) or stimulated with 0.5 ng/mL of LPS or 0.5 μM of FBG-C, -R, -W and -X incubated for 30 min with polymyxin B (PMB) or boiled for 15 min. NF-κB activation was measured after 24 h using QUANTI-Blue™. Data shown as mean ± SEM, N=3 independent experiments. Paired t-test PMB or boiled vs non-treated, *p<0.05.

3.6. Protein activity in primary human macrophages

Measuring protein activity in ThP1 NF-κB cell line is an effective and quick method to determine the activation of NF-κB transcription factor by inflammatory stimuli. However, these cells produce low levels of cytokines after FBG or LPS stimulation and a more relevant system is required to measure the protein ability to induce pro-inflammatory cytokines. Thus, the protein activity of FBG-R, -W and -X was also evaluated in primary human macrophages and cytokine synthesis was measured by ELISA. Similarly to FBG-C, FBG-R and -W could induce IL-6, IL-8 and TNF in a dose dependent manner. However, FBG-X did not induce IL-6, and induced very little TNF and IL-8 compared to the other FBG domains of the tenascin family members (Figure 3-15 A). MTT assays were performed and showed that stimulation of primary human macrophages with the FBG domain of the tenascin family members didn't affect cell viability compared to non-stimulated cells (Figure 3-15 B).

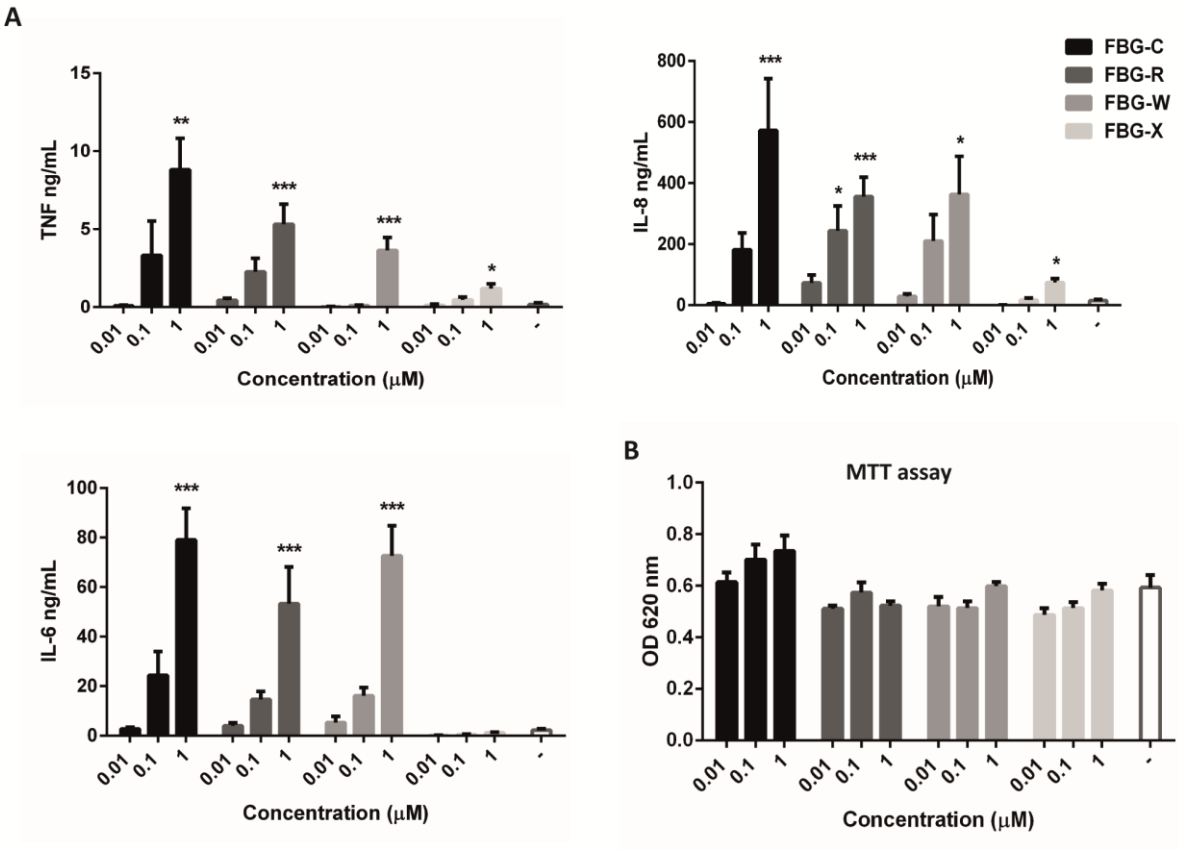

Figure 3-15. FBG-C, -R and -W can induce pro-inflammatory cytokines in primary human macrophages. A. Primary human macrophages were left unstimulated (-) or stimulated with different doses of FBG-C,-R, -W and -X pre-treated with PMB for 30 min. Cytokine synthesis was measured after 24 h by ELISA. **B.** MTT assay of primary human macrophages non-stimulated (-) or stimulated with different doses of FBG-C, -R, -W and -X for 24 h. Data shown as mean ± SEM, N=3 independent donors. One-way ANOVA vs non-stimulated, *p<0.05, **p<0.01, ***p<0.001.

To verify that cytokine induction was not due to LPS contamination of the protein samples, FBG-C, -R, -W and -X were treated with polymyxin B for 30 min or boiled for 15 min. Polymyxin B treatment inhibited LPS cytokine induction but did not affect the activity of FBG-C, -R and -W. However, FBG-X activity was affected by polymyxin B indicating low levels of LPS contamination. Boiling did not inhibit LPS cytokine induction in macrophages but denatured FBG-C, -R, -W and -X and reduced their pro-inflammatory activity (Figure 3-16).

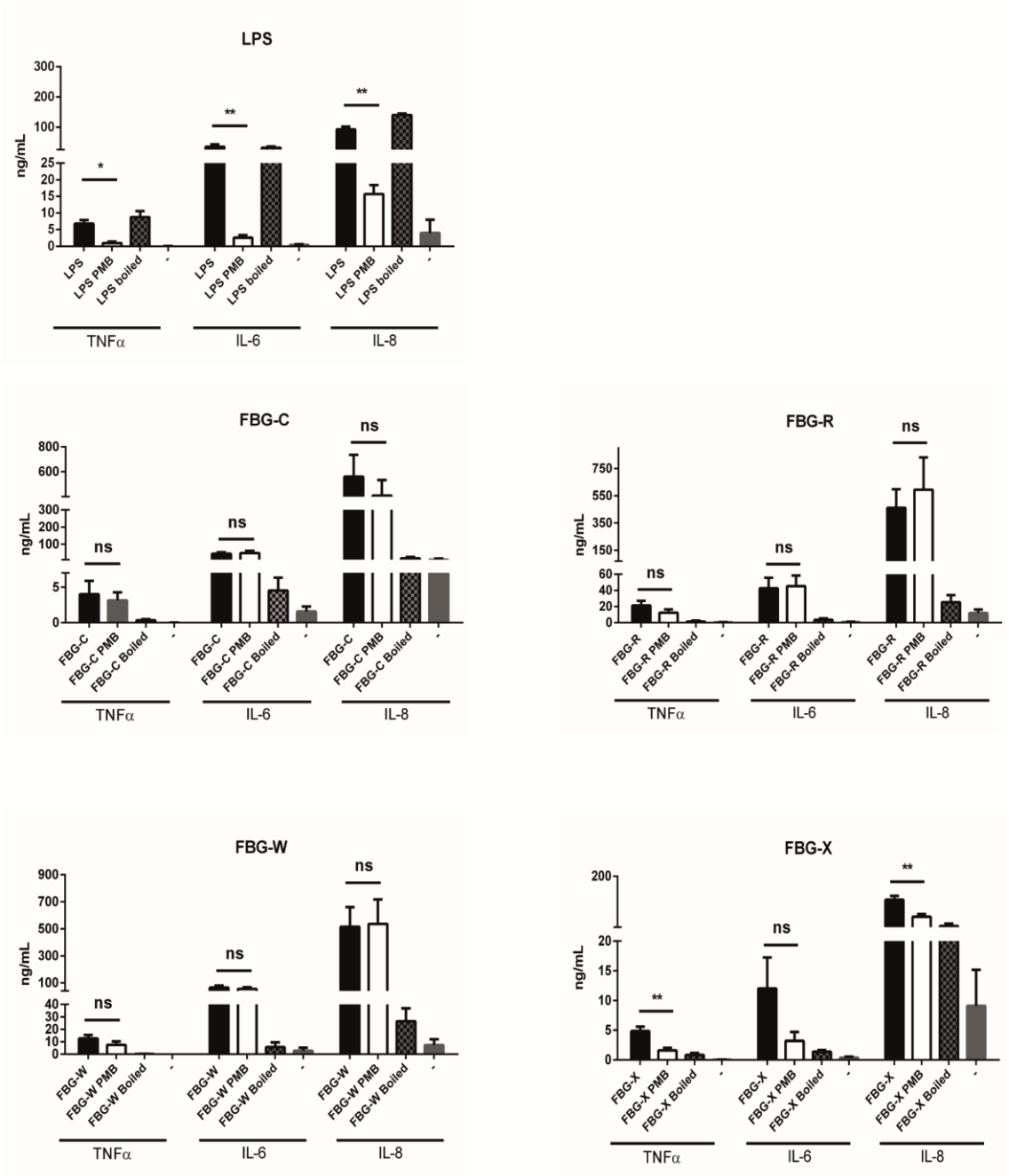

Figure 3-16. FBG-C, -R and -W activity is not due to LPS contamination. Primary human macrophages were left unstimulated (-) or stimulated with 1 ng/mL of LPS or 1 µM of FBG-C, -R, -W or -X for 24 h. Samples were previously incubated for 30 min with polymixyn B (PMB) or boiled for 15 min. Cytokine synthesis was measured by ELISA. Data shown as mean ± SEM, N=3 independent donors. Paired t-test vs non-treated, *p<0.05, **p<0.01, ***p<0.001.

3.7. TLR4 dependency of FBG-C, -R and -W

3.7.1. ThP1 NF-κB cells

FBG-C has been shown to induce cytokine synthesis by activating TLR4 in immune cells [89]. For that reason, I investigated if the pro-inflammatory activity of FBG-R and -W is also TLR4 dependent. The first approach was to use a polyclonal TLR4 function-blocking antibody. TLR4 antibody doses were titrated in ThP1 NF-κB cells stimulated with LPS or FBG-C. TLR4 antibody was effective at inhibiting LPS activity at a concentration of 1, 10 and 25 µg/mL, but no significant effect was observed in the cells stimulated with FBG-C. MTT assay was performed to verify that the doses used didn't affect cell viability (Figure 3-17).

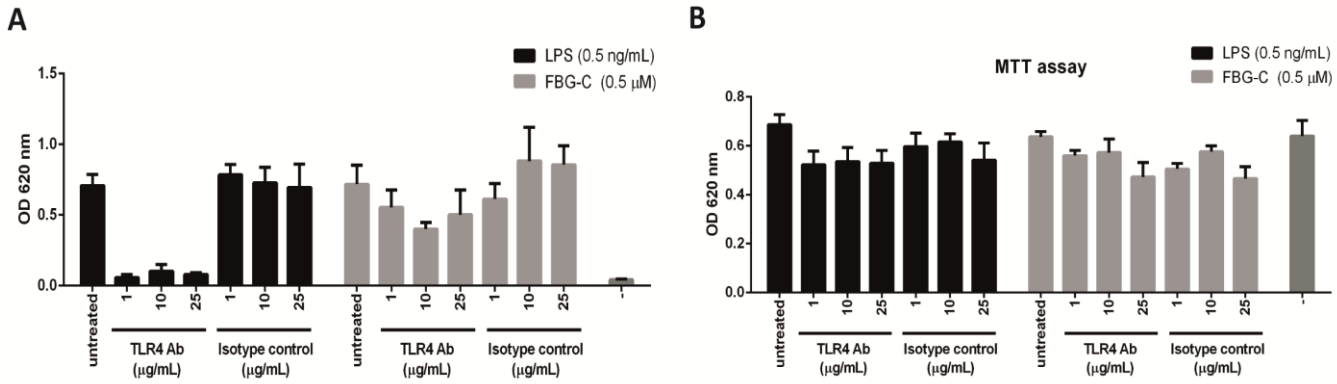

Figure 3-17. Titration of anti-human TLR4 antibody (Ab) in ThP1 NF-κB cells. A. ThP1 NF-κB cells were pre-incubated for 1 h with different doses of the TLR4 Ab or isotype control, prior to stimulation with 0.5 ng/mL of LPS or 0.5 µM of FBG-C. NF-κB activation was measured after 24 h using QUANTI-Blue™. **B.** MTT assay of ThP1 NF-κB cells pre-incubated for 1 h with different doses of the TLR4 antibody or isotype control, prior stimulation with 0.5 ng/mL of LPS or 0.5 µM of FBG-C during 24 h. (-) unstimulated cells. Data shown as mean ± SEM, N=3 independent experiments.

Another approach used to determine TLR4 dependency was pre-incubating the cells with a TLR4 inhibitor (TAK 242). A titration of doses of TAK 242 was performed in the ThP1 NF-κB cells using LPS and FBG-C as positive controls. TAK 242 is dissolved in DMSO, and a DMSO solution at the highest equivalent concentration used was added as a control. TAK 242 was very efficient at inhibiting LPS activity at a concentration >1 μM, but it didn't inhibit FBG-C activity in ThP1 NF-κB cells. The MTT assay confirmed that the TLR4 inhibitor is not toxic to the cells, even at high concentration (10 μM). A similar pattern of inhibition was observed when the cells were stimulated with the different FBG domains of the tenascin family members. While TAK 242 was not able to significantly reduce the activity of these proteins, it could successfully inhibit LPS-induced NF-κB activation in ThP1 NF-κB cells (Figure 3-18). Together, these data showed that the activation of NF-κB by FBG-C is different compared to LPS and confirm LPS-independent activity of FBG-C, -R and -W.

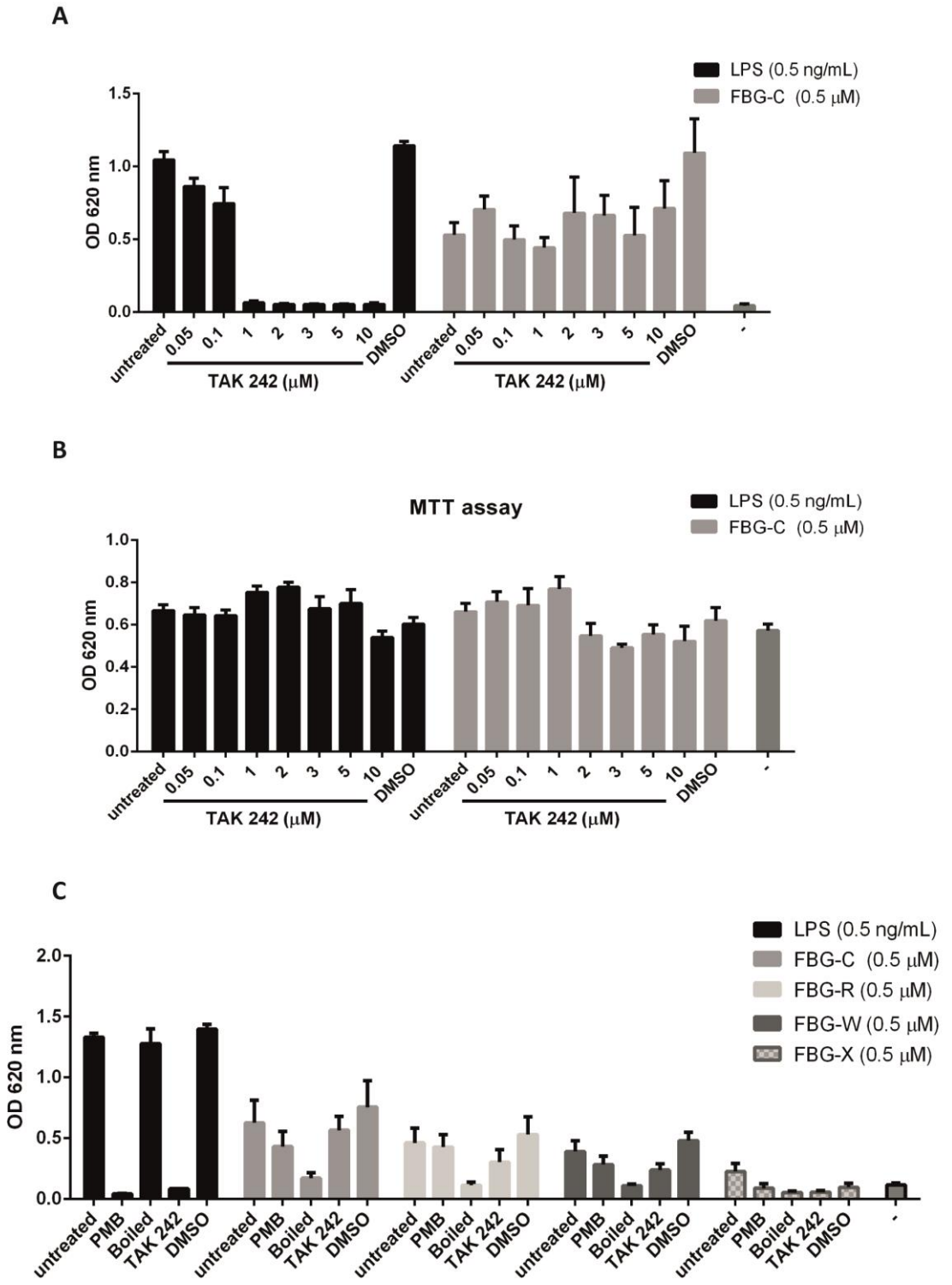

Figure 3-18. Titration of the TLR4 inhibitor TAK 242 in ThP1 NF-κB cells. A. ThP1 NF-κB cells were pre-incubated for 6 h with different doses of the TLR4 inhibitor TAK 242 or DMSO control, prior stimulation with 0.5 ng/mL of LPS or 0.5 μM of FBG-C. NF-κB activation was measured after 24 h using QUANTI-Blue™. **B.** MTT assay of ThP1 NF-κB cells pre-incubated with TAK 242 or DMSO and stimulated with 0.5 ng/mL of LPS or 0.5 μM of FBG-C during 24 h. **C.** ThP1 NF-κB cells were pre-incubated for 6 h with 3 μM of TAK 242 or DMSO control, PMB for 30 min or boiled for 15 min, prior stimulation with 0.5 ng/mL of LPS or 0.5 μM of FBG-C, -R, -W or -X during 24 h. NF-κB activation was measured after 24 h using QUANTI-Blue™. Data shown as mean ± SEM, N=3 independent experiments.

3.7.2. Cytokine synthesis in primary human macrophages

TLR4 dependency was also tested in primary human macrophages, as previously reported for FBG-C [89], to determine if FBG-R and -W were inducing cytokine synthesis via this receptor. Primary human macrophages were pre-incubated with 3 µM of TAK 242, a dose that has been shown to effectively inhibit LPS and DAMP-induced TLR4 activation [312-314]. In primary human macrophages, TAK 242 significantly inhibited the induction of cytokines by LPS, FBG-C, -R and -W (Figure 3-19). The percentage of inhibition of TAK 242 was higher for LPS (>90% inhibition) compared to the FBG proteins (65-85 % inhibition). Among all cytokines, IL-8 showed the lowest levels of inhibition by TAK 242 when cells were stimulated with the FBG proteins (67-79% inhibition) (Table 3-2).

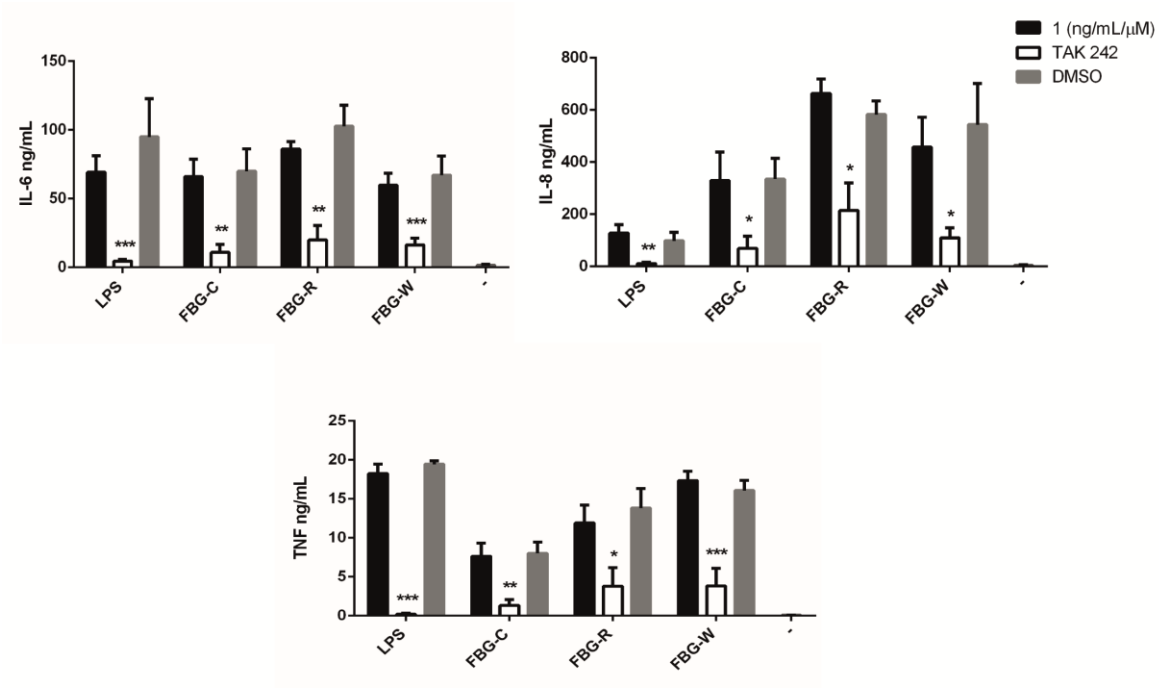

Figure 3-19. TAK 242 can inhibit cytokine induction by LPS, FBG-C, -R and -W. Primary human macrophages were pre-incubated for 6 h with 3 µM of TAK 242, prior stimulation with 1 ng/mL of LPS or 1 µM of FBG-C,-R, -W. Cytokine synthesis was measured after 24 h by ELISA. (-) unstimulated cells. Data shown as mean ± SEM, N=3 independent donors. Paired t-test vs non-treated, *p<0.05, **p<0.01, ***p<0.001.

Table 3-2. % of inhibition of LPS, FBG-C, -R and -W activity by TLR4 inhibitor TAK 242.

Stimulus	IL-6	IL-8	TNF
LPS	93.59	91.97	98.97
FBG-C	83.53	79.22	82.95
FBG-R	76.95	67.72	68.23
FBG-W	72.85	76.18	78.00

A function-blocking anti-TLR4 antibody was also used in primary human macrophages to determine TLR4 dependency. A dose of 25 µg/mL was chosen as it was shown previously to block effectively protein activity on these cells [89]. TLR4 antibody significantly inhibited the activity of LPS, FBG-C, -R and -W (Figure 3-20). More specifically, it was very effective at inhibiting TNF and IL-6 synthesis by LPS, FBG-C, -R and -W. Lower levels of inhibition were observed for IL-8 induction by LPS and FBG-W (Table 3-3).

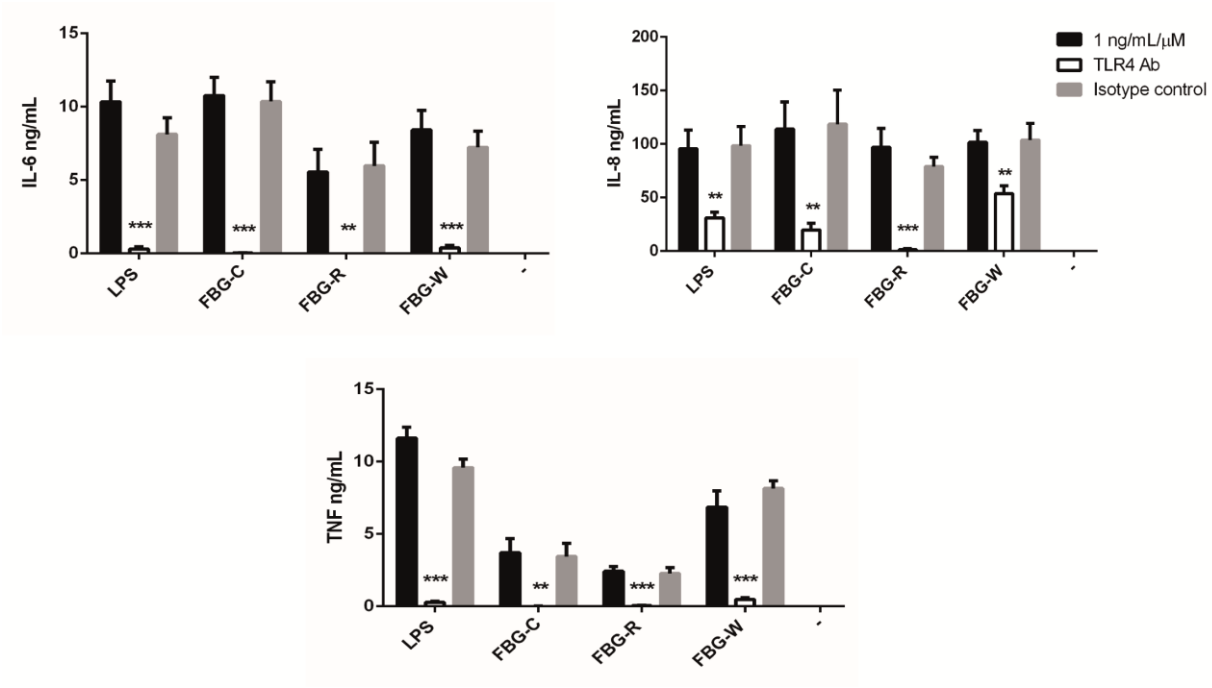

Figure 3-20. TLR4 antibody (Ab) can inhibit cytokine synthesis by LPS, FBG-C, -R and -W. Primary human macrophages were pre-incubated for 1 h with 25 µg/mL of TLR4 Ab or isotype control, prior stimulation with 1 ng/mL of LPS or 1 µM of FBG-C,-R, -W. Cytokine synthesis was measured after 24 h by ELISA. (-) unstimulated cells. Data shown as mean ± SEM, N=3 independent donors. Paired t-test vs non-treated, *p<0.05, **p<0.01, ***p<0.001.

Table 3-3. % of inhibition of LPS, FBG-C, -R and -W activity by TLR4 antibody.

Stimulus	IL-6	IL-8	TNF
LPS	97.31	67.58	97.83
FBG-C	99.84	82.71	99.78
FBG-R	100	98.82	98.48
FBG-W	95.54	47.39	93.15

Together these data showed that FBG-R and -W also signal through TLR4 and induce cytokine synthesis similarly to FBG-C.

3.8. Solid phase binding to TLR4

To assess direct binding of FBG-C to TLR4, a solid phase binding assay was developed. Dr. Anna Piccinini established a protocol where 96 MaxiSorp well plates were coated with TLR4 and different domains of tenascin-C were then added in a dose dependent manner to determine their binding affinity to the receptor. The data showed that only FBG-C binds to TLR4 while other domains, including the FNIII repeats (1-3, 3-5 and 6-8), do not bind to the receptor or to wells coated with PBS as a negative control. In addition, it was investigated if FBG-C could bind to other members of the TLR family. The wells were coated with TLR2, TLR3 or TLR4 and FBG-C was added in a dose dependent manner. The results showed that FBG-C binds with the highest affinity to TLR4, and with lower affinity to TLR2, while it does not bind to TLR3 (Figure 3-21).

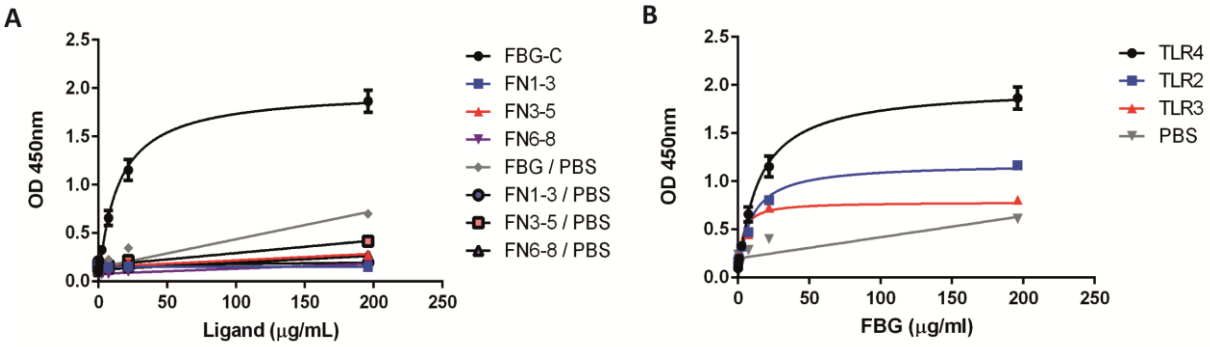

Figure 3-21. Solid phase binding assay of tenascin-C domains to TLRs. A. 96 well plates were coated with TLR4 or PBS and different tenascin-C domains were added in a dose dependent manner. Curve fitted using one binding site (hyperbola) function and data is shown as mean ± SEM, N=3 for FBG-C, N=2 for fibronectin-type 3 repeats. FN 1-3: fibronectin-type 3 repeats 1-3. FN 3-5: fibronectin-type 3 repeats 3-5, FN 6-8: fibronectin-type 3 repeats 6-8. **B.** 96 well plates were coated with TLR4, TLR2, TLR3 or PBS and FBG-C were added in a dose dependent manner. Curve fitted using one binding site (hyperbola) function and data is shown as mean ± SEM, N=3 for TLR4, N=2 for TLR2 and TLR3.

This method relies on detecting the FBG domain using an anti-FBG antibody. Due to the lack of antibodies for all the FBG domains of the tenascin family members, the solid phase binding assay was then reversed. Specifically, I coated 96 wells plates with the FBG domains and TLR4 was added in a dose dependent manner to determine the affinity of the two proteins using the dissociation constant (K_D value). Additionally, it was investigated if FBG-C could bind to TLR4 when it is in complex with MD-2. MD-2 is a co-receptor necessary for the activation of TLR4 by LPS. Our group have previously found that FBG-C activation of TLR4 does not require MD-2 [89]. Previous to assessing the FBG domains affinity to TLR4 in this assay, it was verified that the wells were coated to the same extent with TLR4, TLR4-MD-2 and the FBG domain proteins as shown in Figure 3-22. These results showed that there is no difference in the signal obtained when coated with the FBG domains of the tenascin family members or TLR4 proteins.

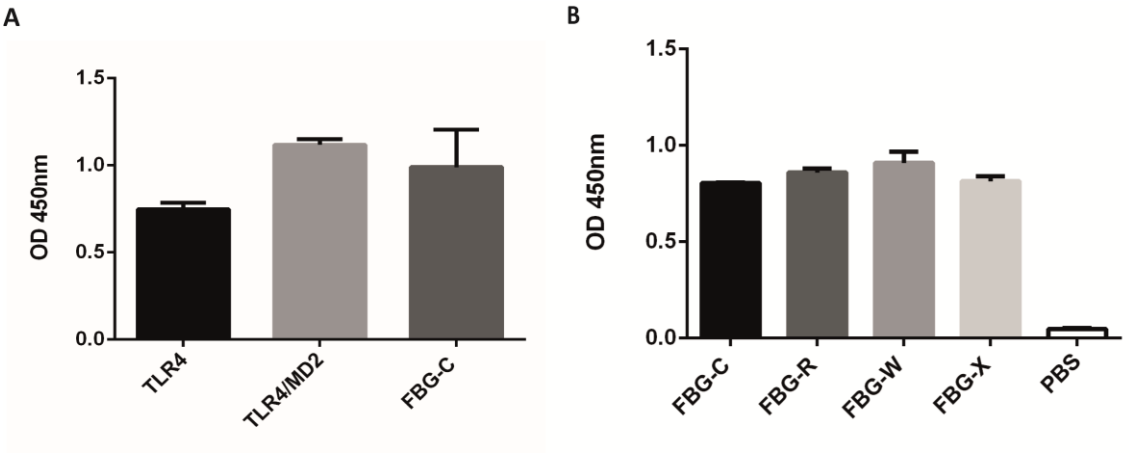

Figure 3-22. Equal coating of 96 wells plate with TLR4, TLR4-MD-2 and FBG-C, -R, -W and -X. A. 96 well plate was coated with 1 µg/mL of TLR4, TLR4-MD-2 and FBG-C and the coating was detected using specific antibodies against these proteins. **B**. 96 wells plate was coated with 1 µg/mL of FBG-C, -R, -W and -X and the coating was detected using anti-His antibody. Data is shown as mean ± SEM, N=3.

Next, I tested the TLR4 affinity to the FBG domains of the tenascin family members. TLR4 exhibited similar binding curves to FBG-C, -R and -W, and bound to these proteins with a K_D ~50-60 nM. However, TLR4 did not bind to FBG-X. These data correlate with the protein activity observed in ThP1 NF-κB cells and primary human macrophages for each FBG domain of the tenascin family (Figure 3-23).

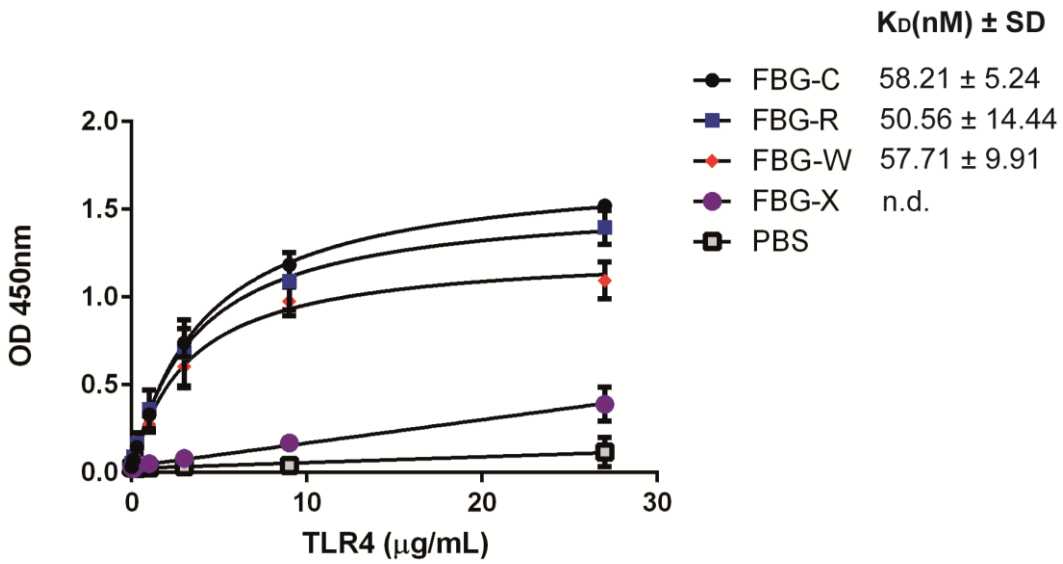

Figure 3-23. Solid phase binding of TLR4 to FBG-C, -R, -W and -X. 96 well plates were coated with 1 μg/mL FBG-C,-R, -W, -X or PBS and TLR4 was added in a dose dependent manner. N.d.: not determined. Curve fitted using one binding site (hyperbola) function and data is shown as mean ± SEM, N=3 independent experiments. K_D was determined using GraphPad Prism 6 software.

Finally, the ability of TLR4-MD-2 to bind to FBG-C was assessed. TLR4-MD-2 binding to FBG-C was significantly lower compared to TLR4, with a K_D: 251.98 nM (Figure 3-24). These results showed a 5 fold difference in binding of TLR4-MD-2 to FBG-C compared to TLR4, suggesting that FBG-C could be competing with MD-2 to bind to the same place in the receptor.

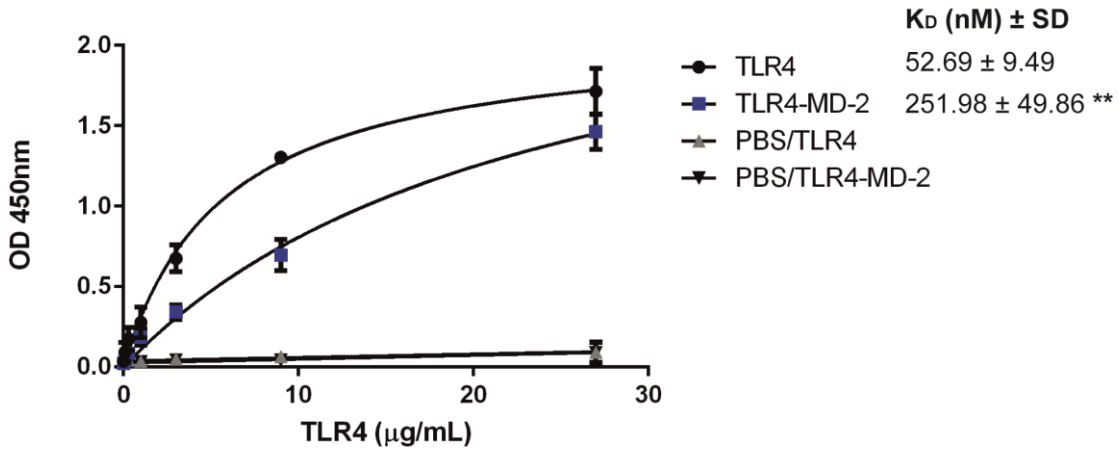

Figure 3-24. Solid phase binding of TLR4 and TLR4-MD-2 to FBG-C. 96 well plates were coated with 1 μg/mL of FBG-C or PBS and TLR4 or TLR4-MD-2 was added in a dose dependent manner. Curve fitted using one binding site (hyperbola) function and data is shown as mean ± SEM, N=3 independent experiments. K_D was determined using GraphPad Prism 6 software. Paired t-test vs TLR4, **p<0.01.

3.9. Discussion

Tenascin-C is highly expressed during tissue injury and infection, and the FBG domain of this protein is responsible for inducing inflammation via activation of TLR4 [89, 213, 214]. In this chapter, I have assessed the ability of the other members of the tenascin family to initiate an inflammatory response similarly to tenascin-C. I have shown for the first time that FBG -R and -W can induce the activation of the NF-κB transcription factor in ThP1 NF-κB cells and the synthesis of pro-inflammatory cytokines in primary human macrophages. In contrast, FBG-X was not able to induce an inflammatory response to the same extent as the other tenascin family members.

Blocking TLR4 using a TLR4 antibody and a TLR4 inhibitor (TAK 242), showed that FBG-R and -W also signal through TLR4 to induce the expression of cytokine in primary human macrophages, similarly to FBG-C. Moreover, solid phase binding assays corroborated that FBG-C, -R and -W bind directly to TLR4 with similar affinity, while FBG-X did not bind. These data indicate that a common mechanism of action is shared among the tenascin family members, which will serve to elucidate how the FBG domain is able to activate and interact with TLR4.

3.9.1. FBG-C, -R and -W can induce an inflammatory response

Human recombinant FBG-R, -W and -X were made as previously described for FBG-C using a bacterial expression system. *E. coli* protein expression was chosen as it generated higher yields of protein per litre of culture compare to a mammalian expression system. A disadvantage of the bacterial expression system is that the FBG domains are found in the insoluble fraction and proteins required refolding. In addition, proteins can be contaminated with LPS as being produced in *E. coli*. However, LPS

was sufficiently removed from protein preparations using triton-X-114 washes during protein purification. In addition, bacterial expression does not introduce any post-translational modification to proteins compared to mammalian expression systems, and it was previously shown that FBG-C does not required any post-translational modification to exert its function [89].

I have shown that FBG-R can induce the activation of NF-κB transcription factor in ThP1 cells as well as cytokine synthesis in primary human macrophages. Tenascin-R is constitutively expressed in adulthood in the central nervous system. However, it is also up-regulated after spinal cord injury to mice in the lesion area [315, 316] and tenascin-R mRNA levels increased after optic nerve lesion and astrocytic activation by oligodendrocytes [317]. As part of the perineuronal nets, tenascin-R restricts synaptic plasticity and inhibits axonal regrowth and remodelling after injury. Thus, tenascin-R null mice recovered better after spinal cord injury compared to wild type mice [316]. *In vitro* studies have shown that the inhibitory effect of tenascin-R in neurite outgrowth is due to the interaction of the EGF-like repeats with the adhesion molecule F3/11 in the neural outgrowth core [267]. Immunization of rats with a polyclonal antibody against the EGF-L of tenascin-R resulted in increased axonal plasticity and sprouting and improved functional recovery after spinal cord injury [318]. Together these data showed that tenascin-R is up-regulated in CNS injury and blocking this protein could be beneficial to enhance the recovery after spinal cord injury.

Different domains of tenascin-R have demonstrated distinct effects *in vitro* on microglial cells. FNIII 6-8 and the FBG domain of tenascin-R can increase microglia adhesion and migration, while the EGF-like repeats is an anti-adhesive substrate for microglia and inhibits their migration. Moreover, it was found that FNIII 6-8 and EGF-L domains can induce the expression of cytokines by microglia including chemokine-

induced cytokine 3 and TNF, as well as different growth factor such as nerve growth factor and brain-derived neutrophic factor [272]. However, in this study it wasn't evaluated if the FBG domain could induce cytokine synthesis in microglia. My data suggest that FBG-R can activate macrophages and could potentially induce the activation of microglia or astrocytes, since these cells express TLR4 and are essential in the inflammatory response in the CNS. However, further studies are necessary to experimentally demonstrate this hypothesis.

Unlike tenascin-C that is little expressed in healthy adults, tenascin-R is constitutively expressed in the CNS suggesting that another level of regulation is needed to control its inflammatory effects on microglia. Tenascin-R is normally part of the perineuronal net, a complex extracellular matrix structure that is degraded as a consequence of tissue injury. It could be hypothesised that the proteolysis of the ECM may release discrete domains of tenascin-R which have a different biological activity compared to full length tenascin-R. Tenascin-R is also over-expressed after CNS injury and the soluble version of the protein compared to the one assemble to the matrix could result in a more active version of it. Further studies are required to understand the regulation of tenascin-R during inflammation and the role of FBG-R in tissue injury in the CNS, specifically the ability of full length tenascin-R vs FBG-R to activate and induce the expression of cytokines by microglia both *in vitro* and *in vivo*.

FBG-W was also able to induce NF-κB activation and cytokine synthesis similarly to FBG-C. Tenascin-W is not normally expressed in healthy tissue but, like tenascin-C, it becomes up-regulated in solid tumours including colorectal and breast cancer [304], oligodendroglioma, astrocytoma and glioblastoma [319], pancreatic and kidney carcinomas, melanomas and lung tumours [303]. Tenascin-W expression in different types of solid tumours makes it as a better biomarker than tenascin-C for

tumour detection and prediction [303]. Moreover, elevated levels of tenascin-W have been found in the sera of patients with breast or colorectal cancer suggesting a link between the expression of this protein and the development of cancer [304]. Tenascin-W is the most recently discovered family member and very little is known about its function. However, in the context of cancer, *in vitro* studies showed that tenascin-W may contribute to the metastasis of mammary tumour cells expressing α8 integrin by increasing their migratory behaviour, but the domain exerting this function hasn't been determined [300]. TNF can induce the expression of tenascin-W, as well as tenascin-C, in mouse embryonic fibroblast, suggesting that tissue injury and inflammation could contribute to the expression of this protein [300]. TLR4 has also been shown to be up-regulated in different types of cancer including colorectal, liver, pancreatic and breast cancer [320]. Under inflammatory conditions, the activation of TLR4 and the NF-κB pathways have been linked to increased cancer cell migration and invasion [321, 322]. Furthermore, LPS activation of TLR4 promoted cancer cell survival and proliferation in hepatocellular carcinoma cell lines [323]. It could be speculated that tenascin-W expression by stromal cells could activate TLR4 in cancer cells and promote cell migration, proliferation and survival. This effect could be mediated by the FBG domain of tenascin-W, which could also participate in the activation of tissue resident macrophages and contribute to the pro-inflammatory niche of the tumour stroma.

FBG-X wasn't able to activate the NF-κB transcription factor or cytokine synthesis at the same level as the other tenascin family members. Tenascin-X is expressed in loose connective tissue in adults and *in vivo* models of wound healing have shown that it plays a role in the maturation of the extracellular matrix after wound closure increasing the strength of the wound [289]. *In vitro*, FBG-X is able to interact with collagen I and tropoelastin, contributing to the organization of the extracellular

matrix and mediating the stability and maturation of the elastic skin fibres [275, 287]. Tenascin-X has been also shown to influence epithelial-to-mesenchymal transition via the interaction of its FBG domain with the small latent complex of TGF-β (SLC), producing a conformational change that exposes active TGF-β. This mechanism is dependent on the binding of the FBG domain to $\alpha_{11}\beta_1$ integrin in the cell surface [293] suggesting a distinct binding site for the integrin and SLC.

Altogether these data show that similarly to FBG-C, FBG-R and -W can induce an inflammatory response. Unlike tenascin-C that is expressed during inflammation indistinctively of the injury site, tenascin–W is up-regulated in cancer but tenascin-R and -X are constitutively expressed. Further studies are necessary to understand the regulation of expression of tenascin-R and tenascin–W in disease, which form of the protein is inducing cytokine synthesis (full length vs discrete domains; soluble vs matrix-assembled) and corroborate *in vitro* data in animal models to verify their function *in vivo*.

3.9.2. FBG-C, -R and -W activity is TLR4-dependent

I have shown that the induction of cytokine synthesis by FBG-C, -R and -W is TLR4-dependent in primary human macrophages. Previous work determined that FBG-C signals through TLR4 using bone marrow derived macrophages from TLR4 null mice and a function-blocking anti-human polyclonal TLR4 antibody [89]. The same TLR4 antibody was also used in this case to determine FBG-R and FBG-W TLR4-dependent protein activity in primary human macrophages. Additionally, TAK 242, an intracellular specific TLR4 inhibitor, was used to corroborate these results. TAK 242 binds to Cys747 of TLR4 intracellular domain and hinders the interaction of this domain with the adaptor molecules essential to trigger the signalling cascade

downstream of TLR4 [324]. TAK 242 is very effective inhibiting TLR4 activation by LPS at a lower dose (1 μM) and it has been used as a tool to establish TLR4-dependent function of other DAMPs including fibronectin EDA [325] and HMGB1 [313] using similar doses to those in this study (3 μM).

My results showed diverse levels of inhibition for LPS and the FBG domain of the tenascin family members. TAK 242 efficiently inhibited LPS-induced cytokine synthesis (>90% inhibition). However, different levels of inhibition were observed for the FBG domain of the tenascin family member: TAK 242 wasn't able to inhibit the synthesis of IL-8 by more than 79%. Anti-TLR4 antibody was very effective inhibiting the expression of IL-6 and TNF, but lower levels of inhibition were observed for the induction of IL-8 by LPS and FBG-C and -W. In summary, the expression of IL-8 was less affected compared to the other cytokines assessed using the TLR4 blocking agents.

IL-8 is a cytokine that can be induced also by TNF via the p38 pathway in monocytes [326]. A dose of 10 ng/mL of TNF is sufficient to robustly induce IL-8 mRNA expression more than 20 fold in rheumatoid synovial fibroblasts [327]. Residual levels of TNF were observed for FBG-R and FBG-W after TAK 242 treatment (31.77% and 22% respectively) and might have contributed to the low expression of IL-8. For example, in the presence of TAK 242, 32.28% and 23.82% of IL-8 was expressed by cells stimulated with FBG-R and FBG-W respectively compared to non-treated cells. The TLR4 antibody was able to inhibit effectively TNF and IL-6 expression in human macrophages after stimulation with FBG-C, -R and -W (>90% inhibition). Nevertheless, an incomplete inhibition in IL-8 synthesis was observed for FBG-C and FBG-W suggesting a different mechanism of TLR activation compared to LPS.

Our group found that FBG-C doesn't require MD-2 or CD14 to activate TLR4 [89], but it is still not known if it requires other co-receptors to induce an inflammatory response. Some DAMPs require only CD14 to activate TLR4 such as lactoferrin [159] and surfactant protein A, D [151, 160]; or only MD-2 to activate this receptor such as fibronectin extra domain A [161]. Other DAMPs, such as hyaluronan, require different co-receptors to form a complex with TLR4 involving CD44 and MD-2 [162]. FBG-C can also interact with αvβ3 integrin promoting cell adhesion [198, 328] and the sequence involved in integrin binding is highly homologous among the FBG domains of the tenascin family members. Other studies have linked αvβ3 with inflammation as it is able to contribute to the inflammatory response exerted by primary human macrophages. αvβ3 ligation promotes the activation of the NF-κB transcription factor inducing the secretion of TNF in primary human macrophages, and can increase the mRNA levels of pro-inflammatory cytokines including IL-8 and IL-6. This effect was enhanced when primary human macrophages were stimulated with LPS suggesting that αvβ3 engagement contribute to the differentiation of macrophages into a sustained pro-inflammatory phenotype [329]. Tenascin-C has been shown to induce IL-6 in peritoneal macrophages from mice via activation of αvβ3 and the NF-κB pathway [238]. It could be hypothesised that FBG-C might also be acting through this receptor contributing to the inflammatory response already mounted by the activation of TLR4. This theory could also explain why blocking TLR4 in ThP1 NF-κB cells didn't inhibit completely the activation of the NF-κB transcription factor by FBG-C.

Another hypothesis is that FBG-C could also activate TLR2. Other extracellular matrix proteins that activate TLR4 can also exert their function via TLR2 including biglycan [155], decorin [152], versican [330] and hyaluronan fragments [162, 331]. Other DAMPs such as HMGB1 can signal through TLR2 and TLR4 in RAW264.7

macrophages [332]. In addition, HMGB1 is able to induced IL-8 expression in mature human chondrocytes [333] which has been shown to expressed TLR1 and TLR2 [334]. Triggering the inflammatory response after ligand binding to TLR4 or TLR2 is very similar: the intracellular domains of TLR4 and TLR2 recruit the same adaptor molecules and they activate similar signalling pathways including MyD88 and NF-κB [335]. Moreover, they are confined to microdomains of the lipid rafts on the plasma membrane of monocytes after bacterial stimulation [336]. Previously, our group has published that bone marrow derived macrophages and embryonic fibroblast from TLR2 null mice did not present a defect in the expression of IL-6 after FBG-C stimulation. Similarly, functional blocking antibody against human TLR2 did not affect TNF synthesis in primary human macrophages by FBG-C [89]. However, the impact on IL-8 production hasn't been assessed. The solid phase binding assay revealed that FBG-C could bind to TLR2 with low affinity compared to TLR4. Activation of TLR2 by FBG-C could also contribute to the activation of NF-κB and could also explain why blocking TLR4 in ThP1 cells didn't inhibit completely NF-κB activation as observed with LPS. Further studies are needed to understand the contribution of αvβ3 and TLR2 in the inflammatory response induced by FBG domain of the tenascin family members. Other approaches that could be used is assessing the activity of the proteins in TLR4 or TLR2 null cells, as it has been shown before for FBG-C [89], or using function blocking antibodies for αvβ3 integrin. Altogether these data suggest that the FBG proteins have a different mechanism of activation of TLR4 compared to pathogenic stimuli.

In summary, FBG-C, -R and -W can signal through TLR4 to induce the expression of pro-inflammatory cytokines in primary human macrophages suggesting a conserved mechanism or epitope among these proteins to activate this receptor. This hypothesis is going to be assessed and discussed in chapter 4.

3.9.3. FBG-C, -R and –W can bind *in vitro* to TLR4

A solid phase binding assay was developed to assess the ability of the FBG proteins to interact directly with TLR4. Firstly, it was confirmed that the FBG was the only domain of tenascin-C that could interact with TLR4. These data corroborate previous studies where FBG-C was the only domain being able to induce an inflammatory response via TLR4 to the same extent as full-length tenascin-C [89]. The other domain of tenascin-C that can induce inflammation is the FNIII 3, but it acts through the activation of α9 integrin [239]. In addition, the solid phase binding assay revealed that FBG-C binds with the highest affinity to TLR4 and with low affinity to TLR2, while no biding was observed for TLR3. These results suggest that FBG-C could be also a ligand for TLR2 as discussed above. However, FBG-C binds with higher affinity to TLR4 and exerts its inflammatory function mainly through this receptor.

FBG-C, -R and -W could bind *in vitro* to TLR4; in contrast, FBG-X did not show binding to this receptor. These data corroborate the results obtained in ThP1 NF-κB cells and in primary human macrophages where FBG-R and -W were able to induce an inflammatory response similarly to FBG-C, but FBG-X couldn't induce the same level of activation. The dissociation constants (K_D) of the FBG domains of the tenascin family members to TLR4 were ~50-60 nM. The solid phase binding assay is a commonly used technique to measure affinity constants as it is easy to perform, sensitive, quantitative and allows comparison of different samples in the same experiment. Another sensitive method commonly used to determine the dissociation constant is surface plasmon resonance (SPR). Briefly, a protein is immobilised on the surface of an SPR crystal. Then, a second protein is added in a solution and, as the proteins form a complex, an increase in the SPR signal measuring the association rate is

registered in response units. Finally, a solution without the protein is added to measure the dissociation rate and from these values the equilibrium dissociation constant can be calculated. This method allows measuring the interaction among proteins in real time but specialised equipment (i.e. BiaCore) is needed to perform the experiments. Each *in vitro* technique can result in a different value in the K_D calculated, and this has to be taken into consideration when comparing results obtained using different methods. For example, the binding affinity of TLR4-MD-2 measured by SPR is 62.9 nM [337]. However, in a solid phase binding assay, the K_D estimated was 12 nM for the TLR4-MD-2 complex [338].

In the laboratory of Prof. Nick Gay (University of Cambridge) other *in vitro* methods were used to interrogate the direct interaction among FBG-C and TLR4, such as analytical gel filtration and gel shift assay. In these experiments, proteins were incubated together for 30 min at room temperature and then loaded into a gel filtration column or native gel. However, these methods did not show direct binding among the proteins, indicating differences in protein interactions in solution compared to methods where the proteins are immobilised. It would be interesting and more physiologically relevant to measure protein-protein interaction in live cells, especially the interaction of cell surface receptors with the extracellular matrix. Endogenous HMGB1 has been shown to interact with TLR4 in synovial fibroblast using proximity ligation assay [150]. This method consists of targeting the proteins in cells with a specific antibody raised in different species. Then, secondary species-specific antibodies are added that contain short DNA strands which can interact with each other. After joining of the two added oligonucleotides by enzymatic ligation, they are amplified via rolling circle amplification, and the duplicated DNA is labelled to highlight the product. This results in high concentration of fluorescence in each single-molecule amplification product

which is visible with a fluorescence microscope. HMGB1 has also been shown to interact with TLR4 and TLR2 using FRET in RAW264.7 cells [339]. This technique measures the interaction among two proteins labelled with a donor or acceptor chromophore, where the energy transfer only occurs when the molecules are in close proximity. FRET has been used to determine TLR dimerization and interaction with other molecules [110, 340, 341]. Both of these methods are highly sensitive and specific and could be used to corroborate the results obtained in *in vitro* assays.

The K_D value has been estimated for the LPS and TLR4 complex, including the other co-receptors required for the activation of TLR4. LPS binds to TLR4-MD-2 complex with high affinity (K_D= 3nM). Additionally, the K_D of other DAMPs in complex with TLRs has been determined (Table 3-4). For example, the K_D of surfactant protein D-TLR4 was 15.8 nM [151] and S100A12 protein affinity to TLR4 was of 92 nM [157]. Microscale thermophoresis showed that the extracellular matrix protein biglycan binds to TLR-4 with a K_D of 28 ± 8 nM [94]. These values are in the range of the binding affinity of the FBG proteins to TLR4.

Table 3-4. Affinity constants (K_D) for protein complexes including TLR4.

Protein complex	K_D	Method used	Reference
LPS-CD14	8.7 µM	SPR	[342]
LPS-MD-2	2.33 µM	SPR	[342]
LPS-TLR4	14.1 µM	SPR	[342]
LPS-MD-2-TLR4	3 nM	^{3}H-lipid A binding assay	[126]
TLR4-MD-2	62.9 nM	SPR	[337]
TLR4-MD-2	12 nM	Solid phase binding assay	[338]
HMGB1-TLR4-MD-2	1.5 uM	SPR	[150]
HMGB1- MD-2	12 nM	SPR	[163]
Surfactant protein D-TLR4	15.8 nM	Solid phase binding assay	[151]
S100A12-TLR4	92 nM	SPR	[157]
Biglycan-TLR4	28 nM	Microscale thermophoresis	[94]
Decorin-TLR4	37 nM	Microscale thermophoresis	[152]

In summary, the dissociation constants determined for endogenous molecules are higher compared to the K_D of LPS to TLR4-MD-2 complex. These findings stress the difference in inflammatory processes induced by endogenous and pathogenic stimuli. In the context of sterile inflammation, an immune response is favoured towards tissue repair, cell proliferation and wound regeneration. In contrast, after infection, the immune system needs to mount a quick response to contain the spread of microorganisms and prevent more tissue damage. In addition, some of these endogenous molecules are constitutively expressed in the tissue in healthy conditions and only when they are over-expressed, secreted by cells or degraded from the ECM, they become largely available to be detected as a danger signal suggesting that the threshold level of detection for these molecules is higher.

Finally, the binding assay showed that FBG-C binds with lower affinity to TLR4 when it is in complex with MD-2 (K_D: 251.98 nM). These data corroborate previous findings that FBG-C does not require MD-2 to activate TLR4 [89]. The low affinity binding observed for FBG-C to TLR4-MD-2 could be due to a small proportion of the TLR4 not being in complex with MD-2. The human recombinant proteins are purchased already in complex and I was not able to determine the % of TLR4 or MD-2 that were not bound. MD-2 is the only known protein that has been co-crystallised with TLR4, binding to the concave interface of the receptor and bridging with a second TLR4 to induce dimerization and activation [116]. It could be speculated that FBG-C might not require MD2 to bind to TLR4 because it occupies the same space in the receptor. To assess this hypothesis, future work could include competition assay *in vitro* where the ability of TLR4 to form a complex MD-2 could be hindered by pre-incubating the receptor with FBG-C.

3.10. Summary

In conclusion, I have shown for the first time that FBG -R and -W can induce the activation of the NF-κB transcription factor in ThP1 NF-κB cells and the synthesis of pro-inflammatory cytokines in primary human macrophages by activating and binding to TLR4, similarly to FBG-C. In contrast, FBG-X was not able to induce an inflammatory response or bind to TLR4. In the next chapter, I will perform an *in silico* analysis of the sequences of the tenascin family members to determine the amino acids sequences that are common among FBG-C, -R and -W and different to FBG-X. Additionally, I will use peptide mapping to determine the region of FBG-C implicated in TLR4 activation.

Chapter 4 – Identification of candidate residues that mediate FBG domain activation of TLR4

Chapter 4. Identification of candidate residues that mediate FBG domain activation of TLR4

4.1. Introduction

In the previous chapter, I demonstrated that the FBG domains of tenascin -C, -R and -W, but not -X, can induce an inflammatory response via activation of TLR4. In this chapter, I aim to determine the amino acids potentially involved in TLR4 activation and binding by the FBG domains using *in silico* analysis and peptide mapping. Multiple sequence alignments will be used to identify the common regions in FBG-C, -R and -W, and differences in the amino acid composition compared to FBG-X. I will also use peptide mapping to dissect specifically the regions of FBG-C required for TLR4 activation. I'll assess the ability of 9 overlapping peptides comprising the entire sequence of FBG-C to activate NF-κB in ThP1 cells and cytokine synthesis in primary human macrophages. Together these data will highlight potential amino acid sequences in the tenascin FBG domains involved in the activation of TLR4.

4.2. Sequence homology of the tenascin family members

The sequences of the tenascin family FBG domains are 50-60% identical (Table 3-1). To examine the sequences of active FBG domains (-C, -R and -W) and compare them to the inactive FBG-X, I used multiple alignment analysis. In this approach, the sequences of FBG-C, -R, -W and -X are aligned according to their identity, but also the amino acids are grouped and coloured according to their property (hydrophobic, positive or negatively charged, polar, etc.). This analysis confirmed the high degree of conservation among the FBG domains of the tenascin family members, especially towards the C-terminus of the proteins (Figure 4-1). There are regions of hydrophobic amino acids (blue) and columns of positively charged amino acids (red), which are highly homologous among the proteins. The positions of the 4 cysteines are also conserved suggesting a similar pattern of folding. Regions which are different among the FBG domains were also observed, for example in the middle section of the proteins (amino acids 100-150), where there is less conservation in their sequence. Looking for sequences common for the active FBG proteins (FBG-C, -R, -W) and different to FBG-X, it was found that, at the C-terminus, FBG-X is the only family member without a cluster of positively charged amino acids (see red box, Figure 4-1), suggesting that this region could potentially be involved in TLR4 activation or binding.

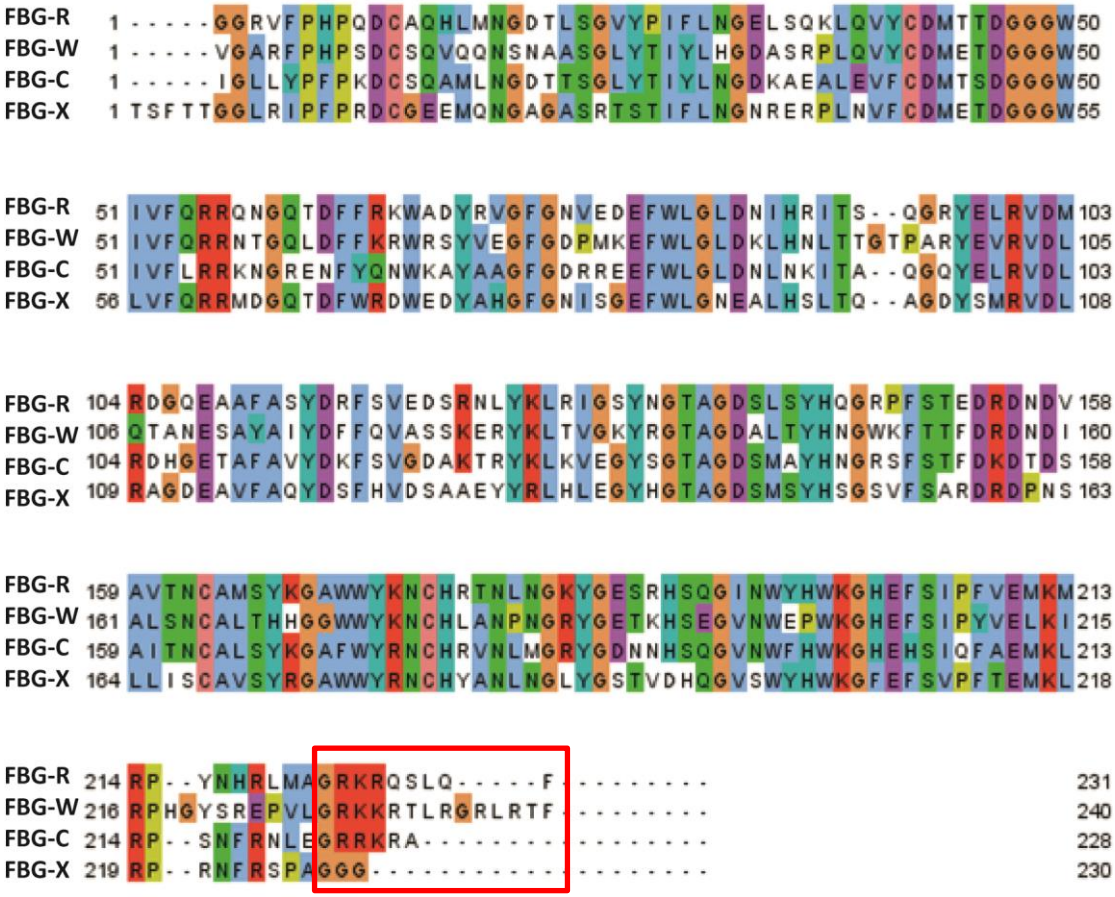

Figure 4-1. Homology between the FBG domains of the human tenascin family members. Multiple alignment analysis determined conserved regions between the FBG domains of tenascin family members using Clustal Omega software. The alignment was coloured according to the Clustal colour scheme. Light blue: hydrophobic. Red: positively charged. Green: Polar. Pink: conserved column of cysteine. Violet: negatively charged. Orange: glycine. Yellow: proline. Cyan: aromatics. Red box indicates differences in the amino acid composition of FBG-X compared to FBG-C, -R and –W.

4.3. Modelling the FBG domain of the tenascin family members

Sequence comparison showed regions of high homology, and differences, among the FBG domain of the tenascin family members. It is also important to compare the structure of the proteins, where similarities and differences might be found in the distribution of the amino acids in FBG-C, -R, and -W compared to FBG-X. The structure of the FBG domains of the tenascin family members hasn't been determined. For that reason, the proteins were modelled using the published structure of the C-

terminus fibrinogen γ chain. Fibrinogen is a large glycoprotein comprising pairs of three non-identical polypeptide chains $(\alpha\ \beta\ \gamma)_2$, which radiate out from a central nodule containing the N-terminus of each peptide (Figure 4-2 A). The C-terminal regions of the β and γ chain each form a 30 kDa globular domain that is absent in the α chain and which exhibits a unique fold and structure containing three distinct sub-domains: A, B and P (Figure 4-2 B) [308].

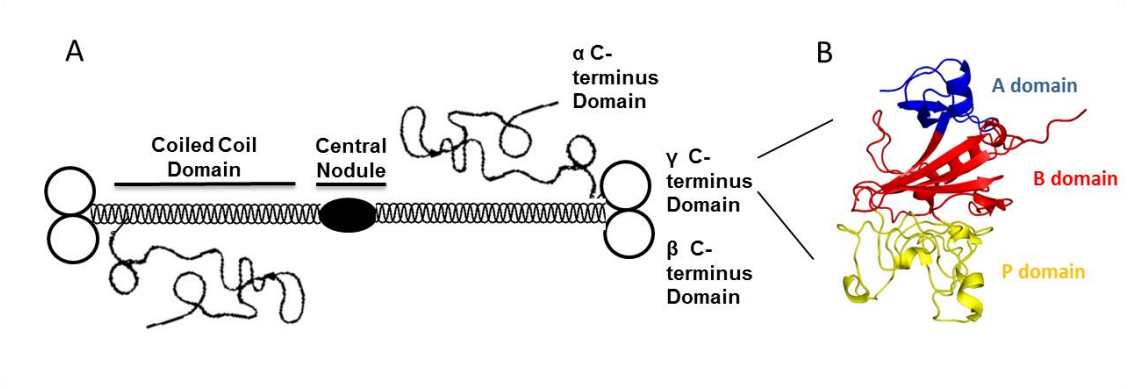

Figure 4-2. Fibrinogen and its C-terminal globular domain. **A.** Schematic structure of fibrinogen showing the central nodule, coiled coil domain and α, β and γ C-terminus domain. **B.** 3D structure of the γ C-terminus globule showing its constituent 3 sub-domains: A (blue), B (red) and P (yellow). The A sub-domain is located in the N-terminus and contains a twisted three-stranded antiparallel β sheet flanked by a short helix, and the first disulphide bond (Cys153 – Cys182) which anchors the helix to the middle strand of the sheet. The B sub-domain is located in the centre of the structure and contains a seven-stranded antiparallel β sheet with two short helices and a hairpin loop aligned against one its faces. The middle strand of the B domain is made up of a segment of residues that appears sequentially after amino acids that make up the third sub-domain. The P sub-domain has little regular secondary structure and is composed predominantly of loops. One lobe of the P domain contains 2 short helices and the second disulphide bond (Cys326 – Cys329) in the structure. This image was modified from [308] protein data bank (PDB) number 1FID, and coloured using PyMOL Molecular Graphics System.

Pairwise alignment showed 30-40% protein identity among the sequences of the FBG domain of the tenascin family members and C-terminus of the fibrinogen γ and β chains (Table 4-1). Proteins were modelled using SWISS-MODEL software based on the C-terminus fibrinogen γ chain. The models of the FBG domain of the tenascin family members showed a pattern of folding and sub-domain organisation similar to

fibrinogen γ chain. Sub-domain A is located in the N-terminus and contains β sheets, a short helix and the first disulphide bond. The B sub-domain is located in the centre of the structure and comprises antiparallel β-sheets with two short helices similar to fibrinogen. In the C-terminus is located the P sub-domain, which has little regular secondary structure and is composed predominantly of loops. It contains the second disulphide bond and only one α-helix, differing from the fibrinogen γ chain that contains 2 short helices (Figure 4-3).

Table 4-1. Identity between the FBG domains of human tenascin-C, -R, -X and -W and fibrinogen ϒ and β chain. Pairwise alignment analysis with Clustal Omega was used to determine the % of identity of the tenascin family members against C-terminus fibrinogen ϒ and β chain.

	Fibrinogen β	**Fibrinogen ϒ**
FBG-C	29.89 %	31.15 %
FBG-R	33.33 %	31.94 %
FBG -X	32.06 %	31.91 %
FBG -W	35.50 %	31.60 %
Fibrinogen ϒ	39.92 %	-

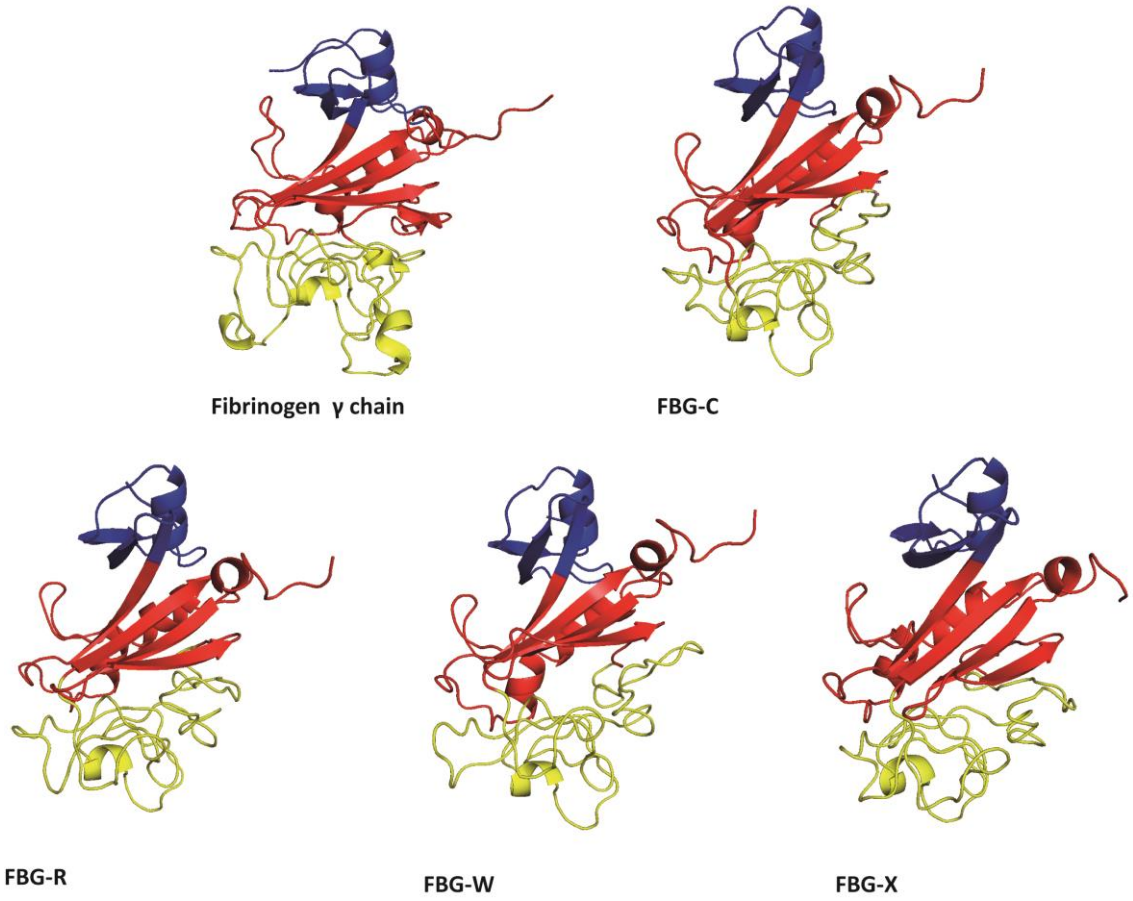

Figure 4-3. Modelling the structure of FBG-C, -R, -W and –X. The structures of FBG-C, -R, -W and –X were modelled based on C-terminus fibrinogen γ chain crystal structure. Sub-domain protein organisation is highlighted: A-subdomain in blue, B sub-domain in red and P subdomain in yellow. Proteins were modelled using SWISS-MODEL software and coloured using PyMOL Molecular Graphics System.

The models of FBG-C, -R, -W and -X were aligned using PyMOL software to determine regions of high homology structurally. Figure 4-4 A showed that the FBG domain of the tenascin family members shared many regions of sequence homology as shown previously in the sequence alignments. However, they also present conserved regions structurally and a similar pattern of folding, especially in the B and P-subdomain (Figure 4-4 B).

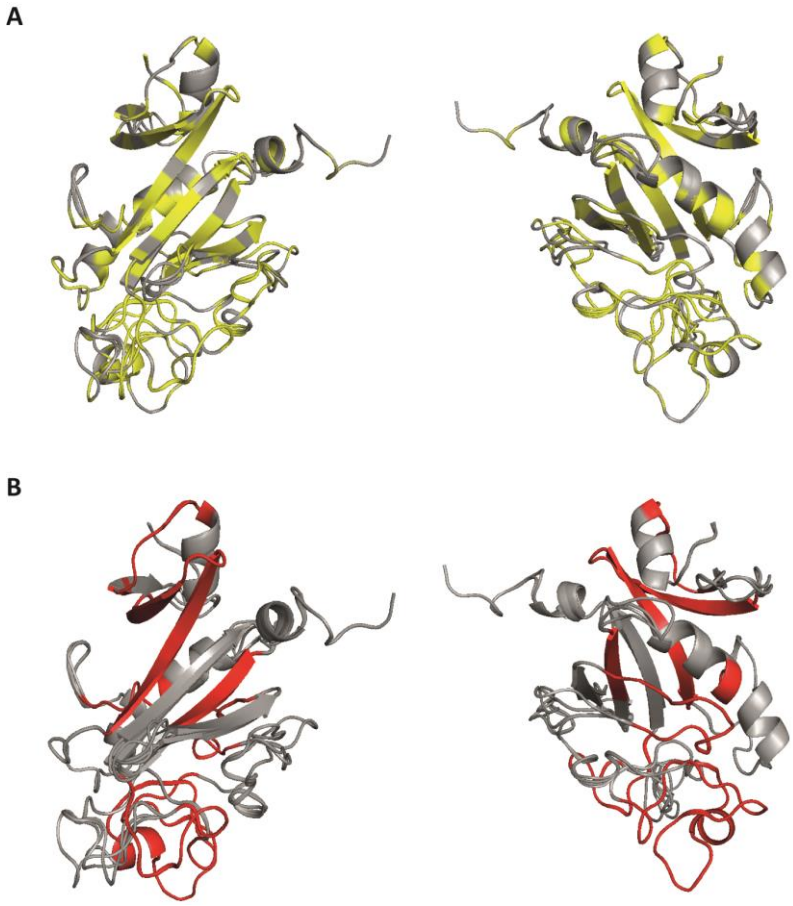

Figure 4-4. Alignment of the structural models of FBG-C, -R, -W and –X. Proteins were aligned and coloured using PyMOL Molecular Graphics System. **A.** Alignment of FBG-C, -R, -W and –X models highlighting in yellow conserved amino acid sequences. **B.** Alignment of FBG-C, -R, -W and –X models highlighting in red conserved structure.

In summary, the high homology among the sequences of the FBG domain of the tenascin family was shown also in the structural models. Alone this makes it difficult to select a specific region or set of amino acids that might be involved in TLR4 activation or binding. This analysis highlighted only one potential region different in FBG-X compared to FBG-C, -R and -W at the C-terminus of the proteins, where FBG-X lacks positive residues in this region.

4.4. Peptide mapping of the FBG-C pro-inflammatory epitope

Peptide mapping was then used to determine which amino acids of FBG-C are required to induce an inflammatory response. Peptide mapping is a method used previously to determine the binding site of FBG-C to the integrin αvβ3 [198]. Peptides were synthesised, each was ~30 amino acids long and together spanned the entire sequence of FBG-C. In addition, their sequence contains an overlapping region among two contiguous peptides (Figure 4-5).

A

1974 TIGLLYPFPKDCSQAMLNGDTTSGL YTI YL NGDKAQALEVFCDMTSDGGG
WIVFL RRKNGRENFYQNWKAYAAGF GDRRE EFWLGLDLNKITAQGQY
ELRVD LRDHGETAFAVYDKFSVGDA KTRYK LKVEGYSGTAGDSMAYHNG
RSFST FDKDTDSAITNCALSYKGAF WYRN CHRVNLMGRYGDNNHSQGVNW
FHWKG HEHSIQFAEMKLRPSNFRNLEGRRKRA 2201

B

P1	TIGLLYPFPKDCSQAMLNGDTTSGL**YTIYL**
P2	**YTIYL**NGDKAEALEVFCDMTSDGGG**WIVFL**
P3	**WIVFL**RRKNGRENFYQNWKAYAAGF**GDRRE**
P4	**GDRRE**EFWLGLDNLNKITAQGQY**ELRVD**
P5	**ELRVD**LRDHGETAFAVYDKFSVGDA**KTRYK**
P6	**KTRYK**LKVEGYSGTAGDSMAYHNG**RSFST**
P7	**RSFST**FDKDTDSAITNCALSYKGAF**WYRN**
P8	**WYRN**CHRVNLMGRYGDNNHSQGVNW**FHWKG**
P9	**FHWKG**HEHSIQFAEMKLRPSNFRNLEGRRKRA

Figure 4-5. Amino acid sequences of peptides 1-9. Nine peptides of ~30 amino acids long were used to map FBG-C active site. They comprise the entire sequence of FBG-C and each peptide contains a sequence that overlaps with the contiguous peptide. **A**. FBG-C sequence is presented highlighting each peptide in a different colour. **B.** Sequences of peptides 1-9 showing overlapping amino acid sequence in bold.

4.4.1. Peptide activity in ThP1 NF-κB cells

The peptides ability to activate NF-κB was assessed in ThP1 NF-κB cells and compared to full length FBG-C. Only peptides 5 and 6 were able to induce NF-κB activation in a dose dependent manner. Peptide 4 could induce NF-κB activation but only at higher doses, and levels of activation were lower compared to peptide 5 and 6 (Figure 4-6 A). The other peptides assessed did not show activation of NF-κB. MTT assays confirmed that the different peptides concentrations used were not affecting cell viability, with the exception of P1 which reduced cell viability at the highest concentration (Figure 4-6 B).

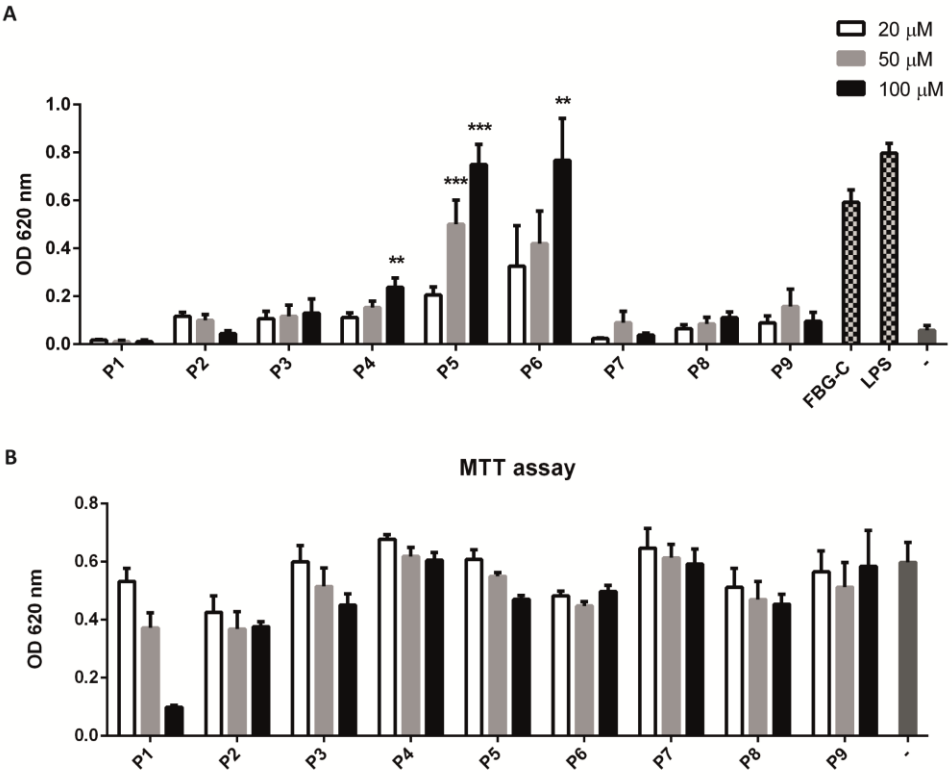

Figure 4-6. P5 and P6 can induce NF-κB activation in a dose dependent manner. **A.** ThP1 NF-κB cells were unstimulated (-) or stimulated with LPS (0.5 ng/mL), FBG-C (0.5 µM) or 20, 50 or 100 µM of peptides 1-9 for 24 h. NF-κB activation was measured using QUANTI-Blue™ . **B.** MTT assay of ThP1 NF-κB cells unstimulated (-) or stimulated with LPS (0.5 ng/mL), FBG-C (0.5 µM) or 20, 50 or 100 µM of peptides 1-9 for 24 h. Data shown as mean ± SEM, N=4 independent experiments. One-way ANOVA vs unstimulated cells, *p<0.05, **p<0.01, ***p<0.001.

The overlapping region of peptide 5 and 6 corresponds to the amino acids KTRYK. I mapped the secondary structure of the FBG domains of the tenascin family members and labelled all α helices, β sheets and loops in the multiple sequence alignment. During this analysis, I found that the amino acids KTRYK are part of loop 5 in the predicted structure of the FBG domains of the tenascin family members. This loop is in the surface of the P sub-domain (Figure 4-7).

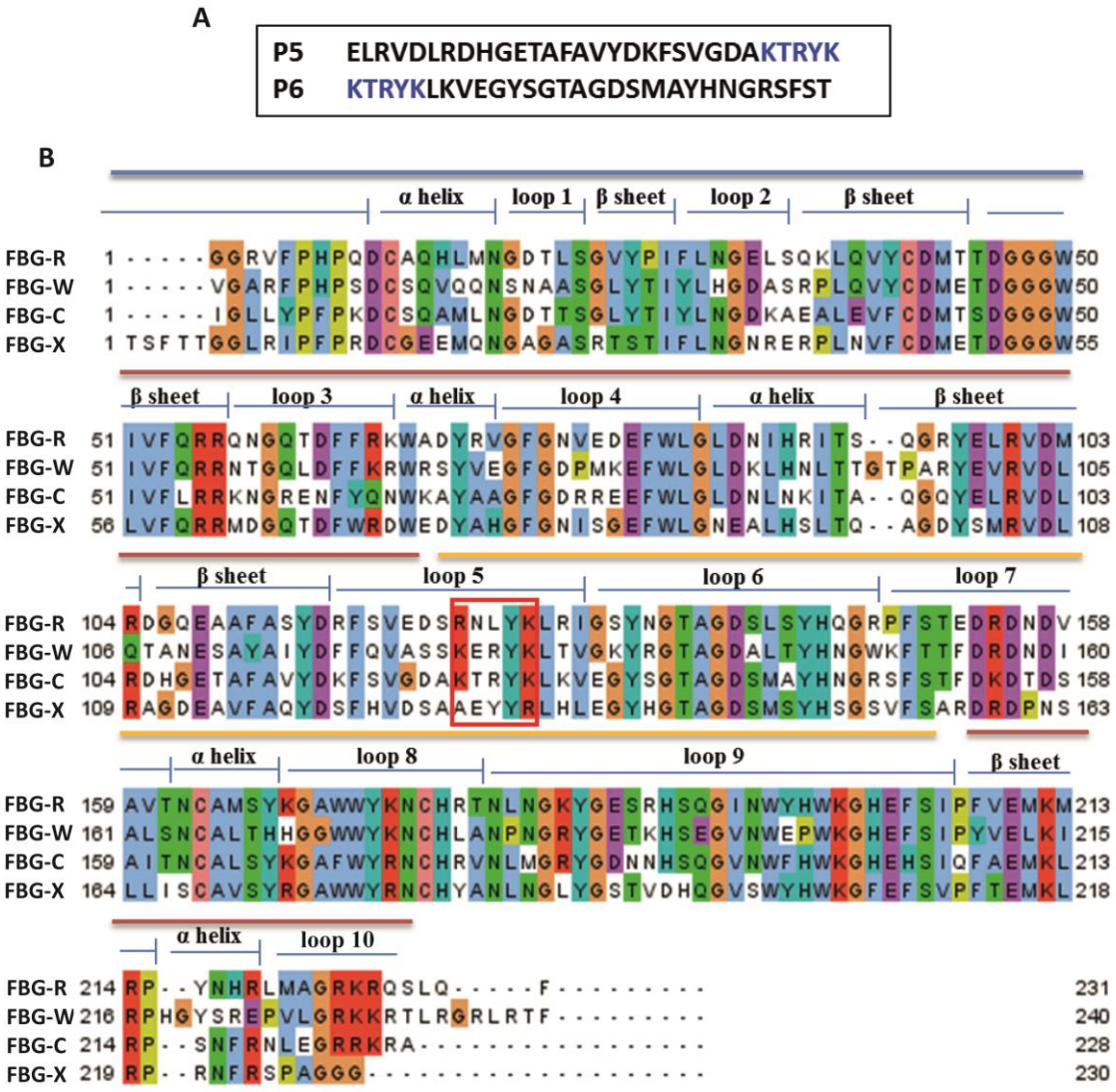

Figure 4-7. The overlapping sequence of P5 and P6 corresponds to loop 5. A. Sequences of P5 and P6 highlighting in blue the overlapping amino acids. **B.** Multiple alignment analysis of FBG domain of tenascin family members highlighting the secondary structure of the predicted protein models. Blue thick line indicates A-subdomain, red thick line indicates B-subdomain and yellow thick line indicates P-subdomain. The overlapping region of P5 and P6 (KTRYK) is located in loop 5 (red box).

Scrambled versions of peptides 5, 6 and 9 as a negative control, were made to verify that peptide activity was sequence specific. In addition, short and long peptide versions of loop 5 were designed to establish the minimum number of amino acids necessary to activate NF-κB in ThP1 cells. Peptide loop 5-1 includes only the overlapping region of P5 and P6 (KTRYK). Peptides loop 5-2 and loop 5-3 are shorter peptide versions of loop 5, incorporating surrounding amino acids of P5 and P6. Loop 5-4 is a 30 amino acids long peptide that includes loop 5 and part of loop 6 and the β-sheet (Table 4-2).

Table 4-2. Amino acid sequences of scramble peptides (P9S, P5S and P6S) and variations of loop 5. Scrambled peptides were designed as controls to determine sequence specificity of peptide 9, 5 and 6. Three peptides were designed incorporating peptide 5 and 6 overlapping sequence (bold) and varying the number of surrounding amino acids.

P5S	KGVFLTRYVTDARDVHFDKYGASRELEAKD
P6S	YKGTSDHFRVGSNSRYETSMGKGAATLKY
P9S	AFERHMKWKRKLRGAGHREPELHSNSNRIFQF
Loop 5-1	**KTRYK**
Loop 5-2	GDA**KTRYK**LKVEG
Loop 5-3	DKFSVGDA**KTRYK**LKVEGYSG
Loop 5-4	AFAVYDKFSVGDA**KTRYK**LKVEGYSGTAGD

Scrambled versions of peptide 5, 6 and 9 showed no activation of NF-κB transcription factor in ThP1 cells, indicating that the activity of these peptides is due to the specificity of their sequences. Loop 5-1 and loop 5-2 had no activity, only the medium and long version of loop 5 (loop 5-3 and loop 5-4) were able to induce NF-κB activation. Loop 5-3 showed lower levels of activation, while loop 5-4 could activate NF-κB to the same extent as P5 or P6. These results suggest that the amino acids

surrounding KTRYK are also required for the activity of the peptides (Figure 4-8 A). MTT assays showed that cell viability was not affected by the addition of the peptides at different concentrations (Figure 4-8 B).

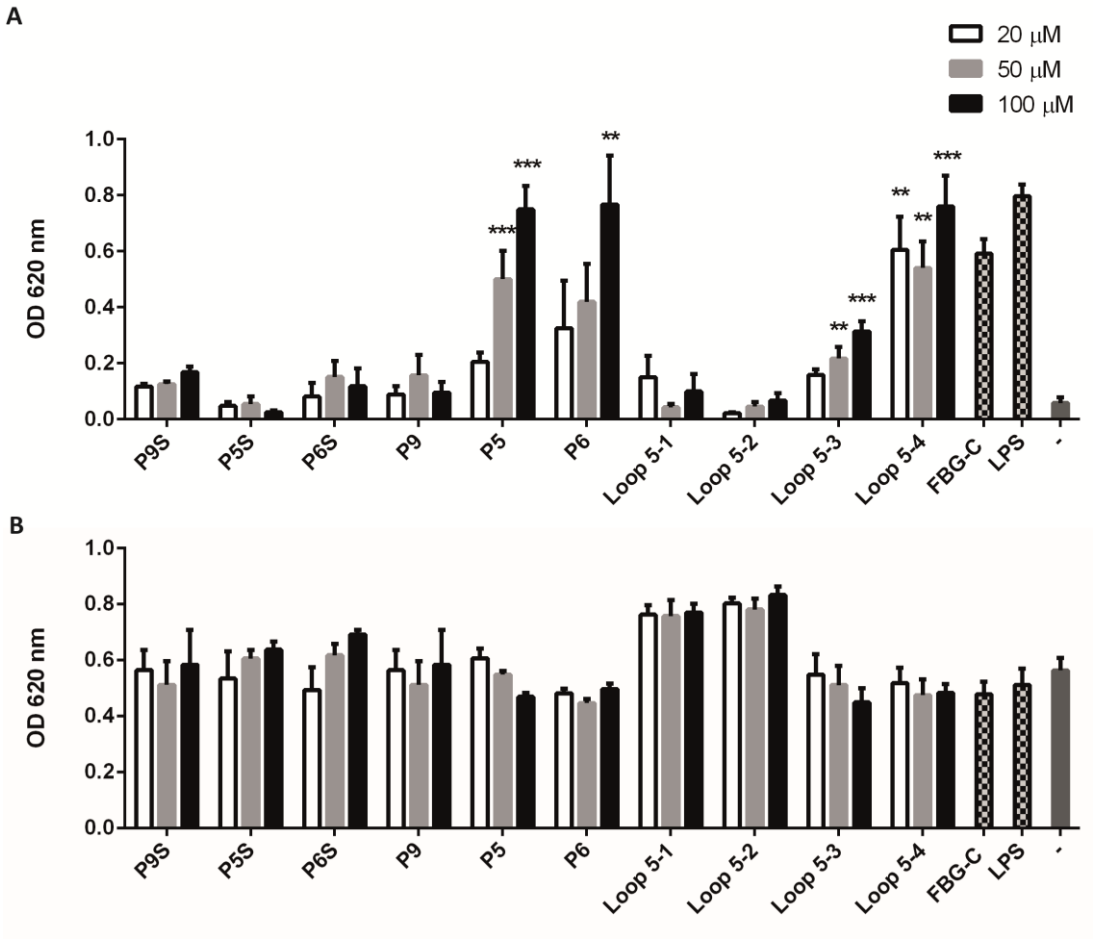

Figure 4-8. Control peptides and peptide variations in ThP1 NF-κB cells. A. ThP1 NF-κB cells were unstimulated (-) or stimulated with 20, 50 or 100 μM of peptide variations for 24 h and NF-κB activation was measured using QUANTI-Blue™ . **B.** MTT assay of ThP1 NF-κB cells unstimulated (-) or stimulated with 20, 50 or 100 μM of peptide variations for 24 h. Data shown as mean ± SEM, N=3 independent experiments. One-way ANOVA vs unstimulated cells, *p<0.05, **p<0.01, ***p<0.001.

Additional tests were performed to determine if lower concentrations of peptide 5, 6 and loop 5-4 were able to activate NF-κB transcription factor in ThP1 cells. All peptides were able to induce NF-κB in a dose dependent manner and the minimum concentration required for NF-κB activation was 20 μM (Figure 4-9 A). Polymyxin B

and boiling treatment confirmed that the activity of loop 5-4 was not due to LPS contamination (Figure 4-9 B).

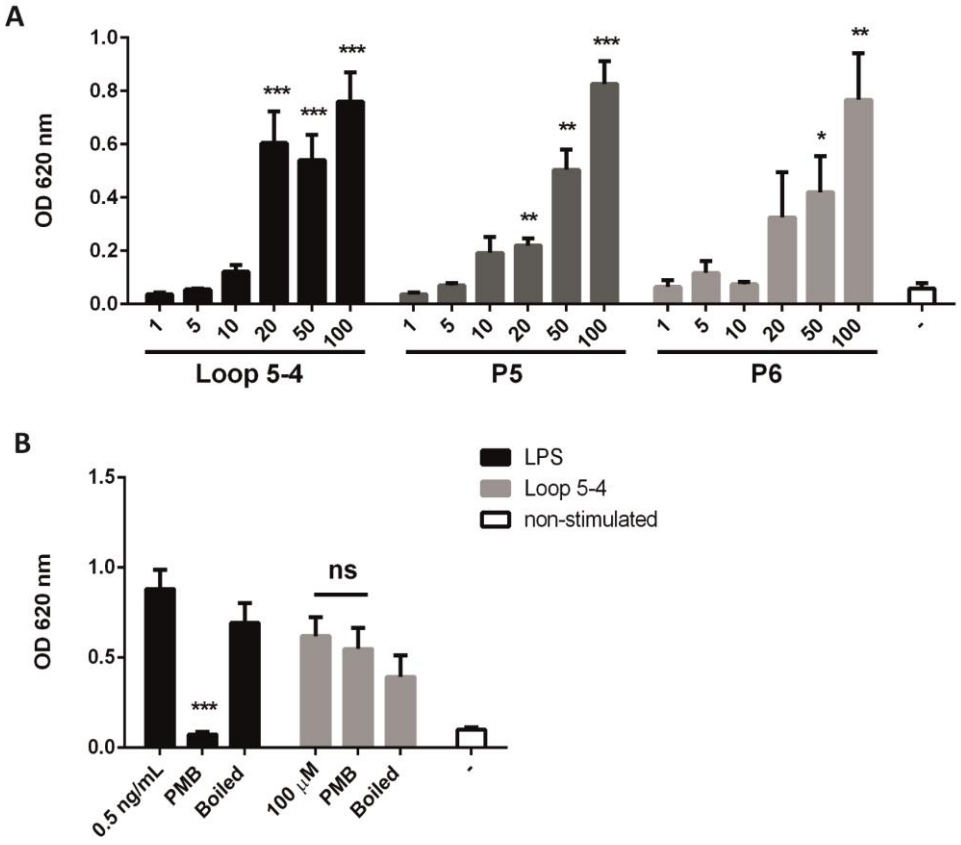

Figure 4-9. Peptides activate NF-κB in a doses dependent manner, and the peptide activity is not due to LPS contamination. A. ThP1 NF-κB cells were left unstimulated (-) or stimulated with 1, 5,10, 20, 50 or 100 μM of peptides for 24 h. NF-κB activation was measured using QUANTI-Blue™. **B.** ThP1 NF-κB cells were left unstimulated (-) or stimulated with 0.5 ng/mL of LPS or 100 μM of loop 5-4 for 24 h. Samples were previously incubated for 30 min with polymyxin B (PMB) or boiled for 15 min. NF-κB activation was measured using QUANTI-Blue™. Data shown as mean ± SEM, N=3 independent experiments. **A**. One-way ANOVA vs unstimulated cells. **B.** Paired t-test vs non-treated, *p<0.05, **p<0.01, ***p<0.001.

4.4.2. Peptide activity in primary human macrophages

Peptide activity was also determined in primary human macrophages. Prof. Midwood stimulated primary human macrophages with peptides 1-9 and observed that only peptides 5 and 6 could induce IL-8 to the same levels as FBG-C (Figure 4-10 A). To corroborate these data, I stimulated human macrophages with different doses of

peptide 5 and loop 5-4 and found that they could induce IL-8 in a dose dependent manner. However, the synthesis of IL-6 and TNF was variable among the donors and not significantly induced compared to unstimulated cells (Figure 4-10 B).

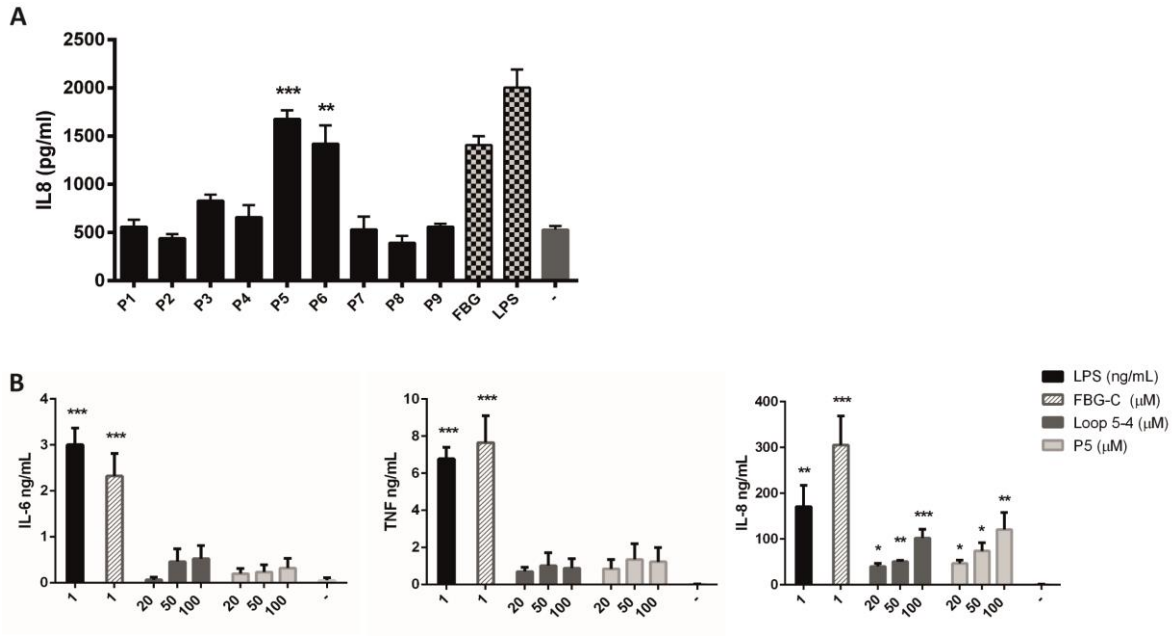

Figure 4-10. P5 and P6 induce IL-8 in primary human macrophages. A. Primary human macrophages were left unstimulated (-) or stimulated with LPS (1ng/mL), FBG-C (1 μM) or 20 μM of peptides 1-9 for 24 h, and cytokine synthesis was measured by ELISA. **B.** Primary human macrophages were left unstimulated or stimulated with LPS (1ng/mL) or 20, 50, 100 μM of peptides 5 or loop 5-4 for 24 h, and cytokine synthesis was measured by ELISA. Data shown as mean ± SEM, N=3 independent donors. One-way ANOVA vs unstimulated cells, *p<0.05, **p<0.01, ***p<0.001.

The anti-TLR4 function-blocking antibody and TAK 242 were used to determine if the activity of peptides 5 and loop 5-4 was TLR4 dependent. TAK 242 significantly reduced LPS and FBG-C induction of IL-8, and decreased the synthesis of IL-8 by peptides 5 and loop 5-4. However, the TLR4 antibody did not inhibit IL-8 induction by peptides 5 and loop 5-4.

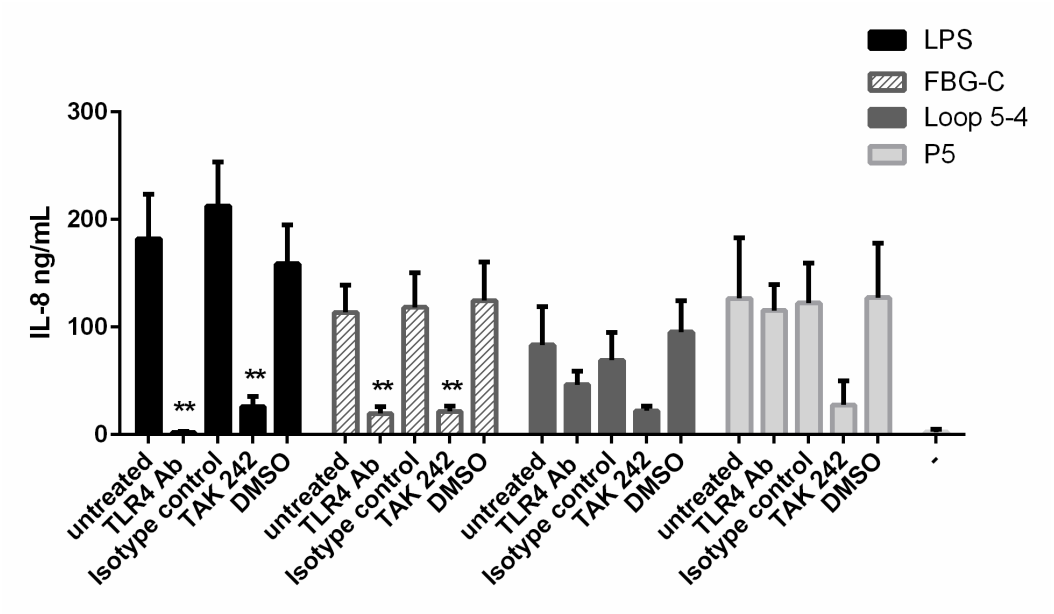

Figure 4-11. TLR4 dependency of the activity of P5 and loop 5-4. Primary human macrophage were pre-incubated for 1 h with 25 µg/mL of TLR4 antibody (TLR4 Ab) or isotype control or 6 h with 3 µM of TAK 242 or DMSO, prior to stimulation with 1 ng/mL of LPS or 100 µM of peptide 5 or loop-5-4. Cytokine synthesis was measured after 24 h by ELISA. (-) unstimulated cells. Data shown as mean ± SEM, N=3 independent donors. One-way ANOVA vs non-treated, *p<0.05, **p<0.01.

In summary, peptides 5 and 6 can induce NF-κB activation in ThP1 NF-κB cells in a dose dependent manner. Scrambled controls showed that the activity of P5 and P6 is sequence specific. The overlapping region of peptide 5 and 6 (KTRYK) corresponds to loop 5 in the sequence of the FBG-C. The peptide containing only the overlapping sequence of P5 and P6 (loop 5-1) showed no activity, however, longer versions including this loop (loop 5-3 and loop 5-4) could also activate NF-κB in a dose dependent manner. These results were corroborated in primary human macrophages where peptides 5, 6 and loop 5-4 could induce IL-8 in a dose dependent manner and this activity was TLR4 dependent when TLR4 activation was blocked using TAK 242.

4.4.3. Blocking assays using peptides

Next, I examined if the peptides 1-9 were able to block the interaction between FBG-C and TLR4 in the solid phase binding assay. TLR4 was pre-incubated with the peptides prior to being added to plates coated with FBG-C. P5, P6 and P7 could significantly block the binding of TLR4 to FBG-C, reducing the binding affinity among these proteins. In contrast, P4 and P8 increased the binding affinity of TLR4 to FBG-C (Figure 4-12, Table 4-3).

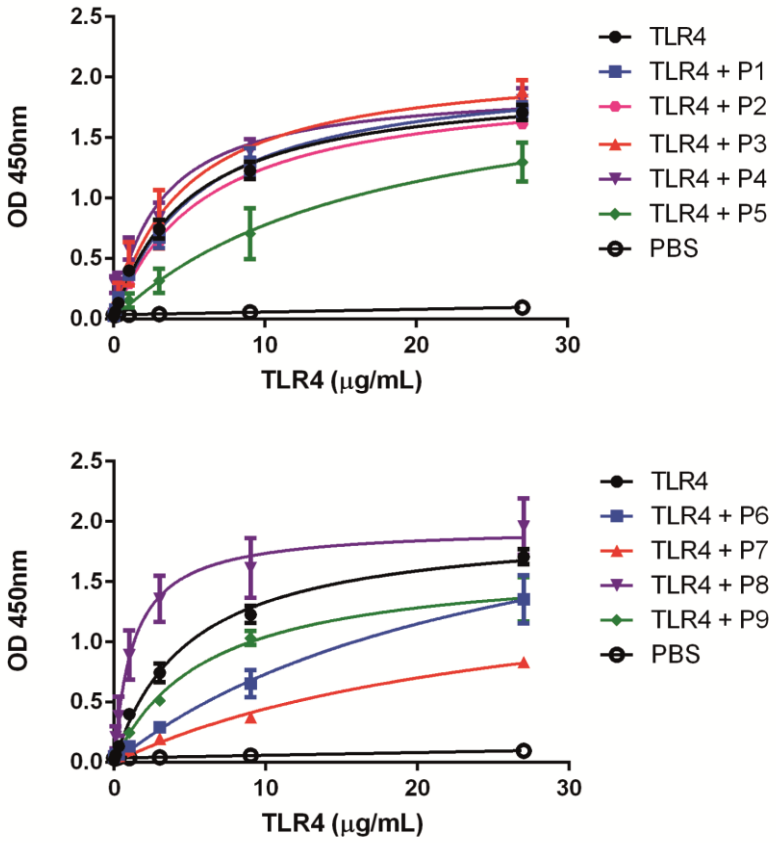

Figure 4-12. Peptides 5, 6 and 7 partially block TLR4-FBG-C interaction *in vitro*. Increasing doses of TLR4 were pre-incubated with 200 µM of peptides before adding them to 96 well plates coated with FBG-C. Curves were fitted in GraphPad Prism using one binding site hyperbola analysis. Data shown as mean ± SEM, N=3.

Table 4-3. Changes in the affinity of TLR4 to FBG-C after incubation with peptides.

Protein	K_D (nM) ± SD	p value
TLR4 only	68.85 ± 7.79	
TLR4 + P1	78.75 ± 11.33	0.280
TLR4 + P2	83.29 ± 5.24	0.056
TLR4 + P3	64.45 ± 15.67	0.672
TLR4 + P4	42.63 ± 10.06	* 0.023
TLR4 + P5	241.22 ± 89.15	* 0.028
TLR4 + P6	370.82 ± 141.64	* 0.021
TLR4 + P7	383.71 ± 113.31	** 0.008
TLR4 + P8	31.87 ± 8.22	* 0.048
TLR4 + P9	86.26 ± 16.57	0.17

To determine if any of the peptides could inhibit the activity of FBG-C, ThP1 NF-κB cells were pre-incubated with the peptides prior to stimulation with FBG-C. Peptide 5 and 6 increased the activation of NF-κB transcription factor compared to FBG-C only. Peptide 7 could reduce the activity of FBG-C (56.6%) but this result did not reach significance (*p* value=0.06) (Figure 4-13).

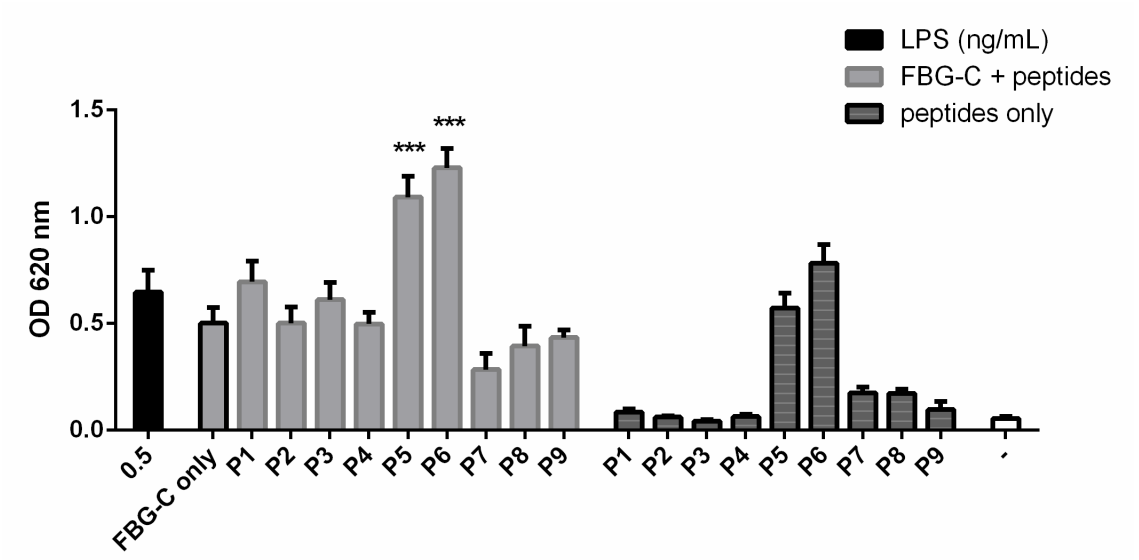

Figure 4-13. FBG-C activation of NF-κB is not blocked by peptides in ThP1 NF-κB cells. ThP1 NF-κB cells were left unstimulated (-) or pre-incubated with 100 µM peptides (except P1 and P3 where 50 µM was used) prior to stimulation with 0.5 µM of FBG-C for 24 h. NF-κB activation was measured using QUANTI-Blue™. Data shown as mean ± SEM, N=3 independent experiments. Paired t-test vs FBG-C only, *p<0.05, **p<0.01, ***p<0.001.

Together these data revealed that peptides 5, 6 and 7 could significantly diminish the affinity of TLR4 binding to FBG-C, indicating that these regions are involved in the interaction with the receptor. Adding P5 or P6 to ThP1 NF-κB cells prior to stimulation with FBG-C, demonstrated an additive effect when the peptides and protein are used together to stimulate the cells. In summary, the regions corresponding to peptide 5 and 6 could be involved in activation and binding to TLR4, while the region including peptide 7 may be required for binding to the receptor.

4.5. Analysis of loops 5, 7-8 and 10 in the FBG domain of the tenascin family members

Multiple sequence alignments of the FBG domain of the tenascin family members revealed a positively charged region at the C-terminus of the proteins that was conserved in FBG-C, -R and -W but not in FBG-X. Measuring the activity of the peptides in ThP1 NF-κB and primary human macrophages showed that peptide 5 and 6 can induce an immune response. Blocking studies using the peptides revealed that the region corresponding to peptide 5 and 6 is also involved in TLR4 binding. In addition, these data showed that peptide 7 can block the interaction between FBG-C and TLR4 in the solid phase binding assay, and reduced NF-κB activation by FBG-C. Next, I will examine and compare these regions in the FBG domains of the tenascin family members to establish which amino acids are conserved in the active FBG domains (-C, -R and -W) and which are different in the inactive FBG-X.

4.5.1. Peptides 5 and 6

The overlapping sequence of peptide 5 and 6 corresponds to loop 5 in the structural models of the FBG domains of the tenascin family members. Loop 5 is located in the P-subdomain and includes amino acids that are exposed in all the FBG domains. Conservation of positively charged amino acids (lysines and arginines) is observed for FBG-C, -R and -W, in addition to serines, hydrophobic and negatively charged amino acids. However, FBG-X exhibits a different amino acid composition in this loop: only one arginine is found in this sequence, and the other positive charges have been replaced by hydrophobic amino acids. FBG-X also contains two histidines that are not present in the other tenascin family members (Figure 4-14).

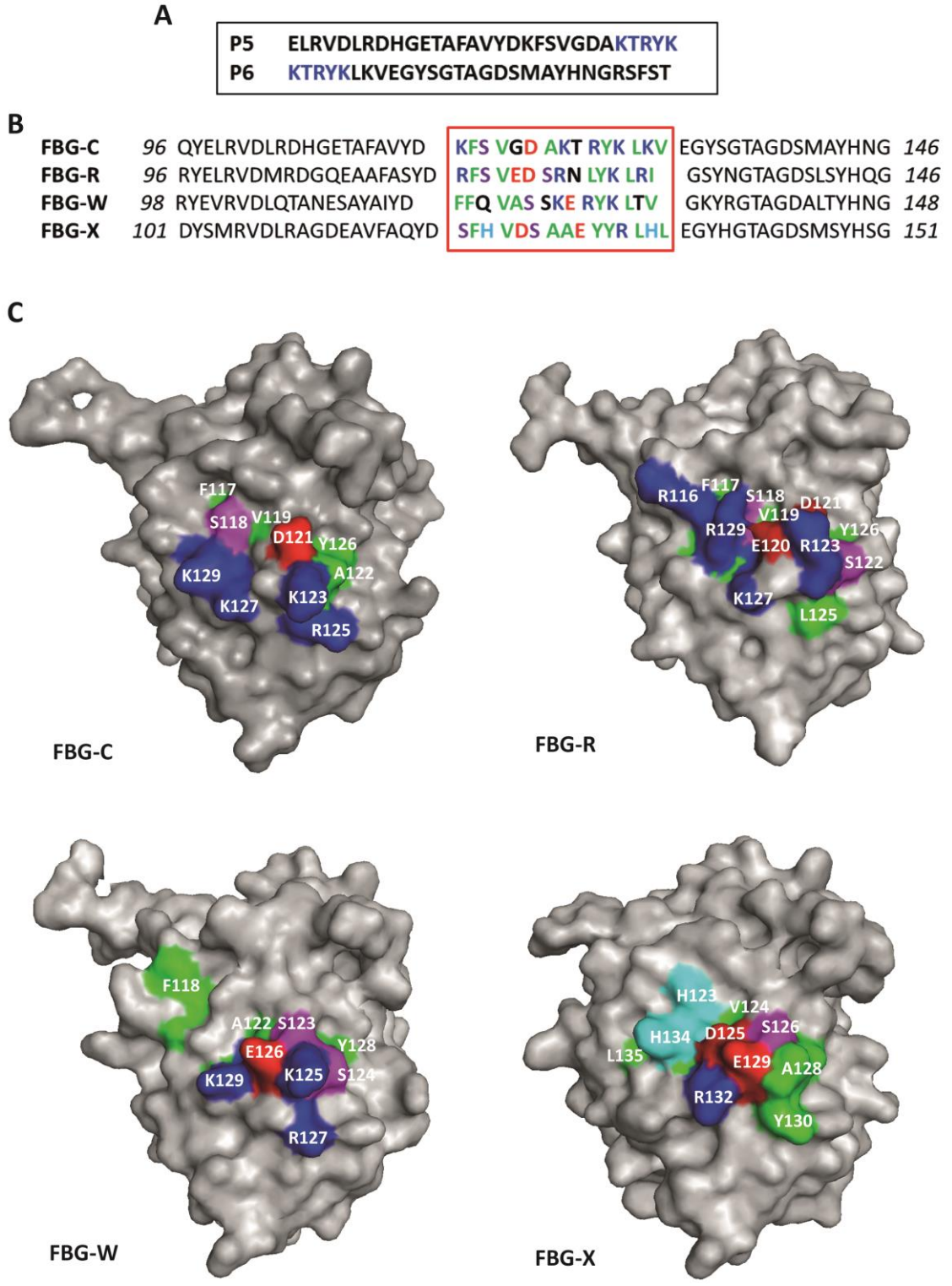

Figure 4-14. Models of loop 5 in the FBG domain of the tenascin family members. A. Sequence of peptide 5 and 6 highlighting overlapping amino acids. **B.** Sequence alignment of the FBG domains of the tenascin family members showing amino acid composition of loop 5 (red box). Hydrophobic amino acids are in green, positively charged amino acids in blue, negatively charged amino acids in red, serines in purple and histidines in cyan. **C.** Models of the FBG domain of tenascin-C, -R, -W and –X highlighting the amino acid composition in loop 5.

Electrostatics maps of FBG-C, -R, -W and -X structural models were calculated in PyMOL and also showed differences in the region corresponding to loop 5. Positively charged regions are conserved in FBG-C, -R and -W, but not in FBG-X. This analysis highlights the differences in charges in the overall structure of the proteins and correlates with their respective isoelectric points (Figure 4-15).

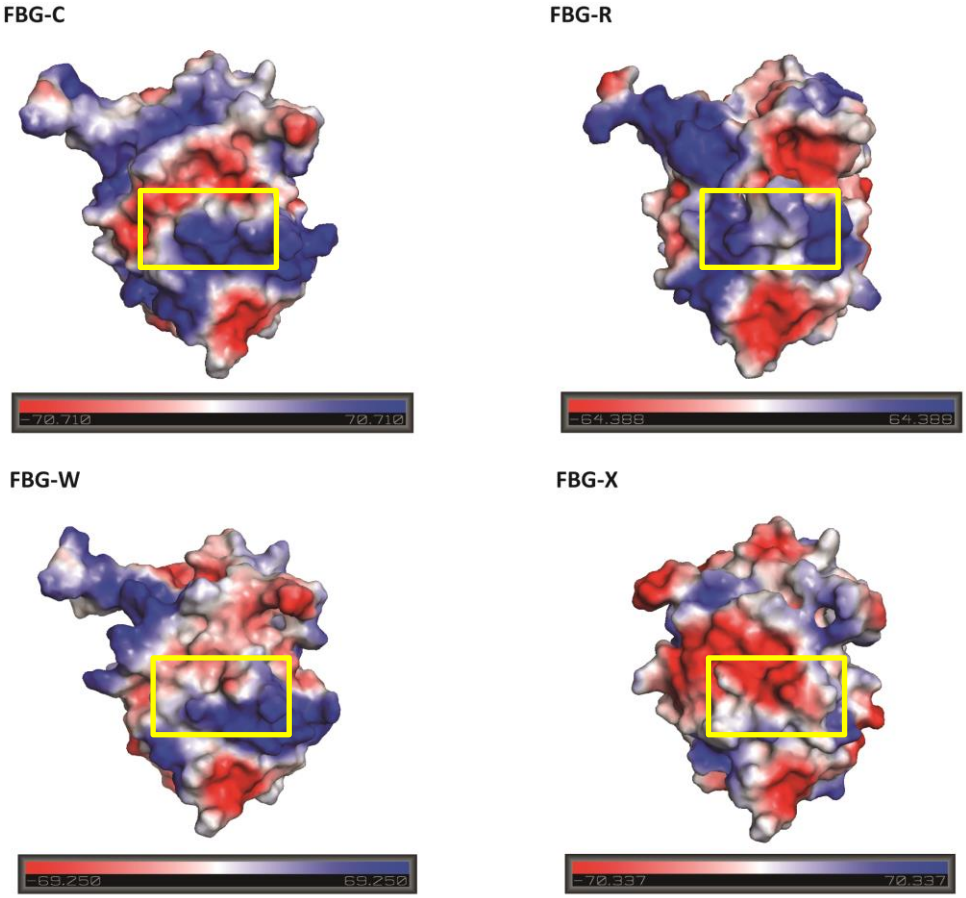

Figure 4-15. Electrostatic maps of FBG-C, -R, -W and -X. The electrostatic maps of FBG-C,-R, -W and -X were calculated using the vacuum electrostatic function of PyMOL Molecular Graphics System. Blue: positively charged. Red: negatively charged. Yellow box indicates the region corresponding to loop 5. The isoelectric points of the FBG domains are: FBG-C: 8.78; FBG-R: 8.63; FBG-W: 9.18; FBG-X: 5.54.

4.5.2. Peptide 7

Peptide 7 couldn't activate cells but did reduce the binding of TLR4 to FBG-C, suggesting that this region could be involved in the interaction of these proteins. Peptide 7 corresponds to the sequence of loop 7, α helix and loop 8 of the FBG domains of the tenascin family members (Figure 4-16).

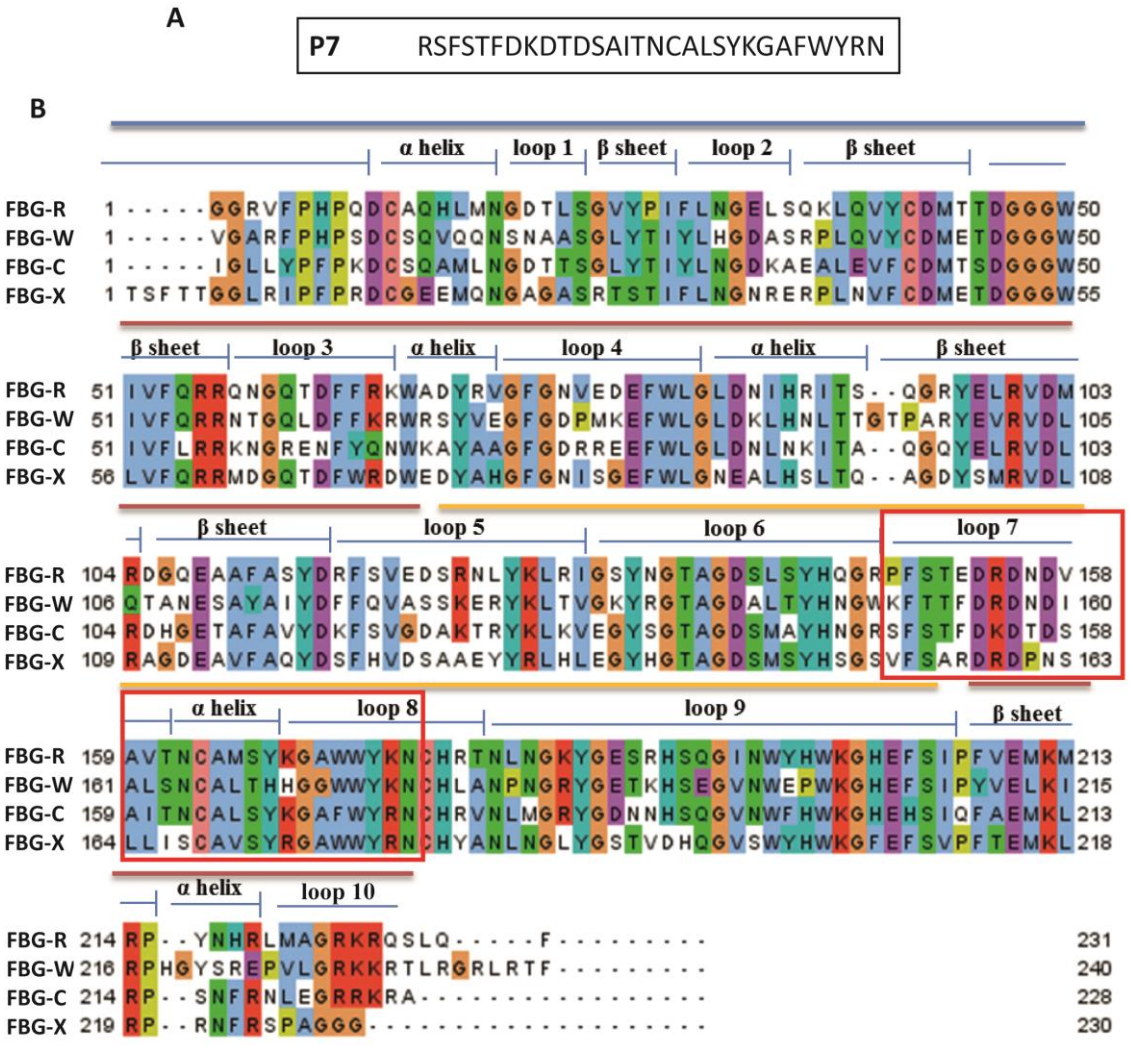

Figure 4-16. P7 corresponds to loops 7-8. A. Peptide 7 sequence. **B.** Multiple alignment analysis of the FBG domain of tenascin family members highlighting the region corresponding to P7 (red boxes).

Analysis of the region corresponding to peptide 7 in the structurala models of the FBG domain of the tenascin family members showed that it is located in the P-subdomain and comprised two loops that are in the surface of the proteins. This area is highly homologous among the FBG domains and it is characterised by exposed hydrophobic and polar amino acids, in addition to positively and negatively charged regions (Figure 4-17). There are some differences in specific amino acids between FBG-C, -R and -W and FBG-X. For example, FBG-X has R157 where the other FBG domains have a hydrophobic amino acid (F), except FBG-R which has a negative charged amino acid (E152). FBG-C, -R and –W also have polar and negatively charged amino acids (T156, D157 in FBG-C), while in FBG-X this sequence has been substituted by a P161 and N162. Finally, a slight variation can be observed in the position of the cluster of exposed hydrophobic and polar amino acids in FBG-C (I160, T161 and N162) compared to FBG-X (L165, I166 and S167).

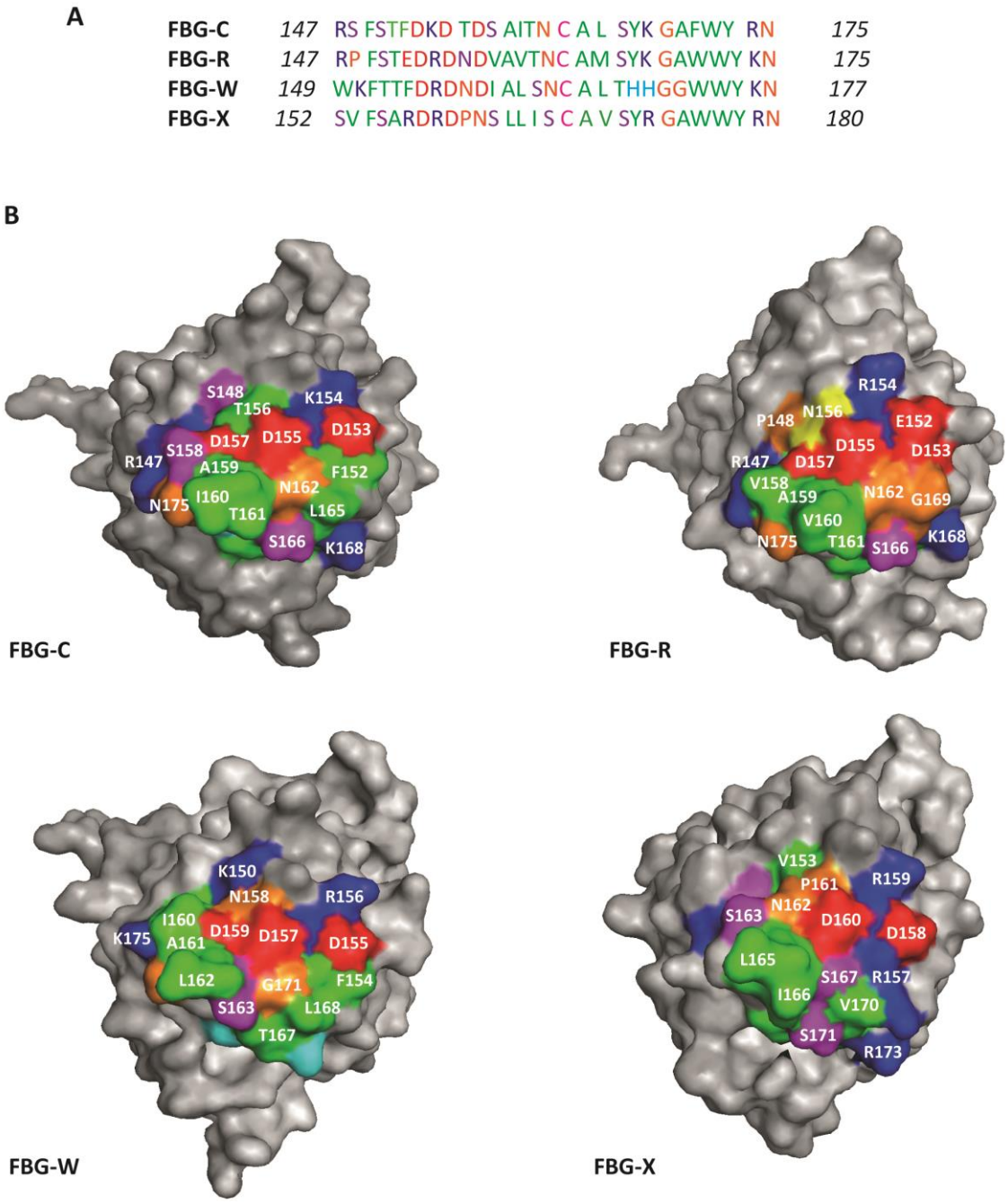

Figure 4-17. **Amino acid composition of peptide 7. A.** Sequence alignment of the FBG domains of the tenascin family members showing amino acid composition of peptide 7. Hydrophobic amino acids are in green, positively charged amino acids in blue, negatively charged amino acids in red, serines in purple, histidines in cyan and other amino acids in orange. **B.** Models of the FBG domain of tenascin-C, -R, -W and -X highlighting P7 amino acids composition.

4.5.3. C-terminus of the FBG domains

Multiple sequence alignments showed a region that was diverse among the FBG domain of the tenascin family members, which corresponds to loop 10 at the C-terminus of the proteins. Structural models of the FBG domains showed that the amino acid composition, specifically the positively charged amino acids, is conserved in FBG-C, -R and -W but not in FBG-X, shortening the C-terminal region of FBG-X compared to the other proteins. Loop 10 is part of the B-subdomain and comprises a surface loop that protrudes from FBG-C, -R and -W (Figure 4-18).

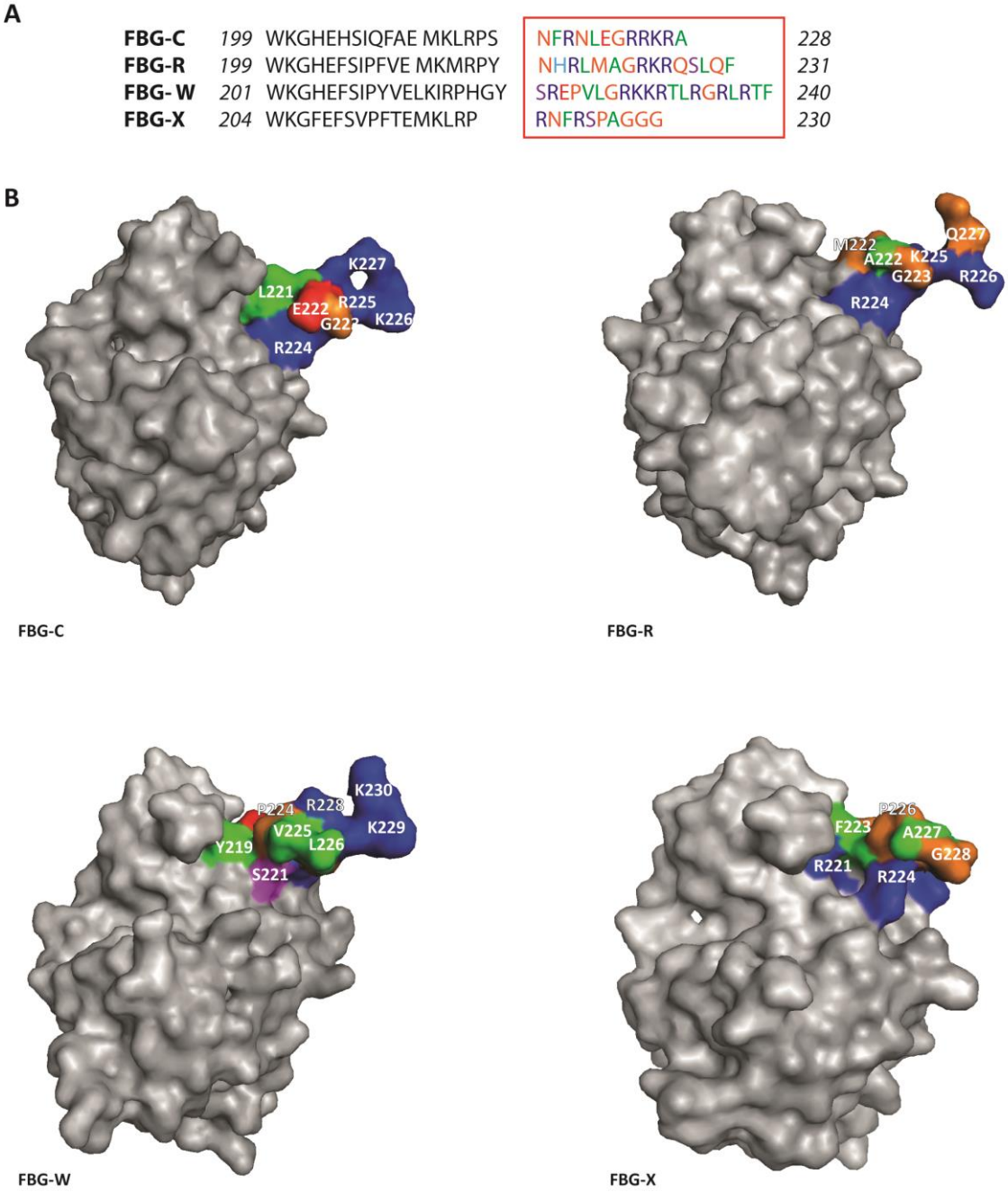

Figure 4-18. Amino acid composition of loop 10 of the FBG domain of the tenascin family members. A. Sequence alignment of the FBG domains of the tenascin family members showing amino acid composition of loop 10. Hydrophobic amino acids are in green, positively charged amino acids in blue, negatively charged amino acids in red, serines in purple, histidines in cyan and other amino acids in orange. **B.** Models of the FBG-C, -R, -W and -X labelling the amino acid composition in loop 10.

In summary, these analyses have revealed three regions that contain amino acids conserved in FBG-C, -R and -W but not in FBG-X, suggesting that these residues could be involved in the activation and binding to TLR4. In Figure 4-19, the three regions are coloured in the predicted model of FBG-C, to highlight their position in the overall model of the protein. Loop 5 and loop 7-8 are in close proximity, while loop 10 is protruding at one side of the protein.

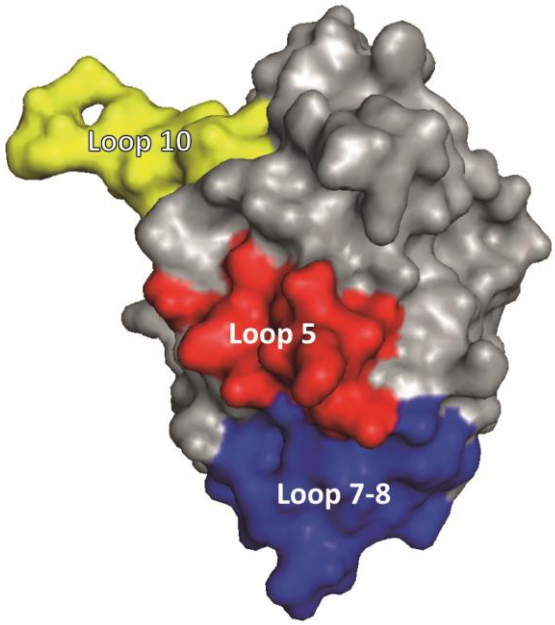

Figure 4-19. Position of loop 5, loop 7-8 and loop 10 in the predicted model of FBG-C. The regions corresponding to loop 5, loop 7-8 and loop 10 were coloured in red, blue and yellow respectively using PyMOL Molecular Graphics System.

4.6. Discussion

Using a combination of approaches, in this chapter I identified 3 regions of interest that could be involved in the activation of TLR4. Peptide mapping showed that peptides 5 and 6 were the only peptides able to activate NF-κB in ThP1 NF-κB cells and IL-8 synthesis in primary human macrophages, and this activity was TLR4 dependent. The overlapping region among these peptides corresponds to loop 5 in the FBG domain of the tenascin family members. In addition, peptide 5, 6 and 7 could inhibit the interaction between TLR4 and FBG-C in the solid binding assay, reducing the affinity of FBG-C binding to the receptor. The region comprising peptide 7 corresponds to loop 7-8 in the structural models of the FBG domains. Finally, comparison of the amino acid sequences and predicted structural models showed a high degree of conservation among the FBG domains of the tenascin family members, but also highlighted some diverse regions such as loop 10. These data suggest that loop 5, loops 7-8 and loop 10 could be involved in the binding and activation of TLR4 and these regions will be further investigated in chapter 5.

4.6.1. Sequence comparison and modelling of the FBG domains of the tenascin family members

I used the multiple sequence alignment software Clustal Omega to compare the identity and similarity of the FBG domains of the tenascin family and fibrinogen. The new version of this software provides a high quality alignment, based on a "guide tree" algorithm, where the sequences are aligned fast and accurately based on their identity and similarity [343]. Pairwise alignments showed a high % of sequence identity among the FBG domains of the tenascin family members. Multiple sequence alignment demonstrated that some regions of the proteins which are not identical, presented

conservation in the properties of their amino acid sequences, for example hydrophobic or charged regions. These alignments allowed the direct comparison of the FBG domains of the tenascin family together and highlighted other regions that were different among the proteins. The amino acid composition in loop 10 at the C-terminus of the proteins was conserved in FBG-C, -R and -W but not in FBG-X, indicating that this could be a potential region involved in TLR4 activation or binding.

Another *in silico* approach used was protein homology modelling, due to the lack of crystal structure for the FBG domains of the tenascin family. Protein homology modelling is a commonly used tool to predict conserved binding or catalytic sites in proteins, to design antibody epitopes or inhibitors and to refine NMR structures [344]. The data obtained with this analysis could generate new hypotheses that can be tested experimentally to be proven. The models of the FBG domains of the tenascin family members presented a similar pattern of folding as the fibrinogen γ chain. Alignments of the models of the FBG domains of the tenascin family demonstrated conservation also at the structural level. However, this analysis is based on theoretical approaches and not the crystal structure of the proteins. For this reason, conclusions from this comparison have to be validated experimentally.

SWISS-MODEL was selected as the modelling software, as it is the most widely used structure modeller server that is completely automated. SWISS-MODEL allows the user to select the template for modelling the target protein from their PDB template library (SMTL), or manually select the template, which was the option used in this project. Template-protein alignment can also be entered in the platform, providing information to calculate sequence identity and agreement between predicted secondary structure and solvent accessibility between target and template, increasing the reliability of the model. The model is then generated automatically using Pro-ModII or

MODELLER software, and the model quality is assessed and scored estimating a value of model accuracy [307]. Other automated softwares commonly used are 3D-JIGSAW and ROSETTA, the latter being able to create *de novo* prediction models without a protein template [345]. However, SWISS-MODEL has a user-friendly interface and can also predict oligomeric structures or ligand and cofactors for the target protein based on the conservation between the target protein and the templates in the PDB library [307]. MODELLER is the most widely used modelling software and allows refinement and optimisation of the structural model, especially the regions with no secondary structure [346]. However, it requires that the user has advance programing skills as it has a complex interface.

Protein modelling has limitations as it is based on theoretical analyses and only qualitative conclusions can be drawn based on this method. The different softwares available can predict diverse protein structures based on the algorithm used and the parameters set to create the models. The reliability of the model is also determined by the degree of sequence identity among the target and template protein. In this case, the % of identity among the FBG domains of the tenascin family members and fibrinogen γ chain is approximately 30 %. This is considered the bottom limit to model any protein, as below this level of similarity, large numbers of gaps and errors can occur in the alignment leading to the generation of inaccurate models [344, 347]. The FBG domains were also modelled by Brian Marsden using FIBCD1 as a template, which is 43% identical to the FBG domain of the tenascin family, and little differences were observed compared to the models made using fibrinogen γ chain as a template. The global quality estimation score (GMQE) is another measurement generated by SWISS-MODEL, which estimates the quality of the model. GMQE is defined with a number between 0 and 1, where higher numbers indicate higher reliability. The models

generated for the FBG-C, -R, -W and -X had a GMQE of 0.7, which is acceptable, but the software highlighted some regions where the proteins were poorly modelled, such as areas of little secondary structure. In particular, the C-terminal region of the FBG domains were not accurately modelled as a structural template is not found in the crystal structure of the fibrinogen γ chain. The conformational state of the proteins used as a template is another factor that will be retained in the resultant homology model, and this is particularly important when modelling protein channels or the Apo (unbound) versus Holo (bound) state of a ligand binding site [347].

Due to the limitations of the predicted structural models of the FBG domains, I started, in collaboration with the group of Prof. Oppermann in the Structure Genomic Centre, to establish the conditions to crystallise the FBG domain of tenascin-C. Microcrystals were obtained for this protein (Figure 4-20), but further optimization was required for X-ray diffraction analysis. By the time of submission of this DPhil thesis the crystal structure of the FBG-C hasn't yet been determined.

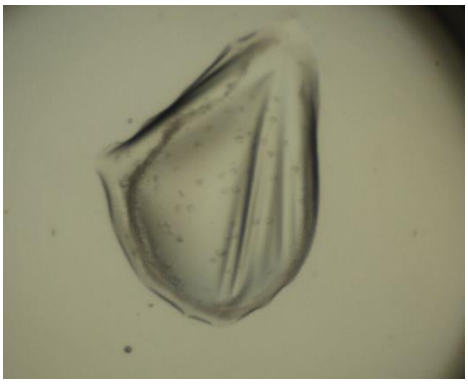

Figure 4-20. Microcrystal of the FBG domain of tenascin-C. FBG-C was purified and concentrated to 9 mg/mL and then transferred to crystallization plates at 20°C and 4°C. Microcrystals were obtained after 3 months at 20°C.

Altogether these data suggest that multiple sequence alignment analysis and protein structural modelling are tools which could help to predict the structure of

proteins and areas involved in protein interactions; however, they do not provide any factual evidence of the significance of these regions in protein complexes.

4.6.2. Peptide mapping of the active site of FBG-C

Peptide mapping is a technique used before to map the binding site of FBG-C and the C-terminus domain of fibrinogen γ chain to $\alpha_v\beta_3$ integrin. LaFleur *et al*. [328] found that aortic smooth cells adhered to plates coated with the FBG domain but not the FNIII repeats of tenascin-C, and this interaction was integrin dependent. To map the specific region of FBG-C involved in cell adhesion, they evaluated the same 9 peptides used in this DPhil project, and found that only peptide 8 could block the adhesion of cells to plates coated with FBG-C or full length tenascin-C. In addition, aortic smooth cells could only adhere to plates coated with peptide 8 or FBG-C, but not the other peptides. Yokoyama *et al.* [198] then used peptide mapping to elucidate the specific region of the C-terminus domain of fibrinogen γ chain and FBG-C that binds to $\alpha_v\beta_3$ integrin, which contribute to cell adhesion. Using CHO cells expressing $\alpha_v\beta_3$ and control CHO cells, they found that $\alpha_v\beta_3$ CHO cells can adhere to plates coated with FBG-C and this interaction could be blocked using RGD peptides, EDTA or $\alpha_v\beta_3$ function blocking antibody. $\alpha_v\beta_3$ CHO cells could adhere to plates coated with peptide 8 in a dose dependent manner, and this peptide shares a similar sequence with the peptides γC346–358 and γC190–202 of fibrinogen γ chain. From these data, the authors suggested a common binding site of peptide 8 and fibrinogen γ chain to $\alpha_v\beta_3$ integrin.

Using this approach, I found that only peptide 5 and 6 could induce the activation of NF-κB transcription factor in ThP1 cells and IL-8 expression in primary human macrophages. The overlapping sequence of these peptides corresponds to a surface loop (loop 5) in the structural model of the FBG domains of the tenascin family members.

Analysis of this region in the predicted models of the FBG domains revealed that positively charged amino acids are conserved in FBG-C, -R and -W, but not in FBG-X. These data correlate with the activity of the FBG domains described in the previous chapter, where only FBG-C,-R and -W can induce an immune response, and suggest that this loop is involved in the activation of TLR4. Shorter versions of loop 5 (< 20 amino acids) could not activate NF-κB transcription factor indicating that adjacent amino acids could be necessary for the peptide to form a structure to bind to the receptor, or they could be also contributing to the activation of TLR4.

One of the limitations of using peptides is that high concentrations are needed to obtain an immune response similar to FBG-C. In addition, the addition of higher concentration of peptides can result in cell toxicity, such as the case of peptide 1. IL-8 was the only cytokine induced consistently by the active peptides, indicating that a 30 amino acids peptide is not sufficient to induce the synthesis of cytokines similarly to FBG-C and other regions of the protein might also be necessary.

The activity of the peptides was inhibited by the intracellular TLR4 inhibitor TAK 242, showing that they are acting via TLR4. However, the TLR4 antibody was not able to reduce IL-8 expression by the peptides. These data suggests that the antibody could be binding to a region in TLR4 which is not interfering with the activation of the receptor by the peptides. The anti-TLR4 antibody is a polyclonal antibody and the epitopes to which the antibody is binding are not known. To corroborate the TLR4-dependent activity of the peptides, experiments could be performed using TLR4 null cells, as this approach has been used before to demonstrate that FBG-C was acting via this receptor [89].

Blocking assays with peptides revealed that in addition to P5 and P6, P7 could significantly block the binding of TLR4 to FBG-C reducing the affinity of the protein for the receptor. These results suggest that the region corresponding to peptide 7 can be involved in the binding of FBG-C to TLR4. In the structural models of the FBG domain of the tenascin family members, peptide 7 corresponds to loop7-8, a region comprising exposed loops in the P sub-domain of the proteins. This region is highly homologous among all the FBG domains of the tenascin family, however only a few amino acids were conserved in FBG-C, -R and -W and different in the amino acid sequence of FBG-X. These data suggest that loop 7-8 could be involved in binding but is not essential in the activation of TLR4.

Other peptides showed the opposite effect compared to peptide 7, such as peptide 4 and 8, which increased the affinity of TLR4 to FBG-C. Although this effect was significant, the increase in the binding affinity of the proteins was modest (<2 fold), suggesting that this could be an artificial effect due to the limitations of the assay. However, these peptides could be assisting in the binding of TLR4 to FBG-C. The peptides could be binding to FBG-C and changing its conformation increasing its affinity for TLR4, as we have observed in our lab that FBG-C could form oligomers. Peptides could also be binding to TLR4 in a non-specific manner, bridging two TLR4 monomers and inducing TLR4 dimerization, enhancing then the binding affinity to FBG-C. Peptide 4 is able to activate at low levels NF-κB transcription factor in ThP1 cells; however when it was added in combination with FBG-C, it did not enhance the protein activity. The lack of activity of these peptides in ThP1 NF-κB cells and primary human macrophages suggests that this effect could be an experimental artefact, but further analyses are needed to determine the involvement of these regions in the interaction between FBG-C and TLR4.

The activity of FBG-C was also assessed in the presence of the peptides in ThP1 NF-κB cells, by pre-incubating the cells with the peptides prior to stimulation with FBG-C. The results showed that peptide 5 and 6 could enhance the protein activity, and peptide 7 could partially block the activation of NF-κB, but this effect was not significant. These results suggest an additive effect when the peptides and FBG-C are added in combination to stimulate cells, indicating that peptide 5 and 6 do not interfere with the activity of FBG-C at the concentrations used. Further analyses could include adding higher concentrations of peptides, but this could have an effect on cell viability, or use sub-optimal doses of FBG-C or the peptides to assess competition for the binding site in TLR4.

Altogether peptide mapping revealed that loop 5 and loops 7-8 of FBG-C could be regions involved in binding and activation of TLR4. Further experiments will be performed to corroborate the significance of these sequences in the TLR4-FBG-C interaction.

4.7. Summary

Multiple sequence alignment, protein structural modelling and peptide mapping highlighted specific regions (loop 5, loops 7-8 and loop 10) involved in binding and activation of TLR4 conserved in FBG-C, -R and -W, but different in FBG-X. However, further analyses are needed to corroborate the importance of these regions. In the next chapter, mutagenesis experiments will be performed, where specific amino acids in loops 5, 7-8 and 10 of FBG-C and -X, will be mutated to dissect their involvement in the binding and activation of TLR4.

Chapter 5 – Identification of the pro-inflammatory epitope of FBG-C

Chapter 5. Identification of the pro-inflammatory epitope of FBG-C

5.1. Introduction

In the previous chapter, I identified 3 regions that could be potentially involved in TLR4 activation and binding, which were conserved in FBG-C, -R and –W, but different in FBG-X. These regions correspond to loop 5 and loops 7-8 in the P-sub domain, and loop 10 at the C-terminus. In this chapter, I will mutate specific amino acids in these regions of FBG-C to assess their involvement in TLR4 activation. In addition, I will mutate the same regions in FBG-X to attempt to recover its activity. The activity of mutant proteins will be assessed in ThP1 NF-κB cells and primary human macrophages. The binding affinity of the mutant proteins to TLR4 will also be tested using the solid phase binding assay. This analysis will determine which amino acids are essential for the activation and binding of FBG-C to TLR4.

5.2. Mutations in loop 5 – peptides

Peptide mapping determined that only peptides 5 and 6 could activate immune cells. The overlapping sequence of these two peptides KTRYK locates in loop 5 in the active FBG domain of the tenascin family members. In chapter 4, another peptide was designed (loop 5-4), which comprises the overlapping region between peptide 5 and 6 and the adjacent amino acids. This peptide was able to induce the activation of NF-κB in ThP1 cells and cytokine synthesis in primary human macrophages (Figure 4-8). In loop 5, a cluster of positively charged amino acids are conserved in the sequence of FBG-C, -R and –W (KTRYKLK) but not in FBG-X. Mutant peptides were then designed to assess the involvement of these residues in the activation of immune cells.

Four new peptides were made: loop 5-deletion has the sequence KTRYKLK of loop 5 deleted; loop 5-mutant 1 or 2 has mutations in the first or second pair of positively charged amino acids respectively. Loop 5-mutant 3 has the four positively charged amino acids in KTRYKLK substituted by alanine (Table 5-1)

Table 5-1. Amino acid sequences of loop 5 mutant peptides. The overlapping sequence of peptide 5 and 6 locates in loop 5, which corresponds to a cluster of positively charged amino acids KTRYKLK. 4 peptides were designed to mutate or delete this sequence (blue). Deletion is indicated by a red arrow. 3 peptides were designed containing alanine substitutions (red) to positively charged amino acids in this sequence.

Loop 5-4	AFAVYDKFSVGDA**KTRYKLK**VEGYSGTAGD
Loop 5-deletion	GETAFAVYDKFSVGDA▼VEGYSGTAGDSMAY
Loop 5-mutant 1	AFAVYDKFSVGDA**A**T**A**YKLKVEGYSGTAGD
Loop 5-mutant 2	AFAVYDKFSVGDAKTRY**A**L**A**VEGYSGTAGD
Loop 5-mutant 3	AFAVYDKFSVGDA**A**T**A**Y**A**L**A**VEGYSGTAGD

The activity of the mutant peptides was assessed in ThP1 NF-κB cells and primary human macrophages. Loop 5-deletion showed a significant reduction in the activation of NF-κB and IL-8 induction. Loop 5-mutant 1, 2 and 3 also presented a significant reduction in NF-κB activation and IL-8 production compared to loop 5-4 (Figure 5-1). These data showed that more than 2 positively charged amino acids in loop 5 are necessary for the activation of immune cells by the peptides.

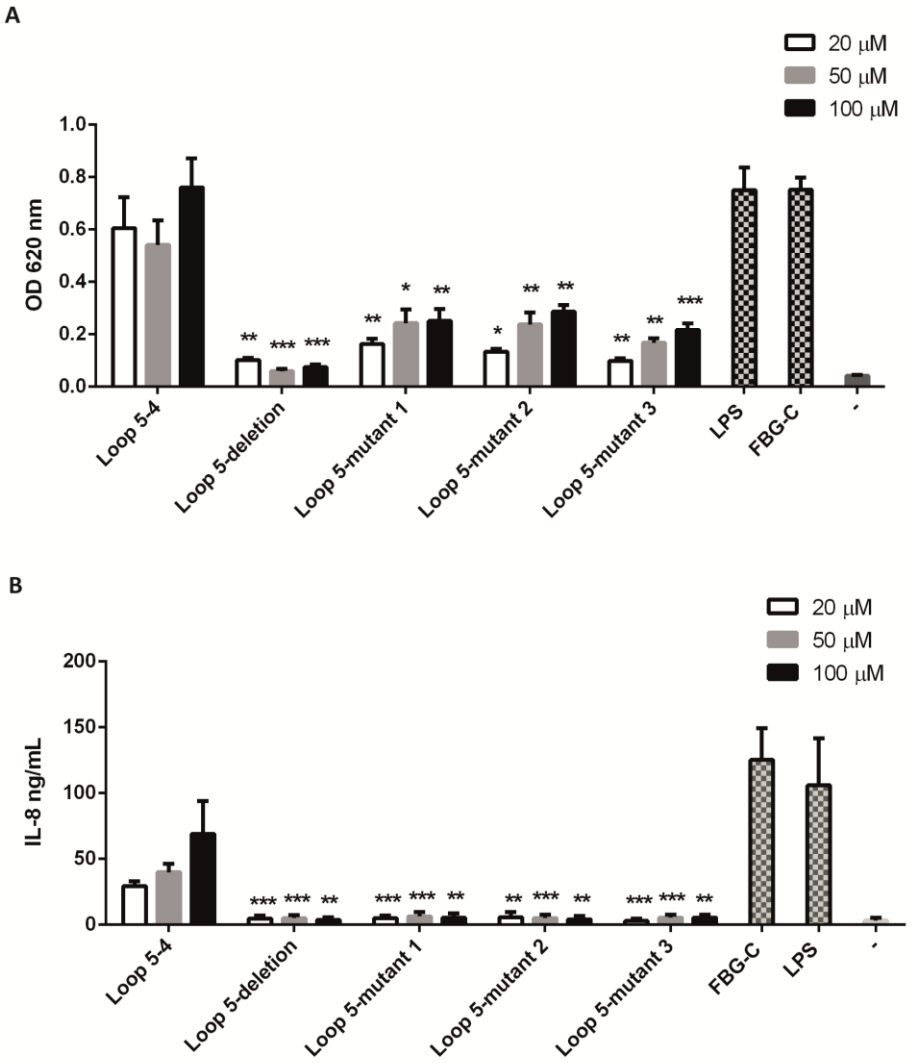

Figure 5-1. Positive charges in loop 5 are essential for loop 5-4 activity. A. ThP1 NF-κB cells were left unstimulated (-) or stimulated with 0.5 µM of FBG-C, 0.5 ng/mL of LPS, 20, 50 and 100 µM of loop 5-4, loop 5-deletion, loop 5-mutation 1, 2 or 3. NF-κB activation was measured after 24 h using QUANTI-Blue™. **B.** Primary human macrophages were left unstimulated (-) or stimulated for 24h with 1 µM of FBG-C, 1 ng/mL of LPS, 20, 50 and 100 µM of loop 5-4, loop 5-mutation 1, 2 or 3. IL-8 synthesis was measured by ELISA. Data shown as mean ± SEM, N=3 independent donors or 3 independent experiments. Paired t-test vs loop5-4, *p<0.05, **p<0.01, ***p<0.001.

5.3. Mutations in loop 5 - FBG-C protein

I also designed 3 mutant FBG-C proteins. FBG-C mutant 1 and 2 have double mutations in the sequence KTRYKLK of loop 5 in the first or second pair respectively of positively charged amino acids, where they were substituted by alanine. FBG-C mutant 3 has all 4 positively charged amino acids mutated to alanine (Table 5-2)

Table 5-2. FBG-C mutant 1-3 protein sequences. Mutant proteins comprise substitutions in loop 5, where positively charged amino acids (blue) were mutated to alanine (red).

FBG-C loop 5	VGDA**K**T**R**Y**K**L**K**VEG
FBG-C mutant 1	VGDA**A**T**A**YKLKVEG
FBG-C mutant 2	VGDAKTRY**A**L**A**VEG
FBG-C mutant 3	VGDA**A**T**A**Y**A**L**A**VEG

5.3.1. Biochemical and biophysical characterisation of FBG-C mutant 1, 2 and 3

FBG-C mutant proteins were made using QuikChange site-directed mutagenesis kit. Mutant proteins were expressed and purified as described previously for FBG-C, -R, -W and –X in chapter 3. FBG-C mutant 1, 2 and 3 were biochemically and biophysically characterised by silver staining, western blot, CD spectroscopy, and the LPS content of these proteins was determined. Silver staining showed that protein preparations were pure and anti-His western blot confirmed the identity of the proteins (Figure 5-2 A, B). In addition, no significant changes were observed in the CD spectra of FBG-C mutant 1, 2 and 3 compared to FBG-C (Figure 5-2 C, D). The LPS content of all the mutant proteins was less than 10 pg/mL.

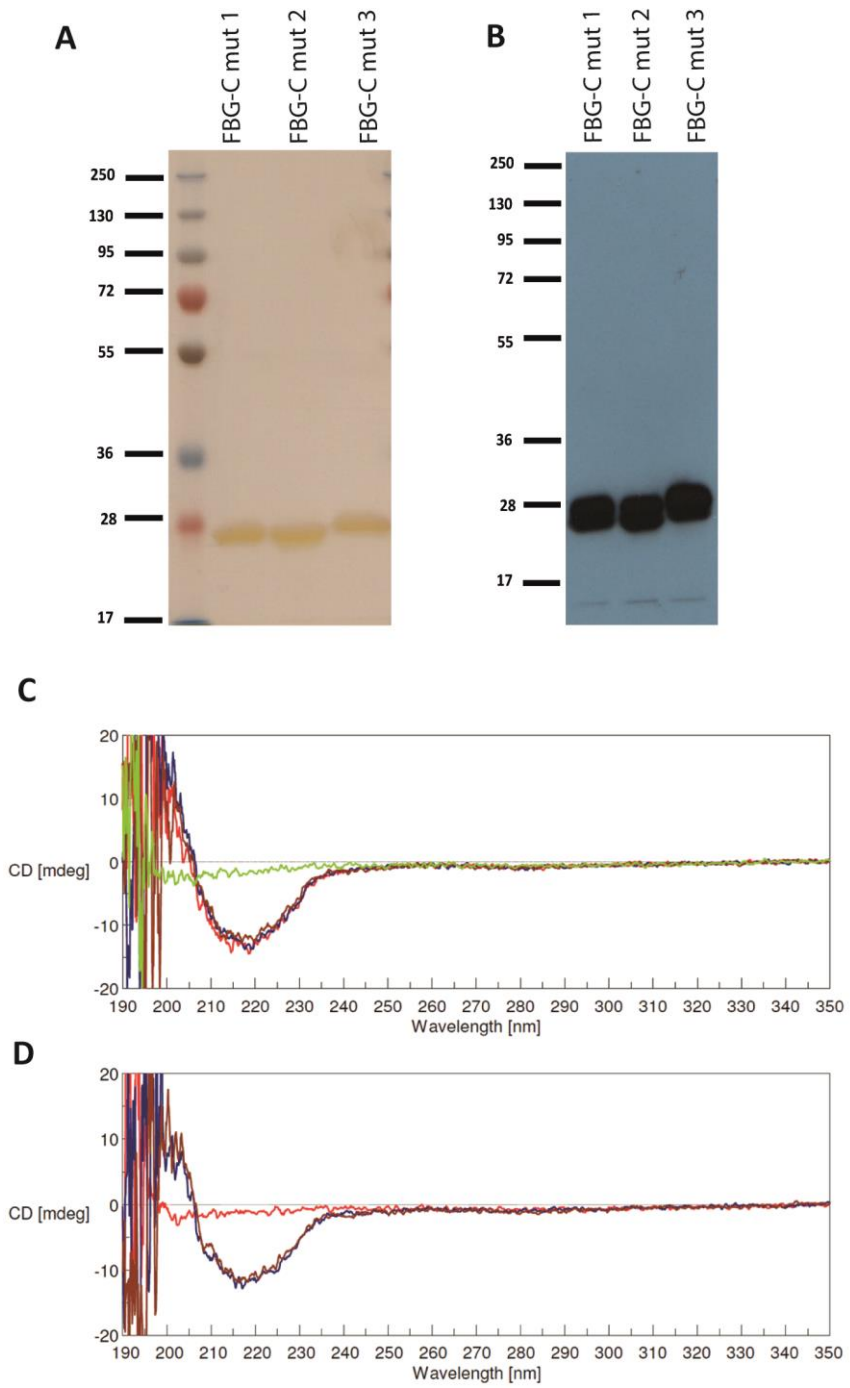

Figure 5-2. Biochemical and biophysical characterization of FBG-C mutant 1, 2 and 3. A. Protein purity was verified by silver staining of 1 µg of protein sample. **B.** Anti-His tag western blot of 1 µg of each protein. **C**. CD spectra in the far UV region of FBG-C mutant 1 (brown) and FBG-C mutant 2 (blue) compared to FBG-C (red). TN buffer signal in green. **D.** CD spectra of FBG-C mutant 3 (brown) compared to FBG-C (blue). TN buffer signal in red.

5.3.2. Activity in ThP1 NF-κB cells

The activity of FBG-C mutant 1, 2 and 3 was assessed in ThP1 NF-κB cells. FBG-C mutant 1 and 2 showed a modest decrease in the activation of NF-κB, while FBG-C mutant 3 showed a complete loss of activity, compared to FBG-C (Figure 5-3 A). MTT assay showed that cell viability was not affected by the FBG-C mutants compared to non-stimulated cells (Figure 5-3 B).

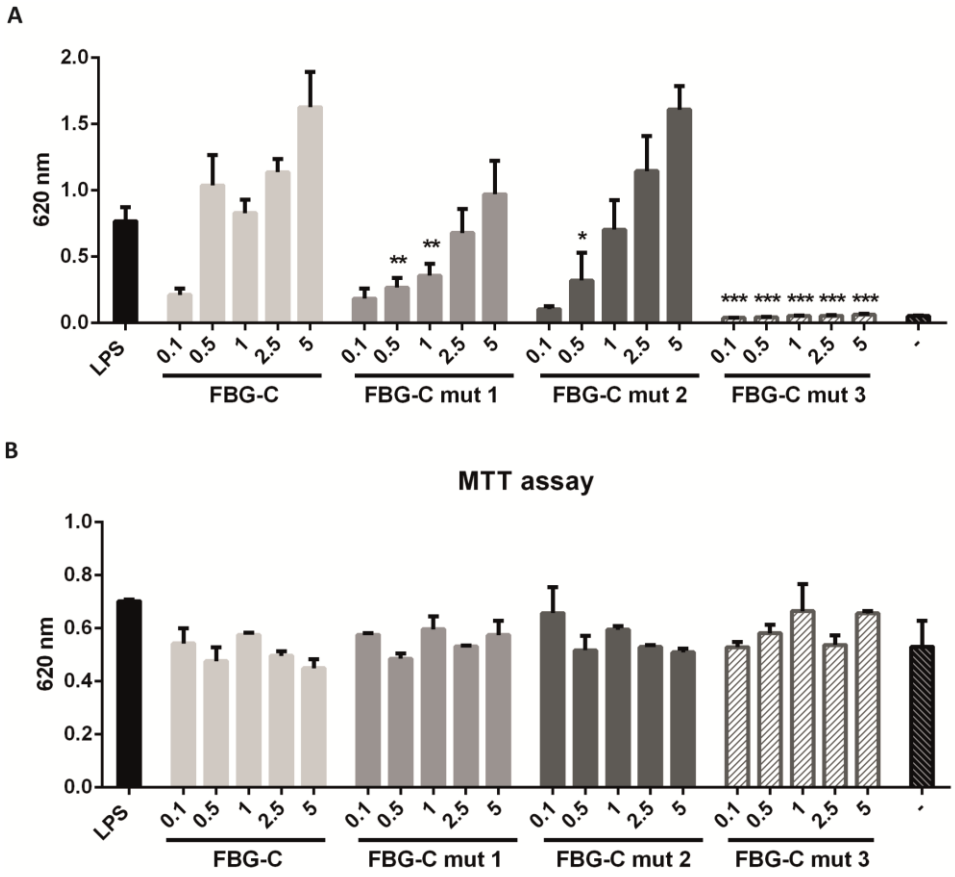

Figure 5-3. Positive charges in loop 5 are essential for the activation of NF-κB by FBG-C. A. ThP1 NF-κB cells were left unstimulated (-) or stimulated for 24 h with 0.5 ng/mL of LPS or increasing doses of FBG-C, FBG-C mutant 1, 2 or 3 pre-treated with PMB for 30 min. NF-κB activation was measured using QUANTI-Blue™. **B.** MTT assay of ThP1 NF-κB cells that were stimulated for 24 h with 0.5 ng/mL of LPS or increasing doses of FBG-C, FBG-C mutant 1, 2 or 3. Data shown as mean ± SEM, N=3 independent experiments. Paired t-test vs FBG-C, *p<0.05, **p<0.01, ***p<0.001.

5.3.3. Activity in primary human macrophages

The activity of FBG-C mutant 1, 2 and 3 was also examined in primary human macrophages. FBG-C mutant 1 and 2 showed a reduction in the induction of IL-6 and IL-8, but no difference was observed in TNF production compared to FBG-C. However, FBG-C mutant 3 showed a significant reduction in IL-6, IL-8 and TNF synthesis compared to FBG-C, even at higher concentrations (Figure 5-4 A). MTT assays confirmed that FBG-C mutant proteins do not affect cell viability compared to unstimulated cells (Figure 5-4 B).

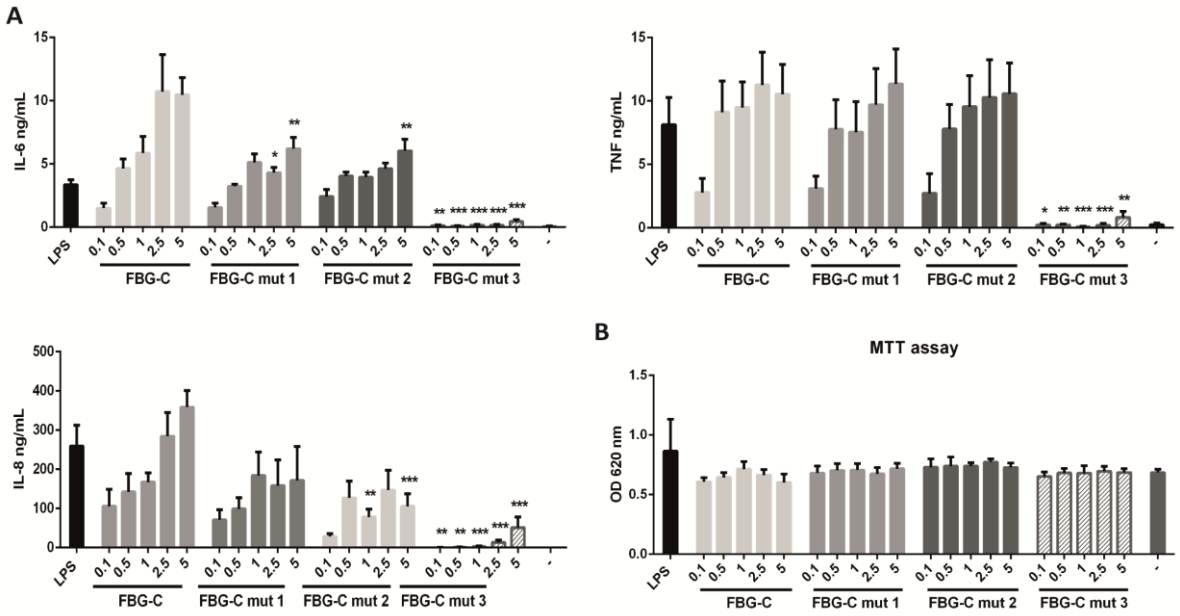

Figure 5-4. Positive charges in loop 5 are essential for the induction of cytokines by FBG-C. A. Primary human macrophages were left unstimulated (-) or stimulated for 24 h with 1 ng/mL of LPS or increasing doses of FBG-C, FBG-C mutant 1, 2 or 3 pre-treated with PMB for 30 min. Cytokines synthesis was measured by ELISA. **B.** MTT assay of primary human macrophages that were stimulated for 24 h with 1 ng/mL of LPS or increasing doses of FBG-C, FBG-C mutant 1, 2 or 3. Data shown as mean ± SEM, N=3 independent donors. Paired t-test vs FBG-C, *p<0.05, **p<0.01, ***p<0.001.

To determine if the activity of FBG-C mutant 1 and 2 was TLR4 dependent, cells were pre-incubated with TLR4 inhibitor (TAK 242) or TLR4 function-blocking antibody. TAK 242 and TLR4 antibody could significantly reduce the induction of cytokines by FBG-C mutant 1 and 2, indicating that these proteins are acting via TLR4 (Figure 5-5)

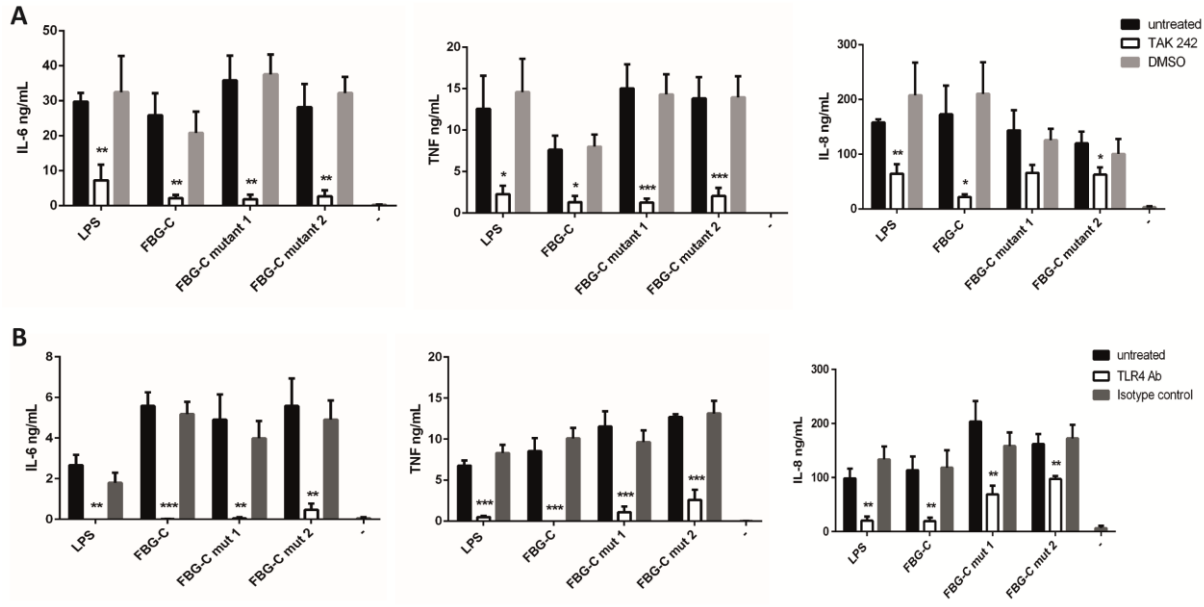

Figure 5-5. Activity of FBG-C mutant 1 and 2 is TLR4 dependent. Primary human macrophages were left unstimulated (-) or pre-incubated for 6 h with 3 µM of TAK 242 (**A**) or 1 h with 25 µg/mL of TLR4 antibody or isotype control (**B**), prior stimulation with 1 ng/mL of LPS or 1 µM of FBG-C, FBG-C mutant 1 or 2. Cytokine synthesis was measured after 24 h by ELISA. Data shown as mean ± SEM, N=3 independent donors. Paired t-test vs untreated, *p<0.05, **p<0.01, ***p<0.001.

5.3.4. Solid phase binding assay

The ability of FBG-C mutant 1, 2 and 3 to bind to TLR4 was evaluated in the solid phase binding assay. FBG-C mutant 2 showed no significant difference in binding to TLR4 compared to FBG-C, while a modest but significant reduction in the affinity to TLR4 was observed with FBG-C mutant 1. However, TLR4 bound with the lowest affinity to FBG-C mutant 3 compared to FBG-C, suggesting that mutations in the

positively charged amino acids in this region affect the binding of FBG-C to TLR4 (Figure 5-6, Table 5-5)

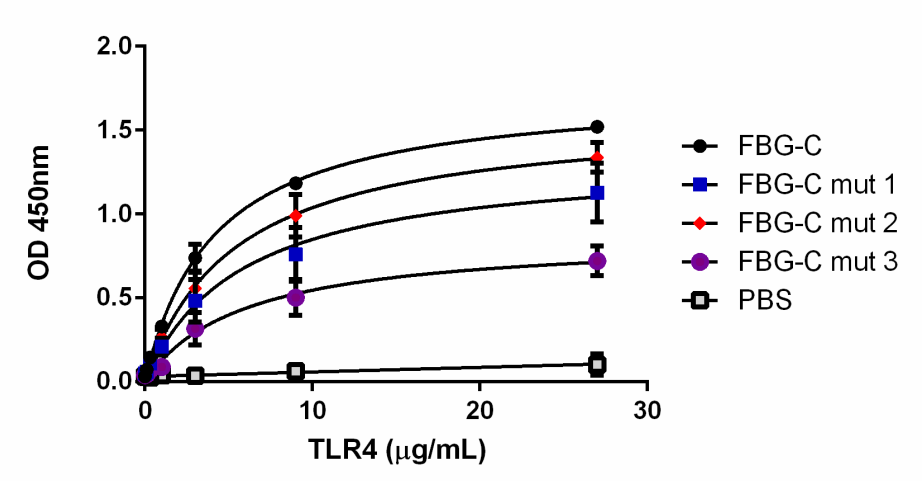

Figure 5-6. TLR4 shows decreased binding to FBG-C mutants in a solid phase binding assay. 96 well plates were coated with FBG-C, FBG-C mutant 1, 2 or 3, and TLR4 was added in a dose dependent manner. Curves were fitted in GraphPad Prism using one binding site hyperbola analysis. Data shown as mean ± SEM, N=4.

Table 5-3. Affinity binding of FBG-C, FBG-C mutant 1, 2 and 3 to TLR4 based on solid phase binding assay. Data shows mean ± SD, N=4. Un-paired t-test vs FBG-C.

Protein	K_D (nM) ± SD	p value
FBG-C	58.21 ± 5.24	
FBG-C mutant 1	81.01 ± 15.45	* 0.031
FBG-C mutant 2	75.92 ± 15.58	0.074
FBG-C mutant 3	121.10 ± 15.29	*** 0.0002

These results suggest that TLR4 is still binding with low affinity to FBG-C mutant 3, and to corroborate this, TLR4 was pre-incubated with increasing doses of FBG-C mutant 3 before it was added to plates coated with FBG-C. The results showed

that FBG-C mutant 3 can block, in a dose dependent manner, the interaction of TLR4 and FBG-C, indicating that this mutant is still binding to the receptor (Figure 5-7).

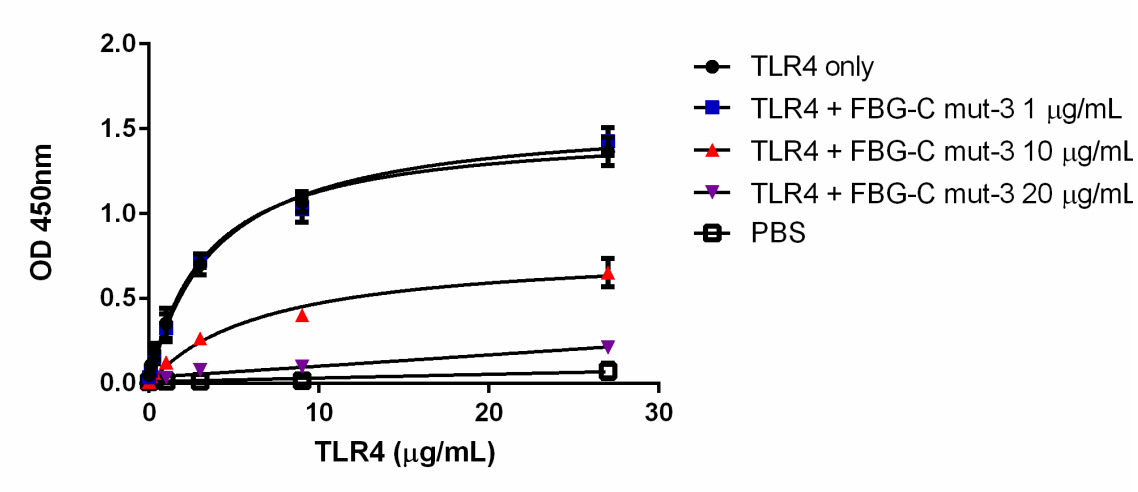

Figure 5-7. Blocking FBG-C-TLR4 interaction by FBG-C mutant 3. TLR4 was pre-incubated with increasing doses of FBG-C mutant 3 before it was added to plates coated with FBG-C. Curves were fitted in GraphPad Prism using one binding site hyperbola analysis. Data shown as mean ± SEM, N=3.

All together, these data suggest that at least 3 positively charged amino acids in loop 5 are needed for the activation of NF-κB in ThP1 cells and the induction of cytokine synthesis in primary human macrophages by FBG-C. In addition, these amino acids contribute to binding to TLR4, although other regions might be necessary for binding efficiently to the receptor.

5.4. Mutations in FBG-C loop 10

Multiple sequence alignment of the FBG domain of the tenascin family members revealed a region that was conserved at the C-terminus of FBG-C, -R and –W but not FBG-X. This sequence is characterised by positively charged amino acids in FBG-C, while these residues in FBG-X are not present. Instead, FBG-X has two glycines in this region creating a truncated version at the C-terminus. To assess the impact of these

residues in the activation of and binding to TLR4, two mutant FBG-C proteins were designed where the FBG-C sequence RRKRA was substituted with the sequence of FBG-X GG. FBG-C mutant 4 has a replacement of the positive charges at loop 10 for two glycines. FBG-C mutant 5 has positively charged amino acids substituted by glycine in loop 10, in addition to the mutations in loop 5 (Table 5-4).

Table 5-4. FBG-C mutants 4 and 5 protein sequences. Mutations were introduced in FBG-C loop 10, where positively charged amino acids (blue) were substituted by glycine (red) or deleted.

FBG-C loop 5	VGDA**K**T**R**Y**K**L**K**VEG
FBG-C loop 10	RNLEG**RRKR**A
FBG-X loop 10	RSPAG**GG**
FBG-C mutant 4	RNLEG**GG**
FBG-C mutant 5	RNLEG**GG** + VGDA**A**T**A**Y**A**L**A**VEG

5.4.1. Biochemical and biophysical characterization of FBG-C mutant 4 and 5

FBG-C mutant 4 and 5 were made as described previously for the FBG-C mutants 1-3. These proteins were expressed in *E. coli* and purified by nickel chromatography. FBG-C mutant 4 and 5 were biochemically and biophysically characterised by silver staining, western blot and CD spectroscopy. The LPS content of the protein solutions was also measured and found to be less than 10 pg/mL. Silver staining showed that the proteins made were pure and anti-His western blot confirmed their identity (Figure 5-8 A, B). CD spectra of FBG-C mutant 4 and 5 exhibited no significant changes in the secondary structure of the mutant proteins compared to FBG-C (Figure 5-8 C, D).

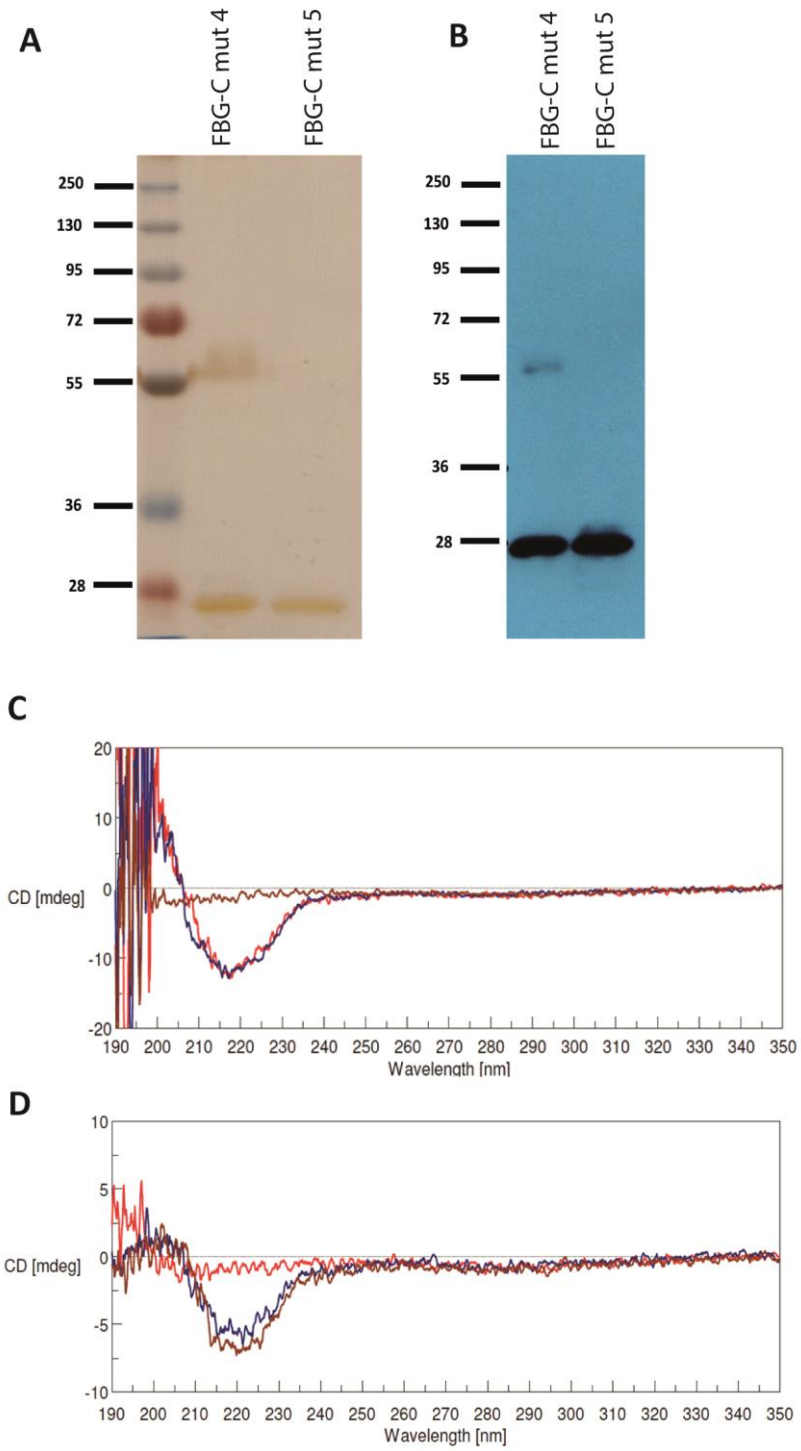

Figure 5-8. Biochemical and biophysical characterization of FBG-C mutant 4 and 5. A. Protein purity was verified by silver staining of 1 µg of protein sample. **B.** Anti-His tag western blot of 1 µg of each protein. **C.** CD spectra in the far UV region of FBG-C mutant 4 (red) compared to FBG-C (blue). TN buffer signal in brown. **D.** CD spectra of FBG-C mutant 5 (blue) compared to FBG-C (brown). TN buffer signal in red.

5.4.2. Activity in ThP1 NF-κB cells

The activity of FBG-C mutant 4 and 5 was measured in ThP1 NF-κB cells. As expected, FBG-C mutant 5 could not induce the activation of NF-κB due to the mutations in loop 5, which were shown to be essential for NF-κB activation and cytokine synthesis. A modest but significant reduction in NF-κB activation was observed with FBG-C mutant 4 (Figure 5-9 A). MTT assays confirmed that protein viability was not affected by the FBG mutant proteins (Figure 5-9 B)

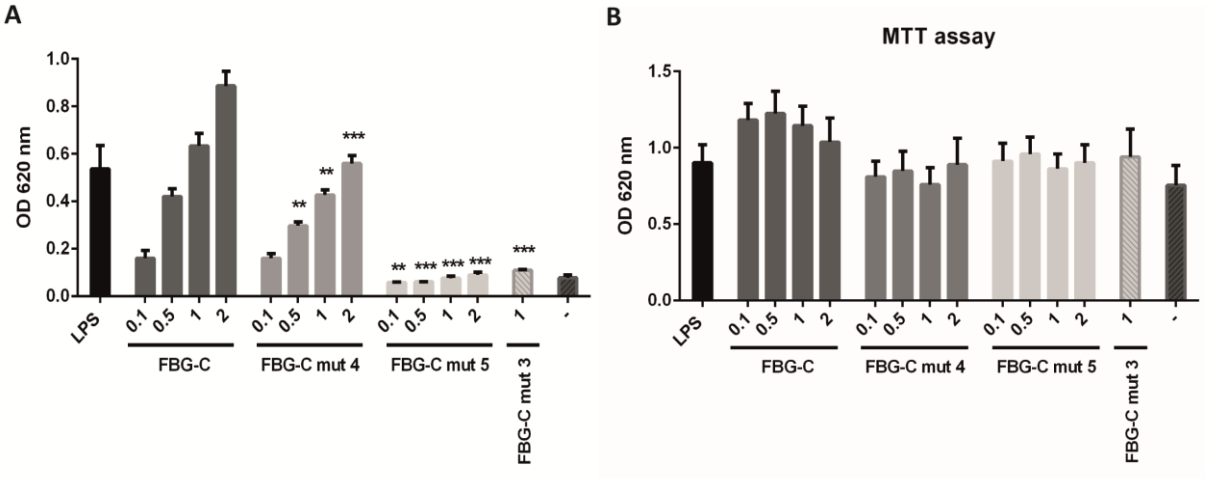

Figure 5-9. Mutations in loop 10 have a modest effect on FBG-C protein activity in ThP1 NF-κB cells. A. ThP1 NF-κB cells were left unstimulated (-) or stimulated for 24 h with 0.5 ng/mL of LPS or increasing doses of FBG-C, FBG-C mutant 4, 5 or 3 pre-treated with PMB for 30 min. NF-κB activation was measured using QUANTI-Blue™ **B.** MTT assay of ThP1 NF-κB cells that were stimulated for 24 h with 0.5 ng/mL of LPS or increasing doses of FBG-C, FBG-C mutant 4, 5 or 3. Data shown as mean ± SEM, N=3 independent experiments. Paired t-test vs FBG-C, *p<0.05, **p<0.01, ***p<0.001.

5.4.3. Activity in primary human macrophages

The activity of FBG-C mutants 4 and 5 was also assessed in primary human macrophages. FBG-C mutant 4 showed no difference in the induction of cytokine synthesis compared to FBG-C, while FBG-C mutant 5 was not able to induce IL-6, IL-8 or TNF, as expected (Figure 5-10 A). MTT assays showed that the mutant proteins had no effect in cell viability compared to unstimulated cells (Figure 5-10 B).

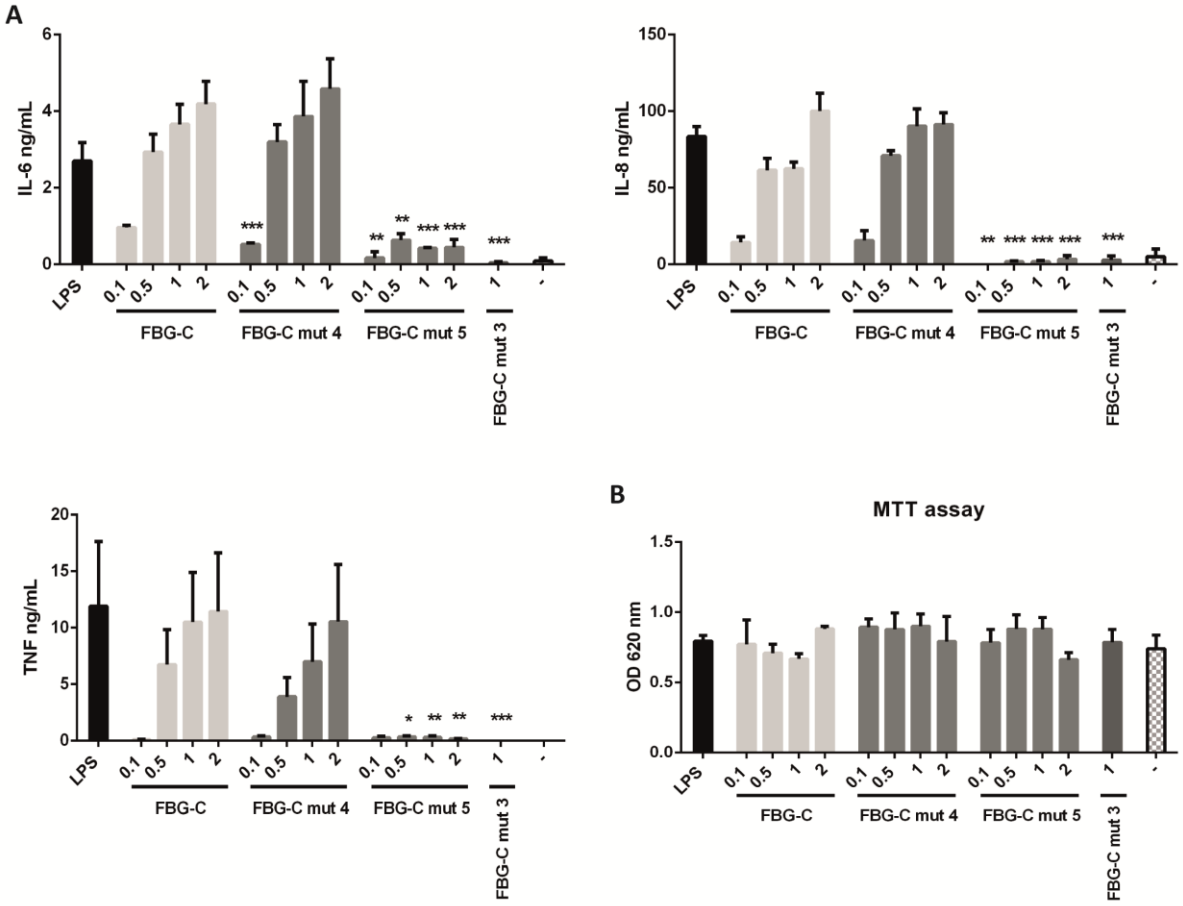

Figure 5-10. Mutations in loop 10 have no effect on FBG-C protein activity in macrophages. A. Primary human macrophages were left unstimulated (-) or stimulated for 24 h with 1 ng/mL of LPS or increasing doses of FBG-C, FBG-C mutant 4, 5 or 3 pre-treated with PMB for 30 min. Cytokines synthesis was measured by ELISA. **B.** MTT assay of primary human macrophages that were stimulated for 24 h with 1 ng/mL of LPS or increasing doses of FBG-C, FBG-C mutant 4, 5 or 3. Data shown as mean ± SEM, N=3 independent donors. Paired t-test vs FBG-C, *p<0.05, **p<0.01, ***p<0.001.

5.4.4. Binding assay

The ability of FBG-C mutant 4 and 5 to bind to TLR4 was assessed using the solid phase binding assay. TLR4 bound with similar affinity to FBG-C mutant 4 compared to FBG-C. However, a significant reduction was observed in the affinity of TLR4 to FBG-C mutant 5, which contains mutations in loop 5 and 10 (Figure 5-11 and Table 5-5).

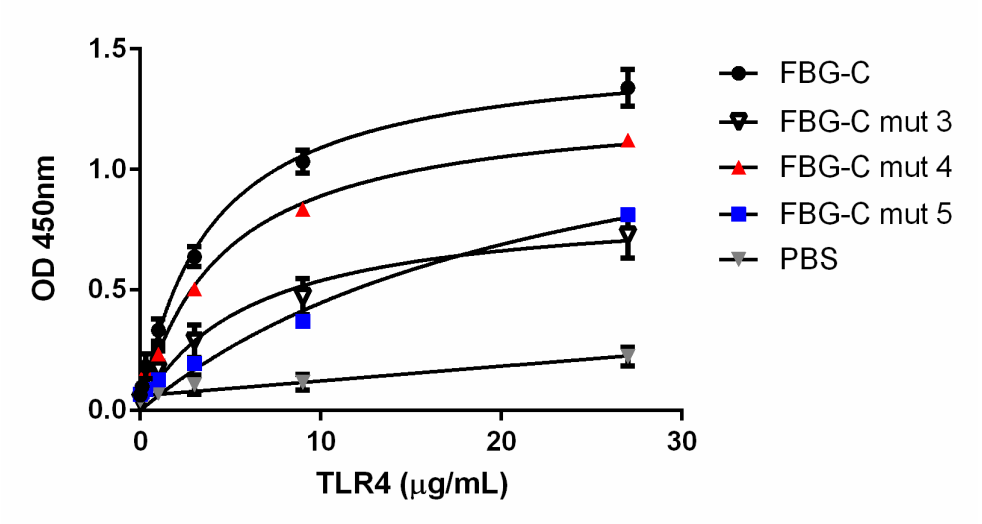

Figure 5-11. TLR4 shows decreased binding to FBG-C mutant 5 in a solid phase binding assay. 96 well plates were coated with FBG-C, FBG-C mutant 3, 4 or 5, and TLR4 was added in a dose dependent manner. Curves were fitted in GraphPad Prism using one binding site hyperbola analysis. Data shown as mean ± SEM; N=3.

Table 5-5. Affinity of FBG-C, FBG-C mutant 4 and 5 to TLR4 based on solid phase binding assay. Data shows mean ± SD, N=3. Un-paired t-test vs FBG-C.

Protein	K_D (nM) ± SD	p value
FBG-C	53.4 ± 7.93	
FBG-C mutant 3	121.10 ± 15.29	** 0.002
FBG-C mutant 4	63.03 ± 8.92	0.234
FBG-C mutant 5	336.4 ± 103.12	** 0.009

In summary, these data show that mutations in loop 10 have little effect on the activation of NF-κB and the induction of cytokine synthesis by FBG-C, indicating that this region is not essential for TLR4 activation. However, mutations in loop 10 and 5 have a significant effect on the binding capability of FBG-C, suggesting that loop 10 could be implicated in stabilizing the binding of FBG-C to TLR4.

5.5. Mutations in FBG-C loop 7

Peptide 7 was able to inhibit the interaction of TLR4 and FBG-C in the solid phase binding assay, and could reduce the induction of NF-κB by FBG-C in ThP1 NF-κB cells. Further comparison of this sequence among the FBG domains of the tenascin family members showed that only 3 amino acids in loop 7 were different in FBG-X compared to FBG-C, -R and -W. To examine the contribution of this sequence to the binding and activation of TLR4, these amino acids were substituted in FBG-C with the residues found in FBG-X. FBG-C mutant 6 has three amino acids substitution: D153P, I160L and N162S. FBG-C mutant 7 has these three mutations and the four positively charged amino acids in loop 5 changed to alanine (Table 5-6).

Table 5-6. FBG-C mutants 6 and 7 protein sequences. Mutations were made in FBG-C loop 7 where the amino acids in FBG-C (blue) were substituted for the residues found in FBG-X (red).

FBG-C loop 5	VGDA**K**T**R**Y**K**L**K**VEG
FBG-C loop 7	TFDKDT**D**SA**I**T**N**CALS
FBG-X loop 7	DRD**P**NSL**L**I**S**CAVS
FBG-C mutant 6	TFDKDT**P**SA**L**T**S**CAL
FBG-C mutant 7	TFDKDT**P**SA**L**T**S**CAL + VGDA**A**T**A**Y**A**L**A**VEG

5.5.1. Biochemical and biophysical characterization FBG-C mutant 6 and 7

FBG-C mutant 6 and 7 were made as described previously for the FBG-C mutant 1-3. These proteins were expressed in *E. coli* and purified by nickel chromatography. FBG-C mutant 6 and 7 were characterised to assess their purity by silver staining and western blots (Figure 5-12 A, B). The LPS content of the protein solutions was also measured and found to be less than 10 pg/mL. CD spectra of FBG-C mutant 6 and 7 confirmed that no significant changes in the secondary structure of the mutant proteins were observed compared to FBG-C (Figure 5-12 C).

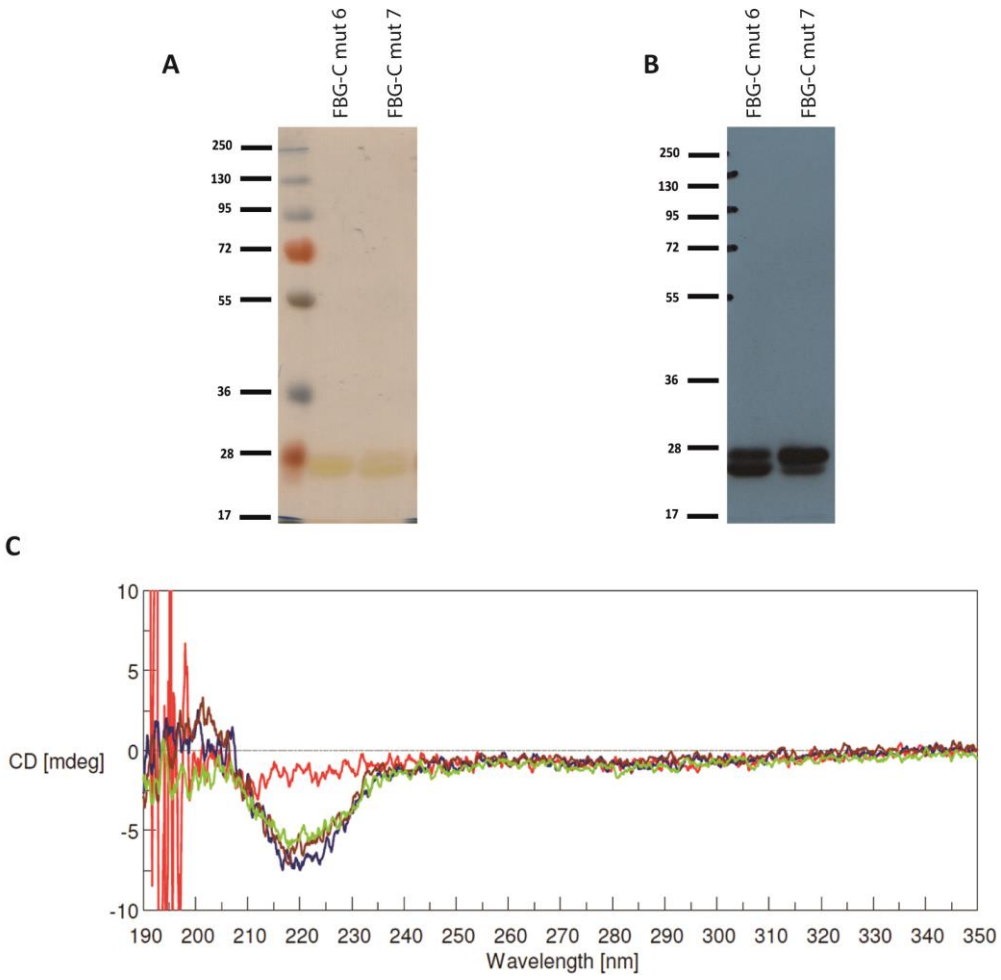

Figure 5-12. Biochemical and biophysical characterization of FBG-C mutant 6 and 7. A. Protein purity was verified by silver staining of 1 µg of protein sample. **B.** Anti-His tag western blot of 1 µg of each protein. **C.** CD spectra in the far UV region of FBG-C mutant 6 (brown) and FBG-C mutant 7 (green) compared to FBG-C (blue). TN buffer signal in brown.

5.5.2. Activity in ThP1 NF-κB cells

The activity of FBG-C mutant 6 and 7 was evaluated in ThP1 NF-κB cells. Mutations only in loop 7 showed a slight but not significant reduction of NF-κB activation in ThP1 cells. FBG-C mutant 7, which also includes mutations in loop 5, showed a complete loss of protein activity as expected (Figure 5-13A). MTT assays were performed to confirm that cell viability was not affected by treatment with the FBG-C mutant proteins (Figure 5-13 B).

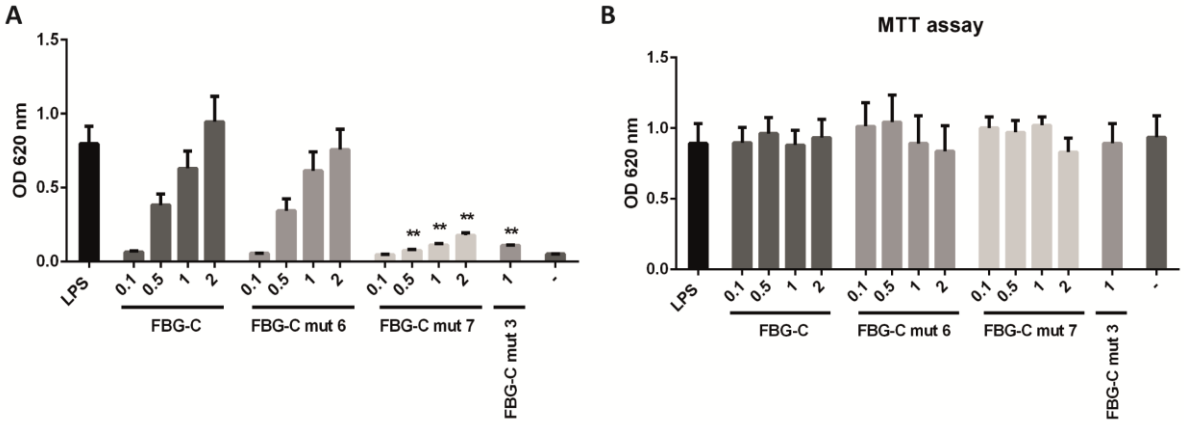

Figure 5-13. Mutations in loop 7 have no effect on the activation of NF-κB. A. ThP1 NF-κB cells were left unstimulated (-) or stimulated for 24 h with 0.5 ng/mL of LPS or increasing doses of FBG-C, FBG-C mutant 6, 7 or 3 pre-treated with PMB for 30 min. NF-κB activation was measured using QUANTI-Blue™ **B.** MTT assay of ThP1 NF-κB cells that were stimulated for 24 h with 0.5 ng/mL of LPS or increasing doses of FBG-C, FBG-C mutant 6, 7 or 3. Data shown as mean ± SEM, N=3 independent experiments. Paired t-test vs FBG-C, *p<0.05, **p<0.01, ***p<0.001.

5.5.3. Activity in primary human macrophages

FBG-C mutant 6 and 7 protein activity was also examined in primary human macrophages. No difference was observed in cytokine induction by FBG-C mutant 6 compared to FBG-C. However, mutations in loop 7 and 5 had an effect in protein activity and FBG-C mutant 7 could not induce IL-6, IL-8 and TNF (Figure 5-14 A).

Macrophage viability was not affected by treatment with the mutant proteins compared to non-stimulated cells (Figure 5-14 B).

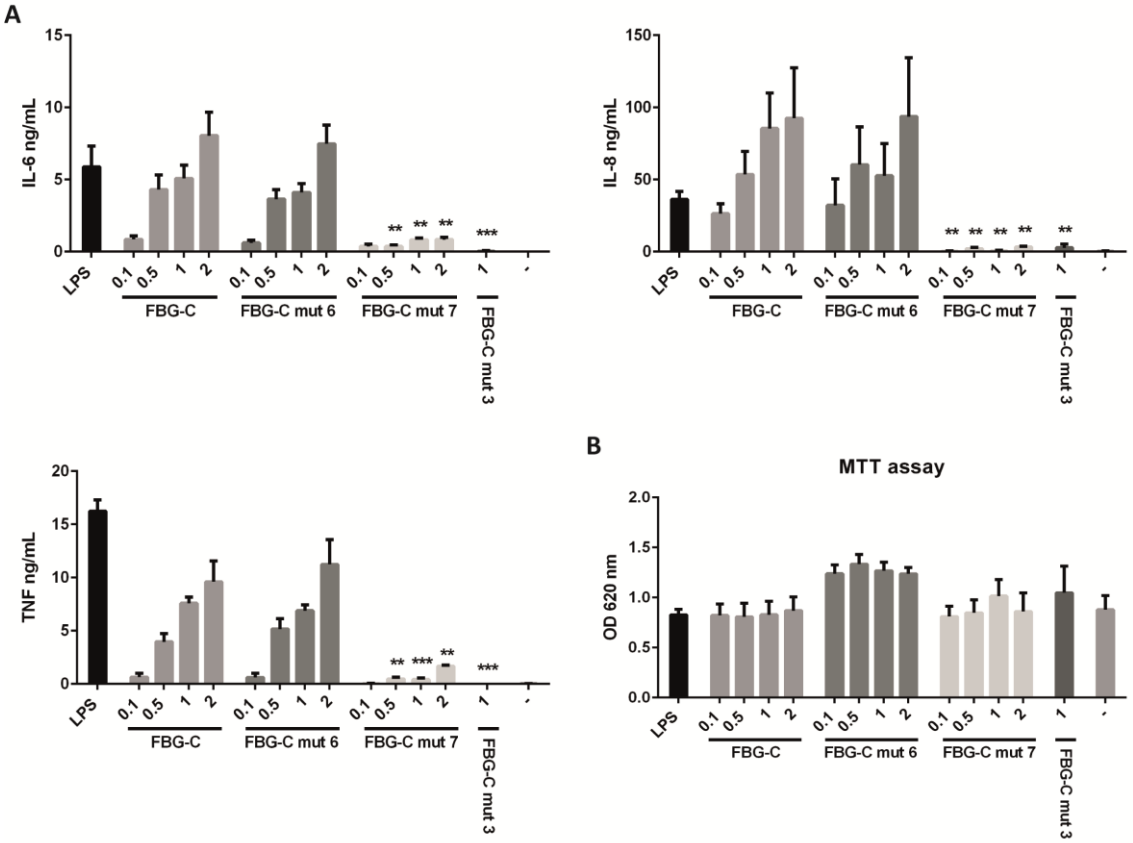

Figure 5-14. Mutations in loop 7 have no effect on FBG-C protein activity in macrophages. **A.** Primary human macrophages were left unstimulated (-) or stimulated for 24 h with 1 ng/mL of LPS or increasing doses of FBG-C, FBG-C mutant 6, 7 or 3 pre-treated with PMB for 30 min. Cytokines synthesis was measured by ELISA. **B.** MTT assay of primary human macrophages that were stimulated for 24 h with increasing doses of FBG-C, FBG-C mutant 6, 7 or 3. Data shown as mean ± SEM, N=3 independent donors. Paired t-test vs FBG-C, *p<0.05, **p<0.01, ***p<0.001.

5.5.4. Binding assay

The binding affinity of FBG-C mutants 6 and 7 to TLR4 was evaluated using the solid phase binding assay. TLR4 showed a decrease in binding affinity to FBG-C mutant 6 but it did not reach statistical significance. TLR4 binds to FBG-C mutant 7 with lower affinity compared to FBG-C, indicating that mutations in loop 7 and 5 affect the binding capabilities of FBG-C to TLR4 (Figure 5-15, Table 5-7).

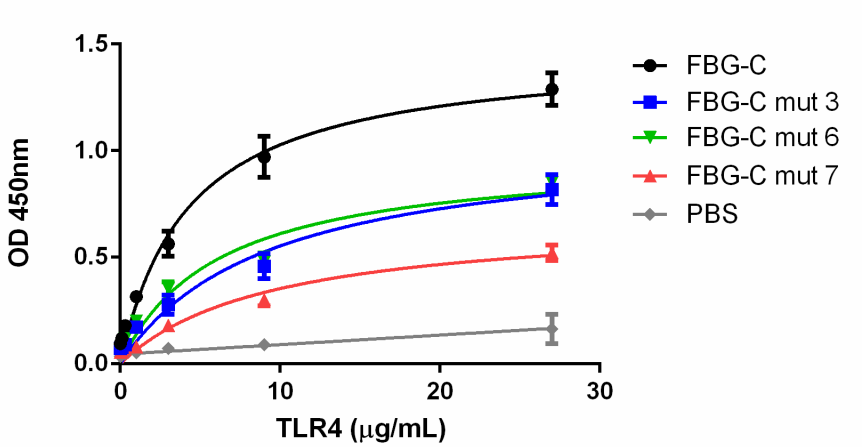

Figure 5-15. TLR4 shows decreased binding to FBG-C mutant 6 and 7 in a solid phase binding assay. 96 well plates were coated with FBG-C, FBG-C mutant 3, 6 and 7, and TLR4 was added in a dose dependent manner. Curves were fitted in GraphPad Prism using one binding site hyperbola analysis. Data shown as mean ± SEM, N=3.

Table 5-7. Affinity of FBG-C, FBG-C mutant 6 and 7 to TLR4 based on solid phase binding assay. Data shows mean ± SD, N=3. Un-paired t-test vs FBG-C.

Protein	**K_D (nM) ± SD**	**p value**
FBG-C	60.48 ± 11.43	
FBG-C mutant 3	121.10 ± 15.29	** 0.005
FBG-C mutant 6	86.69 ± 21.25	0.135
FBG-C mutant 7	123.78 + 28.33	* 0.023

Altogether, these data indicate that mutations in D153, I160 and N162 in loop 7 have no effect on protein activity, and that this region is not involved in the activation of TLR4 by FBG-C. However, mutations in loop 7 and loop 5 resulted in lower binding affinity of TLR4 to FBG-C, suggesting that loop 7 contributes to binding of FBG-C to the receptor.

In summary, three regions in FBG-C have been identified that participate in the activation of and binding to TLR4. Positively charged amino acids in loop 5 are essential for activation of the receptor and also contribute to binding. Basic amino acids

in loop 10 are involved in stabilizing the binding to TLR4, while polar amino acids in loop 7 contribute to the binding of FBG-C to this receptor.

5.6. Mutations in FBG-X

To confirm that the three regions identified in FBG-C involved in binding and activation of TLR4 are sufficient to create an FBG domain capable of activating this receptor, I generated several mutant versions of the inactive FBG-X. In these mutants, I substituted the sequences in FBG-X with the amino acids found in FBG-C in loop 5, 7 and 10 to be involved in the activation and binding to TLR4. Four mutant proteins were designed: FBG-X mutant 1 has positively charged amino acids substituting 2 hydrophobic amino acids in loop 5, while FBG-X mutant 2 has the complete sequence of loop 5 changed to the sequence of FBG-C. FBG-X mutant 3 includes the mutations made in FBG-X mutant 2 plus positively charged amino acids at the C-terminus. Finally, FBG-X mutant 4 includes mutations in all three regions showed to be involved in activation and binding to TLR4: loop 5 and 10 changed to FBG-C sequence and three amino acids substitution in loop 7: P161D, L165I and S167N (Table 5-8). The ability of the FBG-X mutant proteins to activate and bind to TLR4 was assessed in ThP1 NF-κB cells, primary human macrophages and the solid phase binding assay.

Table 5-8. FBG-X mutant 1-4 protein sequences. FBG-X chimeric proteins were designed to substitute the residues in FBG-X loop 5, 7 and 10 for the amino acids found in FBG-C to be involved in the activation and binding to TLR4.

FBG-X loop 5	V**DS**A**AEY**YRL**H**LEG
FBG-X loop 7	DRD**P**NSL**LI**S**C**AVS
FBG-X loop 10	RSPAG**GG**
FBG-C loop 5	VGDA**K**T**R**Y**K**L**K**VEG
FBG-C loop 7	TFDKDT**D**SA**I**T**N**CALS
FBG-C loop 10	RNLEG**RRKR**A
FBG-X mutant 1	VDSA**KAK**YRLHLEG
FBG-X mutant 2	V**GD**A**KTK**YRL**K**LEG
FBG-X mutant 3	V**GD**A**KTK**YRL**K**LEG + RSPAG**RRKRA**
FBG-X mutant 4	V**GD**A**KTK**YRL**K**LEG + RSPAG**RRKRA** + DRD**D**NSL**I**I**N**CAVS

5.6.1. Biochemical and biophysical characterization FBG-X mutant 1, 2, 3 and 4

FBG-X mutants were made as described previously for the FBG-C mutant proteins. These proteins were expressed in *E. coli* and purified by nickel chromatography. FBG-X mutants were biochemically characterised to assess their purity by silver staining and western blots (Figure 5-16 A, B). The LPS content of the protein solutions was also measured and found to be less than 10 pg/mL. CD spectra of FBG-X mutant 1, 2 and 3 showed no significant changes in the secondary structure of the mutant proteins compared to FBG-X (Figure 5-16 C, D, E). However, variations in the secondary structure were observed in FBG-X mutant 4, suggesting that the insertion of these mutations could generate changes in the overall folding of the protein (Figure 5-16 F).

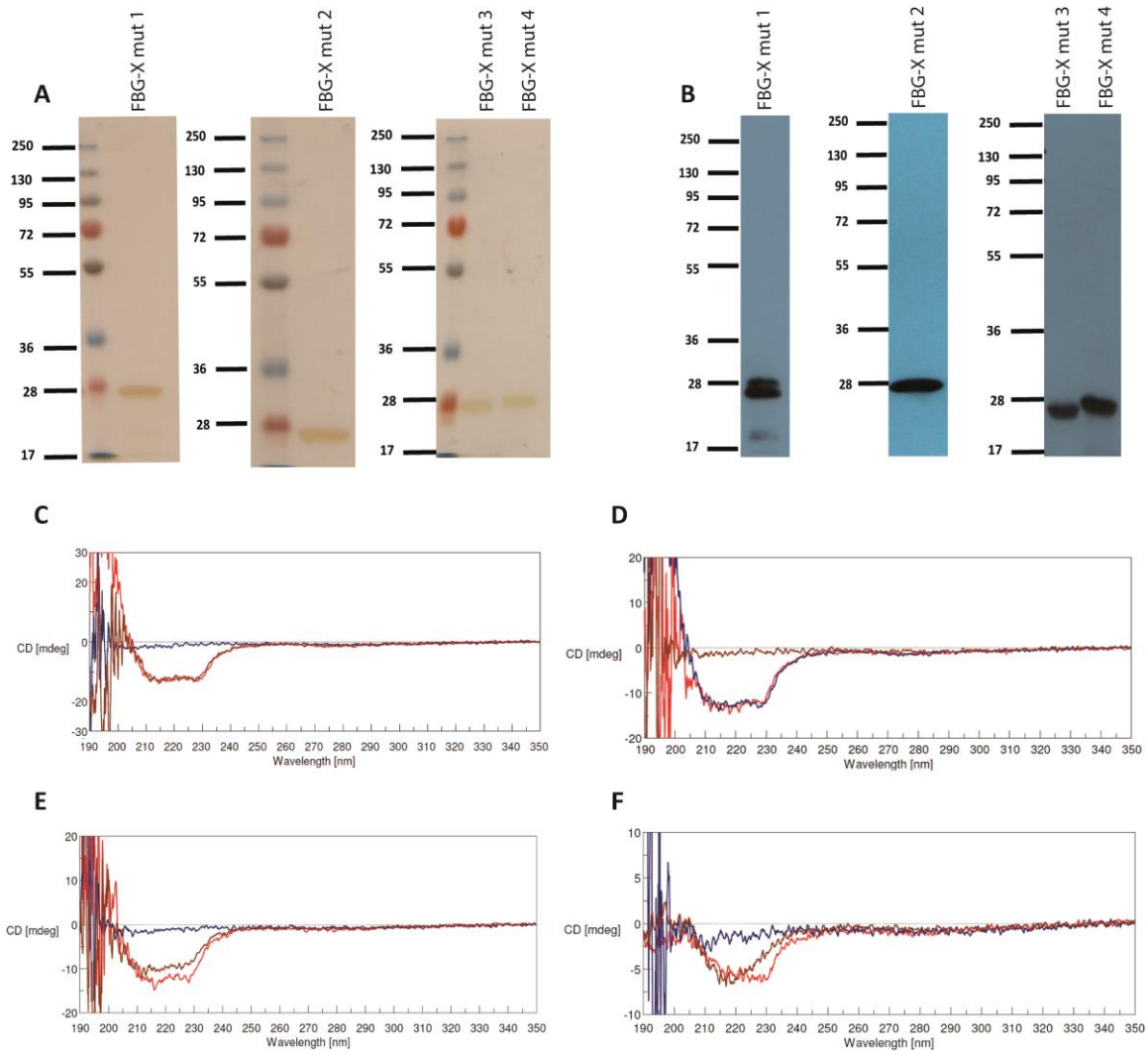

Figure 5-16. Biochemical and biophysical characterization of FBG-X mutant 1, 2, 3 and 4. **A.** Protein purity was verified by silver staining of 1 µg of protein sample. **B.** Anti-His tag western blot of 1 µg of FBG-X mutant 1, 2, 3 and 4. **C.** CD spectra in the far UV region of FBG-X mutant 1 (brown) compared to FBG-X (red). TN buffer signal in blue. **D.** CD spectra in the far UV region of FBG-X mutant 2 (red) compared to FBG-X (blue). TN buffer signal in blue. **E.** CD spectra in the far UV region of FBG-X mutant 3 (brown) compared to FBG-X (red). TN buffer signal in blue. **F.** CD spectra in the far UV region of FBG-X mutant 4 (brown) compared to FBG-X (red). TN buffer signal in blue.

5.6.2. Activity in ThP1 NF-κB cells

The protein activity of the FBG-X mutants was examined in ThP1 NF-κB cells. FBG-X mutant 1 could not induce NF-κB activation similar to FBG-X. FBG-X mutant 2 could partially induce NF-κB activation at high concentration (2 μM). FBG-X mutant 3, where mutations were made in loop 5 and 10, could induce NF-κB activation in a dose dependent manner. In addition, FBG-X mutant 4 that includes mutations in loop 5, 7 and 10 could also activate ThP1 NF-κB cells similarly to FBG-C (Figure 5-17 A). MTT assays confirmed that cell viability was not affected by FBG-X mutant proteins (Figure 5-17 B).

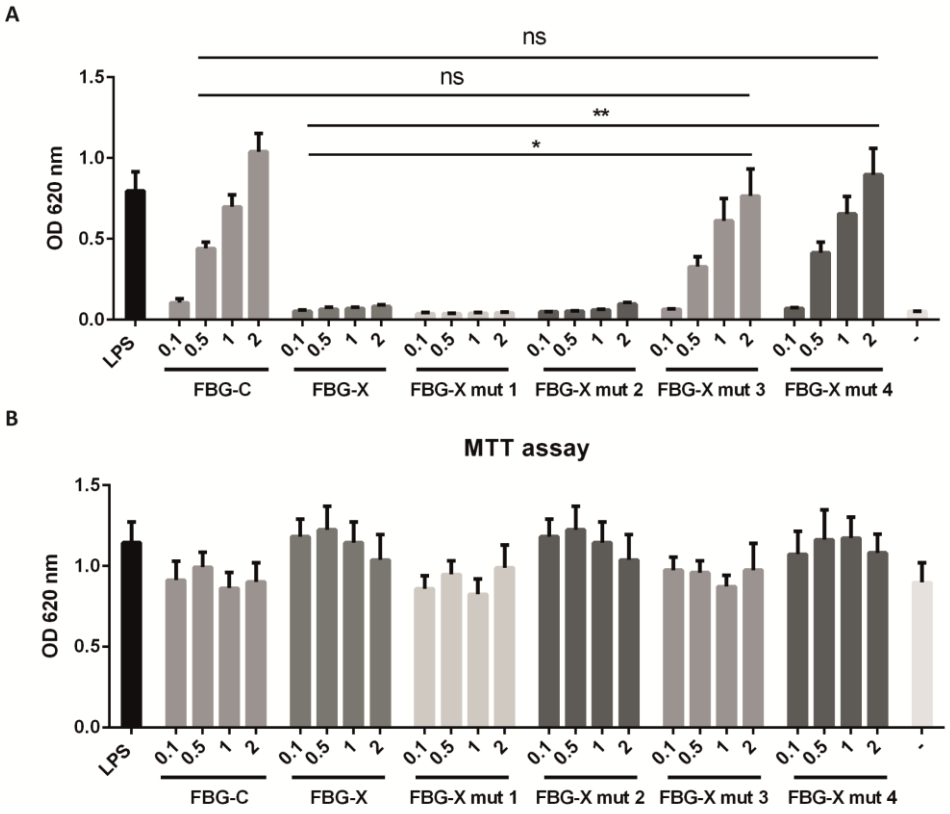

Figure 5-17. Mutations in FBG-X recover protein activity in ThP1 NF-κB cells. A. ThP1 NF-κB cells were left unstimulated (-) or stimulated for 24 h with 0.5 ng/mL of LPS or increasing doses of FBG-C, FBG-X, FBG-X mutant 1, 2, 3 and 4 pre-treated with PMB for 30 min. NF-κB activation was measured using QUANTI-Blue™. **B.** MTT assay of ThP1 NF-κB cells that were stimulated for 24 h with 0.5 ng/mL of LPS or increasing doses of FBG-C, FBG-X, FBG-X mutant 1, 2, 3 and 4. Data shown as mean ± SEM, N=3 independent experiments. One-way ANOVA vs FBG-C or FBG-X. *p<0.05, **p<0.01, ns: non-significant.

5.6.3. Activity in primary human macrophages

To corroborate the results obtained in ThP1 NF-κB cells, the activity of FBG-X mutant proteins was also evaluated in primary human macrophages. Similarly to ThP1 NF-κB cells, no difference was observed in the activity of FBG-X mutant 1 and FBG-X. FBG-X mutant 2 could partially induce IL-6, IL-8 and TNF at high concentrations (2 µM). FBG-X mutants 3 and 4, could induce cytokine synthesis in primary human macrophages in a dose dependent manner, similarly to FBG-C (Figure 5-18 A). MTT assays confirmed that cell viability was not affected by FBG-X mutant proteins (Figure 5-18 B).

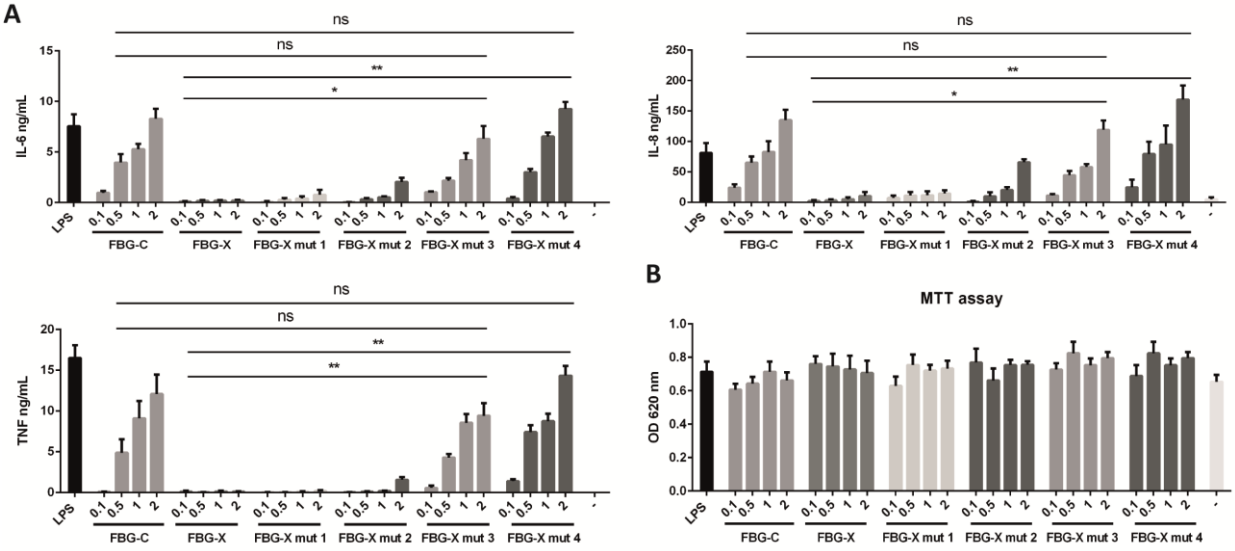

Figure 5-18. Mutations in FBG-X recover protein activity in primary human macrophages. A. Primary human macrophages were left unstimulated (-) or stimulated for 24 h with 1 ng/mL of LPS or increasing doses of FBG-C, FBG-X, FBG-X mutant 1, 2, 3 and 4 pre-treated with PMB for 30 min. Cytokines synthesis was measured by ELISA. **B.** MTT assay of primary human macrophages that were stimulated for 24 h with 1 ng/mL of LPS or increasing doses of FBG-C, FBG-X, FBG-X mutant 1, 2, 3 and 4. Data shown as mean ± SEM, N=3 independent donors. One-way ANOVA vs FBG-C or FBG-X. *p<0.05, **p<0.01, ns: non-significant.

5.6.4. Binding assay

The solid phase binding assay was used to determine if the mutations made in FBG-X are able to recover the binding capability of the protein to TLR4. TLR4 showed no binding to FBG-X as expected, and also did not bind to FBG-X mutant 1. Lower binding affinity was observed to FBG-X mutant 2 and 3 compared to FBG-C (Figure 5-19, Table 5-9). However, TLR4 binds to FBG-X mutant 4 with similar affinity compared to FBG-C, suggesting that mutations in the three regions (loop 5, loop 7 and loop 10) are sufficient to recover the binding capability of the protein to the receptor (Figure 5-19, Table 5-9).

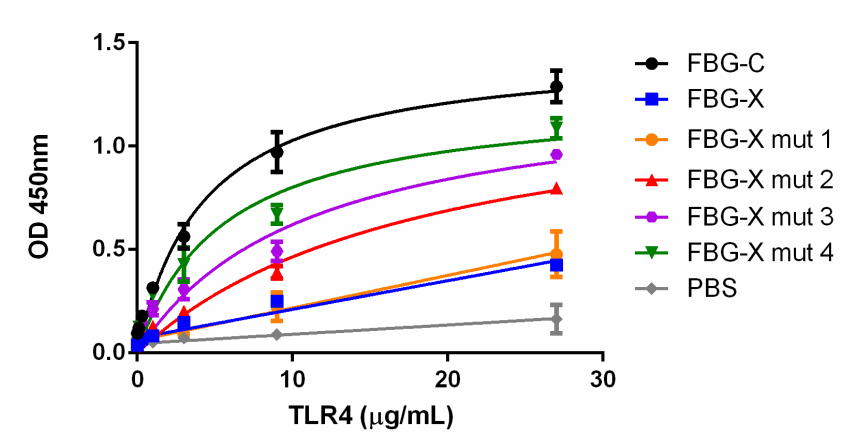

Figure 5-19. Mutations in FBG-X recover the binding ability of the protein to TLR4. 96 wells plate was coated with FBG-C, FBG-X, FBG-X mutant 1, 2, 3 and 4 and TLR4 was added in a dose dependent manner. Data shown as mean ± SD, N=4 independent experiments.

Table 5-9. Affinity of FBG-C, -X, FBG-X mutant 1, 2, 3 and 4 to TLR4 based on solid phase binding assay. Data shows mean ± SD, N=4. n.d.: not determined.

Protein	K_D (nM) ± SD
FBG-C	59.77 ± 7.08
FBG-X	n.d.
FBG-X mutant 1	n.d.
FBG-X mutant 2	173.09 ± 56.66
FBG-X mutant 3	154.96 + 46.74
FBG-X mutant 4	78.33 + 18.41

Together these data indicates that the addition of only two positively charged amino acids in loop 5 of FBG-X is not sufficient to induce NF-κB activation, cytokine synthesis or binding to TLR4. Mutating the sequence of loop 5 of FBG-X to that of FBG-C could partially recover the activation of NF-κB, induction of cytokine synthesis and binding to TLR4, indicating that other regions are necessary for receptor binding and full recovery of protein activity. This was confirmed with mutant 3 and 4, where the addition of mutations in loop 7 and 10 in FBG-X could induce the activation of NF-κB and cytokines synthesis to similar levels as FBG-C. In addition, TLR4 bound to FBG-X mutant 4 with an affinity constant comparable to that of FBG-C.

5.7. Discussion

In this chapter, I identified specific amino acids in FBG-C involved in the activation of and binding to TLR4. Positively charged amino acids in loop 5 (KTRYKLK) were found to be essential for receptor activation, and positive residues in loop 10 (RRKRA) stabilised the interaction with TLR4. In addition, polar interactions in loop 7 contribute to binding to the receptor (Figure 5-20). These findings were also corroborated when the activity of FBG-X was recovered. Changing the sequence of FBG-X loop 5 to that of FBG-C partially recovers protein activity and binding. However, adding positively charged amino acids at the C-terminus and changing specific residues in loop 7 completely recover protein activity and binding to TLR4. These data indicates that these three regions are necessary to fully bind to TLR4 and induce NF-κB activation and cytokine synthesis by the FBG domains.

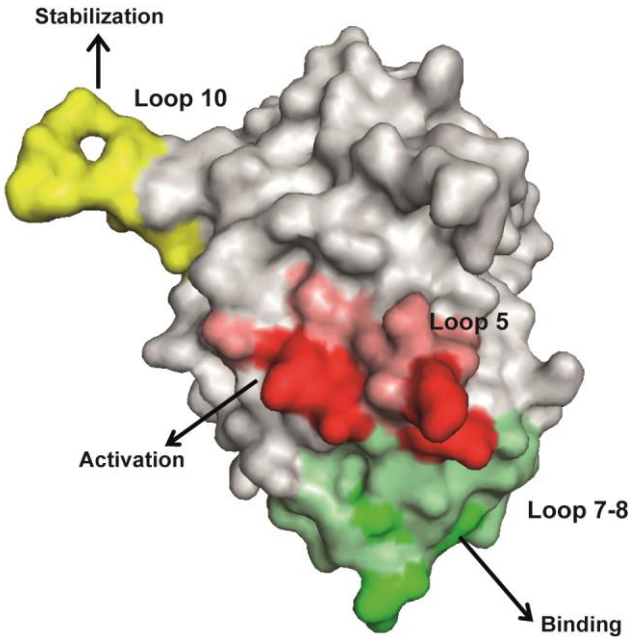

Figure 5-20. Model of FBG-C showing the regions involved in binding and activation of TLR4. Loop 5 is shown in red, loop 7-8 in green and loop 10 in yellow. The amino acids mutated are highlighted in a darker colour.

The first region to be evaluated was loop 5. In the previous chapter, I found that peptides containing this amino acid sequence were able to activate ThP1 cells and primary human macrophages. Comparison of the sequences of the active FBG domains (FBG-C, -R and -W) revealed that positively charged amino acids were conserved in this loop, but they were not present in the inactive FBG-X. For that reason, these residues were mutated to alanine to establish their involvement in TLR4 activation. The lack of all positively charged amino acids in FBG-C mutant 3 or in the peptides, resulted in complete loss of protein activity, indicating that ionic interactions in this region are essential for receptor activation. However, in the solid phase binding assay, it was found that the mutant protein was still binding to TLR4 with low affinity, suggesting that more than one site is contributing to binding to the receptor. This hypothesis was confirmed when TLR4 was pre-incubated with different doses of FBG-C mutant 3, before adding it to plates coated with FBG-C. FBG-C mutant 3 could block completely the interaction between FBG-C and TLR4 at a concentration of 20 µg/mL, which is equivalent to 766.28 nM. The maximum concentration of TLR4 added to the plate is 27 µg/mL (382.44 nM), suggesting that the molar ratio for this interaction is 2:1, or two molecules of FBG for one molecule of TLR4, assuming that TLR4 is a monomer in the solution. In our lab, we have observed that the FBG domain of tenascin-C is able to oligomerise, but additional analyses are necessary to determine if dimerization is essential for binding and activation of TLR4.

To further investigate the contribution of positively charged amino acids in loop 5 to the activation of TLR4, we replaced hydrophobic amino acids in FBG-X (AEYYRLH) with basic residues (KTKYRLH). In FBG-X mutant 1, only two lysines were introduced, and these mutations had no effect on the binding or activation of TLR4. However, when the complete sequence of FBG-X loop 5 was changed to the

sequence of FBG-C, a partial recovery in protein activity was observed at high concentrations. These data supported the hypothesis that positively charged amino acids in loop 5 plus other sites of the FBG domain are required for receptor binding and further activation. In addition, it suggested that these other regions involved in binding are also different in FBG-X compared to FBG-C, -R and -W.

Multiple sequence alignments revealed that at the C-terminus the active FBG domains had positively charged amino acids, while FBG-X presented a truncated version of this region lacking these residues. I then created mutant versions of FBG-C where the sequence at loop 10 was substituted for that of FBG-X. This mutation on its own had little effect on protein activity, indicating that it was not involved in the activation of TLR4. However, in combination with mutations in loop 5, a significant effect was observed in the solid phase biding assay, suggesting that it might contribute to the interaction of FBG-C and TLR4. In addition, when positively charged amino acids were added to loop 10 in FBG-X in combination with mutations in loop 5, FBG-X mutant 3 was able to activate NF-κB and induce cytokine synthesis, corroborating the finding in FBG-C. This region at the C-terminus could be exposed on the surface of the FBG domains and could potentially interact with TLR4 stabilising the binding of the FBG domain to the receptor.

Peptide mapping also revealed that peptide 7 could interfere in the binding of FBG-C to TLR4. Analyses of the FBG domains sequences in this region showed a high degree of conservation and it was difficult to select the amino acids for mutagenesis. However, multiple sequence alignment and examination of the structural models of the FBG domains showed that three amino acids were different in FGB-C compared to FBG-X. These changes create a different distribution of polar amino acids and structural changes in the exposure of hydrophobic amino acids in FBG-X. Three amino

acids in loop 7 were replaced in FBG-C for the ones found in FBG-X to assess their contribution to the interaction of FBG-C and TLR4. Mutations only in loop 7 had no effect in protein activity, but when they were in combination with mutations in loop 5, FBG-C mutant 7 showed a reduction in the affinity to TLR4. Furthermore, mutations of these residues in FBG-X, in conjunction with mutations in loop 5 and loop 10, completely recovered the protein activity to comparable levels as FBG-C. TLR4 was also able to bind to FBG-X mutant 4 in the solid phase binding assay, suggesting that the changes introduced in FBG-X in loop 5, 7 and 10 are sufficient to create a chimeric FBG domain able to activate and bind to TLR4. These mutations also induced changes in the secondary structure of FBG-X, which made it more similar to FBG-C (as shown in the CD spectrum of the protein). These data suggest that mutating these three regions in FBG-X generate structural changes which might contribute to generate an active FBG domain.

Site directed mutagenesis is a technique extensively used to understand the function of specific residues in protein-protein interactions. The amino acids required for the activation of TLR4 by other proteins have been determined using this method. For example, mutagenesis studies showed that substitution of F123 in MD-2 to alanine didn't affect LPS binding but prevented TLR4 activation [131]. Novimmune has determined the mode of action of the TLR4 neutralising antibody Hu 15C1 by site directed mutagenesis, both in TLR4 and Hu 15C1, revealing that the antibody antagonises the receptor dimerization preventing its activation [143]. Mutations in Cys106 in HMGB1 hindered TLR4 activation and cytokine synthesis by this DAMP, indicating that this amino acids is essential for HMGB1 binding and activation of the receptor [150]. Site direct mutagenesis is a useful tool to determine the role of specific amino acids in protein complexes, especially when protein crystallisation is difficult or

not possible. However, one disadvantage of this method is that it doesn't provide structural information of protein-protein interactions. In addition, the introduction of these mutations could disrupt the correct folding of the protein or generate important structural changes that could result in false positive when analysing more than one residue. Biophysical characterization of the mutant proteins is necessary to correctly interpret the results obtained regarding the role of specific residues in protein complexes.

The FBG domain of tenascin-C has been shown to bind to other receptors such as $\alpha_v\beta_3$ [198], receptor protein-tyrosine phosphatase- ζ /β (RPTP- ζ /β) [199] and chicken acidic leucine-rich EGF-like domain containing brain protein (CALEB) [348], and components of the extracellular matrix, including heparin [349], and neurocan [199]. Little is known about the amino acids in the FBG domain involved in these interactions, with the exception of $\alpha_v\beta_3$ and heparin. The integrin $\alpha_v\beta_3$ has been demonstrated to bind to the sequence corresponding to peptide 8 of FBG-C [198]. This region is located in the P-subdomain and it doesn't overlap with the sequences found to be required for the activation or binding to TLR4. Fischer *et al.* [349], by using a short peptide including the C-terminal region of the FBG domain (PSSFRNLEGRRKRA), found that these resides were required for FBG-C binding to heparin. I've shown that this sequence is involved in the stabilization of the binding of FBG-C to TLR4, suggesting that this is a basic loop at the C-terminus that could be involved in the interaction with different binding partners. It would be interesting to examine if heparin binding could prevent TLR4 binding to FBG-C.

5.8. Summary

In this chapter I found the specific residues within the FBG domain of tenascin-C involved in the activation and binding to TLR4. Cationic and polar amino acids in loop 5, 7 and 10 contribute to the interaction between FBG-C and TLR4. Moreover, substituting these amino acids in the inactive FBG-X recovered the activity of this protein, suggesting that they are essential for the induction of inflammation by the active FBG domains. In the next chapter, I will discuss the mode of activation of TLR4 by other molecules and compare it to what I found in FBG-C.

Chapter 6 –Final Discussion

Chapter 6. Final Discussion

Tenascin-C is an ECM protein that is transiently expressed during physiological tissue repair [213], where it triggers an immune response, inducing the synthesis of pro-inflammatory cytokines via activation of TLR4 by its FBG domain [89]. However, persistent tenascin-C expression is associated with chronic sterile pathological inflammation [213]. The mechanism of TLR4 activation by the FBG domain of tenascin-C is still not well understood. Here, I've found three sites within the FBG-C that bind to and activate TLR4, mapping key residues at each site. These data reveal a unique epitope conserved in the active FBG domains of the tenascin family members that is involved in TLR4 activation.

6.1. Modes of TLR4 activation

TLR4 can recognise a variety of ligands including pathogenic stimuli, endogenous molecules and allergens. Different modes of activation has been described for TLR4 (Figure 6-1). Bacterial LPS requires the co-receptor MD-2 to activate the receptor; it exhibits negligible binding to TLR4 alone, but binds with high affinity to the TLR4-MD-2 complex (3 nM). The molecular nature of this complex is well defined, with both the ligand interaction site and the TLR4 dimerization site experimentally validated [116, 131, 350]. The endogenous molecule HMGB1 also requires MD-2 for activity; it also cannot bind TLR4 directly but binds with high affinity to MD-2. This interaction requires one cysteine in HMGB1 and binding, as well as activity *in vitro* and *in vivo*, can be blocked by the peptide tetramer FSSE, which comprises residues 105-108 of HMGB1. This site of HMGB1 is predicted to bind inside the hydrophobic pocket of MD-2 [150, 163]. These data suggest a similar mode of

TLR4 activation with both HMGB1 and LPS interacting with the hydrophobic core of MD-2 (Figure 6-1 A). A second mode of TLR4 activation has been reported for nickel and the cationic lipid diC_{14}-amidine. They both require MD-2 for their activity; however they bind to a different site compared to LPS. Instead, nickel and diC_{14}-amidine induce TLR4 activation by binding to histidines or polar residues respectively in the dimerization interface (Figure 6-1 B) [77, 351]. A third mode of activation is the one reported for the house dust mite allergen Der p 2, which binds to TLR4 in the absence of MD-2 [146]. Der p 2 is a member of the lipid binding family, exhibiting a sandwich β sheet structure enclosing a hydrophobic cavity almost identical to MD-2. Based on their structural homology, Der p 2 has been proposed to house LPS in its hydrophobic pocket and bind to TLR4 in the same location as MD-2 (Figure 6-1 C), driving allergic TLR4 activation upon pathogen sensitization [145, 146]. However, participating residues have not been experimentally interrogated.

The interaction of FBG-C, -R and –W with TLR4 also occurs in the absence of MD-2, consistent with previous data showing that FBG-C activation of TLR4 does not require this co-receptor [89]. Two other endogenous TLR4 agonists, surfactant protein D and biglycan, also bind to TLR4 in the absence of any co-factors, with affinities comparable to the tenascin FBG domains, and to the affinity of MD-2, for TLR4 (Table 3-4). However, these proteins exhibit a different structure compared to MD-2 and Der p 2, suggesting a fourth mode of interaction with the receptor (Figure 6-1 D). Biglycan is a proteoglycan composed of leucine rich repeats [352], while surfactant protein D comprises an α helical coil-coiled structure linked to a globular carbohydrate binding domain [353]. Tenascin FBG domains do not possess a hydrophobic cavity, consistent with them being able to activate TLR4 independently of LPS and with their inability to enhance LPS-mediated TLR4 activation [215]. In addition, FBG-C binds with lower

affinity to TLR4 in complex with MD-2 (Figure 3-24), suggesting competition for a common or overlapping binding site within TLR4.

In order to study the structural possibility of direct binding modes of FBG domains to TLR4, FBG-C homology models were used within protein:protein docking procedures, including only models in which the residues of loops 5 and 7 contact TLR4 (loop 10 has no structural template, therefore was not considered to be modelled accurately). Homology models of FBG-C indicate that the domain is larger in volume than MD-2. However, docking studies suggest that the FBG-C domain may bind in a similar mode than MD-2. Analysis using ICM protein:protein docking and ClusPro showed high frequency hits in the concave surface of TLR4-1 at the N-terminus and central LRR modules, overlapping with some regions of MD-2 interaction with TLR4. FBG-C could also induce TLR4 dimerization by binding to the convex surface of TLR4-2, in a similar fashion than MD-2 (Figure 6-1 D). MD-2 binds to each TLR4 of the receptor homodimer via ionic and polar interactions (TLR4-1: R68, K109, R106, D101, S103, S98, D99, G123; TLR4-2: K125, R90, M85, L87); and the same has been predicted for Der p 2. My data indicate several commonalities with TLRs modes of activation. Firstly, multiple binding sites participate in mediating a high affinity interaction with TLR4, and secondly, similar types of interactions appear to be involved. FBG-C requires charged and polar residues, as well as hydrophobic amino acids to bind and activate TLR4. The interaction between FBG-C and TLR4 could be driven by ionic and hydrophobic bonds similarly to what has been reported for MD-2, where FBG-C is binding to a primary interface in TLR4-1 and to a dimerization interface in TLR4-2. However, the residues in TLR4 involved in binding to FBG-C are still unknown. Future work will include assays using TLR4 mutants to elucidate the specific amino acids in TLR4 interacting with FBG-C.

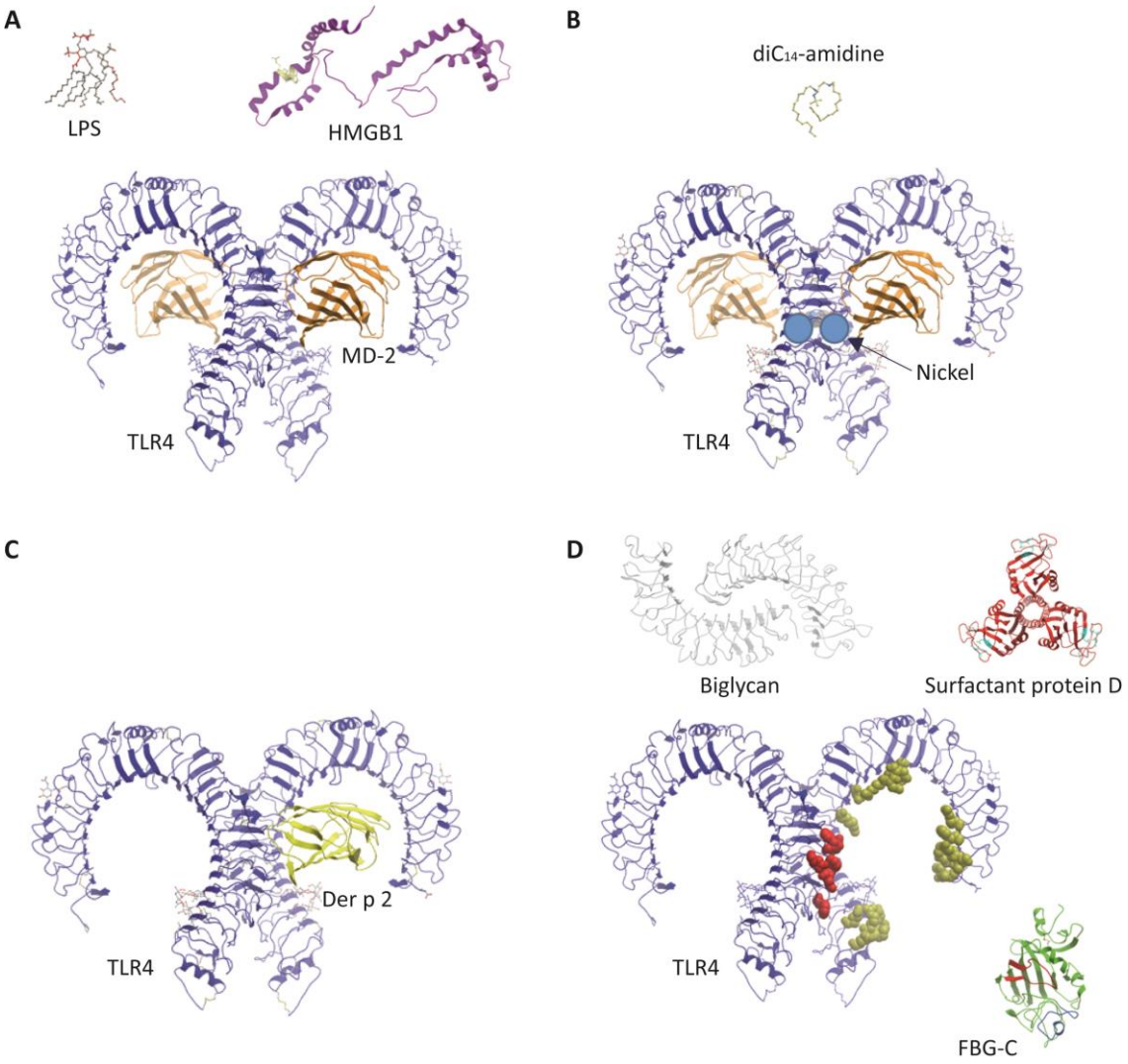

Figure 6-1. Structures of direct and indirect binders of TLR4. The structure of TLR4 (PDB code 4G8A) is shown in blue together with **A.** binders of TLR4 that interact with MD-2 (PDB code 4G8A – orange): LPS (PDB code 4G8A) and HMGB1 (PDB code 2YRQ - purple); **B.** binders of TLR4 that require but do not bind MD-2: Ni^{2+} (blue circles mapped onto critical histidine 456 and 458 of TLR4) and diC_{14}-amidine; **C.** binders of TLR4 that do not require MD-2: DERP-2 (PDB code 1KTJ superimposed upon MD-2 of PDB code 4G8A - yellow); and **D.** endogenous ligands that can bind directly to TLR4: biglycan (bovine structure, PDB code 2FT3 – grey), surfactant protein D (PDB code 1PWB – red; carbohydrate region marked in cyan), tenascin-C FBG-like domain (homology model – green; loop 5 – red; loop 7 - blue) with the TLR4 structure annotated with a high frequency of observed interactions in ICM protein:protein docking with loops 5 and 7 (yellow – TLR4 monomer 1; red – TLR4 monomer 2). Figure generate by Brian D. Marsden.

In summary, I found three specific regions in FBG-C involved in binding and activation of TLR4, which include loop 5, 7 and 10 in the P-subdomain of the protein. Together these data revealed a new mode of TLR4 activation by endogenous molecules,

where FBG-C is predicted to occupy the same space that MD-2 in TLR4. In addition, this information will contribute to the design of specific inhibitors against the FBG domain of tenascin-C, which will be used to treat chronic inflammatory conditions.

6.2. Fibrinogen related proteins

The tenascin family also belong to the group of fibrinogen related proteins (FRePs). These proteins have a domain which is highly homologous to the C-terminal globular structure of the γ and β chain of fibrinogen. This structure has been defined as a fibrinogen-like globe (FBG) domain, also referred to as a fibrinogen related domain (FReD) [354]. Typically, FRePs are multidomain proteins where the FBG domain is at the C-terminus of the molecule.

Although the FBG domain was first describe in fibrinogen, it is an ancient domain. SMART analysis revealed that there are a total of 2515 FRePs in eukaryote, all found in multicellular organism. Whilst some molecules have been found to be homologous to the A sub-domain in choanoflagellates [355], it's in the sea sponge (Phylum Porifera) where the first complete FBG domain can be found. In mammals there are 541 FRePs with 21 different FRePs in human, including fibrinogen, tenascins, ficolins, angiopoietins, angiopoietin-related proteins, fibroleukin, and fibrinogen C domain-containing protein-1 (FIBCD-1) (Figure 6-2).

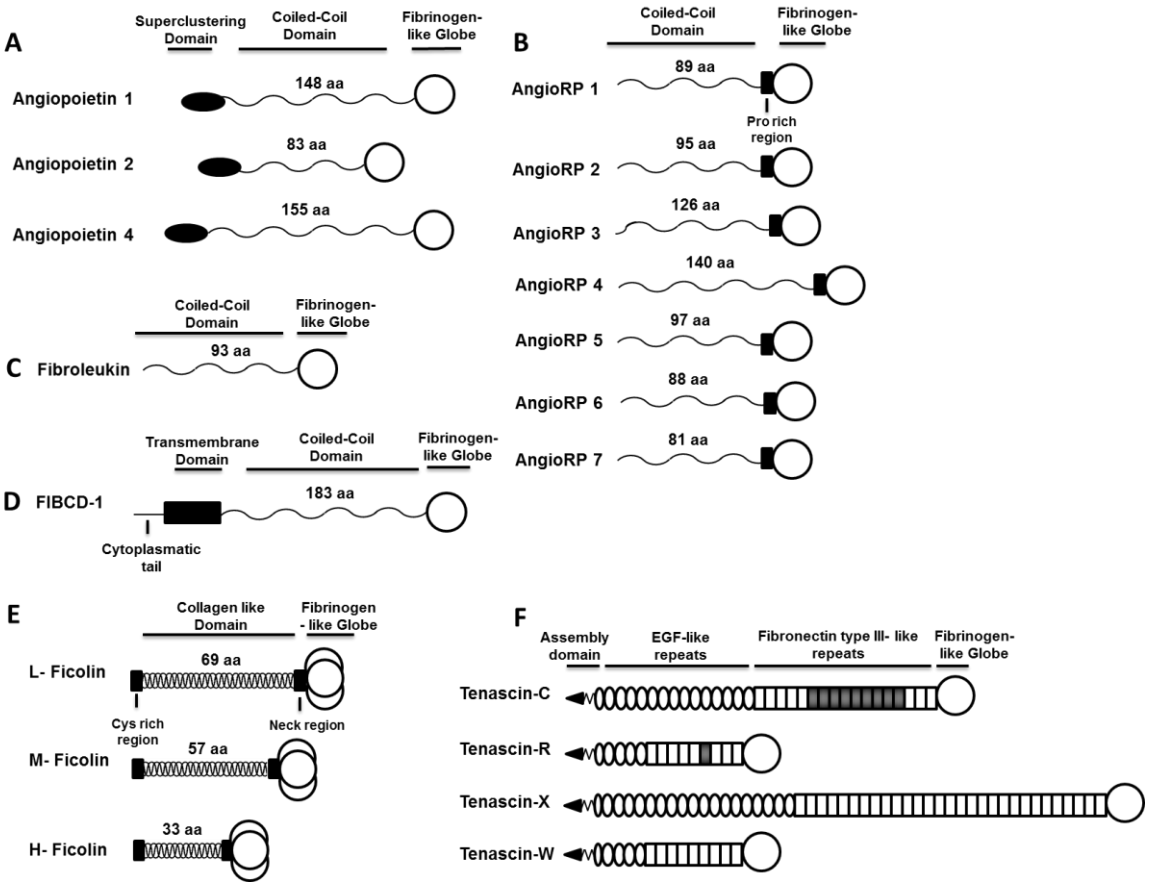

Figure 6-2. Domain organization of human FRePs. A. Angiopoietins contain an N-terminal superclustering domain, followed by a coiled-coil domain in which the number of amino acids varies between family members, and the C-terminus is capped by the FBG domain. **B.** Angiopoietin-related proteins are structurally similar to angiopoietins. They lack a superclustering domain, instead containing a proline rich region before the FBG domain. **C.** Fibroleukin contains a coiled-coil domain and a C-terminal FBG domain. **D.** Fibrinogen-C domain containing protein 1 (FIBCD-1) is the only FReP that is not secreted; it contains a transmembrane domain, followed by coiled-coil domain and FBG domain. **E.** Ficolins contain an N-terminal collagen like domain, which includes a cysteine rich region and a neck region that connects with the FBG domain. **F.** Tenascins have an N-terminal region involved in oligomer formation. Next are the EGF-like repeats, followed by FNIII domains, which number varies among the tenascins, and at the C-terminus is the FBG domain.

There is 30%-40% identity among human FRePs indicating a high level of homology among the sequences of these proteins. This is consistent with the crystal structures published to date for some of the human FRePs, which revealed a well conserved pattern of folding. They all have a common organisation similar to the fibrinogen γ chain, each structure comprising a defined A, B and P sub-domain. The A

sub-domain is formed with anti-parallel β sheets and an α helix, and it's where the first disulphide bond is located. The B domain is in the centre and comprises β sheets and 2 α helices. The P domain is formed mainly of loops and has little secondary structure. The second disulphide bond is located in this region as well as the calcium binding site, which position is conserved among the all structures and involved 2 Asp residues and the cysteines from the disulphide bond (Figure 6-3).

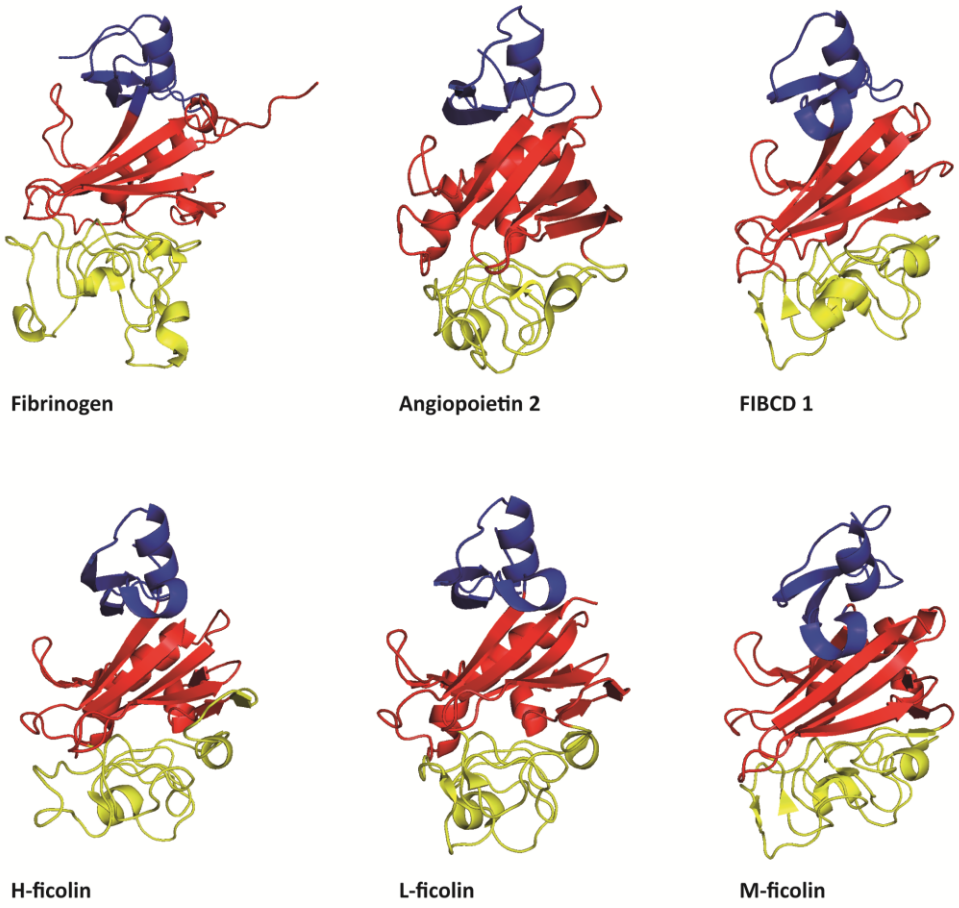

Figure 6-3. 3D structure of C-terminus fibrinogen γ chain and other human FRePs. Protein sub-domain organisation is highlighted: A-subdomain in blue, B sub-domain in red and P subdomain in yellow. Protein structure were obtained in PDB [308, 356-359] and coloured using PyMOL Molecular Graphics System.

Crystal structure analyses have also revealed that FBG domains can oligomerise. All ficolins form homotrimers when crystallised [356, 357], while angiopoietins 1 and 2

can exist as trimeric, tetrameric or pentameric oligomers [360]. Moreover, oligomerization of angiopoietins is essential for binding to the Tie2 receptor [361]. FIBCD-1 also forms homotetramers in the cell membrane and acts as a receptor for chitin binding [362, 363]. The FBG domain of tenascin-C can form dimers and trimers, but it is not known if this is required or might interfere with TLR4 activation.

Human FRePs have diverse and complex functions, being essential in the coagulation cascade, but also involved in cell-cell interaction and signalling. They are part of the extracellular matrix and are key molecules in angiogenesis, as well as the innate immune system [364]. Ligands identified for FRePs include cell surface receptors such as integrins, TLRs and Tie; bacterial components such as sugars; and proteins such as "a" peptide, C-reactive protein and β-amyloid. By direct mutagenesis or crystal structure it has been identified some of the binding site of human FRePs to their ligands (Table 6-1).

Table 6-1. Binding sites of human FRePs ligands. Each ligand is shown with the location of the amino acids involved in the interaction.

FBG domain	Ligand	Binding amino acids	Subdomain
Angiopoietin 1	Tie2	D218, A219, P222, K238, K243, Y246	P [365]
Angiopoietin 2	Tie2	D218, A219, P222, N237-F239, Y245, Y246, S250	P [365]
Fibrinogen βC	β-amyloid 42	N138-G187	B, P [366]
Fibrinogen γC	Integrin $\alpha_{IIb}\beta_3$	H271-V279	P [367]
	Integrin $\alpha_M\beta_2$	G48-V60 / Y248-G266	A, P [368]
	Integrin $\alpha_v\beta_3$	G217-S229	P [198]
	Integrin $\alpha_5\beta_1$	N236-T254	P [369]
	"a" peptide GPRP	Q245, D246, K254-H256, Y279-G282, R291	P [370]
FIBCD-1	Chitin	Y250, H260, Y283, A284	P [363]
H-ficolin	D-fucose	C189, Y190, Y208, V218	P [356]
L-ficolin	Acetylated sugars	F180, C189, H190, G204, F206, Y218, N219	P [356]
	1,3-β-D-glucan	E226, D53, D55, S34, S86	A, B [356]
M-ficolin	Acetylated sugars	F180, C189, H190, Y206, A207, Y218	P [357]
	C-reactive protein	C189-N211	P [371]
Tenascin-C	Integrin $\alpha_v\beta_3$	W151-K189	P [198]
	TLR4	K123-K129, F152-N162, R224-R227	P, B

The P domain is the region where most of the binding sites for ligands are located. In fibrinogen, this region binds to integrins and also to amino-terminal peptide "knobs" originated from the central regions of other fibrinogen molecules, which account for the initial step in fibrin polymerization. This same region contains the ficolin binding sites for sugars and sugar derivative, as well as the residues that angiopoietins required to interact with Tie2 receptor. However, there are key amino acids that aren't conserved and probably confer the proteins their unique function. For example, there are some amino acids insertions in fibrinogen β and γ chain that are not found in other FRePs and are involved in ligand binding. The tenascins lack the region essential for binding acetylated sugars present in ficolins, as a result of a deletion [372]. Multiple sequence alignments of the human FRePs reveals that the binding sites of the tenascin FBG domains to TLR4 are unique to this family, and only the fibrinogen γ chain possesses an extended C-terminal sequence akin to the active tenascin FBG domains (Figure 6-4 B). These data are consistent with the ability of fibrinogen to activate TLR4 [373] and imply that this domain may do so via a similar mode of action to tenascin-C.

Tenascin proteins appeared first in early chordates such as *C. savignyi* and *C. intestinalis* [306, 374]. Multiple alignments of the FBG domain of tenascin-C show a high level of sequence conservation across species. Analysis of the evolutionary change rate of the P subdomain of human FrePs has suggested that when an FBG domain acquires a new function, the rate of change in the P subdomain decreases, and the residues involved in the interaction with other proteins remain conserved among species [372]. Whilst the sequences of loops 5 and 7 and the C-terminus show some divergence in early chordates, they are extraordinarily well conserved in higher

eukaryotes (Figure 6-4 A), suggesting that the involvement of the FBG-C domain in the innate immune response is a more recent acquired function.

Analysis of the sequences of FRePs from ancient organisms revealed similarities in loop 5 and 7 of the mollusc *B. galabrata* and human FBG-C, suggesting that this FReP might be also able to activate TLR4. In invertebrates, FRePs are essential for protection against infection as well as development [375]. The FRePs from *B. glabrata* have been shown to have a role in internal defence, being able to bind and precipitate parasitic antigens [376]. Another well studied example is tachylectin 5A from the horseshoe crab *T. tridendatus*. This FReP can recognise acetyl groups and can agglutinate both Gram-positive and Gram-negative bacteria [377]. Tachylectin 5A has ~40% homology with human ficolins (especially in their ligand binding sites) and these FRePs share similar functions in the immune response. The emergence in vertebrates of a pathogen-independent means of activating immunity suggests an evolutionary pressure to react to threat other than infection.

.

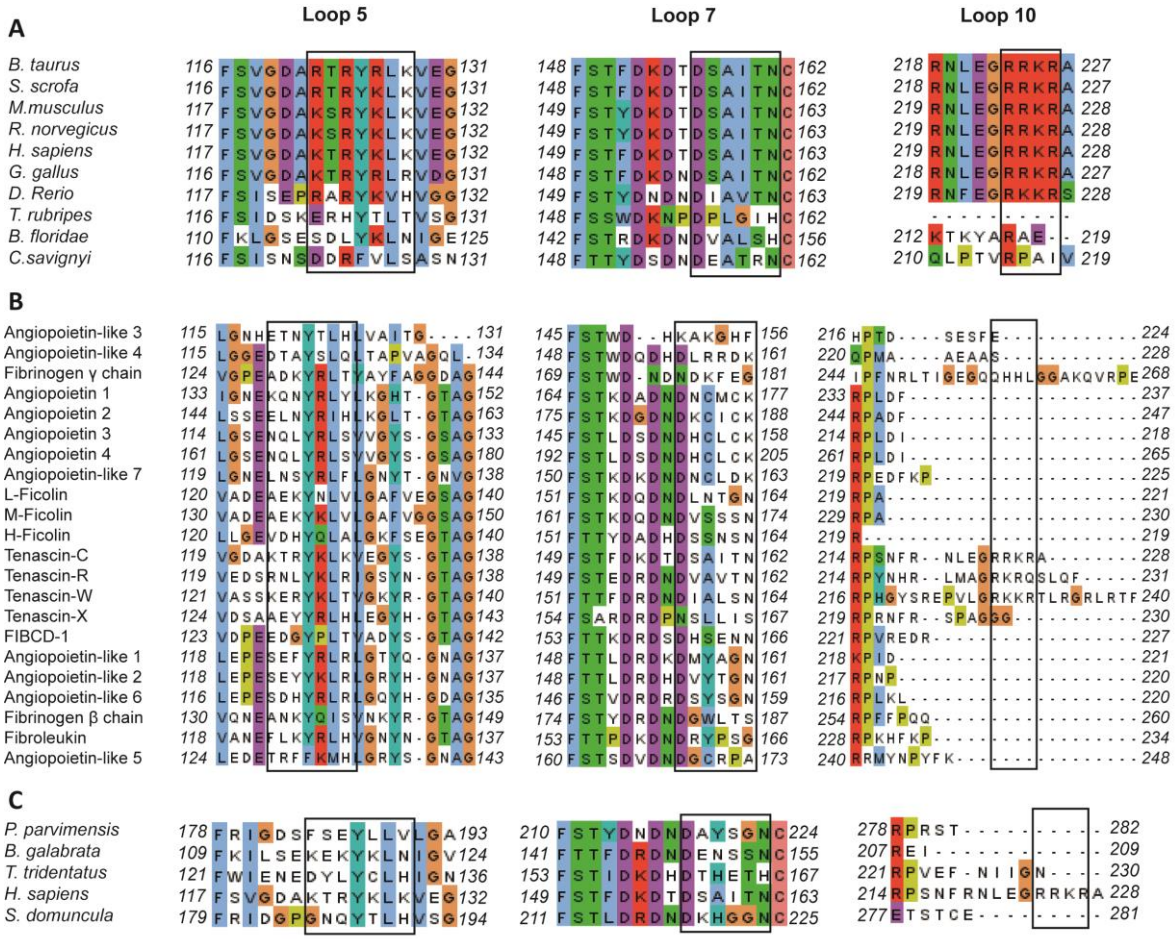

Figure 6-4. Conservation of the FBG-C active epitope across species and in other fibrinogen related proteins. A. Multiple sequence alignment of the FBG domain of tenascin-C of different species. **B.** Multiple sequence alignment of all human FRePs. **C.** Multiple sequence alignment of human FBG-C and fibrinogen related domains from ancient invertebrates. The amino acids involved in TLR4 activation and binding in loop 5, 7 and 10 are highlighted in a black box. The alignment was coloured according to the Clustal colour scheme. Light blue: hydrophobic. Red: positively charged. Green: Polar. Pink: conserved column of cysteine. Violet: negatively charge. Orange: glycine. Yellow: proline. Cyan: aromatics.

In summary, the fibrinogen-like globe is an ancient domain which has diversified to exhibit different functions throughout eukaryotic evolution. Initially involved in immune responses and development, the expansion of these proteins in vertebrates resulted in the development of new complex roles. Whilst a large degree of homology exists among the FBG domains of human FRePs, they interact with multiple diverse binding partners via specific amino acids, which are unique to the same family members. Precise mapping of FBG-binding sites will enable the development of

specific inhibitors that might be useful in controlling diverse processes in human diseases including coagulation, inflammation, angiogenesis, and tissue rebuilding.

6.3. Summary and future plans

I have shown for the first time that, in addition to tenascin-C, other tenascin family members (-R and -W) can induce a TLR4 mediated inflammatory response, where tenascin–X cannot. The pro-inflammatory epitope of the active tenascins lies in loop 5 in the P-subdomain of FBG, where positively charged amino acids are necessary for the activation of TLR4, whilst charged residues in loop 10 and polar and hydrophobic amino acids in 7, assist in mediating high affinity binding to TLR4. Together these data provide the molecular basis of a direct, endogenous TLR4 ligand, which will contribute to better understand how endogenous molecules activate this receptor, as well as be used for the design of specific inhibitors of FBG domain containing TLR stimuli. Future plans will include:

- Determine if FBG-X mutant 3 and 4 activity is dependent on TLR4. TLR4 antibody and TLR4 inhibitor TAK 242 will be used in primary human macrophages prior stimulation with FBG-X mutant 3 and 4 to determine if the protein activity is affected by the inhibition of TLR4.
- Determine the amino acids in TLR4 required for FBG-C recognition. FBG-C activity will be assessed in HEK cells expressing TLR4 mutants. Recombinant TLR4 mutants could be generated to assess *in vitro* binding to FBG-C using the solid phase binding assay. Together these data will elucidate the specific amino acids in TLR4 involved in binding to FBG-C

- Elucidate the differences in the mechanism of activation of TLR4 by FBG-C and LPS. Our group has shown that FBG-C activates the MyD88 pathway downstream of TLR4. However, it is not known if FBG-C could also induce the TRIF pathway or TLR4 internalization like LPS. TRIF-induced cytokines such as interferon, CCL5 and IP-10 could be determined by ELISA in the supernatant from primary human macrophages stimulated with FBG-C or LPS. In addition, TLR4 internalization could be measured by fluorescence-activated cell sorting (FACS) using wild type and TLR4 null bone marrow derived macrophages. These cells will be stimulated with FBG-C and LPS at different time points to track changes in TLR4 localization at the cell surface. These data will determine the differences in TLR4 internalization and the activation of the TRIF pathway induced by LPS or FBG-C, and will indicate a different mode of activation of TLR4 by these ligands.
- Establish if other co-receptors are required for TLR4 activation by FBG-C. The FBG domain of tenascin-C has been shown to bind to integrins; however, it is not known if they contribute to TLR4 activation. Antibodies against different integrin sub-units will be used in cell assays to determine if protein activity is affected by inhibiting possible interactions with integrins. These results will determine if a specific integrin is required as a co-receptor for the activation of TLR4 by FBG-C.
- Determine the crystal structure of FBG-C and FBG-C-TLR4 complex. Recombinant human FBG-C and the extracellular domain of TLR4 will be co-crystallised to confirm and determine the interaction between specific amino acids within these proteins.

- Introduce mutations in loop 5, loop 7 and loop 10 of the FBG domain in full-length tenascin-C. Assess the effect of these changes in the activity of the full-length protein when it is used to stimulate primary human macrophages and ThP1 cells.

References

1. Janeway, C.A., Jr., *Approaching the asymptote? Evolution and revolution in immunology.* Cold Spring Harb Symp Quant Biol, 1989. **54 Pt 1**: p. 1-13.
2. Kumar, H., T. Kawai, and S. Akira, *Pathogen recognition by the innate immune system.* Int Rev Immunol, 2011. **30**(1): p. 16-34.
3. Iwasaki, A. and R. Medzhitov, *Control of adaptive immunity by the innate immune system.* Nat Immunol, 2015. **16**(4): p. 343-53.
4. Kono, H. and K.L. Rock, *How dying cells alert the immune system to danger.* Nat Rev Immunol, 2008. **8**(4): p. 279-89.
5. Matzinger, P., *Tolerance, danger, and the extended family.* Annu Rev Immunol, 1994. **12**: p. 991-1045.
6. Bianchi, M.E., *DAMPs, PAMPs and alarmins: all we need to know about danger.* J Leukoc Biol, 2007. **81**(1): p. 1-5.
7. Chen, G.Y. and G. Nunez, *Sterile inflammation: sensing and reacting to damage.* Nat Rev Immunol, 2010. **10**(12): p. 826-37.
8. Takeuchi, O. and S. Akira, *Pattern recognition receptors and inflammation.* Cell, 2010. **140**(6): p. 805-20.
9. Brubaker, S.W., et al., *Innate immune pattern recognition: a cell biological perspective.* Annu Rev Immunol, 2015. **33**: p. 257-90.
10. Rothfuchs, A.G., et al., *Dectin-1 interaction with Mycobacterium tuberculosis leads to enhanced IL-12p40 production by splenic dendritic cells.* J Immunol, 2007. **179**(6): p. 3463-71.
11. van Kooyk, Y. and G.A. Rabinovich, *Protein-glycan interactions in the control of innate and adaptive immune responses.* Nat Immunol, 2008. **9**(6): p. 593-601.
12. Yamasaki, S., et al., *Mincle is an ITAM-coupled activating receptor that senses damaged cells.* Nat Immunol, 2008. **9**(10): p. 1179-88.
13. Cambi, A. and C. Figdor, *Necrosis: C-type lectins sense cell death.* Curr Biol, 2009. **19**(9): p. R375-8.
14. Ahrens, S., et al., *F-actin is an evolutionarily conserved damage-associated molecular pattern recognized by DNGR-1, a receptor for dead cells.* Immunity, 2012. **36**(4): p. 635-45.
15. Girardin, S.E., et al., *Nod1 detects a unique muropeptide from gram-negative bacterial peptidoglycan.* Science, 2003. **300**(5625): p. 1584-7.
16. Kim, J.G., S.J. Lee, and M.F. Kagnoff, *Nod1 is an essential signal transducer in intestinal epithelial cells infected with bacteria that avoid recognition by toll-like receptors.* Infect Immun, 2004. **72**(3): p. 1487-95.
17. Opitz, B., et al., *Nod1-mediated endothelial cell activation by Chlamydophila pneumoniae.* Circ Res, 2005. **96**(3): p. 319-26.
18. Travassos, L.H., et al., *Nod1 participates in the innate immune response to Pseudomonas aeruginosa.* J Biol Chem, 2005. **280**(44): p. 36714-8.
19. Yu, H.B. and B.B. Finlay, *The caspase-1 inflammasome: a pilot of innate immune responses.* Cell Host Microbe, 2008. **4**(3): p. 198-208.
20. Freche, B., N. Reig, and F.G. van der Goot, *The role of the inflammasome in cellular responses to toxins and bacterial effectors.* Semin Immunopathol, 2007. **29**(3): p. 249-60.

21. Yamasaki, K., et al., *NLRP3/cryopyrin is necessary for interleukin-1beta (IL-1beta) release in response to hyaluronan, an endogenous trigger of inflammation in response to injury.* J Biol Chem, 2009. **284**(19): p. 12762-71.
22. Kanneganti, T.D., et al., *Bacterial RNA and small antiviral compounds activate caspase-1 through cryopyrin/Nalp3.* Nature, 2006. **440**(7081): p. 233-6.
23. Martinon, F., et al., *Gout-associated uric acid crystals activate the NALP3 inflammasome.* Nature, 2006. **440**(7081): p. 237-41.
24. Jimenez-Dalmaroni, M.J., M.E. Gerswhin, and I.E. Adamopoulos, *The critical role of toll-like receptors - From microbial recognition to autoimmunity: A comprehensive review.* Autoimmun Rev, 2016. **15**(1): p. 1-8.
25. Yoneyama, M., et al., *The RNA helicase RIG-I has an essential function in double-stranded RNA-induced innate antiviral responses.* Nat Immunol, 2004. **5**(7): p. 730-7.
26. Kato, H., et al., *Differential roles of MDA5 and RIG-I helicases in the recognition of RNA viruses.* Nature, 2006. **441**(7089): p. 101-5.
27. Saito, T., et al., *Regulation of innate antiviral defenses through a shared repressor domain in RIG-I and LGP2.* Proc Natl Acad Sci U S A, 2007. **104**(2): p. 582-7.
28. Schattgen, S.A. and K.A. Fitzgerald, *The PYHIN protein family as mediators of host defenses.* Immunol Rev, 2011. **243**(1): p. 109-18.
29. Zelensky, A.N. and J.E. Gready, *The C-type lectin-like domain superfamily.* FEBS J, 2005. **272**(24): p. 6179-217.
30. Kim, Y.K., J.S. Shin, and M.H. Nahm, *NOD-Like Receptors in Infection, Immunity, and Diseases.* Yonsei Med J, 2016. **57**(1): p. 5-14.
31. Chen, G., et al., *NOD-like receptors: role in innate immunity and inflammatory disease.* Annu Rev Pathol, 2009. **4**: p. 365-98.
32. Kato, H., et al., *Cell type-specific involvement of RIG-I in antiviral response.* Immunity, 2005. **23**(1): p. 19-28.
33. Nakhaei, P., et al., *RIG-I-like receptors: sensing and responding to RNA virus infection.* Semin Immunol, 2009. **21**(4): p. 215-22.
34. Sun, L., et al., *Cyclic GMP-AMP synthase is a cytosolic DNA sensor that activates the type I interferon pathway.* Science, 2013. **339**(6121): p. 786-91.
35. Gay, N.J. and F.J. Keith, *Drosophila Toll and IL-1 receptor.* Nature, 1991. **351**(6325): p. 355-6.
36. Anderson, K.V., L. Bokla, and C. Nusslein-Volhard, *Establishment of dorsal-ventral polarity in the Drosophila embryo: the induction of polarity by the Toll gene product.* Cell, 1985. **42**(3): p. 791-8.
37. Medzhitov, R., P. Preston-Hurlburt, and C.A. Janeway, Jr., *A human homologue of the Drosophila Toll protein signals activation of adaptive immunity.* Nature, 1997. **388**(6640): p. 394-7.
38. Rock, F.L., et al., *A family of human receptors structurally related to Drosophila Toll.* Proc Natl Acad Sci U S A, 1998. **95**(2): p. 588-93.
39. Ganz, T., *Defensins: antimicrobial peptides of innate immunity.* Nat Rev Immunol, 2003. **3**(9): p. 710-20.
40. Park, H.S., et al., *Cutting edge: direct interaction of TLR4 with NAD(P)H oxidase 4 isozyme is essential for lipopolysaccharide-induced production of reactive oxygen species and activation of NF-kappa B.* J Immunol, 2004. **173**(6): p. 3589-93.
41. Blander, J.M. and R. Medzhitov, *Regulation of phagosome maturation by signals from toll-like receptors.* Science, 2004. **304**(5673): p. 1014-8.

42. Hoshino, K., et al., *Cutting edge: Toll-like receptor 4 (TLR4)-deficient mice are hyporesponsive to lipopolysaccharide: evidence for TLR4 as the Lps gene product.* J Immunol, 1999. **162**(7): p. 3749-52.
43. Takeuchi, O., et al., *Cutting edge: role of Toll-like receptor 1 in mediating immune response to microbial lipoproteins.* J Immunol, 2002. **169**(1): p. 10-4.
44. Takeuchi, O., et al., *Discrimination of bacterial lipoproteins by Toll-like receptor 6.* Int Immunol, 2001. **13**(7): p. 933-40.
45. Larsen, P.H., T.H. Holm, and T. Owens, *Toll-like receptors in brain development and homeostasis.* Sci STKE, 2007. **2007**(402): p. pe47.
46. Michelsen, K.S. and M. Arditi, *Toll-like receptors and innate immunity in gut homeostasis and pathology.* Curr Opin Hematol, 2007. **14**(1): p. 48-54.
47. Micera, A., et al., *Toll-Like Receptors and Tissue Remodeling: The Pro/Cons Recent Findings.* J Cell Physiol, 2016. **231**(3): p. 531-44.
48. Piccinini, A.M. and K.S. Midwood, *DAMPening inflammation by modulating TLR signalling.* Mediators Inflamm, 2010. **2010**.
49. Elgert, K.D., *Immunology : understanding the immune system*. 2nd ed. 2009, Hoboken, N.J.: Wiley-Blackwell. xi, 726 p.
50. Bryant, C.E., et al., *Advances in Toll-like receptor biology: Modes of activation by diverse stimuli.* Crit Rev Biochem Mol Biol, 2015. **50**(5): p. 359-79.
51. Ridnour, L.A., et al., *Molecular pathways: toll-like receptors in the tumor microenvironment--poor prognosis or new therapeutic opportunity.* Clin Cancer Res, 2013. **19**(6): p. 1340-6.
52. Cario, E., G. Gerken, and D.K. Podolsky, *Toll-like receptor 2 controls mucosal inflammation by regulating epithelial barrier function.* Gastroenterology, 2007. **132**(4): p. 1359-74.
53. Ultaigh, S.N., et al., *Blockade of Toll-like receptor 2 prevents spontaneous cytokine release from rheumatoid arthritis ex vivo synovial explant cultures.* Arthritis Res Ther, 2011. **13**(1): p. R33.
54. Nair, A., et al., *Synovial fluid from patients with early osteoarthritis modulates fibroblast-like synoviocyte responses to toll-like receptor 4 and toll-like receptor 2 ligands via soluble CD14.* Arthritis Rheum, 2012. **64**(7): p. 2268-77.
55. Monaco, C., et al., *Toll-like receptor-2 mediates inflammation and matrix degradation in human atherosclerosis.* Circulation, 2009. **120**(24): p. 2462-9.
56. Devaraj, S., et al., *Knockout of toll-like receptor-2 attenuates both the proinflammatory state of diabetes and incipient diabetic nephropathy.* Arterioscler Thromb Vasc Biol, 2011. **31**(8): p. 1796-804.
57. Bohnhorst, J., et al., *Toll-like receptors mediate proliferation and survival of multiple myeloma cells.* Leukemia, 2006. **20**(6): p. 1138-44.
58. Li, X., et al., *Upregulation of Toll-like receptor 2 expression in colorectal cancer infected by human cytomegalovirus.* Oncol Lett, 2015. **9**(1): p. 365-370.
59. Dasu, M.R., et al., *Increased toll-like receptor (TLR) activation and TLR ligands in recently diagnosed type 2 diabetic subjects.* Diabetes Care, 2010. **33**(4): p. 861-8.
60. Chen, S.Y., et al., *Suppression of collagen-induced arthritis by intra-articular lentiviral vector-mediated delivery of Toll-like receptor 7 short hairpin RNA gene.* Gene Ther, 2012. **19**(7): p. 752-60.
61. Alzabin, S., et al., *Investigation of the role of endosomal Toll-like receptors in murine collagen-induced arthritis reveals a potential role for TLR7 in disease maintenance.* Arthritis Res Ther, 2012. **14**(3): p. R142.

62. Tran, N.L., C. Manzin-Lorenzi, and M.L. Santiago-Raber, *Toll-like receptor 8 deletion accelerates autoimmunity in a mouse model of lupus through a Toll-like receptor 7-dependent mechanism.* Immunology, 2015. **145**(1): p. 60-70.
63. Grimmig, T., et al., *TLR7 and TLR8 expression increases tumor cell proliferation and promotes chemoresistance in human pancreatic cancer.* Int J Oncol, 2015. **47**(3): p. 857-66.
64. Lee, S.Y., et al., *Interleukin-17 increases the expression of Toll-like receptor 3 via the STAT3 pathway in rheumatoid arthritis fibroblast-like synoviocytes.* Immunology, 2014. **141**(3): p. 353-61.
65. Jiang, C., et al., *MicroRNA-26a negatively regulates toll-like receptor 3 expression of rat macrophages and ameliorates pristane induced arthritis in rats.* Arthritis Res Ther, 2014. **16**(1): p. R9.
66. Strodthoff, D., et al., *Toll-Like Receptor 3 Influences Glucose Homeostasis and beta-Cell Insulin Secretion.* Diabetes, 2015. **64**(10): p. 3425-38.
67. Nakamura, N., et al., *Toll-like receptor 3 increases allergic and irritant contact dermatitis.* J Invest Dermatol, 2015. **135**(2): p. 411-7.
68. He, J.F., et al., *Genetic polymorphisms of TLR3 are associated with Nasopharyngeal carcinoma risk in Cantonese population.* BMC Cancer, 2007. **7**: p. 194.
69. Sacre, S.M., et al., *Inhibitors of TLR8 reduce TNF production from human rheumatoid synovial membrane cultures.* J Immunol, 2008. **181**(11): p. 8002-9.
70. Roger, T., et al., *Protection from lethal gram-negative bacterial sepsis by targeting Toll-like receptor 4.* Proc Natl Acad Sci U S A, 2009. **106**(7): p. 2348-52.
71. Abdollahi-Roodsaz, S., et al., *Inhibition of Toll-like receptor 4 breaks the inflammatory loop in autoimmune destructive arthritis.* Arthritis Rheum, 2007. **56**(9): p. 2957-67.
72. Szabo, G., et al., *Modulation of non-alcoholic steatohepatitis by pattern recognition receptors in mice: the role of toll-like receptors 2 and 4.* Alcohol Clin Exp Res, 2005. **29**(11 Suppl): p. 140S-145S.
73. Hritz, I., et al., *The critical role of toll-like receptor (TLR) 4 in alcoholic liver disease is independent of the common TLR adapter MyD88.* Hepatology, 2008. **48**(4): p. 1224-31.
74. Michelsen, K.S., et al., *Lack of Toll-like receptor 4 or myeloid differentiation factor 88 reduces atherosclerosis and alters plaque phenotype in mice deficient in apolipoprotein E.* Proc Natl Acad Sci U S A, 2004. **101**(29): p. 10679-84.
75. Higashimori, M., et al., *Role of toll-like receptor 4 in intimal foam cell accumulation in apolipoprotein E-deficient mice.* Arterioscler Thromb Vasc Biol, 2011. **31**(1): p. 50-7.
76. Millien, V.O., et al., *Cleavage of fibrinogen by proteinases elicits allergic responses through Toll-like receptor 4.* Science, 2013. **341**(6147): p. 792-6.
77. Schmidt, M., et al., *Crucial role for human Toll-like receptor 4 in the development of contact allergy to nickel.* Nat Immunol, 2010. **11**(9): p. 814-9.
78. Wu, H., et al., *TLR4 activation mediates kidney ischemia/reperfusion injury.* J Clin Invest, 2007. **117**(10): p. 2847-59.
79. Sheng, W.Y., et al., *Toll-like receptor 4 gene polymorphisms and susceptibility to colorectal cancer: a meta-analysis and review.* Arch Med Sci, 2015. **11**(4): p. 699-707.
80. Yesudhas, D., et al., *Multiple roles of toll-like receptor 4 in colorectal cancer.* Front Immunol, 2014. **5**: p. 334.

81. Gatti, G., et al., *Expression of Toll-like receptor 4 in the prostate gland and its association with the severity of prostate cancer.* Prostate, 2009. **69**(13): p. 1387-97.
82. Lartigue, A., et al., *Role of TLR9 in anti-nucleosome and anti-DNA antibody production in lpr mutation-induced murine lupus.* J Immunol, 2006. **177**(2): p. 1349-54.
83. Nadigel, J., et al., *Cigarette smoke increases TLR4 and TLR9 expression and induces cytokine production from CD8(+) T cells in chronic obstructive pulmonary disease.* Respir Res, 2011. **12**: p. 149.
84. Furi, I., et al., *Epithelial toll-like receptor 9 signaling in colorectal inflammation and cancer: clinico-pathogenic aspects.* World J Gastroenterol, 2013. **19**(26): p. 4119-26.
85. Vaisanen, M.R., et al., *Expression of toll-like receptor-9 is increased in poorly differentiated prostate tumors.* Prostate, 2010. **70**(8): p. 817-24.
86. Di, J.M., et al., *Toll-like receptor 9 agonists up-regulates the expression of cyclooxygenase-2 via activation of NF-kappaB in prostate cancer cells.* Mol Biol Rep, 2010. **37**(4): p. 1849-55.
87. Liu-Bryan, R. and R. Terkeltaub, *Chondrocyte innate immune myeloid differentiation factor 88-dependent signaling drives procatabolic effects of the endogenous Toll-like receptor 2/Toll-like receptor 4 ligands low molecular weight hyaluronan and high mobility group box chromosomal protein 1 in mice.* Arthritis Rheum, 2010. **62**(7): p. 2004-12.
88. van Zoelen, M.A., et al., *Role of toll-like receptors 2 and 4, and the receptor for advanced glycation end products in high-mobility group box 1-induced inflammation in vivo.* Shock, 2009. **31**(3): p. 280-4.
89. Midwood, K., et al., *Tenascin-C is an endogenous activator of Toll-like receptor 4 that is essential for maintaining inflammation in arthritic joint disease.* Nat Med, 2009. **15**(7): p. 774-80.
90. Campo, G.M., et al., *Small hyaluronan oligosaccharides induce inflammation by engaging both toll-like-4 and CD44 receptors in human chondrocytes.* Biochem Pharmacol, 2010. **80**(4): p. 480-90.
91. Black, K.E., et al., *Hyaluronan fragments induce IFNbeta via a novel TLR4-TRIF-TBK1-IRF3-dependent pathway.* J Inflamm (Lond), 2013. **10**(1): p. 23.
92. Brentano, F., et al., *RNA released from necrotic synovial fluid cells activates rheumatoid arthritis synovial fibroblasts via Toll-like receptor 3.* Arthritis Rheum, 2005. **52**(9): p. 2656-65.
93. Barrat, F.J., et al., *Nucleic acids of mammalian origin can act as endogenous ligands for Toll-like receptors and may promote systemic lupus erythematosus.* J Exp Med, 2005. **202**(8): p. 1131-9.
94. Moreth, K., et al., *Biglycan-triggered TLR-2- and TLR-4-signaling exacerbates the pathophysiology of ischemic acute kidney injury.* Matrix Biol, 2014. **35**: p. 143-51.
95. Doddapattar, P., et al., *Fibronectin Splicing Variants Containing Extra Domain A Promote Atherosclerosis in Mice Through Toll-Like Receptor 4.* Arterioscler Thromb Vasc Biol, 2015. **35**(11): p. 2391-400.
96. Prakash, P., et al., *Cellular fibronectin containing extra domain A promotes arterial thrombosis in mice through platelet Toll-like receptor 4.* Blood, 2015. **125**(20): p. 3164-72.
97. Rocha, D.M., et al., *Saturated fatty acids trigger TLR4-mediated inflammatory response.* Atherosclerosis, 2016. **244**: p. 211-5.

98. Kobe, B. and A.V. Kajava, *The leucine-rich repeat as a protein recognition motif.* Curr Opin Struct Biol, 2001. **11**(6): p. 725-32.
99. Matsushima, N., et al., *Comparative Geometrical Analysis of Leucine-Rich Repeat Structures in the Nod-Like and Toll-Like Receptors in Vertebrate Innate Immunity.* Biomolecules, 2015. **5**(3): p. 1955-78.
100. Xu, Y., et al., *Structural basis for signal transduction by the Toll/interleukin-1 receptor domains.* Nature, 2000. **408**(6808): p. 111-5.
101. Khan, J.A., et al., *Crystal structure of the Toll/interleukin-1 receptor domain of human IL-1RAPL.* J Biol Chem, 2004. **279**(30): p. 31664-70.
102. Nyman, T., et al., *The crystal structure of the human toll-like receptor 10 cytoplasmic domain reveals a putative signaling dimer.* J Biol Chem, 2008. **283**(18): p. 11861-5.
103. Song, D.H. and J.O. Lee, *Sensing of microbial molecular patterns by Toll-like receptors.* Immunol Rev, 2012. **250**(1): p. 216-29.
104. Jin, M.S., et al., *Crystal structure of the TLR1-TLR2 heterodimer induced by binding of a tri-acylated lipopeptide.* Cell, 2007. **130**(6): p. 1071-82.
105. Kang, J.Y., et al., *Recognition of lipopeptide patterns by Toll-like receptor 2-Toll-like receptor 6 heterodimer.* Immunity, 2009. **31**(6): p. 873-84.
106. Kim, H.M., et al., *Crystal structure of the TLR4-MD-2 complex with bound endotoxin antagonist Eritoran.* Cell, 2007. **130**(5): p. 906-17.
107. Onji, M., et al., *An essential role for the N-terminal fragment of Toll-like receptor 9 in DNA sensing.* Nat Commun, 2013. **4**: p. 1949.
108. Ohto, U., et al., *Structural basis of CpG and inhibitory DNA recognition by Toll-like receptor 9.* Nature, 2015. **520**(7549): p. 702-5.
109. Triantafilou, M., et al., *Membrane sorting of toll-like receptor (TLR)-2/6 and TLR2/1 heterodimers at the cell surface determines heterotypic associations with CD36 and intracellular targeting.* J Biol Chem, 2006. **281**(41): p. 31002-11.
110. Latz, E., et al., *Ligand-induced conformational changes allosterically activate Toll-like receptor 9.* Nat Immunol, 2007. **8**(7): p. 772-9.
111. Tanji, H., et al., *Structural reorganization of the Toll-like receptor 8 dimer induced by agonistic ligands.* Science, 2013. **339**(6126): p. 1426-9.
112. Leonard, J.N., et al., *The TLR3 signaling complex forms by cooperative receptor dimerization.* Proc Natl Acad Sci U S A, 2008. **105**(1): p. 258-63.
113. Liu, L., et al., *Structural basis of toll-like receptor 3 signaling with double-stranded RNA.* Science, 2008. **320**(5874): p. 379-81.
114. Yoon, S.I., et al., *Structural basis of TLR5-flagellin recognition and signaling.* Science, 2012. **335**(6070): p. 859-64.
115. Tanji, H., et al., *Toll-like receptor 8 senses degradation products of single-stranded RNA.* Nat Struct Mol Biol, 2015. **22**(2): p. 109-15.
116. Park, B.S., et al., *The structural basis of lipopolysaccharide recognition by the TLR4-MD-2 complex.* Nature, 2009. **458**(7242): p. 1191-5.
117. Poltorak, A., et al., *Defective LPS signaling in C3H/HeJ and C57BL/10ScCr mice: mutations in Tlr4 gene.* Science, 1998. **282**(5396): p. 2085-8.
118. Erridge, C., E. Bennett-Guerrero, and I.R. Poxton, *Structure and function of lipopolysaccharides.* Microbes Infect, 2002. **4**(8): p. 837-51.
119. Galanos, C., *Physical state and biological activity of lipopolysaccharides. Toxicity and immunogenicity of the lipid A component.* Z Immunitatsforsch Exp Klin Immunol, 1975. **149**(2-4): p. 214-29.

120. Alexander, C. and E.T. Rietschel, *Bacterial lipopolysaccharides and innate immunity.* J Endotoxin Res, 2001. **7**(3): p. 167-202.
121. Jack, R.S., et al., *Lipopolysaccharide-binding protein is required to combat a murine gram-negative bacterial infection.* Nature, 1997. **389**(6652): p. 742-5.
122. Wright, S.D., et al., *CD14, a receptor for complexes of lipopolysaccharide (LPS) and LPS binding protein.* Science, 1990. **249**(4975): p. 1431-3.
123. Kelley, S.L., et al., *The crystal structure of human soluble CD14 reveals a bent solenoid with a hydrophobic amino-terminal pocket.* J Immunol, 2013. **190**(3): p. 1304-11.
124. Gioannini, T.L., et al., *Isolation of an endotoxin-MD-2 complex that produces Toll-like receptor 4-dependent cell activation at picomolar concentrations.* Proc Natl Acad Sci U S A, 2004. **101**(12): p. 4186-91.
125. Shimazu, R., et al., *MD-2, a molecule that confers lipopolysaccharide responsiveness on Toll-like receptor 4.* J Exp Med, 1999. **189**(11): p. 1777-82.
126. Akashi, S., et al., *Lipopolysaccharide interaction with cell surface Toll-like receptor 4-MD-2: higher affinity than that with MD-2 or CD14.* J Exp Med, 2003. **198**(7): p. 1035-42.
127. Park, B.S. and J.O. Lee, *Recognition of lipopolysaccharide pattern by TLR4 complexes.* Exp Mol Med, 2013. **45**: p. e66.
128. Ohto, U., et al., *Structural analyses of human Toll-like receptor 4 polymorphisms D299G and T399I.* J Biol Chem, 2012. **287**(48): p. 40611-7.
129. Qiao, S., et al., *Structural basis for lipopolysaccharide insertion in the bacterial outer membrane.* Nature, 2014. **511**(7507): p. 108-11.
130. Zipfel, C., *A new receptor for LPS.* Nat Immunol, 2015. **16**(4): p. 340-1.
131. Resman, N., et al., *Essential roles of hydrophobic residues in both MD-2 and toll-like receptor 4 in activation by endotoxin.* J Biol Chem, 2009. **284**(22): p. 15052-60.
132. Teghanemt, A., et al., *Novel roles in human MD-2 of phenylalanines 121 and 126 and tyrosine 131 in activation of Toll-like receptor 4 by endotoxin.* J Biol Chem, 2008. **283**(3): p. 1257-66.
133. Ohto, U., et al., *Crystal structures of human MD-2 and its complex with antiendotoxic lipid IVa.* Science, 2007. **316**(5831): p. 1632-4.
134. Rietschel, E.T., et al., *Bacterial endotoxin: molecular relationships of structure to activity and function.* FASEB J, 1994. **8**(2): p. 217-25.
135. Rietschel, E.T., et al., *The chemical structure of bacterial endotoxin in relation to bioactivity.* Immunobiology, 1993. **187**(3-5): p. 169-90.
136. Arbour, N.C., et al., *TLR4 mutations are associated with endotoxin hyporesponsiveness in humans.* Nat Genet, 2000. **25**(2): p. 187-91.
137. Prohinar, P., et al., *Expression of functional D299G.T399I polymorphic variant of TLR4 depends more on coexpression of MD-2 than does wild-type TLR4.* J Immunol, 2010. **184**(8): p. 4362-7.
138. Figueroa, L., et al., *The Asp299Gly polymorphism alters TLR4 signaling by interfering with recruitment of MyD88 and TRIF*. J Immunol, 2012. **188**(9): p. 4506-15.
139. Connolly, D.J. and L.A. O'Neill, *New developments in Toll-like receptor targeted therapeutics.* Curr Opin Pharmacol, 2012. **12**(4): p. 510-8.
140. Savva, A. and T. Roger, *Targeting toll-like receptors: promising therapeutic strategies for the management of sepsis-associated pathology and infectious diseases.* Front Immunol, 2013. **4**: p. 387.

141. Mullen, L.M., G. Chamberlain, and S. Sacre, *Pattern recognition receptors as potential therapeutic targets in inflammatory rheumatic disease.* Arthritis Res Ther, 2015. **17**: p. 122.
142. Tidswell, M., et al., *Phase 2 trial of eritoran tetrasodium (E5564), a toll-like receptor 4 antagonist, in patients with severe sepsis.* Crit Care Med, 2010. **38**(1): p. 72-83.
143. Loyau, J., et al., *Robust Antibody-Antigen Complexes Prediction Generated by Combining Sequence Analyses, Mutagenesis, In Vitro Evolution, X-ray Crystallography and In Silico Docking.* J Mol Biol, 2015. **427**(16): p. 2647-62.
144. Raghavan, B., et al., *Metal allergens nickel and cobalt facilitate TLR4 homodimerization independently of MD2.* EMBO Rep, 2012. **13**(12): p. 1109-15.
145. Derewenda, U., et al., *The crystal structure of a major dust mite allergen Der p 2, and its biological implications.* J Mol Biol, 2002. **318**(1): p. 189-97.
146. Trompette, A., et al., *Allergenicity resulting from functional mimicry of a Toll-like receptor complex protein.* Nature, 2009. **457**(7229): p. 585-8.
147. Hammad, H., et al., *House dust mite allergen induces asthma via Toll-like receptor 4 triggering of airway structural cells.* Nat Med, 2009. **15**(4): p. 410-6.
148. Kaiser, L., et al., *The crystal structure of the major cat allergen Fel d 1, a member of the secretoglobin family.* J Biol Chem, 2003. **278**(39): p. 37730-5.
149. Herre, J., et al., *Allergens as immunomodulatory proteins: the cat dander protein Fel d 1 enhances TLR activation by lipid ligands.* J Immunol, 2013. **191**(4): p. 1529-35.
150. Yang, H., et al., *A critical cysteine is required for HMGB1 binding to Toll-like receptor 4 and activation of macrophage cytokine release.* Proc Natl Acad Sci U S A, 2010. **107**(26): p. 11942-7.
151. Ohya, M., et al., *Human pulmonary surfactant protein D binds the extracellular domains of Toll-like receptors 2 and 4 through the carbohydrate recognition domain by a mechanism different from its binding to phosphatidylinositol and lipopolysaccharide.* Biochemistry, 2006. **45**(28): p. 8657-64.
152. Merline, R., et al., *Signaling by the matrix proteoglycan decorin controls inflammation and cancer through PDCD4 and MicroRNA-21.* Sci Signal, 2011. **4**(199): p. ra75.
153. Asea, A., et al., *Novel signal transduction pathway utilized by extracellular HSP70: role of toll-like receptor (TLR) 2 and TLR4.* J Biol Chem, 2002. **277**(17): p. 15028-34.
154. Kol, A., et al., *Cutting edge: heat shock protein (HSP) 60 activates the innate immune response: CD14 is an essential receptor for HSP60 activation of mononuclear cells.* J Immunol, 2000. **164**(1): p. 13-7.
155. Schaefer, L., et al., *The matrix component biglycan is proinflammatory and signals through Toll-like receptors 4 and 2 in macrophages.* J Clin Invest, 2005. **115**(8): p. 2223-33.
156. Vogl, T., et al., *Mrp8 and Mrp14 are endogenous activators of Toll-like receptor 4, promoting lethal, endotoxin-induced shock.* Nat Med, 2007. **13**(9): p. 1042-9.
157. Foell, D., et al., *Proinflammatory S100A12 can activate human monocytes via Toll-like receptor 4.* Am J Respir Crit Care Med, 2013. **187**(12): p. 1324-34.
158. Miller, Y.I., et al., *Minimally modified LDL binds to CD14, induces macrophage spreading via TLR4/MD-2, and inhibits phagocytosis of apoptotic cells.* J Biol Chem, 2003. **278**(3): p. 1561-8.

159. Curran, C.S., K.P. Demick, and J.M. Mansfield, *Lactoferrin activates macrophages via TLR4-dependent and -independent signaling pathways.* Cell Immunol, 2006. **242**(1): p. 23-30.
160. Guillot, L., et al., *Cutting edge: the immunostimulatory activity of the lung surfactant protein-A involves Toll-like receptor 4.* J Immunol, 2002. **168**(12): p. 5989-92.
161. Gondokaryono, S.P., et al., *The extra domain A of fibronectin stimulates murine mast cells via toll-like receptor 4.* J Leukoc Biol, 2007. **82**(3): p. 657-65.
162. Taylor, K.R., et al., *Recognition of hyaluronan released in sterile injury involves a unique receptor complex dependent on Toll-like receptor 4, CD44, and MD-2.* J Biol Chem, 2007. **282**(25): p. 18265-75.
163. Yang, H., et al., *MD-2 is required for disulfide HMGB1-dependent TLR4 signaling.* J Exp Med, 2015. **212**(1): p. 5-14.
164. Venereau, E., et al., *Mutually exclusive redox forms of HMGB1 promote cell recruitment or proinflammatory cytokine release.* J Exp Med, 2012. **209**(9): p. 1519-28.
165. Yang, H., et al., *Redox modification of cysteine residues regulates the cytokine activity of high mobility group box-1 (HMGB1).* Mol Med, 2012. **18**: p. 250-9.
166. Hodgkinson, C.P., K. Patel, and S. Ye, *Functional Toll-like receptor 4 mutations modulate the response to fibrinogen.* Thromb Haemost, 2008. **100**(2): p. 301-7.
167. Lin, S.C., Y.C. Lo, and H. Wu, *Helical assembly in the MyD88-IRAK4-IRAK2 complex in TLR/IL-1R signalling.* Nature, 2010. **465**(7300): p. 885-90.
168. Akira, S. and K. Takeda, *Toll-like receptor signalling.* Nat Rev Immunol, 2004. **4**(7): p. 499-511.
169. Kagan, J.C., et al., *TRAM couples endocytosis of Toll-like receptor 4 to the induction of interferon-beta.* Nat Immunol, 2008. **9**(4): p. 361-8.
170. Yoneyama, M., et al., *Direct triggering of the type I interferon system by virus infection: activation of a transcription factor complex containing IRF-3 and CBP/p300.* EMBO J, 1998. **17**(4): p. 1087-95.
171. Yamamoto, M., et al., *Role of adaptor TRIF in the MyD88-independent toll-like receptor signaling pathway.* Science, 2003. **301**(5633): p. 640-3.
172. Fitzgerald, K.A., et al., *LPS-TLR4 signaling to IRF-3/7 and NF-kappaB involves the toll adapters TRAM and TRIF.* J Exp Med, 2003. **198**(7): p. 1043-55.
173. Rosenberger, K., et al., *Intrathecal heat shock protein 60 mediates neurodegeneration and demyelination in the CNS through a TLR4- and MyD88-dependent pathway.* Mol Neurodegener, 2015. **10**: p. 5.
174. Kim, S., et al., *Signaling of high mobility group box 1 (HMGB1) through toll-like receptor 4 in macrophages requires CD14.* Mol Med, 2013. **19**: p. 88-98.
175. Brellier, F., R.P. Tucker, and R. Chiquet-Ehrismann, *Tenascins and their implications in diseases and tissue mechanics.* Scand J Med Sci Sports, 2009. **19**(4): p. 511-9.
176. Tucker, R.P. and R. Chiquet-Ehrismann, *The regulation of tenascin expression by tissue microenvironments.* Biochim Biophys Acta, 2009. **1793**(5): p. 888-92.
177. Hsia, H.C. and J.E. Schwarzbauer, *Meet the tenascins: multifunctional and mysterious.* J Biol Chem, 2005. **280**(29): p. 26641-4.
178. Giblin, S.P. and K.S. Midwood, *Tenascin-C: Form versus function.* Cell Adh Migr, 2015. **9**(1-2): p. 48-82.

179. Gulcher, J.R., et al., *An alternatively spliced region of the human hexabrachion contains a repeat of potential N-glycosylation sites.* Proc Natl Acad Sci U S A, 1989. **86**(5): p. 1588-92.
180. Erickson, H.P. and J.L. Inglesias, *A six-armed oligomer isolated from cell surface fibronectin preparations.* Nature, 1984. **311**(5983): p. 267-9.
181. Chiquet-Ehrismann, R., et al., *Tenascin: an extracellular matrix protein involved in tissue interactions during fetal development and oncogenesis.* Cell, 1986. **47**(1): p. 131-9.
182. Chiquet-Ehrismann, R., *Anti-adhesive molecules of the extracellular matrix.* Curr Opin Cell Biol, 1991. **3**(5): p. 800-4.
183. Midwood, K.S. and J.E. Schwarzbauer, *Tenascin-C modulates matrix contraction via focal adhesion kinase- and Rho-mediated signaling pathways.* Mol Biol Cell, 2002. **13**(10): p. 3601-13.
184. Midwood, K.S., et al., *Coregulation of fibronectin signaling and matrix contraction by tenascin-C and syndecan-4.* Mol Biol Cell, 2004. **15**(12): p. 5670-7.
185. Day, J.M., et al., *Alternative splicing in the aggrecan G3 domain influences binding interactions with tenascin-C and other extracellular matrix proteins.* J Biol Chem, 2004. **279**(13): p. 12511-8.
186. Lundell, A., et al., *Structural basis for interactions between tenascins and lectican C-type lectin domains: evidence for a crosslinking role for tenascins.* Structure, 2004. **12**(8): p. 1495-506.
187. Kammerer, R.A., et al., *Tenascin-C hexabrachion assembly is a sequential two-step process initiated by coiled-coil alpha-helices.* J Biol Chem, 1998. **273**(17): p. 10602-8.
188. Swindle, C.S., et al., *Epidermal growth factor (EGF)-like repeats of human tenascin-C as ligands for EGF receptor.* J Cell Biol, 2001. **154**(2): p. 459-68.
189. Iyer, A.K., et al., *Tenascin cytotactin epidermal growth factor-like repeat binds epidermal growth factor receptor with low affinity.* J Cell Physiol, 2007. **211**(3): p. 748-58.
190. Joshi, P., et al., *Endothelial cells adhere to the RGD domain and the fibrinogen-like terminal knob of tenascin.* J Cell Sci, 1993. **106 (Pt 1)**: p. 389-400.
191. Prieto, A.L., G.M. Edelman, and K.L. Crossin, *Multiple integrins mediate cell attachment to cytotactin/tenascin.* Proc Natl Acad Sci U S A, 1993. **90**(21): p. 10154-8.
192. Yokosaki, Y., et al., *Differential effects of the integrins alpha9beta1, alphavbeta3, and alphavbeta6 on cell proliferative responses to tenascin. Roles of the beta subunit extracellular and cytoplasmic domains.* J Biol Chem, 1996. **271**(39): p. 24144-50.
193. Puente Navazo, M.D., D. Valmori, and C. Ruegg, *The alternatively spliced domain TnFnIII A1A2 of the extracellular matrix protein tenascin-C suppresses activation-induced T lymphocyte proliferation and cytokine production.* J Immunol, 2001. **167**(11): p. 6431-40.
194. Chung, C.Y., J.E. Murphy-Ullrich, and H.P. Erickson, *Mitogenesis, cell migration, and loss of focal adhesions induced by tenascin-C interacting with its cell surface receptor, annexin II.* Mol Biol Cell, 1996. **7**(6): p. 883-92.
195. Michele, M. and A. Faissner, *Tenascin-C stimulates contactin-dependent neurite outgrowth via activation of phospholipase C.* Mol Cell Neurosci, 2009. **41**(4): p. 397-408.

196. Mercado, M.L., et al., *Neurite outgrowth by the alternatively spliced region of human tenascin-C is mediated by neuronal alpha7beta1 integrin.* J Neurosci, 2004. **24**(1): p. 238-47.
197. Srinivasan, J., M. Schachner, and W.A. Catterall, *Interaction of voltage-gated sodium channels with the extracellular matrix molecules tenascin-C and tenascin-R.* Proc Natl Acad Sci U S A, 1998. **95**(26): p. 15753-7.
198. Yokoyama, K., et al., *Identification of amino acid sequences in fibrinogen gamma -chain and tenascin C C-terminal domains critical for binding to integrin alpha vbeta 3.* J Biol Chem, 2000. **275**(22): p. 16891-8.
199. Milev, P., et al., *The fibrinogen-like globe of tenascin-C mediates its interactions with neurocan and phosphacan/protein-tyrosine phosphatase-zeta/beta.* J Biol Chem, 1997. **272**(24): p. 15501-9.
200. Midwood, K.S. and G. Orend, *The role of tenascin-C in tissue injury and tumorigenesis.* J Cell Commun Signal, 2009. **3**(3-4): p. 287-310.
201. Latijnhouwers, M., et al., *Human epidermal keratinocytes are a source of tenascin-C during wound healing.* J Invest Dermatol, 1997. **108**(5): p. 776-83.
202. Chiquet-Ehrismann, R., et al., *Tenascin-C expression by fibroblasts is elevated in stressed collagen gels.* J Cell Biol, 1994. **127**(6 Pt 2): p. 2093-101.
203. Trebaul, A., E.K. Chan, and K.S. Midwood, *Regulation of fibroblast migration by tenascin-C.* Biochem Soc Trans, 2007. **35**(Pt 4): p. 695-7.
204. Canfield, A.E. and A.M. Schor, *Evidence that tenascin and thrombospondin-1 modulate sprouting of endothelial cells.* J Cell Sci, 1995. **108 (Pt 2)**: p. 797-809.
205. Schenk, S., R. Chiquet-Ehrismann, and E.J. Battegay, *The fibrinogen globe of tenascin-C promotes basic fibroblast growth factor-induced endothelial cell elongation.* Mol Biol Cell, 1999. **10**(9): p. 2933-43.
206. Rodrigues, M., et al., *The matrikine tenascin-C protects multipotential stromal cells/mesenchymal stem cells from death cytokines such as FasL.* Tissue Eng Part A, 2013. **19**(17-18): p. 1972-83.
207. Forsberg, E., et al., *Skin wounds and severed nerves heal normally in mice lacking tenascin-C.* Proc Natl Acad Sci U S A, 1996. **93**(13): p. 6594-9.
208. Sumioka, T., et al., *Impaired cornea wound healing in a tenascin C-deficient mouse model.* Lab Invest, 2013. **93**(2): p. 207-17.
209. Okamura, N., et al., *Deficiency of tenascin-C delays articular cartilage repair in mice.* Osteoarthritis Cartilage, 2010. **18**(6): p. 839-48.
210. Betz, P., et al., *Localization of tenascin in human skin wounds--an immunohistochemical study.* Int J Legal Med, 1993. **105**(6): p. 325-8.
211. Latijnhouwers, M.A., et al., *Tenascin expression during wound healing in human skin.* J Pathol, 1996. **178**(1): p. 30-5.
212. Mackie, E.J., W. Halfter, and D. Liverani, *Induction of tenascin in healing wounds.* J Cell Biol, 1988. **107**(6 Pt 2): p. 2757-67.
213. Udalova, I.A., et al., *Expression and immune function of tenascin-C.* Crit Rev Immunol, 2011. **31**(2): p. 115-45.
214. Goh, F.G., et al., *Transcriptional regulation of the endogenous danger signal tenascin-C: a novel autocrine loop in inflammation.* J Immunol, 2010. **184**(5): p. 2655-62.
215. Piccinini, A.M. and K.S. Midwood, *Endogenous control of immunity against infection: tenascin-C regulates TLR4-mediated inflammation via microRNA-155.* Cell Rep, 2012. **2**(4): p. 914-26.

216. McCachren, S.S. and V.A. Lightner, *Expression of human tenascin in synovitis and its regulation by interleukin-1.* Arthritis Rheum, 1992. **35**(10): p. 1185-96.
217. Salter, D.M., *Tenascin is increased in cartilage and synovium from arthritic knees.* Br J Rheumatol, 1993. **32**(9): p. 780-6.
218. Goh, F.G., et al., *Transcriptional regulation of the endogenous danger signal tenascin-C: a novel autocrine loop in inflammation.* J Immunol. **184**(5): p. 2655-62.
219. Van Eyken, P., et al., *Localization and cellular source of the extracellular matrix protein tenascin in normal and fibrotic rat liver.* Hepatology, 1992. **15**(5): p. 909-16.
220. Kaarteenaho-Wiik, R., et al., *Tenascin is increased in epithelial lining fluid in fibrotic lung disorders.* Lung, 1998. **176**(6): p. 371-80.
221. Dalkowski, A., et al., *Increased expression of tenascin C by keloids in vivo and in vitro.* Br J Dermatol, 1999. **141**(1): p. 50-6.
222. Wallner, K., et al., *Tenascin-C is expressed in macrophage-rich human coronary atherosclerotic plaque.* Circulation, 1999. **99**(10): p. 1284-9.
223. Karjalainen, E.M., et al., *Airway inflammation and basement membrane tenascin in newly diagnosed atopic and nonatopic asthma.* Respir Med, 2003. **97**(9): p. 1045-51.
224. Gutowski, N.J., J. Newcombe, and M.L. Cuzner, *Tenascin-R and C in multiple sclerosis lesions: relevance to extracellular matrix remodelling.* Neuropathol Appl Neurobiol, 1999. **25**(3): p. 207-14.
225. Salas, A., et al., *Subepithelial myofibroblasts and tenascin expression in microscopic colitis.* Histopathology, 2003. **43**(1): p. 48-54.
226. Catalan, V., et al., *Increased tenascin C and Toll-like receptor 4 levels in visceral adipose tissue as a link between inflammation and extracellular matrix remodeling in obesity.* J Clin Endocrinol Metab, 2012. **97**(10): p. E1880-9.
227. Orend, G. and R. Chiquet-Ehrismann, *Tenascin-C induced signaling in cancer.* Cancer Lett, 2006. **244**(2): p. 143-63.
228. Riedl, S., et al., *Serum tenascin-C is an indicator of inflammatory bowel disease activity.* Int J Colorectal Dis, 2001. **16**(5): p. 285-91.
229. Page, T.H., et al., *Raised circulating tenascin-C in rheumatoid arthritis.* Arthritis Res Ther, 2012. **14**(6): p. R260.
230. Liabeuf, S., et al., *High circulating levels of large splice variants of tenascin-C is associated with mortality and cardiovascular disease in chronic kidney disease patients.* Atherosclerosis. **215**(1): p. 116-24.
231. Fujimoto, N., et al., *Incremental prognostic values of serum tenascin-C levels with blood B-type natriuretic peptide testing at discharge in patients with dilated cardiomyopathy and decompensated heart failure.* J Card Fail, 2009. **15**(10): p. 898-905.
232. Hisatomi, K., et al., *Elevated levels of tenascin-C in patients with cryptogenic organizing pneumonia.* Intern Med, 2009. **48**(17): p. 1501-7.
233. Ruhmann, M., et al., *Endogenous activation of adaptive immunity: tenascin-C drives interleukin-17 synthesis in murine arthritic joint disease.* Arthritis Rheum, 2012. **64**(7): p. 2179-90.
234. Kanayama, M., et al., *alpha9beta1 integrin-mediated signaling serves as an intrinsic regulator of pathogenic Th17 cell generation.* J Immunol, 2011. **187**(11): p. 5851-64.
235. Nakahara, H., et al., *Deficiency of tenascin C attenuates allergen-induced bronchial asthma in the mouse.* Eur J Immunol, 2006. **36**(12): p. 3334-45.

236. Kuriyama, N., et al., *Tenascin-C: a novel mediator of hepatic ischemia and reperfusion injury.* Hepatology, 2011. **54**(6): p. 2125-36.
237. Xie, K., et al., *Tenascin-C deficiency ameliorates Alzheimer's disease-related pathology in mice.* Neurobiol Aging, 2013. **34**(10): p. 2389-98.
238. Shimojo, N., et al., *Tenascin-C May Accelerate Cardiac Fibrosis by Activating Macrophages via the Integrin alphaVbeta3/Nuclear Factor-kappaB/Interleukin-6 Axis.* Hypertension, 2015. **66**(4): p. 757-66.
239. Asano, T., et al., *alpha9beta1 integrin acts as a critical intrinsic regulator of human rheumatoid arthritis.* Rheumatology (Oxford), 2014. **53**(3): p. 415-24.
240. Kanayama, M., et al., *Alpha9 integrin and its ligands constitute critical joint microenvironments for development of autoimmune arthritis.* J Immunol, 2009. **182**(12): p. 8015-25.
241. Patel, L., et al., *Tenascin-C induces inflammatory mediators and matrix degradation in osteoarthritic cartilage.* BMC Musculoskelet Disord, 2011. **12**: p. 164.
242. Liu, R., et al., *Tenascin-C produced by oxidized LDL-stimulated macrophages increases foam cell formation through Toll-like receptor-4.* Mol Cells, 2012. **34**(1): p. 35-41.
243. Fujimoto, M., et al., *Tenascin-C induces prolonged constriction of cerebral arteries in rats.* Neurobiol Dis, 2013. **55**: p. 104-9.
244. Machino-Ohtsuka, T., et al., *Tenascin-C aggravates autoimmune myocarditis via dendritic cell activation and Th17 cell differentiation.* J Am Heart Assoc, 2014. **3**(6): p. e001052.
245. Chiquet-Ehrismann, R. and R.P. Tucker, *Tenascins and the importance of adhesion modulation.* Cold Spring Harb Perspect Biol, 2011. **3**(5).
246. Bartsch, S., et al., *Expression of tenascin in the developing and adult cerebellar cortex.* J Neurosci, 1992. **12**(3): p. 736-49.
247. Celio, M.R. and R. Chiquet-Ehrismann, *'Perineuronal nets' around cortical interneurons expressing parvalbumin are rich in tenascin.* Neurosci Lett, 1993. **162**(1-2): p. 137-40.
248. Hagihara, K., et al., *Immunohistochemical evidence for the brevican-tenascin-R interaction: colocalization in perineuronal nets suggests a physiological role for the interaction in the adult rat brain.* J Comp Neurol, 1999. **410**(2): p. 256-64.
249. El Ayachi, I., et al., *Spatiotemporal distribution of tenascin-R in the developing human cerebral cortex parallels neuronal migration.* J Comp Neurol, 2011. **519**(12): p. 2379-89.
250. Woodworth, A., et al., *Neuronal-specific synthesis and glycosylation of tenascin-R.* J Biol Chem, 2004. **279**(11): p. 10413-21.
251. Montag-Sallaz, M. and D. Montag, *Severe cognitive and motor coordination deficits in tenascin-R-deficient mice.* Genes Brain Behav, 2003. **2**(1): p. 20-31.
252. Freitag, S., M. Schachner, and F. Morellini, *Behavioral alterations in mice deficient for the extracellular matrix glycoprotein tenascin-R.* Behav Brain Res, 2003. **145**(1-2): p. 189-207.
253. Dufresne, D., et al., *Homozygous deletion of Tenascin-R in a patient with intellectual disability.* J Med Genet, 2012. **49**(7): p. 451-4.
254. Haunso, A., et al., *Morphology of perineuronal nets in tenascin-R and parvalbumin single and double knockout mice.* Brain Res, 2000. **864**(1): p. 142-5.

255. Bruckner, G., et al., *Postnatal development of perineuronal nets in wild-type mice and in a mutant deficient in tenascin-R.* J Comp Neurol, 2000. **428**(4): p. 616-29.
256. Sykova, E., et al., *Reduced extracellular space in the brain of tenascin-R- and HNK-1-sulphotransferase deficient mice.* Eur J Neurosci, 2005. **22**(8): p. 1873-80.
257. Nikonenko, A., et al., *Tenascin-R-deficient mice show structural alterations of symmetric perisomatic synapses in the CA1 region of the hippocampus.* J Comp Neurol, 2003. **456**(4): p. 338-49.
258. Saghatelyan, A.K., et al., *Reduced perisomatic inhibition, increased excitatory transmission, and impaired long-term potentiation in mice deficient for the extracellular matrix glycoprotein tenascin-R.* Mol Cell Neurosci, 2001. **17**(1): p. 226-40.
259. Manavalan, A., et al., *Brain site-specific proteome changes in aging-related dementia.* Exp Mol Med, 2013. **45**: p. e39.
260. Morawski, M., et al., *Tenascin-R promotes assembly of the extracellular matrix of perineuronal nets via clustering of aggrecan.* Philos Trans R Soc Lond B Biol Sci, 2014. **369**(1654): p. 20140046.
261. Kwok, J.C., et al., *Extracellular matrix and perineuronal nets in CNS repair.* Dev Neurobiol, 2011. **71**(11): p. 1073-89.
262. Xiao, Z.C., et al., *Tenascin-R is a functional modulator of sodium channel beta subunits.* J Biol Chem, 1999. **274**(37): p. 26511-7.
263. Okuda, H., et al., *Chondroitin sulfate proteoglycan tenascin-R regulates glutamate uptake by adult brain astrocytes.* J Biol Chem, 2014. **289**(5): p. 2620-31.
264. Saghatelyan, A.K., et al., *The extracellular matrix molecule tenascin-R and its HNK-1 carbohydrate modulate perisomatic inhibition and long-term potentiation in the CA1 region of the hippocampus.* Eur J Neurosci, 2000. **12**(9): p. 3331-42.
265. Probstmeier, R., et al., *Tenascin-R interferes with integrin-dependent oligodendrocyte precursor cell adhesion by a ganglioside-mediated signalling mechanism.* Eur J Neurosci, 1999. **11**(7): p. 2474-88.
266. Pesheva, P., et al., *Tenascin-R is an intrinsic autocrine factor for oligodendrocyte differentiation and promotes cell adhesion by a sulfatide-mediated mechanism.* J Neurosci, 1997. **17**(12): p. 4642-51.
267. Xiao, Z.C., et al., *Distinct effects of recombinant tenascin-R domains in neuronal cell functions and identification of the domain interacting with the neuronal recognition molecule F3/11.* Eur J Neurosci, 1996. **8**(4): p. 766-82.
268. Xiao, Z.C., et al., *Defasciculation of neurites is mediated by tenascin-R and its neuronal receptor F3/11.* J Neurosci Res, 1998. **52**(4): p. 390-404.
269. Revest, J.M., et al., *Bidirectional signaling between neurons and glial cells via the F3 neuronal adhesion molecule.* Adv Exp Med Biol, 1999. **468**: p. 309-18.
270. Pesheva, P. and R. Probstmeier, *The yin and yang of tenascin-R in CNS development and pathology.* Prog Neurobiol, 2000. **61**(5): p. 465-93.
271. Angelov, D.N., et al., *Tenascin-R is antiadhesive for activated microglia that induce downregulation of the protein after peripheral nerve injury: a new role in neuronal protection.* J Neurosci, 1998. **18**(16): p. 6218-29.
272. Liao, H., et al., *Tenascin-R plays a role in neuroprotection via its distinct domains that coordinate to modulate the microglia function.* J Biol Chem, 2005. **280**(9): p. 8316-23.

273. Burch, G.H., et al., *Embryonic expression of tenascin-X suggests a role in limb, muscle, and heart development.* Dev Dyn, 1995. **203**(4): p. 491-504.
274. Geffrotin, C., et al., *Distinct tissue distribution in pigs of tenascin-X and tenascin-C transcripts.* Eur J Biochem, 1995. **231**(1): p. 83-92.
275. Lethias, C., et al., *A model of tenascin-X integration within the collagenous network.* FEBS Lett, 2006. **580**(26): p. 6281-5.
276. Luczak, J.A., S.D. Redick, and J.E. Schwarzbauer, *A single cysteine, Cys-64, is essential for assembly of tenascin-C hexabrachions.* J Biol Chem, 1998. **273**(4): p. 2073-7.
277. Schalkwijk, J., et al., *A recessive form of the Ehlers-Danlos syndrome caused by tenascin-X deficiency.* N Engl J Med, 2001. **345**(16): p. 1167-75.
278. Voermans, N.C., et al., *Ehlers-Danlos syndrome due to tenascin-X deficiency: muscle weakness and contractures support overlap with collagen VI myopathies.* Am J Med Genet A, 2007. **143A**(18): p. 2215-9.
279. Mao, J.R., et al., *Tenascin-X deficiency mimics Ehlers-Danlos syndrome in mice through alteration of collagen deposition.* Nat Genet, 2002. **30**(4): p. 421-5.
280. Voermans, N.C., et al., *Mild muscular features in tenascin-X knockout mice, a model of Ehlers-danlos syndrome.* Connect Tissue Res. **52**(5): p. 422-32.
281. Zweers, M.C., et al., *Deficiency of tenascin-X causes abnormalities in dermal elastic fiber morphology.* J Invest Dermatol, 2004. **122**(4): p. 885-91.
282. Minamitani, T., H. Ariga, and K. Matsumoto, *Deficiency of tenascin-X causes a decrease in the level of expression of type VI collagen.* Exp Cell Res, 2004. **297**(1): p. 49-60.
283. Veit, G., et al., *Collagen XII interacts with avian tenascin-X through its NC3 domain.* J Biol Chem, 2006. **281**(37): p. 27461-70.
284. Elefteriou, F., et al., *Binding of tenascin-X to decorin.* FEBS Lett, 2001. **495**(1-2): p. 44-7.
285. Margaron, Y., et al., *Tenascin-X increases the stiffness of collagen gels without affecting fibrillogenesis.* Biophys Chem, 2010. **147**(1-2): p. 87-91.
286. Minamitani, T., et al., *Modulation of collagen fibrillogenesis by tenascin-X and type VI collagen.* Exp Cell Res, 2004. **298**(1): p. 305-15.
287. Egging, D., et al., *Interactions of human tenascin-X domains with dermal extracellular matrix molecules.* Arch Dermatol Res, 2007. **298**(8): p. 389-96.
288. Egging, D.F., et al., *Dermal connective tissue development in mice: an essential role for tenascin-X.* Cell Tissue Res, 2006. **323**(3): p. 465-74.
289. Egging, D., et al., *Wound healing in tenascin-X deficient mice suggests that tenascin-X is involved in matrix maturation rather than matrix deposition.* Connect Tissue Res, 2007. **48**(2): p. 93-8.
290. Elefteriou, F., et al., *Cell adhesion to tenascin-X mapping of cell adhesion sites and identification of integrin receptors.* Eur J Biochem, 1999. **263**(3): p. 840-8.
291. Fujie, S., et al., *Tenascin-X induces cell detachment through p38 mitogen-activated protein kinase activation.* Biol Pharm Bull, 2009. **32**(10): p. 1795-9.
292. Valcourt, U., et al., *Tenascin-X: beyond the architectural function.* Cell Adh Migr, 2015. **9**(1-2): p. 154-65.
293. Alcaraz, L.B., et al., *Tenascin-X promotes epithelial-to-mesenchymal transition by activating latent TGF-beta.* J Cell Biol, 2014. **205**(3): p. 409-28.
294. Weber, P., et al., *Zebrafish tenascin-W, a new member of the tenascin family.* J Neurobiol, 1998. **35**(1): p. 1-16.

295. Scherberich, A., et al., *Murine tenascin-W: a novel mammalian tenascin expressed in kidney and at sites of bone and smooth muscle development.* J Cell Sci, 2004. **117**(Pt 4): p. 571-81.
296. Brellier, F., et al., *The adhesion modulating properties of tenascin-W.* Int J Biol Sci, 2012. **8**(2): p. 187-94.
297. Degen, M., et al., *Tenascin-W is a novel marker for activated tumor stroma in low-grade human breast cancer and influences cell behavior.* Cancer Res, 2007. **67**(19): p. 9169-79.
298. Martina, E., et al., *Tenascin-W is a specific marker of glioma-associated blood vessels and stimulates angiogenesis in vitro.* FASEB J, 2010. **24**(3): p. 778-87.
299. Meloty-Kapella, C.V., et al., *Effects of tenascin-W on osteoblasts in vitro.* Cell Tissue Res, 2008. **334**(3): p. 445-55.
300. Scherberich, A., et al., *Tenascin-W is found in malignant mammary tumors, promotes alpha8 integrin-dependent motility and requires p38MAPK activity for BMP-2 and TNF-alpha induced expression in vitro.* Oncogene, 2005. **24**(9): p. 1525-32.
301. Kimura, H., et al., *Tenascin-W inhibits proliferation and differentiation of preosteoblasts during endochondral bone formation.* Biochem Biophys Res Commun, 2007. **356**(4): p. 935-41.
302. Mikura, A., et al., *Association of tenascin-W expression with mineralization in mouse calvarial development.* Congenit Anom (Kyoto), 2009. **49**(2): p. 77-84.
303. Brellier, F., et al., *Tenascin-W is a better cancer biomarker than tenascin-C for most human solid tumors.* BMC Clin Pathol, 2012. **12**: p. 14.
304. Degen, M., et al., *Tenascin-W, a new marker of cancer stroma, is elevated in sera of colon and breast cancer patients.* Int J Cancer, 2008. **122**(11): p. 2454-61.
305. Chiovaro, F., et al., *Transcriptional regulation of tenascin-W by TGF-beta signaling in the bone metastatic niche of breast cancer cells.* Int J Cancer, 2015. **137**(8): p. 1842-54.
306. Tucker, R.P. and R. Chiquet-Ehrismann, *Evidence for the evolution of tenascin and fibronectin early in the chordate lineage.* Int J Biochem Cell Biol, 2009. **41**(2): p. 424-34.
307. Biasini, M., et al., *SWISS-MODEL: modelling protein tertiary and quaternary structure using evolutionary information.* Nucleic Acids Res, 2014. **42**(Web Server issue): p. W252-8.
308. Yee, V.C., et al., *Crystal structure of a 30 kDa C-terminal fragment from the gamma chain of human fibrinogen.* Structure, 1997. **5**(1): p. 125-38.
309. Comeau, S.R., et al., *ClusPro: an automated docking and discrimination method for the prediction of protein complexes.* Bioinformatics, 2004. **20**(1): p. 45-50.
310. Reichelt, P., C. Schwarz, and M. Donzeau, *Single step protocol to purify recombinant proteins with low endotoxin contents.* Protein Expr Purif, 2006. **46**(2): p. 483-8.
311. Magalhaes, P.O., et al., *Methods of endotoxin removal from biological preparations: a review.* J Pharm Pharm Sci, 2007. **10**(3): p. 388-404.
312. Kawamoto, T., et al., *TAK-242 selectively suppresses Toll-like receptor 4-signaling mediated by the intracellular domain.* Eur J Pharmacol, 2008. **584**(1): p. 40-8.
313. Zhang, C., et al., *High-mobility group box 1 (HMGB1) impaired cardiac excitation-contraction coupling by enhancing the sarcoplasmic reticulum (SR)*

Ca(2+) leak through TLR4-ROS signaling in cardiomyocytes. J Mol Cell Cardiol, 2014. **74**: p. 260-73.
314. Tsou, T.C., et al., *Crucial role of Toll-like receptors in the zinc/nickel-induced inflammatory response in vascular endothelial cells.* Toxicol Appl Pharmacol, 2013. **273**(3): p. 492-9.
315. Deckner, M., et al., *Differential expression of tenascin-C, tenascin-R, tenascin/J1, and tenascin-X in spinal cord scar tissue and in the olfactory system.* Exp Neurol, 2000. **166**(2): p. 350-62.
316. Apostolova, I., A. Irintchev, and M. Schachner, *Tenascin-R restricts posttraumatic remodeling of motoneuron innervation and functional recovery after spinal cord injury in adult mice.* J Neurosci, 2006. **26**(30): p. 7849-59.
317. Becker, T., et al., *Tenascin-R inhibits regrowth of optic fibers in vitro and persists in the optic nerve of mice after injury.* Glia, 2000. **29**(4): p. 330-46.
318. You, J., et al., *Passive immunization with tenascin-R (TN-R) polyclonal antibody promotes axonal regeneration and functional recovery after spinal cord injury in rats.* Neurosci Lett, 2012. **525**(2): p. 129-34.
319. Martina, E., et al., *Tenascin-W is a specific marker of glioma-associated blood vessels and stimulates angiogenesis in vitro.* FASEB J. **24**(3): p. 778-87.
320. Mai, C.W., Y.B. Kang, and M.R. Pichika, *Should a Toll-like receptor 4 (TLR-4) agonist or antagonist be designed to treat cancer? TLR-4: its expression and effects in the ten most common cancers.* Onco Targets Ther, 2013. **6**: p. 1573-87.
321. Ikebe, M., et al., *Lipopolysaccharide (LPS) increases the invasive ability of pancreatic cancer cells through the TLR4/MyD88 signaling pathway.* J Surg Oncol, 2009. **100**(8): p. 725-31.
322. Kelsh, R.M. and P.J. McKeown-Longo, *Topographical changes in extracellular matrix: Activation of TLR4 signaling and solid tumor progression.* Trends Cancer Res, 2013. **9**: p. 1-13.
323. Wang, L., et al., *Lipopolysaccharide-induced toll-like receptor 4 signaling in cancer cells promotes cell survival and proliferation in hepatocellular carcinoma.* Dig Dis Sci, 2013. **58**(8): p. 2223-36.
324. Takashima, K., et al., *Analysis of binding site for the novel small-molecule TLR4 signal transduction inhibitor TAK-242 and its therapeutic effect on mouse sepsis model.* Br J Pharmacol, 2009. **157**(7): p. 1250-62.
325. Lefebvre, J.S., et al., *Extra domain A of fibronectin primes leukotriene biosynthesis and stimulates neutrophil migration through activation of Toll-like receptor 4.* Arthritis Rheum, 2011. **63**(6): p. 1527-33.
326. Manthey, C.L., et al., *SB202190, a selective inhibitor of p38 mitogen-activated protein kinase, is a powerful regulator of LPS-induced mRNAs in monocytes.* J Leukoc Biol, 1998. **64**(3): p. 409-17.
327. Suzuki, M., et al., *The role of p38 mitogen-activated protein kinase in IL-6 and IL-8 production from the TNF-alpha- or IL-1beta-stimulated rheumatoid synovial fibroblasts.* FEBS Lett, 2000. **465**(1): p. 23-7.
328. LaFleur, D.W., et al., *Aortic smooth muscle cells interact with tenascin-C through its fibrinogen-like domain.* J Biol Chem, 1997. **272**(52): p. 32798-803.
329. Antonov, A.S., et al., *alphaVbeta3 integrin regulates macrophage inflammatory responses via PI3 kinase/Akt-dependent NF-kappaB activation.* J Cell Physiol, 2011. **226**(2): p. 469-76.
330. Kim, S., et al., *Carcinoma-produced factors activate myeloid cells through TLR2 to stimulate metastasis.* Nature, 2009. **457**(7225): p. 102-6.

331. Quero, L., et al., *Hyaluronic acid fragments enhance the inflammatory and catabolic response in human intervertebral disc cells through modulation of toll-like receptor 2 signalling pathways.* Arthritis Res Ther, 2013. **15**(4): p. R94.
332. Park, J.S., et al., *Involvement of toll-like receptors 2 and 4 in cellular activation by high mobility group box 1 protein.* J Biol Chem, 2004. **279**(9): p. 7370-7.
333. Amin, A.R. and A.B. Islam, *Genomic analysis and differential expression of HMG and S100A family in human arthritis: upregulated expression of chemokines, IL-8 and nitric oxide by HMGB1*. DNA Cell Biol, 2014. **33**(8): p. 550-65.
334. Sillat, T., et al., *Toll-like receptors in human chondrocytes and osteoarthritic cartilage.* Acta Orthop, 2013. **84**(6): p. 585-92.
335. O'Neill, L.A. and A.G. Bowie, *The family of five: TIR-domain-containing adaptors in Toll-like receptor signalling.* Nat Rev Immunol, 2007. **7**(5): p. 353-64.
336. Triantafilou, M., et al., *Lateral diffusion of Toll-like receptors reveals that they are transiently confined within lipid rafts on the plasma membrane.* J Cell Sci, 2004. **117**(Pt 17): p. 4007-14.
337. Hyakushima, N., et al., *Interaction of soluble form of recombinant extracellular TLR4 domain with MD-2 enables lipopolysaccharide binding and attenuates TLR4-mediated signaling.* J Immunol, 2004. **173**(11): p. 6949-54.
338. Visintin, A., et al., *Pharmacological inhibition of endotoxin responses is achieved by targeting the TLR4 coreceptor, MD-2.* J Immunol, 2005. **175**(10): p. 6465-72.
339. Park, J.S., et al., *High mobility group box 1 protein interacts with multiple Toll-like receptors.* Am J Physiol Cell Physiol, 2006. **290**(3): p. C917-24.
340. Horvath, G., S. Young, and E. Latz, *Toll-like receptor interactions imaged by FRET microscopy and GFP fragment reconstitution.* Methods Mol Biol, 2009. **517**: p. 33-54.
341. Raby, A.C., et al., *Soluble TLR2 reduces inflammation without compromising bacterial clearance by disrupting TLR2 triggering.* J Immunol, 2009. **183**(1): p. 506-17.
342. Shin, H.J., et al., *Kinetics of binding of LPS to recombinant CD14, TLR4, and MD-2 proteins.* Mol Cells, 2007. **24**(1): p. 119-24.
343. Sievers, F., et al., *Fast, scalable generation of high-quality protein multiple sequence alignments using Clustal Omega.* Mol Syst Biol, 2011. **7**: p. 539.
344. Baker, D. and A. Sali, *Protein structure prediction and structural genomics.* Science, 2001. **294**(5540): p. 93-6.
345. Das, R., et al., *Structure prediction for CASP7 targets using extensive all-atom refinement with Rosetta@home.* Proteins, 2007. **69 Suppl 8**: p. 118-28.
346. Webb, B. and A. Sali, *Protein structure modeling with MODELLER.* Methods Mol Biol, 2014. **1137**: p. 1-15.
347. Marti-Renom, M.A., et al., *Comparative protein structure modeling of genes and genomes.* Annu Rev Biophys Biomol Struct, 2000. **29**: p. 291-325.
348. Schumacher, S. and E.M. Stube, *Regulated binding of the fibrinogen-like domains of tenascin-R and tenascin-C to the neural EGF family member CALEB.* J Neurochem, 2003. **87**(5): p. 1213-23.
349. Fischer, D., et al., *A single heparin binding region within the fibrinogen-like domain is functional in chick tenascin-C.* J Biol Chem, 1995. **270**(7): p. 3378-84.

350. Meng, J., E. Lien, and D.T. Golenbock, *MD-2-mediated ionic interactions between lipid A and TLR4 are essential for receptor activation.* J Biol Chem, 2010. **285**(12): p. 8695-702.
351. Lonez, C., et al., *Critical residues involved in Toll-like receptor 4 activation by cationic lipid nanocarriers are not located at the lipopolysaccharide-binding interface.* Cell Mol Life Sci, 2015. **72**(20): p. 3971-82.
352. Scott, P.G., et al., *Crystal structure of the biglycan dimer and evidence that dimerization is essential for folding and stability of class I small leucine-rich repeat proteoglycans.* J Biol Chem, 2006. **281**(19): p. 13324-32.
353. Hakansson, K., et al., *Crystal structure of the trimeric alpha-helical coiled-coil and the three lectin domains of human lung surfactant protein D.* Structure, 1999. **7**(3): p. 255-64.
354. Doolittle, R.F., *A detailed consideration of a principal domain of vertebrate fibrinogen and its relatives.* Protein Sci, 1992. **1**(12): p. 1563-77.
355. King, N., et al., *The genome of the choanoflagellate Monosiga brevicollis and the origin of metazoans.* Nature, 2008. **451**(7180): p. 783-8.
356. Garlatti, V., et al., *Structural insights into the innate immune recognition specificities of L- and H-ficolins.* EMBO J, 2007. **26**(2): p. 623-33.
357. Garlatti, V., et al., *Structural basis for innate immune sensing by M-ficolin and its control by a pH-dependent conformational switch.* J Biol Chem, 2007. **282**(49): p. 35814-20.
358. Barton, W.A., D. Tzvetkova, and D.B. Nikolov, *Structure of the angiopoietin-2 receptor binding domain and identification of surfaces involved in Tie2 recognition.* Structure, 2005. **13**(5): p. 825-32.
359. Shrive, A.K., et al., *Crystal structure of the tetrameric fibrinogen-like recognition domain of fibrinogen C domain containing 1 (FIBCD1) protein.* J Biol Chem, 2014. **289**(5): p. 2880-7.
360. Kim, K.T., et al., *Oligomerization and multimerization are critical for angiopoietin-1 to bind and phosphorylate Tie2.* J Biol Chem, 2005. **280**(20): p. 20126-31.
361. Davis, S., et al., *Angiopoietins have distinct modular domains essential for receptor binding, dimerization and superclustering.* Nat Struct Biol, 2003. **10**(1): p. 38-44.
362. Schlosser, A., et al., *Characterization of FIBCD1 as an acetyl group-binding receptor that binds chitin.* J Immunol, 2009. **183**(6): p. 3800-9.
363. Thomsen, T., et al., *The recognition unit of FIBCD1 organizes into a noncovalently linked tetrameric structure and uses a hydrophobic funnel (S1) for acetyl group recognition.* J Biol Chem, 2010. **285**(2): p. 1229-38.
364. Zuliani-Alvarez, L. and K.S. Midwood, *Fibrinogen-Related Proteins in Tissue Repair: How a Unique Domain with a Common Structure Controls Diverse Aspects of Wound Healing.* Adv Wound Care (New Rochelle), 2015. **4**(5): p. 273-285.
365. Barton, W.A., et al., *Crystal structures of the Tie2 receptor ectodomain and the angiopoietin-2-Tie2 complex.* Nat Struct Mol Biol, 2006. **13**(6): p. 524-32.
366. Ahn, H.J., et al., *Alzheimer's disease peptide beta-amyloid interacts with fibrinogen and induces its oligomerization.* Proc Natl Acad Sci U S A, 2010. **107**(50): p. 21812-7.
367. Farrell, D.H. and P. Thiagarajan, *Binding of recombinant fibrinogen mutants to platelets.* J Biol Chem, 1994. **269**(1): p. 226-31.

368. Ugarova, T.P., et al., *Identification of a novel recognition sequence for integrin alphaM beta2 within the gamma-chain of fibrinogen.* J Biol Chem, 1998. **273**(35): p. 22519-27.
369. Podolnikova, N.P., et al., *Identification of a novel binding site for platelet integrins alpha IIb beta 3 (GPIIbIIIa) and alpha 5 beta 1 in the gamma C-domain of fibrinogen.* J Biol Chem, 2003. **278**(34): p. 32251-8.
370. Pratt, K.P., et al., *The primary fibrin polymerization pocket: three-dimensional structure of a 30-kDa C-terminal gamma chain fragment complexed with the peptide Gly-Pro-Arg-Pro.* Proc Natl Acad Sci U S A, 1997. **94**(14): p. 7176-81.
371. Zhang, J., et al., *Pathophysiological condition changes the conformation of a flexible FBG-related protein, switching it from pathogen-recognition to host-interaction.* Biochimie, 2011. **93**(10): p. 1710-9.
372. Doolittle, R.F., K. McNamara, and K. Lin, *Correlating structure and function during the evolution of fibrinogen-related domains.* Protein Sci, 2012. **21**(12): p. 1808-23.
373. Smiley, S.T., J.A. King, and W.W. Hancock, *Fibrinogen stimulates macrophage chemokine secretion through toll-like receptor 4.* J Immunol, 2001. **167**(5): p. 2887-94.
374. Tucker, R.P., et al., *Phylogenetic analysis of the tenascin gene family: evidence of origin early in the chordate lineage.* BMC Evol Biol, 2006. **6**: p. 60.
375. Hanington, P.C. and S.M. Zhang, *The primary role of fibrinogen-related proteins in invertebrates is defense, not coagulation.* J Innate Immun, 2011. **3**(1): p. 17-27.
376. Hertel, L.A., et al., *Biomphalaria glabrata hemolymph lectins: binding to bacteria, mammalian erythrocytes, and to sporocysts and rediae of Echinostoma paraensei.* J Invertebr Pathol, 1994. **64**(1): p. 52-61.
377. Gokudan, S., et al., *Horseshoe crab acetyl group-recognizing lectins involved in innate immunity are structurally related to fibrinogen.* Proc Natl Acad Sci U S A, 1999. **96**(18): p. 10086-91.